UNIVERSIDADE FEDERAL RURAL DO RIO DE JANEIRO
INSTITUTO DE TECNOLOGIA
PROGRAMA DE PÓS-GRADUAÇÃO EM CIÊNCIA E TECNOLOGIA DE ALIMENTOS

BRUNO SÉRGIO TOLEDO BARBOSA

CONJUGADOS FORMADOS POR PROTEÍNAS DA CLARA DE OVO E ÁCIDO FERÚLICO PARA SUA APLICAÇÃO EM SISTEMAS DE CARREAMENTO DE SUBSTÂNCIAS BIOATIVAS HIDROFÓBICAS

SEROPÉDICA
2026

BRUNO SÉRGIO TOLEDO BARBOSA

CONJUGADOS FORMADOS POR PROTEÍNAS DA CLARA DO OVO E ÁCIDO FERÚLICO PARA SUA APLICAÇÃO EM SISTEMAS DE CARREAMENTO DE SUBSTÂNCIAS BIOATIVAS HIDROFÓBICAS

Tese apresentada ao Programa de Pós-Gradução em Ciência e Tecnologia de Alimentos da Universidade Federal Rural do Rio de Janeiro, como requisito parcial para a obtenção do grau de Doutor em Ciência e Tecnologia de Alimentos.

Orientador: Edwin Elard Garcia Rojas.

SEROPÉDICA
2026

Universidade Federal Rural do Rio de Janeiro
Biblioteca Central / Seção de Processamento Técnico

Ficha catalográfica elaborada
com os dados fornecidos pelo(a) autor(a)

B238c

Barbosa, Bruno Sérgio Toledo, 1995-
Conjugados formados por proteínas da clara de ovo e ácido ferúlico para sua aplicação em sistemas de carreamento de substâncias bioativas hidrofóbicas / Bruno Sérgio Toledo Barbosa. - Seropédica, 2026.
190 f.: il.

Orientador: Edwin Elard Garcia Rojas.
Tese(Doutorado). -- Universidade Federal Rural do Rio de Janeiro, Programa de Pós Graduação em Ciência e Tecnologia de Alimentos, 2026.

1. Conjugados. 2. Microencapsulação. 3. Emulsões Pickering. 4. Filmes . 5. Proteínas do ovo. I. Elard Garcia Rojas, Edwin , 1972-, orient. II Universidade Federal Rural do Rio de Janeiro. Programa de Pós Graduação em Ciência e Tecnologia de Alimentos III. Título.

O presente trabalho foi realizado com apoio da Coordenação de Aperfeiçoamento de Pessoal de Nível Superior – Brasil (CAPES) – Código de Financiamento 001.

MINISTÉRIO DA EDUCAÇÃO
UNIVERSIDADE FEDERAL RURAL DO RIO DE JANEIRO
PROGRAMA DE PÓS-GRADUAÇÃO EM CIÊNCIA E TECNOLOGIA DE ALIMENTOS

TERMO Nº 227/2026 - PPGCTA (12.28.01.00.00.00.00.41)

Nº do Protocolo: 23083.017397/2026-49

Seropédica-RJ, 15 de abril de 2026.

BRUNO SÉRGIO TOLEDO BARBOSA

Tese submetida como requisito parcial para obtenção do grau de doutor em Ciência e Tecnologia de Alimentos, no Curso de Pós-Graduação em Ciência e Tecnologia de Alimentos, área de Concentração em Ciência de Alimentos.

TESE APROVADA EM 10/04/2026

EDWIN ELARD GARCIA ROJAS, (Dr) UFF (orientador)

CÉSAR AUGUSTO SODRÉ DA SILVA, (Dr) UFV

RENATA VALERIANO TONON, (Dra) EMBRAPA

TATIANA SALDANHA, (Dra) UFRRJ

YAGO ALVES DE AGUIAR BERNARDO, (Dr) UFRRJ

Documento não acessível publicamente

(Assinado digitalmente em 16/04/2026 19:14)
TATIANA SALDANHA
PROFESSOR DO MAGISTERIO SUPERIOR
DTA (12.28.01.00.00.00.00.46)
Matrícula: ###634#2

(Assinado digitalmente em 15/04/2026 18:12)
YAGO ALVES DE AGUIAR BERNARDO
PROFESSOR DO MAGISTERIO SUPERIOR
DTA (12.28.01.00.00.00.00.46)
Matrícula: ###317#4

(Assinado digitalmente em 15/04/2026 18:00)
CESAR AUGUSTO SODRE DA SILVA
ASSINANTE EXTERNO
CPF: ###.###.776-##

(Assinado digitalmente em 15/04/2026 17:59)
EDWIN ELARD GARCIA ROJAS
ASSINANTE EXTERNO
CPF: ###.###.996-##

(Assinado digitalmente em 16/04/2026 09:21)
RENATA VALERIANO TONON
ASSINANTE EXTERNO
CPF: ###.###.418-##

RESUMO

BARBOSA, Bruno Sérgio Toledo. **Conjugados formados por proteínas da clara de ovo e ácido ferúlico para sua aplicação em sistemas de carreamento de substâncias bioativas hidrofóbicas**. 2026. 190p. Tese (Doutor em Ciência e Tecnologia de Alimentos). Instituto de Tecnologia de Alimentos. Universidade Federal Rural do Rio de Janeiro, Seropédica, RJ, 2026.

A crescente demanda por alimentos funcionais e sustentáveis tem impulsionado a busca por ingredientes naturais capazes de oferecer benefícios à saúde além da nutrição básica. Nesse contexto, proteínas e compostos fenólicos destacam-se por suas propriedades tecnofuncionais e biológicas. A interação entre proteínas e polifenóis pode ocorrer por associações não covalentes ou covalentes. A interação covalente, também denominada conjugação, resulta em modificações estruturais irreversíveis na proteína, impactando sua solubilidade, capacidade emulsificante, formação de espuma e capacidade antioxidante. Dessa forma, a formação de conjugados proteína–fenólico surge como uma estratégia promissora para a obtenção de novos componentes alimentares com funcionalidades ampliadas. A tese teve como objetivo desenvolver e caracterizar conjugados formados entre ovalbumina e lisozima, principais proteínas da clara de ovo, e o ácido ferúlico, bem como avaliar sua aplicação como agentes emulsificantes em emulsões Pickering para o carreamento de compostos bioativos e posterior incorporação em filmes comestíveis. A conjugação promoveu modificações estruturais significativas nas proteínas. No caso da ovalbumina, a conjugação covalente com o ácido ferúlico, obtida por meio da técnica alcalina, promoveu alterações nas estruturas secundária e terciária, além de aumento da hidrofobicidade superficial, resultando em melhorias expressivas na capacidade emulsificante e na capacidade de formação de espuma da proteína, bem como em aumento estatisticamente significativo da capacidade antioxidante. Para os conjugados lisozima–ácido ferúlico, obtidos pela técnica de radicais livres, também foram observadas modificações estruturais relevantes, refletindo em aprimoramento das propriedades tecnofuncionais. Adicionalmente, a conjugação contribuiu para a proteção da capacidade antioxidante do ácido ferúlico após simulação gastrointestinal *in vitro*, indicando maior estabilidade frente às condições digestivas. Os conjugados mostraram-se alternativas eficazes como agentes emulsificantes em emulsões Pickering óleo em água. As emulsões formuladas com conjugados de ovalbumina–ácido ferúlico apresentaram boa estabilidade cinética, sem separação de fases por até 8 dias, além de menor oxidação lipídica em comparação às emulsões estabilizadas apenas com ovalbumina nativa. Para a encapsulação de vitamina D, observou-se elevada eficiência de encapsulação, 92,13 ± 1,14%, contribuindo para a proteção do micronutriente frente à degradação fotoquímica. Emulsões Pickering formuladas com conjugados de lisozima–ácido ferúlico e carregadas com β-caroteno também apresentaram alta estabilidade cinética e oxidativa, além de eficiência de encapsulação de 88,99 ± 2,02%. A incorporação das emulsões em filmes de pectina modificou as propriedades estruturais e de barreira do material. Os filmes contendo β-caroteno microencapsulado apresentaram coloração amarelada, maior barreira à luz, menor permeabilidade ao vapor de água e menor solubilidade. A adição das emulsões aumentou a hidrofobicidade superficial dos filmes. A liberação do β-caroteno foi descrita pelos modelos de Ritger–Peppas e Peppas–Sahlin, com comportamento de difusão Fickiana. Em conjunto, os resultados demonstram que a conjugação proteína–ácido ferúlico constitui uma estratégia eficiente para o desenvolvimento de componentes multifuncionais com potencial aplicação em alimentos funcionais e embalagens bioativas.

Palavras-chave: emulsões Pickering; microencapsulação; vitamina D; β-caroteno; filmes bioativos.

ABSTRACT

BARBOSA, Bruno Sérgio Toledo. **Conjugates formed by egg white proteins and ferulic acid for application in delivery systems of hydrophobic bioactive compounds**. 2026. 190p. Thesis (Doctorate in Food Science and Technology). Institute of Food Technology. Universidade Federal do Rio de Janeiro, Seropédica, RJ, 2026.

The growing demand for functional and sustainable foods has driven the search for natural ingredients capable of providing health benefits beyond basic nutrition. In this context, proteins and phenolic compounds stand out due to their techno-functional and biological properties. Protein–polyphenol interactions may occur through non-covalent or covalent associations. Covalent interaction, also referred to as conjugation, results in irreversible structural modifications of proteins, affecting their solubility, emulsifying capacity, foaming properties, and antioxidant activity. Thus, the formation of protein–phenolic conjugates emerges as a promising strategy for obtaining novel food components with enhanced functionalities. This thesis aimed to develop and characterize conjugates formed between ovalbumin and lysozyme, the main egg white proteins, and ferulic acid, as well as to evaluate their application as emulsifying agents in Pickering emulsions for the delivery of bioactive compounds and subsequent incorporation into edible films. Conjugation promoted significant structural modifications in the proteins. In the case of ovalbumin, covalent conjugation with ferulic acid obtained by the alkaline method led to changes in secondary and tertiary structures, along with increased surface hydrophobicity, resulting in marked improvements in emulsifying and foaming capacities, as well as a statistically significant increase in antioxidant activity. For lysozyme–ferulic acid conjugates obtained by the free radical method, relevant structural modifications were also observed, leading to improved techno-functional properties. In addition, conjugation protected the antioxidant activity of ferulic acid after *in vitro* gastrointestinal simulation, indicating greater stability under digestive conditions. The conjugates proved to be effective alternatives as emulsifying agents in oil-in-water Pickering emulsions. Emulsions formulated with ovalbumin–ferulic acid conjugates exhibited good kinetic stability, with no phase separation for up to 8 days, and lower lipid oxidation compared with emulsions stabilized with native ovalbumin. For vitamin D encapsulation, a high encapsulation efficiency, 92.13 ± 1.14%, was achieved, contributing to the protection of the micronutrient against photochemical degradation. Pickering emulsions formulated with lysozyme–ferulic acid conjugates and loaded with β-carotene also showed high kinetic and oxidative stability, as well as an encapsulation efficiency of 88.99 ± 2.02%. The incorporation of these emulsions into pectin-based films modified the structural and barrier properties of the material. Films containing microencapsulated β-carotene exhibited a characteristic yellowish coloration, enhanced light barrier properties, reduced water vapor permeability, and lower water solubility. The addition of the emulsions increased the surface hydrophobicity of the films. β-Carotene release was described by the Ritger–Peppas and Peppas–Sahlin models, with Fickian diffusion behavior. Overall, the results demonstrate that protein–ferulic acid conjugation is an efficient strategy for developing multifunctional components with potential applications in functional foods and bioactive packaging.

Keywords: Pickering emulsions; microencapsulation; vitamin D; β-carotene; bioactive films.

LISTA DE FIGURAS

Figura 1. Fluxograma representativo da estrutura da tese, apresentando a síntese dos conjugados de ácido ferúlico com ovalbumina (OVA-AF) e lisozima (LIS-AF) e suas respectivas aplicações em sistemas de carreamento de substâncias bioativas. 18
Figura 2. Estrutura da ovalbumina. 24
Figura 3. Estrutura da lisozima. 25
Figura 4. Estrutura básica dos flavonoides, em que A e B são os anéis aromáticos. 26
Figura 5. Estrutura das formas isoméricas do ácido ferúlico (a) Cis e (b) Trans. 27
Figura 6. Interações não covalentes presentes entre polifenóis e proteínas. 30
Figura 7. Interação covalente a partir do método alcalino e enzimático entre proteínas e polifenóis. 31
Figura 8. Interação covalente a partir do método de radical livre entre proteínas e polifenóis. 32
Figura 9. Diagrama de processos que causam instabilidade em emulsões. 38
Figura 10. Esquema do comportamento das partículas em emulsões de Pickering em função da molhabilidade. 40
Figura 11. Representação esquemática do processo de formação de filmes pelo método de evaporação de solvente. 43
Figura 12. Estrutura da vitamina D. 48
Figura 13. Estrutura do β-caroteno. 50
Figure 14. S-type model (Equation 10) of the binding capacity of ferulic acid in the OVA-FA conjugate as a function of the initial concentration of FA added to the system. 72
Figure 15. Free SH groups in control ovalbumin and in OVA-FA conjugates formed from different initial concentrations of FA added to the system. Values followed by the same letters do not present statistically significant difference in the Tukey test ($p < 0.05$). 73
Figure 16. SDS-PAGE (12% resolution gel) of control ovalbumin and OVA-FA conjugate. . 75
Figure 17. Far UV CD spectra of control ovalbumin (green) and the OVA-FA conjugate (purple). 76
Figure 18. FTIR spectra of ovalbumin (red) and OVA-FA conjugate (blue). Peaks are shown by arrows. 77

Figure 19. Intrinsic fluorescence spectra of control ovalbumin (blue line) and OVA-FA conjugate (red line). Excitation was set at 280 nm, and dashed line is the peak of control OVA. 78
Figure 20. UV-VIS spectrum of ovalbumin and OVA-FA conjugate. 79
Figure 21. Techo-functional properties of ovalbumin and the OVA-FA conjugate. Solubility (A), emulsion properties (B), foaming properties (C) and antioxidant activity (D) are presented as mean ± standard deviation. Values followed by the same letters do not present statistically significant difference in the Tukey test ($p < 0.05$). 82
Figure 22. (A) Dynamic interfacial tension of different OVA-FA concentrations at the oil-water interface, with the model proposed by Equation 1 (–). (B) Oil-water three-phase contact angle with the OVA-FA conjugate..... 98
Figure 23. Creaming index of the different Pickering O/W emulsion samples, where (A), (B), (C), and (D) correspond to oil fractions of 0.25, 0.5, 0.6, and 0.7, respectively. Values followed by the same letters do not show statistically significant differences in the Tukey test ($p < 0.05$). Lowercase letters match samples and uppercase letters match time. 100
Figure 24. Adsorption of the OVA-FA conjugate at the oil-water interface of Pickering O/W emulsions. Values are presented as mean ± standard deviation. Values followed by the same letters do not show statistically significant differences in the Tukey test ($p < 0.05$)..... 101
Figure 25. Optical microscopy image of B4, C4, and D4 samples, Pickering O/W emulsions, composed of an aqueous phase containing 4% OVA-FA and different oil fractions (0.5, 0.6, and 0.7, respectively)..... 102
Figure 26. Rheological properties of Pickering emulsions at different oil fractions: (A) Apparent viscosity as a function of time; (B) Storage modulus (G'), loss modulus (G'') and damping factor (tan δ). 105
Figure 27. Antioxidant capacity, evaluated using the $ABTS^+$ (A) and DPPH (B) assays, of emulsions containing different oil fractions (B4 = 0.5, C4 = 0.6, D4 = 0.7), an emulsion stabilized with ovalbumin only (OVAE), and a ferulic acid solution (0.1 mg/mL). Results are expressed as mean ± standard deviation. Means followed by the same letter are not significantly different according to the Tukey test ($p < 0.05$). 106
Figure 28. (A) Lipid oxidation of Pickering O/W emulsions at different oil fractions. (B) Photochemical stability of vitamin D3 under UV irradiation in Pickering emulsions stabilized by OVA-FA, with different oil fractions. 109

Figure 29. Vitamin D3 release in *in vitro* gastrointestinal simulations of Pickering O/W emulsions with different oil fractions (B4 = 0.5, C4 = 0.6, D4 = 0.7), an emulsion stabilized with ovalbumin only (OVAE), and an unencapsulated vitamin D3 in oil (Control). 111
Figure 30. Bioaccessibility of vitamin D3 in a simulated *in vitro* gastrointestinal model from emulsions with different oil fractions (B4 = 0.5, C4 = 0.6, D4 = 0.7), an emulsion stabilized with ovalbumin only (OVAE), and an unencapsulated vitamin D3 in oil (Control). Values followed by the same letters do not show statistically significant differences in the Tukey test ($p < 0.05$). 112
Figure 31. (A) Fluorescence emission spectra of LYS and LYS-FA in the presence of increasing concentrations of FA, ranging from 2.7 to 38.8 μmol/L with excitation at 280 nm. (B) Stern-Volmer plot of LYS fluorescence quenching as a function of FA concentration. (C) Double logarithm plot for LYS-FA conjugates..... 135
Figure 32. SDS-PAGE analysis of LYS and LYS-FA performed on a 15% polyacrylamide gel showing the molecular weight marker, native LYS and LYS-FA conjugates..... 137
Figure 33. FTIR spectra of LYS and LYS-FA conjugates recorded in the spectral range of 400 to 4000 cm-1..... 138
Figure 34. UV-Vis absorption spectra of LYS and LYS-FA conjugates recorded in the wavelength range of 240 to 450 nm. 139
Figure 35. (A) Antioxidant activity of FA, LYS and LYS-FA conjugates evaluated by DPPH and ABTS radical scavenging assays. Emulsifying properties of LYS and LYS-FA conjugates expressed as (B) Emulsifying Activity Index (EAI), and (C) Emulsion Stability Index (ESI). (D) Foaming ability and stability of LYS and LYS-FA samples. Values are presented as mean ± standard deviation. Different letters indicate statistically significant differences according to the Tukey test ($p < 0.05$)..... 141
Figure 36. (A) Dynamic interfacial tension of different LYS-FA concentrations at the oil-water interface, with the model proposed by Equation 10 (–). (B) Oil-water three-phase contact angle with the LYS-FA conjugate..... 143
Figure 37. DPPH radical scavenging activity of FA, LYS and LYS-FA conjugates during in vitro simulated gastrointestinal digestion..... 144
Figure 38. (A) Creaming index of Pickering O/W emulsions stabilized by LYS-FA conjugates at concentrations of 2%, 3%, and 4% as a function of storage time. (B) Protein adsorption of the LYS-FA conjugates at the oil-water interface of the emulsions. Values are presented as mean

± standard deviation. Different letters indicate statistically significant differences according to the Tukey test ($p < 0.05$). 145
Figure 39. Rheological properties of Pickering emulsions stabilized by LYS-FA conjugates at different concentrations: (A) Apparent viscosity as a function of time; (B) Storage modulus (G') and loss modulus (G''). 148
Figure 40. (A) Antioxidant capacity of Pickering O/W emulsions stabilized by LYS-FA conjugates at concentrations of 2%, 3%, and 4%, assessed by DPPH and ABTS radical scavenging assays. (B) and (C) Evaluation of the oxidative stability of the emulsions over time through the quantification of lipid hydroperoxides and malondialdehyde (MDA) content, respectively, compared to soybean oil control. Values are presented as mean ± standard deviation. Different letters indicate statistically significant differences according to the Tukey test ($p < 0.05$). 150
Figure 41. (A) β-carotene encapsulation efficiency of Pickering emulsions prepared using LYS–FA conjugates as emulsifiers at different concentrations. (B) Photochemical stability of β-carotene in soybean oil (control) and in Pickering emulsions prepared using LYS–FA conjugates as emulsifiers during UV exposure. Data are expressed as mean ± standard deviation. Different lowercase letters indicate significant differences among samples ($p < 0.05$). 170
Figure 42. Visual appearance of the pectin-based films: (A) control film; (B) LYSFA 1%; (C) LYSFA 3%; (D) LYSFA 5%; (E) BC–LYSFA 1%; (F) BC–LYSFA 3%; and (G) BC–LYSFA 5%. 171
Figure 43. (A) UV–visible light transmittance spectra of pectin-based films containing LYS–FA conjugates at different concentrations, with or without β-carotene. (B) Radical scavenging activity of the films evaluated by $ABTS^{+}$ and DPPH assays. Results are expressed as mean ± standard deviation. Different lowercase letters indicate significant differences among samples within each assay ($p < 0.05$). 172
Figure 44. FTIR spectra of pectin-based films: control film, films containing LYS–FA emulsions at different concentrations (1, 3 and 5%), and films incorporating β-carotene–loaded LYS–FA emulsions (BC-LYSFA1%, BC-LYSFA3% and BC-LYSFA5%). 175
Figure 45. Contact angle images of the pectin-based films: (A) control film; (B) LYSFA 1%; (C) LYSFA 3%; (D) LYSFA 5%; (E) BC–LYSFA 1%; (F) BC–LYSFA 3%; and (G) BC–LYSFA 5%. 179
Figure 46. Kinetic modeling of β-carotene release from pectin-based films containing β-carotene-loaded Pickering emulsions prepared using LYS–FA conjugates as emulsifiers at

different concentrations: (A) 1%, (B) 3%, and (C) 5% (w/w). Experimental data were fitted to first-order, Higuchi, Ritger–Peppas, and Peppas–Sahlin models. Symbols represent experimental data and solid lines correspond to the predicted values from each kinetic model. 181

LISTA DE TABELAS

Tabela 1. Estudos sobre formação de conjugados a partir de proteínas e compostos fenólicos. 34

Tabela 2. Estudos sobre a utilização de conjugados proteína-composto fenólico como emulsificante em emulsões Pickering. 41

Tabela 3. Estudos sobre a formação e a caracterização de filmes comestíveis, incluindo materiais, métodos de formação e propriedades avaliadas. 44

Tabela 4. Conjugados proteína–polifenol empregados na encapsulação de ingredientes bioativos e seus principais resultados. 47

Table 5. Dynamic interfacial tension parameters between the external aqueous phase with different concentrations of OVA-FA conjugate and soybean oil estimated from equation 1. ..97

Table 6. Rheological models fit with Power Law, Bingham, and Herschel-Bulkley for emulsions with oil fractions of 0.5 (B4), 0.6 (C4), and 0.7 (D4), and 4% w/w OVA-FA as the emulsifier in the aqueous phase. 104

Table 7. Encapsulation efficiency of vitamin D3 in emulsions with different oil fractions. Values are presented as mean ± standard deviation. Values followed by the same letters do not show statistically significant differences in the Tukey test ($p < 0.05$). 108

Table 8. Dynamic interfacial tension parameters between the external aqueous phase with different concentrations of LYS-FA conjugate and soybean oil estimated from Equation 10. 142

Table 9. Rheological parameters of Power Law, Bingham, and Herschel-Bulkley models for Pickering emulsions stabilized with different LYS-FA conjugate concentrations..... 147

Table 10. Opacity, color parameters (L*, a*, b*), chroma (C*), hue angle (h°), and yellowness index (Yi) of control films and films containing unloaded and β-carotene–loaded Pickering emulsions at different concentrations. 174

Table 11. Thickness, mechanical properties, opacity, moisture content, solubility, water vapor permeability of control films and films incorporated with unloaded and β-carotene–loaded Pickering emulsions at different concentrations. 180

Table 12. Kinetic parameters of release obtained from different mathematical models for films containing varying concentrations of β-carotene–loaded Pickering emulsions. 182

SUMÁRIO

INTRODUÇÃO **16**

OBJETIVOS **19**

Objetivo Geral 19

Objetivos Específicos 19

CAPÍTULO I. REVISÃO BIBLIOGRÁFICA **20**

1 Componentes Alimentares 21

1.1 Proteínas 21

1.2 Compostos fenólicos 25

1.3 Polissacarídeos 27

2 Formação de Complexos e Conjugados 28

2.1 Interação não-covalente proteína-composto fenólico. 29

2.2 Interação covalente proteína-composto fenólico. 31

2.3 Fatores que afetam a interação proteína-composto fenólico 32

3 Efeitos Biológicos dos Complexos e Conjugados Proteína-Composto Fenólico 35

3.1 Bioacessibilidade 35

3.2 Capacidade Antioxidante 35

3.3 Propriedades Antimicrobianas 36

3.4 Imunogenicidade 36

4 Aplicações Tecnológicas dos Complexos e Conjugados Proteína-Composto Fenólico 37

4.1 Emulsões 37

4.2 Filmes 42

4.3 Microencapsulação 45

5 Substâncias Bioativas 48

5.1 Vitamina D 48

5.2 β-Caroteno 50

6 Conclusões 51

7 Referências 52

CAPÍTULO II. IMPACT OF THE COVALENT INTERACTION BETWEEN FERULIC ACID AND OVALBUMIN ON THE STRUCTURE AND FUNCTIONAL PROPERTIES OF THE PROTEIN 62

1 Introduction 64

2 Material and Methods 65

2.1 Material 65

2.2 Formation of OVA-FA Conjugates 66

2.3 Determination of FA Binding Equivalent Capacity to OVA 66

2.4 Determination of the Thiol Sulfhydryl Group 67

2.5 Structural Analysis of the OVA-FA Conjugate 67

2.6 Techno-Functional Properties 69

2.7 Antioxidant Activity 70

2.8 Statistical analysis 71

3 Results and Discussion 71

3.1 Ferulic Acid Binding Capacity 71

3.2 Structural Analysis of the OVA-FA Conjugate. 74

3.3 Functional Properties of the Conjugate Formed by OVA-FA 80

3.4 Antioxidant Activity of the OVA-FA Conjugate 81

4 Conclusions 83

5 References 84

CAPÍTULO III. EFFECT OF OVALBUMIN-FERULIC ACID CONJUGATES ON THE STABILITY AND BIOACCESSIBILITY OF VITAMIN D3 IN PICKERING EMULSIONS 86

1 Introduction 88

2 Material and Methods 89

2.1 Material 89

2.2 Preparation of OVA-FA Conjugates 90

2.3 Characterization of OVA-FA Conjugates 90

2.4 Formation of O/W Pickering Emulsions 91

2.5 Characterization of Pickering Emulsions 92

2.6 Microencapsulation of Vitamin D3 in O/W Pickering Emulsions 94
2.7 *In vitro* Gastrointestinal Simulation of Vitamin D3 Microcapsules 95
2.8 Statistical Analysis 96
3 Results and discussion 96
3.1 Characterization of the OVA-FA Conjugate 96
3.2 Formation and Stability of Pickering Emulsions 98
3.3 Characterization of Pickering Emulsions 101
3.4 Microencapsulation of Vitamin D3 in O/W Pickering Emulsions 107
3.5 In vitro gastrointestinal simulation of Vitamin D3 microcapsules 109
4 Conclusions 112
5 References 113
CAPÍTULO IV. KINETIC AND OXIDATIVE STABILITY OF OIL-IN-WATER PICKERING EMULSIONS STABILIZED BY LYSOZYME-FERULIC ACID CONJUGATES. 120
1 Introduction 122
2 Materials and Methods 124
2.1 Materials 124
2.2 Preparation of LYS–FA conjugates 124
2.3 Structural characterization of the LYS–FA conjugate 125
2.4 Techno-functional properties of the LYS–FA conjugate 127
2.5 In vitro gastrointestinal digestion simulation of the LYS–FA conjugate 129
2.6 Oil-in-water (O/W) Pickering emulsion formation 130
2.7 Characterization of O/W Pickering emulsions 131
2.8 Statistical analysis 133
3 Results and Discussion 134
3.1 Formation of the LYS–FA conjugate 134
3.2 Structural Analysis of the LYS–FA conjugate 136
3.3 Characterization of the LYS–FA conjugate 139
3.4 *In vitro* gastrointestinal digestion simulation of the LYS–FA conjugate 143

3.5 Formation and stability of Pickering emulsions 144
3.6 Characterization of Pickering emulsions 145
4 Conclusions 151
5 References 152
CAPÍTULO V. BIOACTIVE PECTIN FILMS INCORPORATED WITH BETA-CAROTENE PICKERING EMULSIONS USING LYSOZYME-FERULIC ACID CONJUGATES AS EMULSIFIERS 159
1 Introduction 161
2 Material and Methods 162
2.1 Material 162
2.2 Preparation of Particles from the LYS–FA Conjugate 163
2.3 Formation of β-Carotene-Loaded Pickering Emulsions 163
2.4 Stability of β-Carotene in Pickering Emulsions 163
2.5 Preparation of Pectin-Based Films 164
2.6 Characterization of Pectin-Based Films 165
2.7 β-Carotene Release Kinetics from Pectin-Based Films 168
2.8 Statistical Analysis 169
3 Results and Discussion 169
3.1 Microencapsulation of β-Carotene in Pickering Emulsions 169
3.2 Characterization of Pectin-Based Films 171
3.3 β-Carotene Release Kinetics from Pectin-Based Films 181
4 Conclusions 183
5 References 184
CONCLUSÃO 189

INTRODUÇÃO

Nos últimos anos, tem-se intensificado a busca por uma alimentação mais saudável e sustentável, associada ao conceito de “alimentos funcionais e verdes”, que abrange produtos capazes de oferecer benefícios à saúde além da nutrição básica, por meio da presença de compostos bioativos, e que são desenvolvidos a partir de práticas produtivas ambientalmente responsáveis (Dias; Ferreira; Barreiro, 2015; Janowicz *et al.*, 2023). Nesse contexto, a substituição de aditivos sintéticos por ingredientes de origem natural tem sido amplamente incentivada, impulsionando o estudo e a aplicação de macromoléculas alimentares com propriedades tecnofuncionais relevantes.

Entre os principais componentes explorados destacam-se as proteínas, os polissacarídeos e os compostos fenólicos. As proteínas apresentam propriedades emulsificantes, espumantes e formadoras de filmes, os polissacarídeos contribuem com funções espessantes, gelificantes e estruturantes, enquanto os polifenóis se destacam por sua reconhecida capacidade antioxidante e potencial bioativo (Baba; McClements; Maqsood, 2021; Liu *et al.*, 2023). A integração dessas diferentes funcionalidades em um mesmo sistema tem sido alvo de intenso interesse científico, uma vez que a combinação estratégica desses componentes pode resultar em ingredientes com desempenho tecnológico e biológico superior ao de seus constituintes isolados. Nesse cenário, as interações entre proteínas e polifenóis têm recebido especial atenção. Essas interações podem ocorrer por meio de forças físicas, como ligações de hidrogênio, interações hidrofóbicas e forças eletrostáticas, originando complexos não covalentes, ou por meio de reações químicas que resultam na formação de conjugados covalentes (Baba; McClements; Maqsood, 2021; Quan *et al.*, 2019). A formação de complexos e conjugados proteína–polifenol pode induzir modificações estruturais nas proteínas, impactando suas propriedades interfaciais, solubilidade, estabilidade térmica e capacidade antioxidante. Além disso, tais alterações estruturais podem influenciar características biológicas relevantes, como digestibilidade, alergenicidade e bioacessibilidade (Liu *et al.*, 2023, 2019; Quan *et al.*, 2019).

Os conjugados proteína–composto fenólico apresentam elevado potencial tecnológico, especialmente em virtude de sua capacidade de atuar como agentes emulsificantes em sistemas coloidais (McClements; Decker, 2018). A modificação estrutural decorrente da conjugação pode aumentar a hidrofobicidade superficial e a flexibilidade molecular das proteínas, favorecendo sua adsorção na interface óleo–água e contribuindo para a formação de sistemas emulsificados mais estáveis (Zhang *et al.*, 2021). Entre essas aplicações, destaca-se a

estabilização de emulsões Pickering, nas quais partículas sólidas substituem surfactantes convencionais, promovendo maior estabilidade cinética e resistência à coalescência (Chevalier; Bolzinger, 2013). Essas emulsões podem atuar como plataformas de microencapsulação, permitindo o carreamento, a proteção e a liberação controlada de substâncias bioativas lipofílicas, como vitaminas e carotenoides, durante o processamento, armazenamento e digestão gastrointestinal (Neekhra *et al.*, 2022).

Na presente tese, proteínas do ovo, ovalbumina (OVA) e lisozima (LIS), foram modificadas por meio de interação covalente com o ácido ferúlico (AF), visando à formação de conjugados proteína–composto fenólico com propriedades estruturais e interfaciais aprimoradas. Esses conjugados foram investigados quanto ao seu desempenho como agentes emulsificantes em emulsões Pickering destinadas ao carreamento de substâncias bioativas. Adicionalmente, avaliou-se a aplicação desses sistemas na modificação estrutural de filmes bioativos.

Os capítulos que compõem o presente trabalho correspondem a artigos científicos publicados ou submetidos a periódicos especializados.

O Capítulo I apresenta os fundamentos teóricos que sustentam esta tese, abordando os principais aspectos relacionados aos biopolímeros de interesse, às interações entre proteínas e compostos fenólicos, bem como aos conceitos de emulsões, emulsões Pickering, microencapsulação e compostos bioativos. O Capítulo II descreve a formação e a caracterização estrutural e funcional de conjugados de ovalbumina e ácido ferúlico (OVA-AF), com ênfase nas modificações conformacionais e nas propriedades tecnofuncionais resultantes da conjugação. No Capítulo III, é apresentada a formação e a caracterização de emulsões Pickering estabilizadas pelo conjugado OVA-AF avaliando seu desempenho como agente emulsificante na encapsulação da vitamina D, bem como a estabilidade e a bioacessibilidade do composto encapsulado. O Capítulo IV aborda o desenvolvimento e a aplicação de conjugados lisozima–ácido ferúlico (LIS-AF) na estabilização de emulsões Pickering, investigando suas propriedades físico-químicas, estruturais e funcionais em sistemas de encapsulação. Por fim, o Capítulo V trata da microencapsulação de β-caroteno por meio de emulsões Pickering estabilizadas por LIS-AF, bem como da incorporação desses sistemas na fabricação de filmes bioativos, avaliando-se suas propriedades estruturais, mecânicas, ópticas e antioxidantes. A Figura 1 apresenta uma representação esquemática dos capítulos da tese.

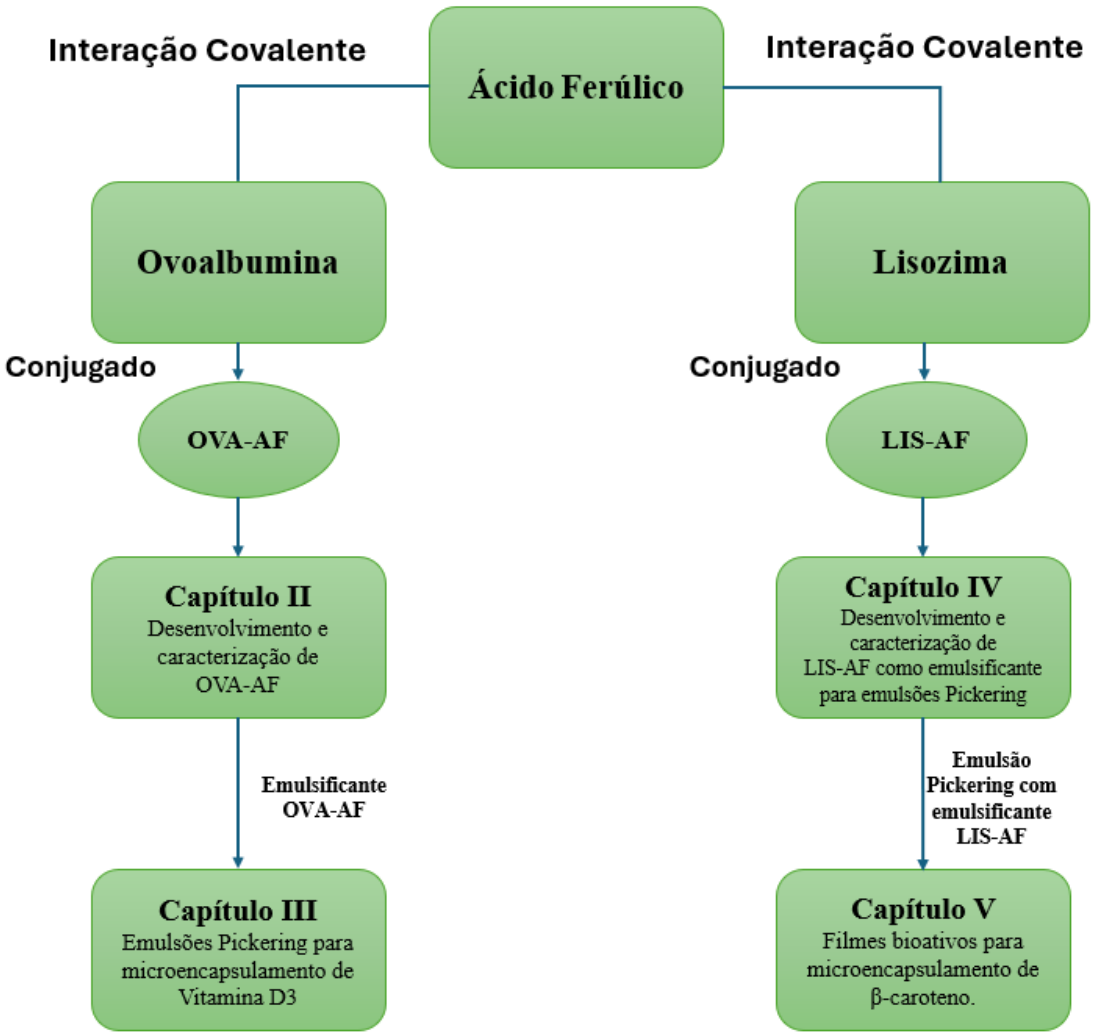

Figura 1. Fluxograma representativo da estrutura da tese, apresentando a síntese dos conjugados de ácido ferúlico com ovalbumina (OVA-AF) e lisozima (LIS-AF) e suas respectivas aplicações em sistemas de carreamento de substâncias bioativas.

OBJETIVOS

Objetivo Geral

Desenvolver e caracterizar conjugados formados entre proteínas da clara de ovo, ovalbumina ou lisozima, e ácido ferúlico, visando sua aplicação como agentes estruturantes, antioxidantes e emulsificantes em sistemas de carreamento de compostos bioativos hidrofóbicos.

Objetivos Específicos

- Investigar o mecanismo de formação dos conjugados entre ovalbumina ou lisozima e ácido ferúlico, avaliando alterações estruturais, propriedades tecnofuncionais e capacidade antioxidante.
- Desenvolver e caracterizar emulsões Pickering óleo-em-água estabilizadas por conjugados proteína–ácido ferúlico, avaliando suas propriedades físico-químicas, estruturais e antioxidantes.
- Aplicar as emulsões Pickering na microencapsulação de vitamina D, avaliando a eficiência de encapsulação, estabilidade cinética, estabilidade oxidativa e bioacessibilidade do composto.
- Incorporar emulsões Pickering estabilizadas por conjugados lisozima–ácido ferúlico em filmes bioativos para o carreamento de β-caroteno, investigando propriedades estruturais, mecânicas, ópticas e de estabilidade dos sistemas desenvolvidos.

CAPÍTULO I. REVISÃO BIBLIOGRÁFICA

1 Componentes Alimentares

As proteínas, os polissacarídeos e os polifenóis são importantes compostos alimentares com diferentes propriedades tecnofuncionais, como emulsificação, formação de espumas e capacidade espessante (Liu *et al.*, 2023). Esta revisão bibliográfica apresenta estes diferentes tipos de compostos alimentares, assim como as interações entre estes compostos para a formação de novos componentes, também discute os efeitos biológicos que esses novos componentes exibem, além das aplicações tecnológicas desses componentes.

1.1 Proteínas

As proteínas são biopolímeros formados por cadeias de aminoácidos ligados por ligações peptídicas, cuja sequência determina sua conformação tridimensional e propriedades físico-químicas. No contexto alimentar, as proteínas assumem papel central tanto do ponto de vista nutricional quanto tecnológico. Proteínas alimentares são definidas como aquelas que apresentam elevada digestibilidade, perfil adequado de aminoácidos essenciais, ausência de toxicidade e capacidade de serem funcionalmente incorporadas em matrizes alimentares (Damodaran; Parkin, 2017; Phillips; Williams, 2011). Com base em sua conformação tridimensional e organização estrutural, as proteínas podem ser classificadas em duas grandes categorias: proteínas globulares e proteínas fibrilares. As proteínas globulares apresentam conformação compacta e geralmente assumem forma aproximadamente esférica, desempenhando funções metabólicas e enzimáticas. Já as proteínas fibrilares possuem estrutura alongada, organizada em filamentos ou fibras, exercendo predominantemente funções estruturais, como resistência mecânica e suporte (Damodaran; Parkin, 2017). Do ponto de vista nutricional, as proteínas são macronutrientes fundamentais na dieta humana, fornecendo aminoácidos essenciais necessários para síntese proteica, manutenção de tecidos e regulação metabólica. Além da relevância fisiológica, as proteínas desempenham papel central na ciência e tecnologia de alimentos devido às suas propriedades tecnofuncionais (Meganaharshini *et al.*, 2023).

A funcionalidade das proteínas está diretamente relacionada à sua organização estrutural hierárquica, tradicionalmente dividida em quatro níveis: primário, secundário, terciário e quaternário. A estrutura primária corresponde à sequência linear de aminoácidos. A estrutura secundária refere-se ao arranjo espacial local da cadeia polipeptídica, formando principalmente α-hélices e folhas β, estabilizadas por ligações de hidrogênio. A estrutura terciária representa o dobramento tridimensional completo da cadeia polipeptídica, resultado de interações

intramoleculares como ligações de hidrogênio, interações hidrofóbicas, interações eletrostáticas, forças de van der Waals e pontes dissulfeto. Por fim, a estrutura quaternária ocorre quando duas ou mais cadeias polipeptídicas se associam, formando complexos proteicos funcionalmente ativos (Phillips; Williams, 2011). Essas interações intermoleculares e intramoleculares são determinantes para a estabilidade conformacional das proteínas e, consequentemente, para suas propriedades funcionais. Alterações nas condições ambientais, como pH, temperatura, força iônica e presença de agentes químicos, podem promover mudanças estruturais, incluindo desnaturação parcial ou total, afetando diretamente o comportamento proteico em sistemas biológicos e alimentares (Damodaran; Paraf, 2019).

Dentre as principais características tecnofuncionais destacam-se a solubilidade, a capacidade emulsificante e capacidade de formação de espuma. Essas propriedades determinam o comportamento das proteínas em matrizes alimentares complexas e são fortemente dependentes de sua estrutura molecular.

A solubilidade é uma das propriedades tecnofuncionais mais relevantes das proteínas, pois condiciona diretamente sua aplicabilidade em sistemas alimentares. A solubilidade proteica depende de fatores extrínsecos, como temperatura, pH, força iônica e presença de íons metálicos e surfactantes, bem como de fatores intrínsecos, relacionados à sua sequência de aminoácidos e ao ponto isoelétrico. Em valores de pH próximos ao ponto isoelétrico, a redução da repulsão eletrostática entre as moléculas favorece a agregação e a precipitação proteica, resultando em menor solubilidade. Dessa forma, a solubilidade está intimamente relacionada à distribuição de cargas superficiais e à exposição de regiões hidrofílicas da proteína (Damodaran; Paraf, 2019; Qing *et al.*, 2022).

A capacidade emulsificante das proteínas decorre de seu caráter anfifílico, que permite a adsorção rápida na interface óleo–água, reduzindo a tensão interfacial e formando uma camada interfacial ao redor das gotas dispersas. Esse processo depende da estrutura da proteína, da exposição de regiões hidrofóbicas e da velocidade de reorganização estrutural na interface. De maneira semelhante, a capacidade espumante está associada à habilidade das proteínas em adsorver e estabilizar a interface ar–água, formando filmes coesos capazes de resistir à coalescência e ao colapso das bolhas. Em ambos os casos, a estabilidade do sistema está relacionada ao equilíbrio entre solubilidade, mobilidade molecular e interações intermoleculares após a adsorção interfacial (Phillips; Williams, 2011).

As proteínas alimentares podem ser obtidas de fontes vegetais e animais. Fontes vegetais incluem cereais, leguminosas e sementes oleaginosas, enquanto as fontes animais abrangem leite, carnes, peixes, aves e ovos (Loveday, 2019).

Entre as fontes de origem animal, o ovo destaca-se como uma das principais fontes de proteína de alta qualidade biológica, amplamente consumida em nível mundial. O ovo é constituído por casca, clara e gema, composto aproximadamente por 75% de água, 12% de proteínas, 12% de lipídios e cerca de 1% de carboidratos e minerais (Razi *et al.*, 2023). As proteínas estão distribuídas tanto na gema quanto na clara, sendo esta última composta predominantemente por água (≈88%) e proteínas (≈11%). Entre as principais proteínas da clara destacam-se a ovalbumina (≈54%), ovotransferrina (≈12%), ovomucóide (≈11%), lisozima (≈3,5%) e ovomucina (≈3,5%) (Abeyrathne; Lee; Ahn, 2013; Razi *et al.*, 2023).

A composição, estrutura e propriedades funcionais das proteínas da clara do ovo tornam-nas particularmente relevantes para aplicações tecnológicas, especialmente em sistemas emulsificados, espumas e matrizes estruturadas, consolidando o ovo como modelo amplamente explorado na pesquisa em ciência de alimentos.

1.1.1 Ovalbumina

A ovalbumina é a principal proteína da clara do ovo. Trata-se de uma fosfoglicoproteína globular com massa molar em torno de 45 kDa. Seu ponto isoelétrico situa-se em aproximadamente pH 4,5, enquanto sua temperatura de desnaturação é próxima de 84 °C (Rostamabadi *et al.*, 2023). Do ponto de vista tecnológico, a ovalbumina destaca-se principalmente por sua elevada capacidade de formação e estabilização de espumas.

Estruturalmente, a ovalbumina é composta por 385 resíduos de aminoácidos, apresentando uma distribuição equilibrada entre regiões hidrofílicas e hidrofóbicas, o que confere à proteína caráter anfifílico. Sua estrutura é apresentada na Figura 2. A molécula contém seis resíduos de cisteína, responsáveis pela presença de grupos sulfidrila e pontes dissulfeto. Além disso, a ovalbumina possui dez resíduos de tirosina e três resíduos de triptofano em sua sequência, os quais atuam como fluoróforos intrínsecos (Guha; Majumder; Mine, 2019; Nisbet *et al.*, 1981).

No que se refere à capacidade emulsificante, a ovalbumina atua como agente estabilizante devido à sua habilidade de adsorver-se rapidamente na interface óleo–água, reduzindo a tensão interfacial e formando uma camada interfacial viscoelástica ao redor das gotas dispersas. A eficiência desse processo está relacionada à flexibilidade estrutural da proteína, à exposição de regiões hidrofóbicas e à sua capacidade de reorganização na interface. Esse comportamento é fortemente dependente do pH, da força iônica e da presença de outros

biopolímeros no sistema, fatores que modulam a carga líquida e a conformação molecular da proteína (Razi *et al.*, 2023; Rostamabadi *et al.*, 2023).

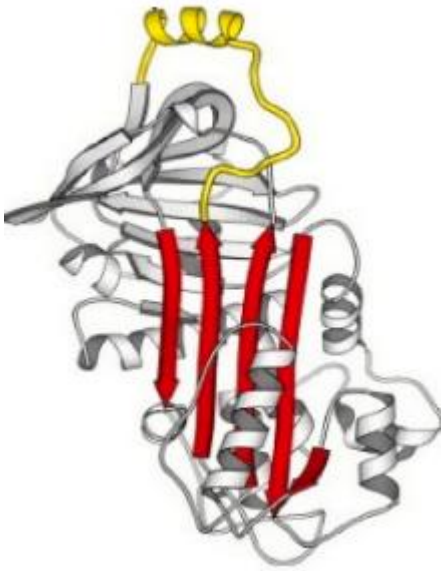

Figura 2. Estrutura da ovalbumina.
Fonte: Rostamabadi *et al.*, 2023.

1.1.2 Lisozima

A lisozima é uma proteína com reconhecida atividade antimicrobiana, cuja principal função está associada à hidrólise das ligações glicosídicas presentes nas cadeias de carboidratos da parede celular bacteriana. Em função desse mecanismo de ação, a lisozima é considerada um antimicrobiano natural, capaz de inibir o crescimento bacteriano em diferentes matrizes alimentares, além de desempenhar papel fundamental no sistema imunológico inato de diversos organismos (Ferraboschi; Ciceri; Grisenti, 2021; Nawaz *et al.*, 2022).

A lisozima está amplamente distribuída na natureza, sendo encontrada em diferentes espécies animais, como em secreções de mamíferos, mucosas de peixes e em invertebrados. No entanto, o ovo destaca-se como a principal fonte para aplicações industriais, devido à sua elevada concentração e facilidade de extração (Ferraboschi; Ciceri; Grisenti, 2021; Khorshidian *et al.*, 2022). Com base em diferenças na sequência de aminoácidos, na estrutura tridimensional e em propriedades imunológicas, as lisozimas são classificadas em três principais tipos: tipo G, presente em diferentes classes de aves; tipo I, encontrada em invertebrados; e tipo C, considerada a forma convencional e obtida a partir do ovo de galinha (Nawaz *et al.*, 2022).

A lisozima do tipo C apresenta massa molecular entre 11 e 15 kDa, um ponto isoelétrico de 10,7 e temperatura de desnaturação de 75 º. Sua estrutura é composta por uma sequência de 129 resíduos de aminoácidos, na qual contém oito resíduos de cisteína, que formam quatro

pontes dissulfeto, não apresentando grupos sulfidrila livres. Além disso, a molécula possui seis resíduos de triptofano e três resíduos de tirosina, os quais atuam como fluoróforos intrínsecos (Jalili-Firoozinezhad *et al.*, 2020; Wu *et al.*, 2019). Sua estrutura é apresentada na Figura 3.

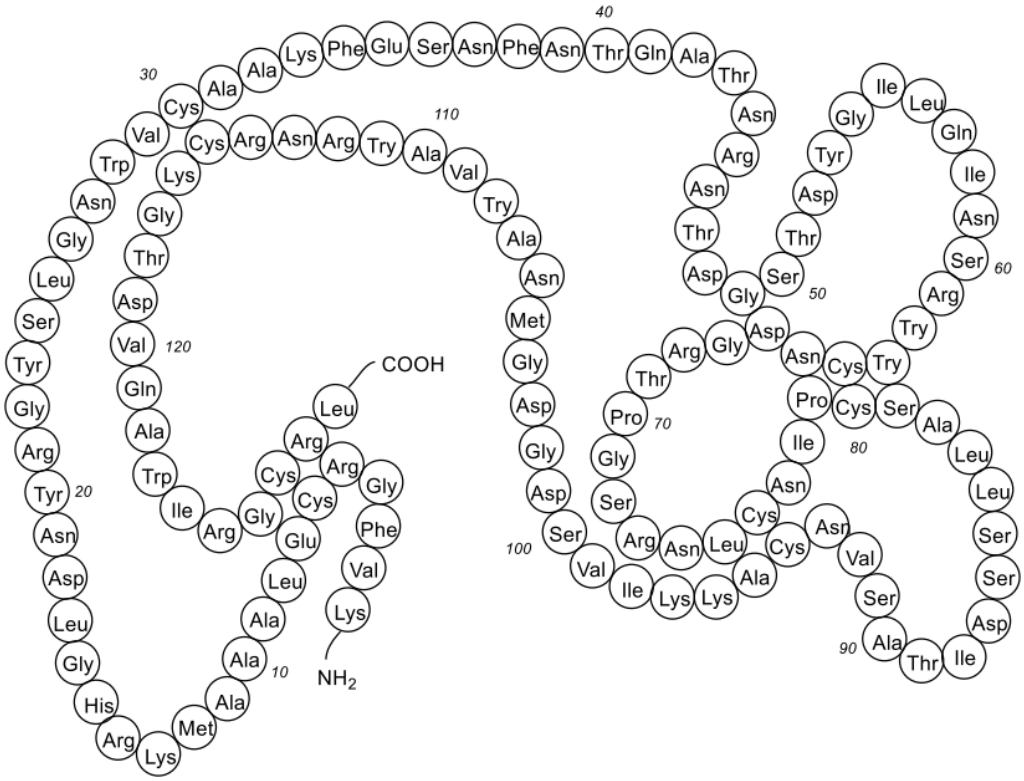

Figura 3. Estrutura da lisozima.
Fonte: Ferraboschi; Ciceri; Grisenti, 2021.

1.2 Compostos fenólicos

Compostos fenólicos são um grupo de compostos orgânicos encontrados em muitas plantas, tendo mais de 8000 compostos caracterizados e mais de 500 são consumidos regularmente na dieta humana (Gebicki; Nauser, 2021; Tsao, 2010). Eles são caracterizados pela presença de um ou mais anéis fenólicos e são conhecidos por terem uma ampla variedade de benefícios para a saúde, desde suas atividades antioxidantes, até prevenção de inflamação, doenças cardiovasculares, câncer e diabetes. Estes compostos são amplamente distribuídos em plantas comestíveis, como frutas, vegetais, grãos, nozes, sementes e chás. Eles também estão presentes em muitos alimentos processados, como bebidas, molhos e condimentos (Abdel-Moneim *et al.*, 2020; Alara; Abdurahman; Ukaegbu, 2021; Tsao, 2010). Compostos fenólicos abrangem diversos tipos de estruturas diferentes, sendo dividido em dois principais subgrupos, os flavonoides e os não flavonoides, que também se dividem em outros subgrupos, esses

subgrupos diferem entre si, além da estrutura, em estabilidade a diferentes meios, biodisponibilidade e nas propriedades benéficas para a saúde humana (Tsao, 2010).

Os flavonoides são os principais polifenóis na dieta humana, eles consistem em dois anéis aromáticos em uma estrutura C6-C3-C6 como mostra a Figura 4. Os flavonoides podem ser categorizados em diferentes grupos, dependendo da quantidade, posição e composição dos grupos químicos presentes em suas moléculas podendo ser classificados como: antocianinas, flavonas, flavonóis, auronas, cauconas, isoflavonas, flavononas, catequinas e dihidroflavonois (Abdel-Moneim *et al.*, 2020; Alara; Abdurahman; Ukaegbu, 2021; Tsao, 2010).

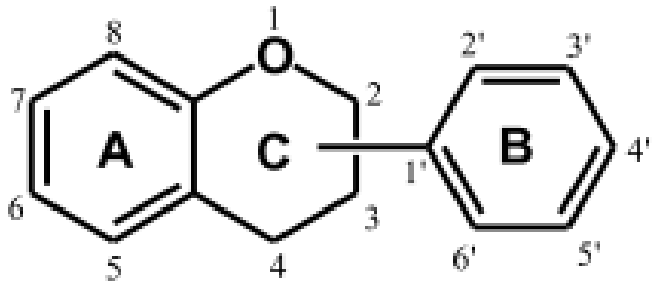

Figura 4. Estrutura básica dos flavonoides, em que A e B são os anéis aromáticos.
Fonte: Adaptado de QUAN *et al.*, 2019.

Os não flavonoides são os grupos que não possuem a estrutura C6-C3-C6. Os estilbenos, as lignanas e as xantonas são não flavonoides que possuem dois anéis aromáticos em sua estrutura, já os taninos podem possuir mais anéis em sua estrutura (Durazzo *et al.*, 2019; Wang *et al.*, 2022). Os ácidos fenólicos são estruturas que possuem apenas um anel aromático ligado a um grupo carboxila, eles podem ser divididos em dois grupos, os derivados do ácido benzoico e os derivados do ácido cinâmico. Nos derivados do ácido benzoico o ácido gálico é uma das principais estruturas, já pelo ácido cinâmico, se destacam o ácido cafeico, o ácido clorogênico e o ácido ferúlico (Durazzo *et al.*, 2019; Tsao, 2010).

1.2.1 Ácido Ferúlico

O ácido ferúlico, ou ácido 4-hidroxi-3-metoxicinâmico, é um ácido fenólico abundante no meio ambiente, podendo ir de 5 g/kg no trigo até 50 g/kg no milho, porém, o ácido ferúlico não é encontrado de forma livre normalmente, e sim ligados em estruturas celulares, principalmente na parede celular das plantas (Ou; Kwok, 2004; Tsao, 2010).

O interesse no ácido ferúlico vem aumentando nos últimos tempos, pois ele é um composto fenólico abundante, com alta capacidade antioxidante, anti-inflamatória e sua capacidade de prevenção de câncer e de diabetes, além disso, o ácido ferúlico é um dos componentes presentes em diferentes ervas medicinais (Han; Dye; Mackie, 2023; Ou; Kwok, 2004; Xue *et al.*, 2023). A estrutura do ácido ferúlico é um anel ferúlico ligado por uma dupla ligação a uma cadeia lateral de carboxila, essa cadeia pode estar disposta a conformação cis ou trans, como mostra a Figura 5 (Kumar; Goel, 2019; Li *et al.*, 2021).

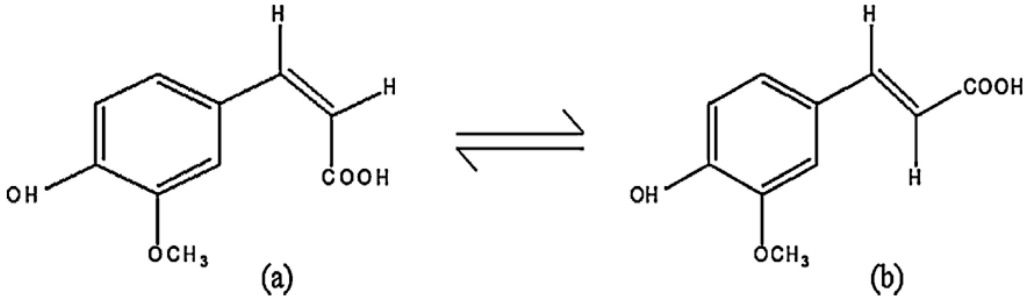

Figura 5. Estrutura das formas isoméricas do ácido ferúlico (a) Cis e (b) Trans.
Fonte: Adaptado de Kumar; Pruthi, 2014.

1.3 Polissacarídeos

Os polissacarídeos são macromoléculas complexas compostas por longas cadeias de açúcares simples, chamados de monossacarídeos, unidos por ligações glicosídicas. Essas biomoléculas desempenham papéis vitais nos organismos vivos, atuando como fonte de energia, reserva de energia e estruturas de suporte (Liu *et al.*, 2023). Em sua estrutura, os polissacarídeos podem se apresentar de forma linear, em que a união dos monossacarídeos é feita em forma de uma cadeia linear, e a forma ramificada, em que existem cadeias laterais ligadas a uma cadeia principal. A celulose possui uma estrutura linear, enquanto a amilopectina possui uma cadeia ramificada (Yang *et al.*, 2020).

Polissacarídeos desempenham múltiplos papéis na indústria alimentícia, servindo para uma variedade de propósitos. Eles são empregados como agentes para coloração e flavorização, proporcionam textura e espessura aos alimentos, e desempenham um papel na formação de emulsões e espumas (McClements, 2014).

Eles podem ser obtidos de diversas fontes, os de origem animal, como a quitosana, são extraídos de crustáceos, os de origem bacteriana como a goma xantana, produzida por meio da fermentação aeróbica de açúcares pela bactéria *Xanthomonas campestris*. Entretanto, a maioria dos polissacarídeos usados na indústria alimentícia provém de fontes vegetais. Nesse contexto,

destacam-se o amido, os alginatos, a celulose e as pectinas como alguns dos principais representantes (Yang *et al.*, 2020).

1.3.1 Pectina

A pectina é um polissacarídeo aniônico estrutural amplamente distribuído na parede celular primária de tecidos vegetais, composta predominantemente por cadeias lineares de ácido D-galacturônico unidas por ligações glicosídicas α-(1→4). Parte desses resíduos pode estar esterificada com grupos metila, o que permite classificar a pectina em de alto ou baixo teor de metoxilação. A presença de numerosos grupos hidroxila e carboxila confere elevada hidrofilicidade ao biopolímero (Freitas *et al.*, 2021; Song *et al.*, 2025).

A obtenção da pectina ocorre principalmente a partir de subprodutos agroindustriais, especialmente cascas de cítricos e bagaço de maçã, por meio de extração ácida seguida de precipitação alcoólica. As condições de extração, como pH, temperatura e tempo, influenciam diretamente o grau de esterificação, a massa molar e a funcionalidade da pectina obtida. Essas características estruturais são determinantes para sua aplicabilidade na indústria de alimentos (Adetunji *et al.*, 2017).

Devido à sua natureza biodegradável, atóxica e renovável, a pectina tem sido amplamente explorada na indústria de alimentos, sendo utilizada principalmente como agente espessante, gelificante, estabilizante e emulsificante em diversos produtos. Além disso, a pectina tem despertado crescente interesse na produção de embalagens biodegradáveis, incluindo filmes e revestimentos comestíveis para aplicações alimentícias. Essas aplicações refletem a versatilidade funcional da pectina e seu potencial no desenvolvimento de sistemas alimentares mais sustentáveis (Freitas *et al.*, 2021; Martău; Mihai; Vodnar, 2019).

2 Formação de Complexos e Conjugados

As proteínas, os polissacarídeos e os polifenóis exibem atributos singulares e habilidades únicas para alterar a estrutura e as características dos alimentos. Isso abrange não apenas sua textura, cor e sabor, mas também engloba suas funcionalidades, como a capacidade de criar espumas, emulsões e géis (Liu *et al.*, 2017, 2023). Esses compostos podem ser empregados em sua forma natural ou submetidos a modificações. Essas modificações podem envolver a combinação desses compostos, resultando na fusão de propriedades desejáveis de dois ou até mesmo dos três compostos. Esse processo visa a criação de ingredientes funcionais aprimorados (Liu *et al.*, 2017, 2023).

As interações entre proteínas, polissacarídeos e compostos fenólicos podem ser classificadas como reversíveis ou irreversíveis, dependendo do tipo de ligação envolvida. As interações reversíveis ocorrem por meio de forças físicas não covalentes, como ligações de hidrogênio, interações hidrofóbicas e eletrostáticas, resultando na formação de complexos. Por outro lado, as interações irreversíveis envolvem ligações químicas covalentes, originando sistemas denominados conjugados (Baba; McClements; Maqsood, 2021)

Entre essas interações, os sistemas formados entre proteínas e compostos fenólicos têm despertado crescente interesse, uma vez que combinam as propriedades funcionais das proteínas com a capacidade antioxidante e bioativa dos compostos fenólicos, ampliando seu potencial de aplicação em sistemas alimentares e em matrizes funcionais.

2.1 Interação não-covalente proteína-composto fenólico.

As interações não covalentes entre proteínas e compostos fenólicos são normalmente reversíveis e ocorrem pela ação de interações hidrofóbicas, eletrostáticas, de Van der Waals e ligações de hidrogênio (Quan *et al.*, 2019; Shahidi; Dissanayaka, 2023). Os compostos formados por essa interação são caracterizados como complexos (Liu *et al.*, 2023, 2019). As interações hidrofóbicas ocorrem pela atração entre os aminoácidos hidrofóbicos das proteínas e os anéis aromáticos dos polifenóis, já as ligações de hidrogênio ocorrem pela ligação entre os átomos de oxigênio das proteínas com o grupo hidroxila dos compostos fenólicos, as interações eletrostáticas ocorrem pela ligação iônica dos aminoácidos positivamente carregadas da proteína, como a lisina e dos grupos hidroxila negativamente carregados dos fenólicos. As principais interações para a formação de complexos proteína-polifenol são as interações hidrofóbicas e as ligações de hidrogênio. A Figura 6 ilustra essas interações (Shahidi; Dissanayaka, 2023; Wang *et al.*, 2022).

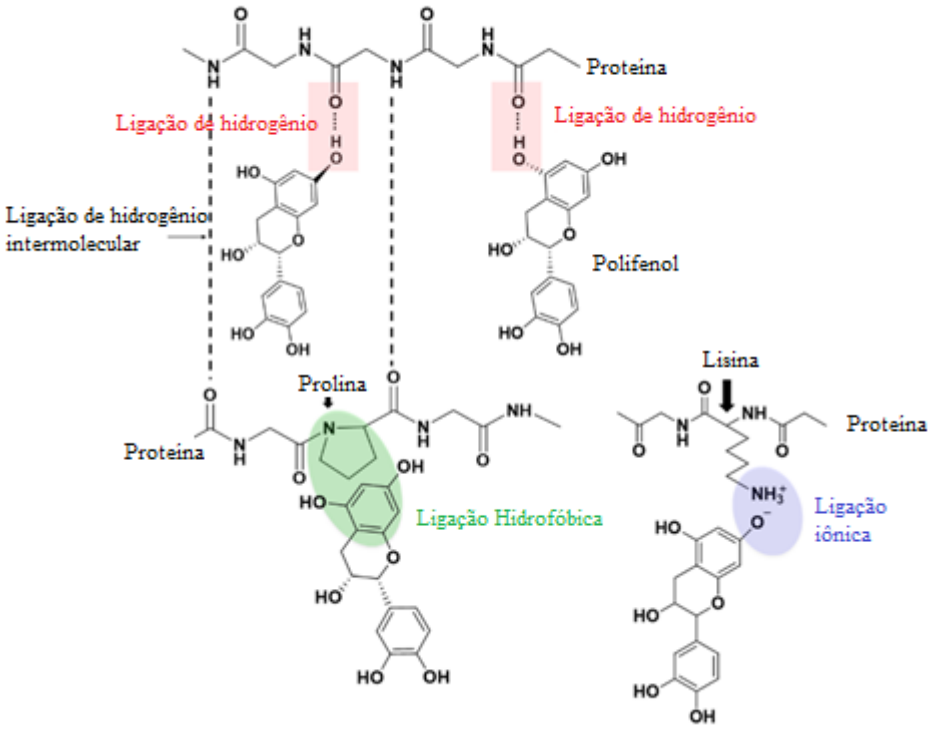

Figura 6. Interações não covalentes presentes entre polifenóis e proteínas.
Fonte: Adaptado de WANG *et al.*, 2022.

A produção de complexos não covalentes é feita pelo simples processo de mistura entre a proteína e o composto fenólico de modo que as interações físicas ocorram. Esse preparo pode ser feito a partir de agitação entre os compostos ou apenas deixando eles em reação em temperatura ambiente por um longo período (Baba; McClements; Maqsood, 2021). Dependendo da interação produzida, os complexos não covalentes podem ter diferentes formas estruturais. Em interações mais fracas pode haver apenas um leve aumento ou achatamento das estruturas da proteína, enquanto em interações mais fortes é possível obter mudanças na estrutura terciária ou secundária da proteína. Assim as propriedades tecno funcionais desses complexos são afetadas pela mudança estrutural da proteína (Baba; McClements; Maqsood, 2021; Sun; Sarteshnizi; Udenigwe, 2022).

Para entender as interações formadas entre as proteínas e os compostos fenólicos diversas técnicas são utilizadas, dentre elas se destacam métodos como o infravermelho com transformada de Fourier, técnicas de fluorescência, espectroscopia de dicroísmo circular e a calorimetria de titulação isotérmica (Baba; McClements; Maqsood, 2021; Ulrih, 2017; Wang *et al.*, 2022).

2.2 Interação covalente proteína-composto fenólico.

As interações não reversíveis entre os ingredientes ocorrem através de interações químicas covalentes, como interações enzimáticas, reações alcalinas e de radical livre. Os compostos formados por esse tipo de interação são caracterizados como conjugados (Liu *et al.*, 2023, 2019).

As interações covalentes entre os polifenóis e as proteínas se dá a partir de interações não reversíveis via ligações entre o carbono e o nitrogênio (C-N) e o carbono e o enxofre (C-S). Essas ligações ocorrem nos resíduos nucleofílicos das proteínas, sendo eles os aminoácidos metionina, lisina, triptofano e cisteína (Quan *et al.*, 2019; Shahidi; Dissanayaka, 2023). Diversas técnicas são utilizadas para formar conjugados entre os compostos fenólicos e as proteínas, entre eles estão o método alcalino, enzimático, radical livre e outros métodos químicos, porém na prática, apenas os métodos alcalinos e de radical livre são os mais utilizados (Baba; McClements; Maqsood, 2021; Shahidi; Dissanayaka, 2023).

Um dos métodos mais comuns para a formação de conjugados entre proteínas e polifenóis é o alcalino. Os polifenóis são propensos a oxidação na presença de oxigênio e pH's alcalinos, próximos de 9. Essa oxidação rearranja os anéis aromáticos dos compostos fenólicos e forma as quinonas, que rapidamente se ligam aos aminoácidos das proteínas. Essa reação é apresentada na Figura 7 (Liu *et al.*, 2019; Quan *et al.*, 2019).

O método enzimático funciona de maneira similar ao método alcalino, as enzimas oxidam os compostos fenólicos na presença de oxigênio formando as quinonas que reagem com as proteínas de maneira similar ao método alcalino. Diferentes enzimas podem ser utilizadas nesse método, como a lacase e a monofenolase, essa reação é apresentada na Figura 8 (Baba; McClements; Maqsood, 2021; Shahidi; Dissanayaka, 2023).

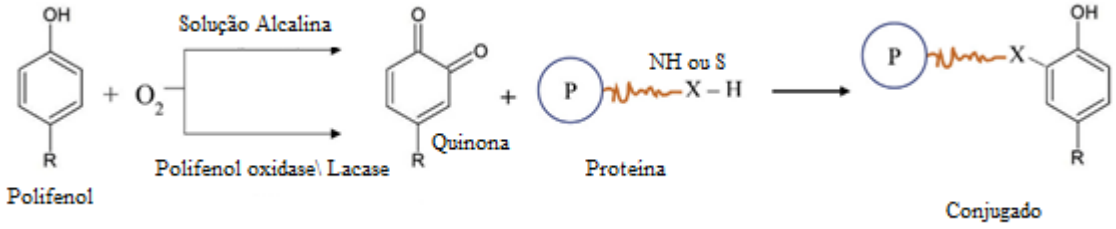

Figura 7. Interação covalente a partir do método alcalino e enzimático entre proteínas e polifenóis.
Fonte: Adaptado de QUAN *et al.*, 2019.

O método de radicais livres é uma técnica promissora na formação dos conjugados, já que é simples e rápida. Nessa metodologia ocorre uma reação redox entre o ácido ascórbico e o peróxido de hidrogênio, formando grupos hidroxila que começam a reação, esses grupos

hidroxila oxidam aminoácidos localizados nas proteínas formando radicais que reagem com os polifenóis formando os conjugados. A Figura 8 ilustra os passos da reação (Quan *et al.*, 2019; Shahidi; Dissanayaka, 2023).

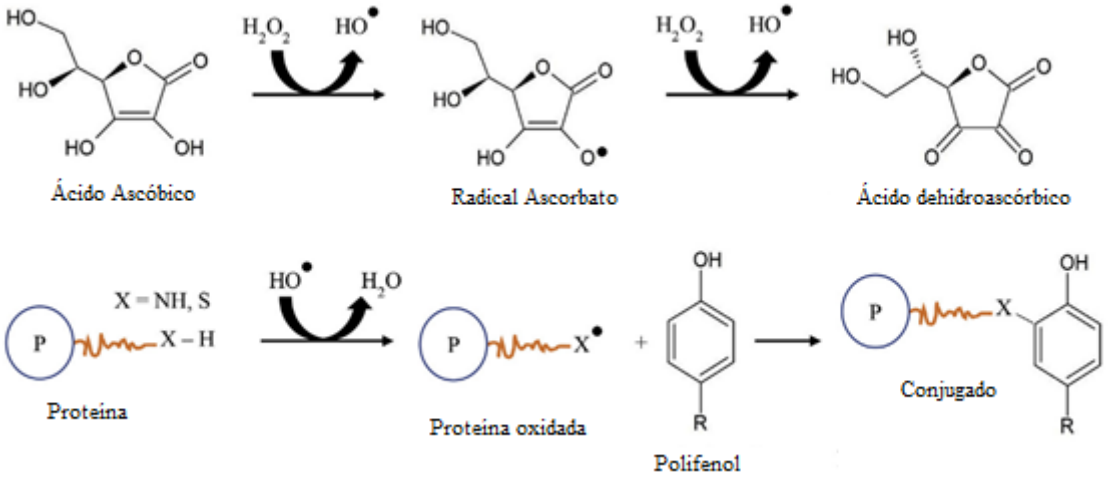

Figura 8. Interação covalente a partir do método de radical livre entre proteínas e polifenóis.
Fonte: Adaptado de QUAN *et al.*, 2019.

A Tabela 1 reúne diferentes estudos sobre a formação de complexos e conjugados entre proteínas e compostos fenólicos, evidenciando os compostos fenólicos e as proteínas utilizadas, os métodos de formação e os principais impactos da conjugação sobre as propriedades das proteínas.

2.3 Fatores que afetam a interação proteína-composto fenólico

A formação de complexos e conjugados depende de diversos fatores, os quais podem estar relacionados às propriedades inerentes dos compostos envolvidos, denominadas fatores intrínsecos, ou às condições do meio em que a interação ocorre, denominadas fatores extrínsecos (Zhang *et al.*, 2021).

2.3.1 Fatores intrínsecos

As características inerentes dos compostos fenólicos e das proteínas influencia diretamente na capacidade de formação de complexo e conjugado, além disso, a concentração desses compostos também interfere na formação dos complexos e conjugados (Zhang *et al.*, 2021). Compostos fenólicos são compostos bastante diversos, existindo vários grupos e subgrupos entre eles, portanto, suas características de hidrofobicidade, massa molecular, flexibilidade estrutural e a presença de grupos funcionais, incluindo grupos hidroxila, metila e glicosil são diferentes, e esses fatores são essenciais para a formação de complexos e

conjugados (Quan *et al.*, 2019; Zhang *et al.*, 2021). As propriedades superficiais das proteínas, assim como sua composição de aminoácidos e sua massa molecular afetam a capacidade de ligação dos complexos, proteínas mais compactas e estruturadas tem menor capacidade de ligação que proteínas com estruturas mais abertas. A presença de prolina na composição da proteína também ajuda na formação de complexos, já que ela tem bastante participação em interações hidrofóbicas (Quan *et al.*, 2019; Zhang *et al.*, 2021).

2.3.2 Fatores extrínsecos

Os principais fatores extrínsecos que afetam a formação de complexos e conjugados são a temperatura, o pH e a força iônica.

A temperatura influencia na estrutura da proteína, modificando sua solubilidade e seus sítios de ligação não covalente, como o aumento de setores hidrofóbicos. Essa modificação pode ajudar ou dificultar a formação de complexos e conjugados, por um lado pode aumentar as interações hidrofóbicas pela sua exposição, e por outro lado facilita a auto agregação da proteína, o que diminui sua área superficial. O aumento da temperatura também facilita a formação de quinonas pelos polifenóis, porém, o aumento da temperatura também pode causar a degradação destes compostos (Quan *et al.*, 2019; Zhang *et al.*, 2021).

As interações entre proteínas e polifenóis podem acontecer em um grande intervalo de pH's (2 a 10). A modificação do pH pode mudar a conformação da proteína, o que modifica a força das interações não covalentes com o polifenol. Em pH's alcalinos há a oxidação dos polifenóis em quinonas, o que geram interações covalentes com as proteínas (Liu *et al.*, 2023; Quan *et al.*, 2019).

A força iônica representa outro elemento que influencia as interações. Essa interferência está intimamente relacionada com o principal tipo de interação que atua no complexo, sendo assim uma maior força iônica pode restringir as ligações eletrostáticas, contudo, também pode desencadear a exposição de sítios hidrofóbicos, intensificando, assim, as ligações hidrofóbicas presentes nos complexos formados (Liu *et al.*, 2023; Zhang *et al.*, 2021)

A presença de outros agentes na solução também pode influenciar nas interações formadas, a presença de enzimas que oxidam os polifenóis, assim como a presença de radicais livres. Esses agentes causam a transformação dos polifenóis em quinonas, facilitando interações covalentes com a proteína (Zhang *et al.*, 2021).

Tabela 1. Estudos sobre formação de conjugados a partir de proteínas e compostos fenólicos.

Proteína	Composto Fenólico	Método de formação	Resultados	Referência
Ovalbumina	Ácido Ferúlico	Alcalino	• Melhora das propriedades emulsificantes e espumantes e da capacidade antioxidante; • Aumento da hidrofobicidade superficial.	Barbosa *et al.*, 2025.
Lisozima	EGCG	Radical livre	• Redução da temperatura de desnaturação; • Aumento da capacidade antioxidante.	Yin *et al.*, 2024.
Extrato de proteína de Amendoim	EGCG Ácido clorogênico	Alcalino	• Melhora das propriedades emulsificantes, espumantes, solubilidade e capacidade antioxidante. • Redução da alergenicidade.	He *et al.*, 2023.
Proteína de soro do leite	Quercetina	Alcalino	• Melhora das propriedades emulsificantes e de espuma; Aumento da hidrofobicidade superficial.	Cheng *et al.*, 2023.
Zeina	Resveratrol	Alcalino Radical livre	• Melhora das propriedades emulsificantes e espumantes; • Aumento da estabilidade térmica.	Ren *et al.*, 2022a.
Proteína de soro do leite	Ácido ferúlico Ácido gálico Ácido tânico	Alcalino	• Aumento da capacidade antioxidante.	Thongzai *et al.*, 2022.

Legenda: EGCG - epigalocatequina-3-galato

3 Efeitos Biológicos dos Complexos e Conjugados Proteína-Composto Fenólico

3.1 Bioacessibilidade

A bioacessibilidade é definida como a fração de um nutriente que se torna solúvel e potencialmente disponível para absorção durante a digestão gastrointestinal. Trata-se de um fator importante na determinação do valor nutritivo das proteínas, uma vez que está diretamente relacionada à sua digestibilidade (Dima; Dima, 2020; McClements; Peng, 2020). A interação entre proteínas e compostos fenólicos pode modificar a estrutura proteica, influenciando sua digestibilidade, a qual pode ser aumentada ou reduzida dependendo da natureza dessas interações (Liu *et al.*, 2023, 2019).

Xu *et al.* (2019) observaram que a formação de conjugados entre isolado proteico do soro de leite e ácido clorogênico resultou em aumento da digestibilidade proteica. Resultados semelhantes foram reportados por (Jiang *et al.*, 2018), que verificaram que o ácido clorogênico aumentou a digestibilidade das proteínas do soro de leite e da caseína. Em contrapartida, (Dufour *et al.*, 2018) relataram que polifenóis extraídos de vegetais exerceram efeitos negativos sobre a digestibilidade proteica, reduzindo a eficiência da digestão.

3.2 Capacidade Antioxidante

Os antioxidantes são agentes capazes de reduzir reações de oxidação, contribuindo para a manutenção da qualidade dos alimentos, uma vez que minimizam processos degradativos, aumentando a vida de prateleira e a segurança dos produtos (Liu *et al.*, 2023). Alimentos com elevada capacidade antioxidante também estão associados a benefícios à saúde humana, pois auxiliam na redução de espécies reativas de oxigênio, contribuindo para a prevenção de diversas doenças crônicas (Liu *et al.*, 2019). Proteínas podem atuar como antioxidantes naturais; entretanto, a maioria apresenta capacidade antioxidante limitada. Nesse contexto, a interação entre proteínas e compostos fenólicos tem sido amplamente explorada como estratégia para potencializar essa atividade (Quan *et al.*, 2019).

Diversos estudos relatam aumento significativo da capacidade antioxidante em conjugados proteína–composto fenólico (Barbosa *et al.*, 2025; He *et al.*, 2023; Pan *et al.*, 2023; Ren *et al.*, 2022a), indicando que esse tipo de interação é capaz de intensificar a capacidade antioxidante das proteínas.

3.3 Propriedades Antimicrobianas

Com o aumento da consciência ecológica dos consumidores, observa-se uma tendência crescente no uso de agentes antimicrobianos naturais para a preservação de alimentos. Proteínas, como a lisozima, apresentam atividade antimicrobiana intrínseca e, por isso, são consideradas alternativas promissoras aos conservantes sintéticos. A formação de conjugados entre proteínas e compostos fenólicos tem sido explorada como estratégia para potencializar essa atividade antimicrobiana ou para agregar novas propriedades funcionais às proteínas, mantendo sua capacidade antimicrobiana (Liu *et al.*, 2023; Rani *et al.*, 2021).

Fu *et al.* (2017) demonstraram que conjugados formados entre gelatina e ácido clorogênico apresentaram maior atividade antibacteriana frente a bactérias Gram-negativas, sendo essa atividade fortemente influenciada pela concentração do composto fenólico. Além disso, os autores observaram que o método de conjugação não afetou significativamente a atividade antimicrobiana. Em contraste, Li *et al.* (2023) relataram que conjugados de lisozima com ácido rosmarínico e ácido gentísico apresentaram menor atividade antimicrobiana em comparação à proteína isolada; entretanto, a incorporação dos compostos fenólicos promoveu melhorias em outras propriedades funcionais da proteína, como o aumento da capacidade antioxidante.

3.4 Imunogenicidade

Proteínas que apresentam níveis elevados de aminoácidos aromáticos, especialmente tirosina, demonstram uma notável imunogenicidade, que é a capacidade de uma substância provocar resposta imune no corpo humano, resultando na manifestação de alergias alimentares e na necessidade de restrições no consumo dessas proteínas. Tipicamente, as reações alérgicas a alimentos são desencadeadas pela habilidade dos anticorpos IgE em identificar antígenos, gerando uma inflamação. A capacidade alergênica das proteínas pode ser mitigada ao bloquear os sítios de ligação da IgE aos alérgenos proteicos por meio da utilização de polifenóis, que se ligarão a esses sítios (Liu *et al.*, 2023, 2019).

Em testes *in vitro* He *et al.* (2019) detectaram que a modificação estrutural no conjugado de ovalbumina e epigalocatequina-3-galato (EGCG) diminuiu a capacidade da proteína em se ligar aos sítios IgE, formando assim um produto menos alergênico. Em testes *in vivo e in vitro,* He *et al.* (2023) também constataram que a mudança estrutural entre o conjugado de proteína de amendoim e EGCG e ácido clorogênico também impediram a proteína de se ligar aos sítios

alergênicos, evidenciando que a interação entre proteínas e polifenóis tem efeito direto na alergenicidade da proteína.

4 Aplicações Tecnológicas dos Complexos e Conjugados Proteína-Composto Fenólico

A formação de complexos e conjugados entre proteínas e compostos fenólicos apresenta grande potencial para a geração de novos ingredientes com aplicações tecnológicas, conferindo características diferenciadas ou propriedades tecnofuncionais aprimoradas.

4.1 Emulsões

As emulsões são sistemas formados pela dispersão de dois líquidos imiscíveis, geralmente óleo e água, nos quais uma das fases encontra-se dispersa na forma de gotículas na outra, denominada fase contínua (Kupikowska-Stobba; Domagała; Kasprzak, 2024; McClements, 2014). De acordo com a natureza da fase dispersa e da fase contínua, as emulsões podem ser classificadas em emulsões óleo em água (O/A), nas quais gotículas de óleo estão dispersas em uma fase aquosa, e emulsões água em óleo (A/O), em que gotículas de água encontram-se dispersas em uma fase oleosa (McClements, 2014; Tamilvanan, 2004). A produção de emulsões ocorre por meio do processo de homogeneização, no qual se aplica energia suficiente ao sistema para promover a quebra de uma fase líquida em gotículas de menor tamanho e aumentar a área interfacial (McClements, 2004, 2014). As emulsões são sistemas termodinamicamente instáveis, que tendem a separar suas fases ao longo do tempo devido à ocorrência de diferentes mecanismos de instabilidade. Esses mecanismos incluem processos gravimétricos, como cremeação e sedimentação, e processos associados à interação entre gotículas, como floculação, coalescência e maturação de Ostwald. Em geral, esses fenômenos podem ocorrer simultaneamente em um mesmo sistema emulsionado, sendo que um mecanismo pode favorecer ou intensificar a ocorrência de outros (Fredrick; Walstra; Dewettinck, 2010; Liu *et al.*, 2024). A Figura 9 apresenta um diagrama dos processos que geram a separação de fases de uma emulsão.

A cremeação e a sedimentação são processos decorrentes da diferença de densidade entre a fase dispersa e a fase contínua. Quando a fase dispersa apresenta densidade menor que a fase contínua, as gotículas tendem a se deslocar para o topo do sistema, caracterizando o fenômeno de cremeação. Por outro lado, a sedimentação ocorre quando a fase dispersa é mais

densa que a fase contínua, promovendo o deslocamento das gotículas para o fundo do sistema (Fredrick; Walstra; Dewettinck, 2010; Liu *et al.*, 2024).

Os processos de floculação e coalescência estão relacionados à agregação das gotículas e ocorrem quando as forças atrativas entre elas superam as forças repulsivas. A floculação consiste na aproximação e no agrupamento de duas ou mais gotículas que mantêm sua integridade individual, enquanto a coalescência ocorre quando há a fusão das gotículas, resultando na formação de gotas maiores. Já a maturação de Ostwald é caracterizada pelo crescimento de gotículas maiores às custas das menores, devido à difusão molecular da fase dispersa através da fase contínua (Fredrick; Walstra; Dewettinck, 2010; Liu *et al.*, 2024).

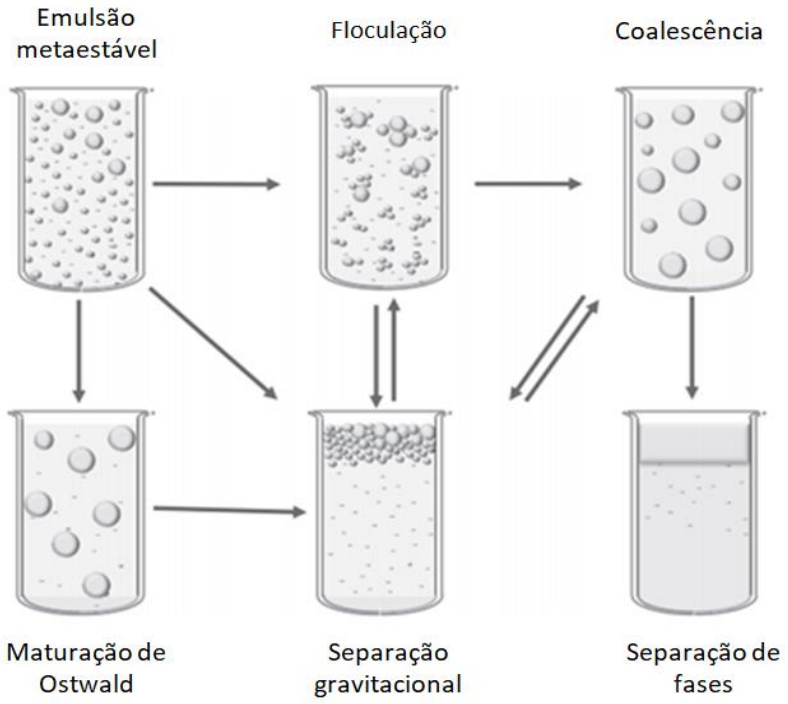

Figura 9. Diagrama de processos que causam instabilidade em emulsões.
Fonte: Adaptado de MCCLEMENTS, 2014.

Devido à instabilidade intrínseca das emulsões, a utilização de emulsificantes é essencial para a formação e estabilização desses sistemas. Os emulsificantes são substâncias capazes de se adsorver na interface óleo–água, reduzindo a tensão interfacial e formando uma camada protetora ao redor das gotículas dispersas, o que impede sua agregação por meio da geração de forças repulsivas. Na indústria de alimentos, proteínas são amplamente empregadas como emulsificantes naturais devido à sua natureza anfifílica, que permite adsorção eficiente na interface óleo–água (Liu *et al.*, 2024; McClements, 2004).

Nesse contexto, os conjugados proteína–composto fenólico têm emergido como alternativas promissoras aos emulsificantes convencionais. A conjugação promove alterações na conformação da proteína e na sua hidrofobicidade superficial, favorecendo uma adsorção mais eficiente e estável na interface óleo–água e resultando em capacidade emulsificante aprimorada. Além disso, a presença de compostos fenólicos confere capacidade antioxidante ao emulsificante, contribuindo para a proteção da fase lipídica contra a oxidação e, consequentemente, para o aumento da estabilidade da emulsão (Liu *et al.*, 2019; Quan *et al.*, 2019).Além das emulsões convencionais, diversos sistemas outros emulsionados têm sido desenvolvidos com o objetivo de ampliar a estabilidade e a funcionalidade dos produtos. Entre eles destacam-se as emulsões duplas, as emulsões multicamadas, as nanoemulsões e as emulsões Pickering (McClements, 2014).

4.1.1 Emulsões Pickering

As emulsões Pickering são sistemas emulsionados estabilizados por partículas sólidas que se adsorvem na interface óleo–água, formando uma barreira física ao redor das gotículas dispersas (Chevalier; Bolzinger, 2013). Diferentemente das emulsões convencionais, as emulsões Pickering apresentam elevada estabilidade cinética, uma vez que a energia necessária para a desorção das partículas da interface é significativamente maior. Essa estabilidade está diretamente relacionada às propriedades das partículas estabilizantes, como tamanho, forma, carga superficial e sua molhabilidade (Albert *et al.*, 2019; Linke; Drusch, 2018).

A molhabilidade das partículas é frequentemente descrita pelo ângulo de contato (θ), que expressa a afinidade da partícula pelas fases óleo e aquosa. Partículas com ângulo de contato próximo a 90° apresentam afinidade equilibrada por ambas as fases, favorecendo uma ancoragem eficiente na interface e resultando em emulsões altamente estáveis. Valores de ângulo de contato menores que 90° indicam maior afinidade pela fase aquosa, favorecendo a formação de emulsões óleo em água, enquanto valores superiores a 90° estão associados à maior afinidade pela fase oleosa e à formação de emulsões água em óleo (Albert *et al.*, 2019; Rayees *et al.*, 2024; Yan *et al.*, 2020). A Figura 10 apresenta um esquema do comportamento das partículas em função de sua molhabilidade em emulsões de Pickering.

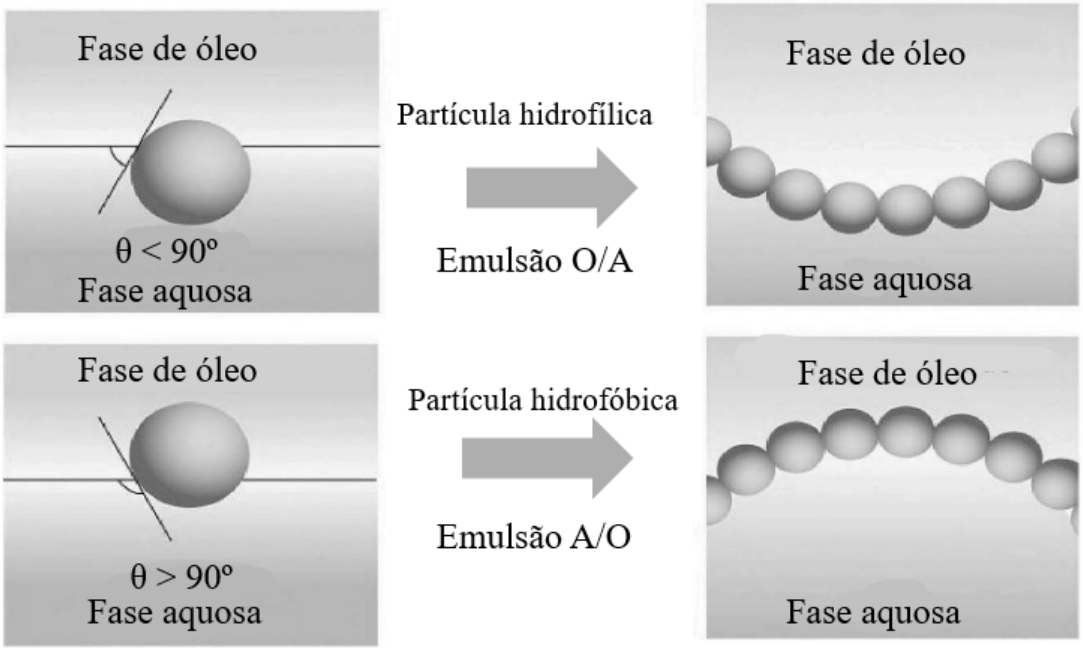

Figura 10. Esquema do comportamento das partículas em emulsões de Pickering em função da molhabilidade. Fonte: Adaptado de Rayees *et al.*, 2024.

Nesse contexto, os conjugados proteína–composto fenólico têm emergido como alternativas promissoras aos emulsificantes Pickering convencionais. A conjugação pode modificar a hidrofobicidade superficial, a carga e a conformação das proteínas, ajustando sua molhabilidade e favorecendo a adsorção estável na interface óleo–água sob a forma de partículas ou agregados (Baba; McClements; Maqsood, 2021; Quan *et al.*, 2019). Além disso, esses conjugados podem conferir funcionalidades adicionais ao sistema, como capacidade antioxidante, contribuindo para a estabilidade oxidativa da fase lipídica (McClements; Decker, 2018). A Tabela 2 apresenta diferentes estudos sobre emulsões Pickering estabilizadas por conjugados proteína–composto fenólico, destacando os sistemas avaliados e os principais resultados obtidos em termos de estabilidade e funcionalidade.

Tabela 2. Estudos sobre a utilização de conjugados proteína-composto fenólico como emulsificante em emulsões Pickering.

Conjugado	Método de formação	Fase dispersa	Resultados	Referência
Ovalbumina-Ácido Ferúlico	Alcalino	Óleo de soja	• Maior capacidade antioxidante da emulsão; • Redução da oxidação lipídica.	Barbosa; Garcia-Rojas, 2025.
Lactoferrina-EGCG	Alcalino	Óleo de peixe	• Redução do tamanho médio das gotas e aumento do potencial zeta; • Redução da oxidação lipídica; • Maior estabilidade frente a estresses ambientais.	Sun *et al.*, 2024.
Caseína-ácido cafeico	Alcalino	Óleo MCT	• Maior estabilidade durante o armazenamento.	Zhang; Wang; Lu, 2023.
BSPI-C3G	Alcalino	Óleo de peixe	• Maior estabilidade térmica e durante o armazenamento; • Redução da oxidação lipídica.	Cui *et al.*, 2022.
Zeína-Resveratrol	Alcalino	Óleo de milho	• Maior estabilidade em diferentes valores de pH e ao longo do tempo de armazenamento; • Redução da oxidação lipídica.	Ren *et al.*, 2022b.
WPI-EGCG	Radical Livre	Óleo MCT	• Redução do tamanho médio das gotas e aumento do potencial zeta; • Aumento da espessura da camada interfacial.	Qin; Gao; Luo, 2021.

Legenda: MCT **-** óleo de triglicerídeos de cadeia média (*Medium-Chain Triglycerides*)**,** BSPI - isolado proteico de soja preta (*Black Soybean Protein Isolate*), C3G - cianidina-3-O-glicosídeo, EGCG - epigalocatequina-3-galato

4.2 Filmes

Os filmes são materiais poliméricos finos e contínuos capazes de atuar como barreiras físicas entre o alimento e o ambiente (Janowicz *et al.*, 2023). Na área de alimentos, esses materiais têm sido amplamente investigados como alternativas sustentáveis às embalagens sintéticas, devido à sua biodegradabilidade e origem renovável (Matloob *et al.*, 2023; Otoni *et al.*, 2017). Os filmes comestíveis constituem uma classe específica de filmes formulados exclusivamente com componentes seguros para consumo humano, podendo ser aplicados diretamente sobre a superfície dos alimentos ou utilizados como embalagens primárias (Janowicz *et al.*, 2023; Otoni *et al.*, 2017). Já os filmes bioativos têm como diferencial a incorporação de compostos ativos capazes de interagir com o alimento ou com o meio, conferindo funcionalidades adicionais ao sistema. Entre esses compostos destacam-se agentes antioxidantes e antimicrobianos, os quais podem atuar na extensão da vida de prateleira e na manutenção da qualidade do alimento (Benbettaïeb; Karbowiak; Debeaufort, 2019; Liyanapathiranage *et al.*, 2023).

Esses filmes são geralmente produzidos a partir de biopolímeros naturais, como polissacarídeos (amido, quitosana, alginato e pectina), proteínas (gelatina, caseína e proteínas do soro do leite) e lipídios (ceras e ácidos graxos), os quais são dissolvidos ou dispersos em meio aquoso para a obtenção de soluções filmogênicas homogêneas (Avramescu *et al.*, 2020). A adição de plastificantes, como glicerol, sorbitol e polietilenoglicol, os quais são compostos de baixa volatilidade, é empregada para aumentar a flexibilidade e reduzir a fragilidade dos filmes, pois, ao serem incorporados a materiais poliméricos, promovem alterações na organização tridimensional da matriz, reduzindo as forças intermoleculares atrativas e aumentando o volume livre e a mobilidade das cadeias (Espitia *et al.*, 2014). Entre os principais métodos de formação, destacam-se a evaporação de solvente e a extrusão.

O método de evaporação de solvente é amplamente empregado em estudos laboratoriais, no qual a solução filmogênica é vertida sobre uma superfície plana e submetida à secagem controlada, promovendo a evaporação do solvente e a reorganização das cadeias poliméricas em uma matriz contínua e coesa. Esse método permite maior controle da espessura e da homogeneidade dos filmes (Janowicz *et al.*, 2023). A Figura 11 ilustra o método de evaporação de solvente. Por outro lado, a extrusão é um processo contínuo e mais compatível com a escala industrial, no qual uma ou duas roscas rotativas em um cilindro promovem o transporte, a mistura, a compressão e a conformação do material polimérico por meio de uma matriz. Esse método apresenta maior produtividade e menor demanda energética associada à remoção de água. No entanto, apesar de seu elevado potencial, ainda são limitados os estudos que abordam

a produção de filmes comestíveis por extrusão, o que é atribuído à complexidade das interações químicas entre os ingredientes e à elevada sensibilidade do processo às variáveis operacionais (Espitia *et al.*, 2014).

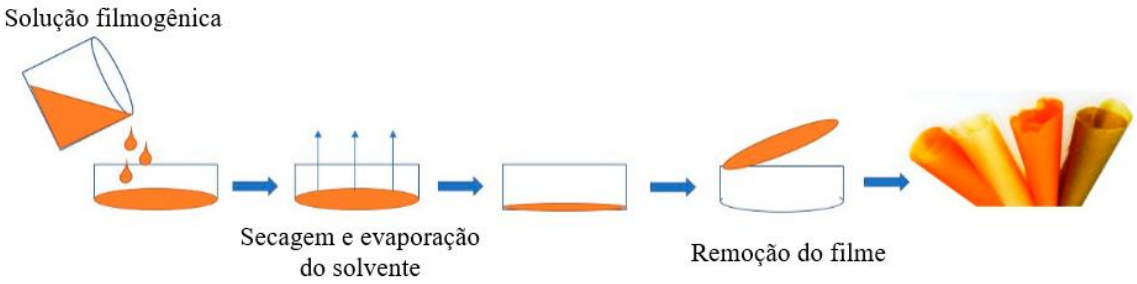

Figura 11. Representação esquemática do processo de formação de filmes pelo método de evaporação de solvente. Fonte: Adaptado de Janowicz *et al.*, 2023.

A aplicabilidade dos filmes na indústria de alimentos depende de diversas propriedades funcionais do material, destacando-se principalmente as propriedades mecânicas, como resistência à tração e alongamento na ruptura, que descrevem a capacidade do filme de resistir a esforços mecânicos e deformações durante o manuseio e o uso. Além disso, as propriedades ópticas, relacionadas à transparência, cor e capacidade de bloquear ou permitir a passagem de luz, e as propriedades de barreira, como a permeabilidade ao vapor de água e a gases, que determinam a taxa de transferência de substâncias através do filme, são fatores essenciais para seu desempenho. Essas características são fortemente influenciadas pela natureza do biopolímero, pela presença de plastificantes e pela organização estrutural da matriz polimérica (Avramescu *et al.*, 2020). A Tabela 3 apresenta estudos sobre a formação de filmes, bem como os materiais empregados, os métodos de formação e as propriedades funcionais avaliadas

Tabela 3. Estudos sobre a formação e a caracterização de filmes comestíveis, incluindo materiais, métodos de formação e propriedades avaliadas.

Matriz polimérica	Plastificante	Formação	Propriedades analisadas	Referência
•Amido de batata doce	Glicerol	Evaporação de Solvente	• Teor de umidade; • Permeabilidade de vapor de água; • Solubilidade; • Opacidade, transparência e cor.	Otero-Herrera *et al.*, 2025.
•Hidroxipropilmetilcelulose •Pectina •Gelatina	Glicerol	Evaporação de Solvente	• Ângulo de contato; • Teor de umidade; • Solubilidade; • Permeabilidade de vapor de água; • Propriedades mecânicas; • Transparência.	Athanasopoulou *et al.*, 2024.
•Pectina	----	Evaporação de Solvente	• Transparência e cor; • Ângulo de contato; • Permeabilidade de vapor de água; • Propriedades mecânicas.	Méndez *et al.*, 2023.
•Amido de mandioca •Gelatina •Óleo de canola •Gordura vegetal •Cera de abelha	Glicerol	Extrusão	• Ângulo de contato; • Solubilidade; • Permeabilidade de vapor de água; • Propriedades mecânicas.	Cheng *et al.*, 2021.
•Polpa de manga •Pectina	----	Extrusão	• Teor de umidade; • Permeabilidade de vapor de água; • Propriedades mecânicas; • Cor.	Oldoni *et al.*, 2021.

Apesar do elevado potencial tecnológico e ambiental, a aplicação industrial de filmes biodegradáveis ainda enfrenta desafios importantes, como a elevada sensibilidade à umidade em comparação às embalagens plásticas convencionais, além de limitações relacionadas à estabilidade dos compostos bioativos ao longo do armazenamento (Espitia *et al.*, 2014). Nesse contexto, a incorporação de conjugados proteína–composto fenólico tem se mostrado uma estratégia promissora para a melhoria das propriedades funcionais dos filmes. Zhao; Li; Xue (2023) observaram que filmes à base de carboximetilcelulose (CMC) incorporados com conjugados de isolado proteico do soro de leite (WPI) com proantocianidina ou curcumina apresentaram melhorias significativas nas propriedades mecânicas e de barreira, incluindo menor permeabilidade ao vapor de água e maior resistência à tração. De forma complementar, a incorporação de emulsões também tem sido reportada como uma estratégia eficaz para modificar e aprimorar as propriedades funcionais dos filmes, uma vez que a presença da fase lipídica pode alterar a microestrutura da matriz e contribuir para o controle da transferência de vapor de água (Almasi; Azizi; Amjadi, 2020).

4.3 Microencapsulação

A microencapsulação é uma técnica na qual gotas, partículas ou gases são incorporados a um agente encapsulante, formando pequenas cápsulas capazes de isolar o material encapsulado do meio externo (Ribeiro; Estevinho; Rocha, 2020). Nesse processo, há o material encapsulado (núcleo) e a substância que o envolve, denominada material de parede. O material de parede, em geral, deve ser insolúvel e quimicamente inerte em relação ao núcleo, além de apresentar baixo custo, ser atóxico e biodegradável (Bamidele; Emmambux, 2021; Nooshkam; Varidi, 2020).

A microencapsulação é amplamente empregada em diferentes setores industriais, como o alimentício, têxtil, farmacêutico, cosmético e agroquímico. Essa tecnologia possibilitou a incorporação de substâncias anteriormente inviáveis de serem aplicadas em processos industriais, como compostos sensíveis ao calor, à luz e às variações de pH. Na indústria de alimentos, a microencapsulação destaca-se como uma importante estratégia para o desenvolvimento de alimentos funcionais e com maior valor agregado, atendendo às novas demandas dos consumidores (Ribeiro; Estevinho; Rocha, 2020; Suljagic; Bratovcic, 2019).

Os objetivos da microencapsulação na indústria de alimentos incluem atuar como barreira contra luz, umidade e oxigênio, bem como possibilitar o mascaramento de sabores e odores indesejáveis. Adicionalmente, essa tecnologia permite a liberação controlada dos compostos encapsulados, protegendo-os contra a degradação durante o processo digestivo e,

consequentemente, garantindo sua estabilidade, absorção ao longo do trato gastrointestinal e aumento da bioacessibilidade (Reque; Brandelli, 2021; Suljagic; Bratovcic, 2019; Ye; Georges; Selomulya, 2018).

Substâncias bioativas têm sido incorporadas a alimentos por meio de técnicas de microencapsulação, como óleos essenciais (Niu *et al.*, 2022), vitaminas (Zhao *et al.*, 2023), minerais (Barbosa; Garcia-Rojas, 2022) e microrganismos (Zhang *et al.*, 2022). Nesse contexto, os conjugados proteína–compostos fenólicos destacam-se como componentes bifuncionais, uma vez que podem atuar simultaneamente como agente bioativo, por apresentarem propriedades biológicas relevantes, como capacidade antioxidante e antimicrobiana e como material encapsulante, por exibirem capacidades tecnofuncionais aprimoradas em comparação às proteínas nativas, dessa forma, os conjugados proteína–compostos fenólicos podem melhorar a eficiência de técnicas já consolidadas, como a microencapsulação via emulsões, promovendo maior estabilidade físico-química dos sistemas e maior proteção dos compostos encapsulados (Liu *et al.*, 2023; Quan *et al.*, 2019).

As cápsulas podem ser classificadas de acordo com o tamanho em macrocápsulas (> 5.000 μm), microcápsulas (0,2 a 5.000 μm) e nanocápsulas (< 0,2 μm), sendo que sua morfologia depende principalmente da técnica de encapsulação empregada e dos ingredientes utilizados (Silva *et al.*, 2014). As cápsulas podem apresentar duas principais conformações estruturais: microcápsulas, nas quais o núcleo se encontra concentrado e envolvido por uma camada contínua do material de parede, e microesferas, caracterizadas pela dispersão do núcleo em uma matriz (Corrêa-Filho; Moldão-Martins; Alves, 2019; Silva *et al.*, 2014) . Também é possível a formação de microcápsulas com múltiplos núcleos ou com múltiplas camadas de parede envolvendo um mesmo núcleo. Diversos métodos de microencapsulação têm sido desenvolvidos, incluindo *spray-drying, spray cooling, spray chilling, freeze-drying*, extrusão, coacervação complexa, além de emulsões (Mehta *et al.*, 2022).

Na encapsulação por emulsões, as substâncias bioativas são solubilizadas na fase interna do sistema e, após a formação e estabilização das gotículas, passam a ficar fisicamente aprisionadas e protegidas pelo sistema interfacial, o que contribui para aumentar sua estabilidade frente às condições do ambiente (McClements, 2014). Nesse contexto, as emulsões de Pickering estabilizadas por conjugados proteína–composto fenólico atuam como sistemas de dupla encapsulação, co-encapsulando tanto a substância bioativa de interesse quanto o próprio composto fenólico presente na interface (McClements; Decker, 2018). A Tabela 4 apresenta estudos sobre emulsões de Pickering estabilizadas por conjugados proteína–composto fenólico aplicadas à encapsulação de substâncias bioativas.

Tabela 4. Conjugados proteína–polifenol empregados na encapsulação de ingredientes bioativos e seus principais resultados.

Conjugado	Fase dispersa	Ingrediente encapsulado	Resultados	Referência
IPS-Curcumina	Óleo MCT	*L. plantarum*	• Proteção de probióticos durante a digestão gastrointestinal e aumento de sua taxa de sobrevivência.	Ye *et al.*, 2025.
OVA-Ácido Ferúlico	Óleo de soja	Vitamina D	• Maior estabilidade fotoquímica; • Bioacessibilidade de até 50%.	Barbosa; Garcia-Rojas, 2025.
WPI-ácido tânico WPI-ácido gálico WPI-polifenóis de chá WPI–ácido vanílico	Óleo de nozes	Vitamina D	• Eficiência de encapsulação de até 84%; • Bioacessibilidade de até 60%.	Zhao *et al.*, 2023.
WPI-EGCG	Água	*L. plantarum*	• Alta viabilidade após a pasteurização e a digestão gastrointestinal.	He; Yang; Qin, 2023.
IPS- EGCG	Óleo de soja	β-caroteno	• Até 86% de estabilidade química do ingrediente ativo por 42 dias; • Bioacessibilidade de até 52%.	Geng *et al.*, 2022.

Legenda: IPS - Isolado proteico de soja, MCT- óleo de triglicerídeos de cadeia média (*Medium-Chain Triglycerides*), OVA- ovalbumina, WPI- Isolado proteico do soro do leite (*Whey Protein Isolate*), EGCG - epigalocatequina-3-galato.

5 Substâncias Bioativas

5.1 Vitamina D

A vitamina D é um nutriente lipossolúvel essencial para o organismo humano, desempenhando papel fundamental na manutenção da homeostase mineral, da saúde óssea e de diversos processos metabólicos e imunológicos. As duas principais formas de vitamina D presentes na dieta e no organismo são a vitamina D2 (ergocalciferol) e a vitamina D3 (colecalciferol) (Göring, 2018). As estruturas químicas da vitamina D2 e da vitamina D3 estão apresentadas na Figura 12, evidenciando pequenas diferenças estruturais que influenciam sua estabilidade e eficiência de absorção no organismo.

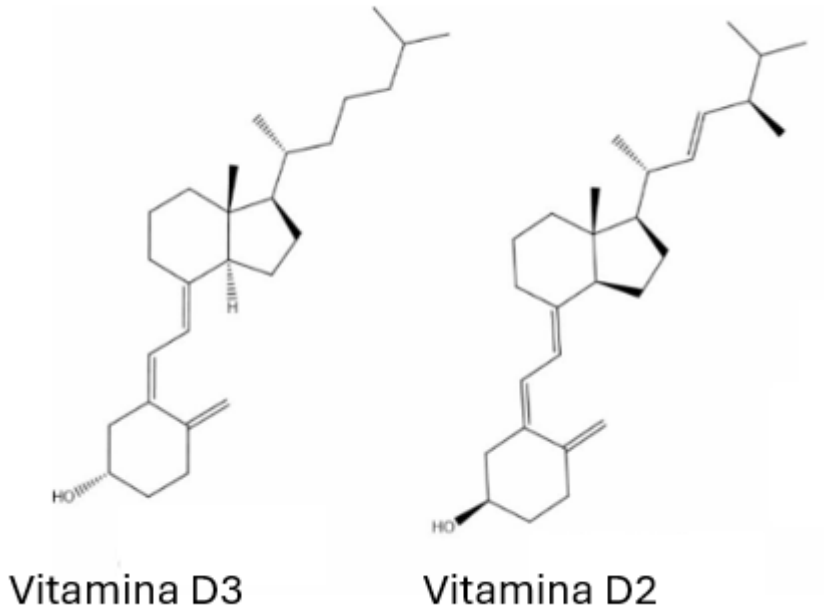

Figura 12. Estrutura da vitamina D.
Fonte: Majeed; Rather, 2025.

A vitamina D2 é obtida predominantemente de fontes vegetais e fúngicas, como cogumelos expostos à radiação ultravioleta, além de estar presente em pequenas quantidades em ovos. Já a vitamina D3 é produzida endogenamente na pele a partir do 7-desidrocolesterol, quando ocorre exposição à radiação ultravioleta B proveniente da luz solar, sendo também encontrada em alimentos de origem animal, como peixes gordurosos, fígado e gema de ovo (Gallo *et al.*, 2013; Ross, 2011).

Após sua obtenção por via dietética ou por síntese cutânea, ambas as formas de vitamina D passam por um processo de ativação metabólica em duas etapas. Inicialmente, no fígado, a vitamina D é hidroxilada, formando a 25-hidroxivitamina D (calcidiol), que constitui a principal

forma circulante e o principal marcador clínico do estado nutricional de vitamina D no organismo. Em seguida, nos rins, o calcidiol sofre nova hidroxilação, originando a forma biologicamente ativa, a 1,25-di-hidroxivitamina D (calcitriol). O calcitriol atua como um hormônio esteroide, ligando-se a receptores nucleares e regulando a expressão gênica de proteínas envolvidas na absorção intestinal de cálcio e fósforo, na mineralização óssea, na função muscular e na modulação do sistema imunológico (Majeed; Rather, 2025).

Os efeitos positivos da vitamina D no corpo humano incluem o aumento da absorção intestinal de cálcio e fósforo, a manutenção da densidade mineral óssea, a contribuição para a função muscular, a modulação da resposta imunológica inata e adaptativa e um possível papel protetor contra doenças inflamatórias, metabólicas e cardiovasculares (Esmaeili *et al.*, 2022; Wilson *et al.*, 2017). Por outro lado, a deficiência de vitamina D constitui um problema de saúde pública em escala global, afetando diferentes faixas etárias e populações. Entre os principais fatores associados à hipovitaminose D destacam-se a baixa exposição solar e dietas pobres nesse nutriente, além da obesidade, processos inflamatórios e condições que comprometem a absorção intestinal de lipídios, como síndrome nefrótica e cirurgias bariátricas (Cashman, 2020). No Brasil, aproximadamente 45% da população apresenta algum grau de deficiência de vitamina D, sendo as maiores incidências observadas nas regiões Sul e Sudeste, embora todas as regiões do país apresentem níveis insuficientes desse nutriente (Borba *et al.*, 2022).

Em crianças, a deficiência pode levar ao raquitismo, caracterizado por deformidades ósseas e atraso no crescimento. Em adultos, está associada à osteomalácia e à osteoporose, com aumento do risco de fraturas. Além disso, níveis reduzidos de vitamina D têm sido relacionados à fraqueza muscular, maior suscetibilidade a infecções, alterações na resposta imunológica e maior risco de desenvolvimento de doenças crônicas, como diabetes tipo 2, doenças cardiovasculares e algumas neoplasias (Esmaeili *et al.*, 2022; Wilson *et al.*, 2017).

Apesar de sua relevância fisiológica, a vitamina D apresenta elevada instabilidade físico-química, sendo suscetível à degradação quando exposta à luz, ao oxigênio e a altas temperaturas, o que limita sua aplicação em alimentos fortificados e suplementos nutricionais (Majeed; Rather, 2025; McClements, 2014). Nesse contexto, a microencapsulação surge como uma estratégia tecnológica promissora para proteger a vitamina D contra fatores ambientais adversos, aumentar sua estabilidade durante o processamento e o armazenamento, além de melhorar sua bioacessibilidade e biodisponibilidade no trato gastrointestinal. Diversas técnicas têm sido exploradas para a microencapsulação da vitamina D, como emulsões (Zhao *et al.*, 2023), coacervação complexa (Zhao *et al.*, 2025), *spray drying* (Bashir *et al.*, 2024) e lipossomas (Fan *et al.*, 2023).

5.2 β-Caroteno

Os carotenoides constituem um grupo diversificado de compostos apolares responsáveis pelas colorações amarela, laranja e vermelha de diversos alimentos, sendo amplamente reconhecidos pelos benefícios que promovem à saúde humana (Bogacz-Radomska; Harasym, 2018; McClements, 2014). Estruturalmente, essas moléculas são caracterizadas pela presença de múltiplas ligações duplas conjugadas e, em muitas delas, por estruturas de anéis de carbono em uma ou ambas as extremidades da molécula (Jomova; Valko, 2013). Dentre essa classe, o β-caroteno assume papel de destaque, sendo classificado como um carotenoide do subgrupo dos hidrocarbonetos, composto exclusivamente por átomos de carbono e hidrogênio, cuja estrutura está apresentada na Figura 13 (Kaczor; Baranska; Czamara, 2016). Devido à sua coloração intensa e à sua segurança, o β-caroteno é amplamente utilizado pela indústria alimentícia e cosmética como pigmento natural e agente corante (Böhm *et al.*, 2021; Jomova; Valko, 2013).

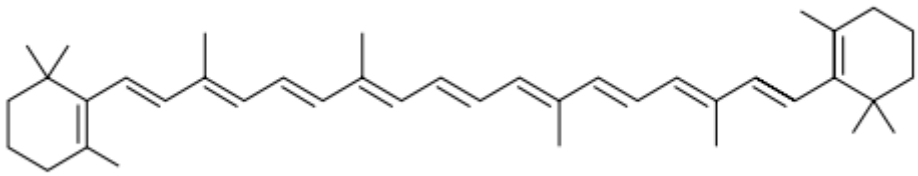

Figura 13. Estrutura do β-caroteno.
Fonte: Jomova; Valko, 2013.

O β-caroteno é encontrado em abundância em diversos vegetais e frutas de coloração laranja, amarela ou verde-escura, incluindo cenouras, abóboras, batata-doce, pimentões, damascos, manga, espinafre, couve, brócolis e folhas verdes escuras (Bogacz-Radomska; Harasym, 2018; Böhm *et al.*, 2021). Nessas plantas, o β-caroteno desempenha funções biológicas essenciais como componente fundamental dos complexos de antena colhedores de luz de organismos fotossintéticos. Nesses sistemas, ele atua na captura de fótons e na transferência de excitações eletrônicas para as moléculas de clorofila, além de exercer um papel crítico na fotoproteção, regulando o fluxo de energia e dissipando o excesso de luz que poderia causar danos oxidativos às células (Kaczor; Baranska; Czamara, 2016).

No organismo humano, o consumo de β-caroteno está associado a diversos efeitos benéficos. Sua potente capacidade antioxidante permite a neutralização de radicais livres de oxigênio, prevenindo danos oxidativos às células e tecidos. Essa propriedade antioxidante está relacionada à redução do risco de doenças como câncer, doenças cardiovasculares,

enfermidades oftalmológicas e doenças neurodegenerativas. Além disso, o β-caroteno contribui para a proteção contra radiação ultravioleta, auxiliando na integridade dos tecidos epiteliais (Bhatt; Patel, 2020). Contudo, sua função biológica mais relevante é a de pró-vitamina A. O β-caroteno um precursor eficiente do retinol (vitamina A). Nos seres humanos, os dois principais sítios de conversão do β-caroteno em vitamina A são o intestino e o fígado, onde ocorre a clivagem enzimática que gera retinol ativo (Harrison, 2012).

A deficiência de vitamina A, constitui um problema de saúde pública em diversas regiões do mundo (Maurya; Bashir; Aggarwal, 2020). Essa deficiência pode resultar em distúrbios oculares, comprometimento do sistema imunológico, aumentando a suscetibilidade a infecções, além de afetar o crescimento infantil e os sistemas reprodutivos masculino e feminino (Wiseman; Bar-El Dadon; Reifen, 2017).

Apesar de sua importância nutricional e industrial, o β-caroteno apresenta desafios significativos de estabilidade. Protegido naturalmente pelas matrizes teciduais de frutas, vegetais e animais, o composto é relativamente estável. Entretanto, uma vez isolado ou extraído, torna-se altamente suscetível à degradação por fatores como luz, oxigênio, variações de pH e temperaturas elevadas (McClements, 2014) . Tais agentes favorecem reações de isomerização e oxidação, resultando na perda da coloração característica, redução da capacidade antioxidante e degradação do valor nutricional (Lavelli; Sereikaitė, 2022).

Diante da vulnerabilidade química do β-caroteno e da sua baixa solubilidade em meios aquosos, a microencapsulação surge como uma estratégia tecnológica promissora. Essa técnica promove o aprisionamento do composto em matrizes protetoras, prolongando sua vida útil e viabilizando sua incorporação em diferentes sistemas alimentares. Entre as técnicas utilizadas destacam-se as emulsões (Geng *et al.*, 2022), a coacervação complexa (Barbosa; Bastos; Garcia-Rojas, 2021), o *spray drying* (Xiao *et al.*, 2026) e lipossomos (Gu *et al.*, 2024).

6 Conclusões

Essa revisão bibliográfica apresenta e discute a relevância de proteínas, polissacarídeos e compostos fenólicos na ciência de alimentos, com ênfase em suas interações e aplicações. A formação de complexos e conjugados entre esses compostos possibilita o aprimoramento de propriedades tecnológicas e biológicas, como emulsificação, capacidade antioxidante e bioacessibilidade. Além disso, aplicações em emulsões, filmes e microencapsulação evidenciam seu potencial no desenvolvimento de sistemas mais estáveis, capazes de proteger e veicular compostos bioativos, contribuindo para a obtenção de alimentos funcionais com maior valor agregado.

7 Referências

ABDEL-MONEIM, Abdel-Moneim E. *et al.* The role of polyphenols in poultry nutrition. **Journal of Animal Physiology and Animal Nutrition**, v. 104, n. 6, p. 1851–1866, 2020.

ABEYRATHNE, E. D. N. S.; LEE, H. Y.; AHN, D. U. Egg white proteins and their potential use in food processing or as nutraceutical and pharmaceutical agents—A review. **Poultry Science**, v. 92, n. 12, p. 3292–3299, 2013.

ADETUNJI, Lanrewaju Ridwan *et al.* Advances in the pectin production process using novel extraction techniques: A review. **Food Hydrocolloids**, v. 62, p. 239–250, 2017.

ALARA, Oluwaseun Ruth; ABDURAHMAN, Nour Hamid; UKAEGBU, Chinonso Ishamel. Extraction of phenolic compounds: A review. **Current Research in Food Science**, v. 4, p. 200–214, 2021.

ALBERT, Claire *et al.* Pickering emulsions: Preparation processes, key parameters governing their properties and potential for pharmaceutical applications. **Journal of Controlled Release**, v. 309, p. 302–332, 2019.

ALMASI, Hadi; AZIZI, Saeedeh; AMJADI, Sajed. Development and characterization of pectin films activated by nanoemulsion and Pickering emulsion stabilized marjoram (*Origanum majorana* L.) essential oil. **Food Hydrocolloids**, v. 99, p. 105338, 2020.

ATHANASOPOULOU, Evmorfia *et al.* Synthesis and characterization of polysaccharide- and protein-based edible films and application as packaging materials for fresh fish fillets. **Scientific Reports**, v. 14, n. 1, p. 517, 2024.

AVRAMESCU, Sorin Marius *et al.* Edible and Functionalized Films/Coatings—Performances and Perspectives. **Coatings**, v. 10, n. 7, p. 687, 2020.

BABA, Waqas N.; MCCLEMENTS, David Julian; MAQSOOD, Sajid. Whey protein–polyphenol conjugates and complexes: Production, characterization, and applications. **Food Chemistry**, v. 365, p. 130455, 2021.

BAMIDELE, Oluwaseun P.; EMMAMBUX, Mohammad Naushad. Encapsulation of bioactive compounds by “extrusion” technologies: a review. **Critical Reviews in Food Science and Nutrition**, v. 61, n. 18, p. 3100–3118, 2021.

BARBOSA, Ahmad El Ghazzaqui; BASTOS, Lívia Pinto Heckert; GARCIA-ROJAS, Edwin Elard. Complex Coacervates Formed between Whey Protein Isolate and Carboxymethylcellulose for Encapsulation of β-Carotene from Sacha Inchi Oil: Stability, *In Vitro* Digestion and Release Kinetics. **Food Biophysics**, v. 16, n. 3, p. 293–305, 2021.

BARBOSA, Bruno Sérgio Toledo *et al.* Impact of the Covalent Interaction Between Ferulic Acid and Ovalbumin on the Structure and Functional Properties of the Protein. **Food Biophysics**, v. 20, n. 1, p. 28, 2025.

BARBOSA, Bruno Sérgio Toledo; GARCIA-ROJAS, Edwin Elard. Double emulsions as delivery systems for iron: Stability kinetics and improved bioaccessibility in infants and adults. **Current Research in Food Science**, v. 5, p. 718–725, 2022.

BARBOSA, Bruno Sérgio Toledo; GARCIA-ROJAS, Edwin Elard. Effect of ovalbumin-ferulic acid conjugates on the stability and bioaccessibility of vitamin D3 in pickering emulsions. **International Journal of Biological Macromolecules**, v. 321, p. 146397, 2025.

BASHIR, Iqra *et al.* Effect of freeze drying and spray drying on physical properties, morphology and *in vitro* release kinetics of vitamin D3 nanoparticles. **Powder Technology**, v. 432, p. 119164, 2024.

BENBETTAÏEB, Nasreddine; KARBOWIAK, Thomas; DEBEAUFORT, Frédéric. Bioactive edible films for food applications:Influence of the bioactive compounds on film structure and properties. **Critical Reviews in Food Science and Nutrition**, v. 59, n. 7, p. 1137–1153, 2019.

BHATT, Takshma; PATEL, Kirtan. Carotenoids: Potent to Prevent Diseases Review. **Natural Products and Bioprospecting**, v. 10, n. 3, p. 109–117, 2020.

BOGACZ-RADOMSKA, Ludmila; HARASYM, Joanna. β-Carotene—properties and production methods. **Food Quality and Safety**, v. 2, n. 2, p. 69–74, 2018.

BÖHM, Volker *et al.* From carotenoid intake to carotenoid blood and tissue concentrations – implications for dietary intake recommendations. **Nutrition Reviews**, v. 79, n. 5, p. 544–573, 2021.

BORBA, Victoria Zeghbi Cochenski *et al.* Epidemiology of Vitamin D (EpiVida)—A Study of Vitamin D Status Among Healthy Adults in Brazil. **Journal of the Endocrine Society**, v. 7, n. 1, p. bvac171, 2022.

CASHMAN, Kevin D. Vitamin D Deficiency: Defining, Prevalence, Causes, and Strategies of Addressing. **Calcified Tissue International**, v. 106, n. 1, p. 14–29, 2020.

CHENG, Jinju *et al.* Impact of binding interaction modes between whey protein concentrate and quercetin on protein structural and functional characteristics. **Food Hydrocolloids**, v. 142, p. 108787, 2023.

CHENG, Yue *et al.* Effect of lipids with different physical state on the physicochemical properties of starch/gelatin edible films prepared by extrusion blowing. **International Journal of Biological Macromolecules**, v. 185, p. 1005–1014, 2021.

CHEVALIER, Yves; BOLZINGER, Marie-Alexandrine. Emulsions stabilized with solid nanoparticles: Pickering emulsions. **Colloids and Surfaces A: Physicochemical and Engineering Aspects**, v. 439, p. 23–34, 2013.

CORRÊA-FILHO, Luiz C.; MOLDÃO-MARTINS, Margarida; ALVES, Vitor D. Advances in the Application of Microcapsules as Carriers of Functional Compounds for Food Products. **Applied Sciences**, v. 9, n. 3, p. 571, 2019.

CUI, Xiaojie *et al.* Formation, structure and stability of high internal phase Pickering emulsions stabilized by BSPI-C3G covalent complexes. **Food Chemistry: X**, v. 16, p. 100455, 2022.

DAMODARAN, S.; PARKIN, K. L. Amino Acids, Peptides, and Proteins. *In*: **Fennema's Food Chemistry**. Fifth ed. Boca Raton: CRC Press, 2017. p. 1123.

DAMODARAN, S.; PARAF, A. **Food Proteins and Their Applications**. 1. ed. Boca Raton: CRC Press, 2019.

DIAS, Maria Inês; FERREIRA, Isabel C. F. R.; BARREIRO, Maria Filomena. Microencapsulation of bioactives for food applications. **Food & Function**, v. 6, n. 4, p. 1035–1052, 2015.

DIMA, Cristian; DIMA, Stefan. Bioaccessibility study of calcium and vitamin D3 co-microencapsulated in water-in-oil-in-water double emulsions. **Food Chemistry**, v. 303, p. 125416, 2020.

DUFOUR, Claire *et al.* The matrix of fruit & vegetables modulates the gastrointestinal bioaccessibility of polyphenols and their impact on dietary protein digestibility. **Food Chemistry**, v. 240, p. 314–322, 2018.

DURAZZO, Alessandra *et al.* Polyphenols: A concise overview on the chemistry, occurrence, and human health. **Phytotherapy Research**, v. 33, n. 9, p. 2221–2243, 2019.

ESMAEILI, Mina *et al.* Encapsulating Vitamin D: A Feasible and Promising Approach to Combat Its Deficiency. **Pharmaceutical Sciences**, v. 28, n. 2, p. 194–207, 2022.

ESPITIA, Paula Judith Pérez *et al.* Edible films from pectin: Physical-mechanical and antimicrobial properties - A review. **Food Hydrocolloids**, v. 35, p. 287–296, 2014.

FAN, Chunli *et al.* Liposomes for encapsulation of liposoluble vitamins (A, D, E and K): Comparation of loading ability, storage stability and bilayer dynamics. **Food Research International**, v. 163, p. 112264, 2023.

FERRABOSCHI, Patrizia; CICERI, Samuele; GRISENTI, Paride. Applications of Lysozyme, an Innate Immune Defense Factor, as an Alternative Antibiotic. **Antibiotics**, v. 10, n. 12, p. 1534, 2021.

FREDRICK, Eveline; WALSTRA, Pieter; DEWETTINCK, Koen. Factors governing partial coalescence in oil-in-water emulsions. **Advances in Colloid and Interface Science**, v. 153, n. 1–2, p. 30–42, 2010.

FREITAS, Cariny Maria Polesca *et al.* Structure and Applications of Pectin in Food, Biomedical, and Pharmaceutical Industry: A Review. **Coatings**, v. 11, n. 8, p. 922, 2021.

FU, Shalu *et al.* Preparation and characterisation of Chlorogenic acid-gelatin: A type of biologically active film for coating preservation. **Food Chemistry**, v. 221, p. 657–663, 2017.

GALLO, Sina *et al.* The change in plasma 25-hydroxyvitamin D did not differ between Breast-Fed Infants That Received a Daily Supplement of Ergocalciferol or Cholecalciferol for 3 Months. **Journal of Nutrition**, v. 143, n. 2, p. 148–153, 2013.

GEBICKI, Janusz M.; NAUSER, Thomas. Fast Antioxidant Reaction of Polyphenols and Their Metabolites. **Antioxidants**, v. 10, n. 8, p. 1297, 2021.

GENG, Mengjie *et al.* Encapsulation of β-carotene in high internal phase Pickering emulsions stabilized by soy protein isolate – epigallocatechin-3-gallate covalent composite microgel particles. **Journal of Molecular Liquids**, v. 360, p. 119511, 2022.

GÖRING, H. Vitamin D in Nature: A Product of Synthesis and/or Degradation of Cell Membrane Components. **Biochemistry (Moscow)**, v. 83, n. 11, p. 1350–1357, 2018.

GU, Jinhui *et al.* Improving the encapsulation of β-carotene by nanoliposomes via potato starch/whey protein coating. **International Journal of Food Science and Technology**, v. 59, n. 4, p. 2524–2534, 2024.

GUHA, Snigdha; MAJUMDER, Kaustav; MINE, Yoshinori. Egg Proteins. *In*: MELTON, Laurence; SHAHIDI, Fereidoon; VARELIS, Peter (Orgs.). **Encyclopedia of Food Chemistry**. 1. ed. Amsterdam: Elsevier, 2019. p. 74–84.

HAN, Haizhen; DYE, Louise; MACKIE, Alan. The impact of processing on the release and antioxidant capacity of ferulic acid from wheat: A systematic review. **Food Research International**, v. 164, p. 112371, 2023.

HARRISON, Earl H. Mechanisms involved in the intestinal absorption of dietary vitamin A and provitamin A carotenoids. **Biochimica et Biophysica Acta (BBA) - Molecular and Cell Biology of Lipids**, v. 1821, n. 1, p. 70–77, 2012.

HE, Weiyi *et al.* Function, digestibility and allergenicity assessment of ovalbumin–EGCG conjugates. **Journal of Functional Foods**, v. 61, p. 103490, 2019.

HE, Weiyi *et al.* Modulating the allergenicity and functional properties of peanut protein by covalent conjugation with polyphenols. **Food Chemistry**, v. 415, p. 135733, 2023.

HE, Xian; YANG, Wanshui; QIN, Xinsheng. Ultrasound-assisted multilayer Pickering emulsion fabricated by WPI-EGCG covalent conjugates for encapsulating probiotics in colon-targeted release. **Ultrasonics Sonochemistry**, v. 97, p. 106450, 2023.

JALILI-FIROOZINEZHAD, Sasan *et al.* Chicken egg white: Hatching of a new old biomaterial. **Materials Today**, v. 40, p. 193–214, 2020.

JANOWICZ, Monika *et al.* The Potential of Edible Films, Sheets, and Coatings Based on Fruits and Vegetables in the Context of Sustainable Food Packaging Development. **Polymers**, v. 15, n. 21, p. 4231, 2023.

JIANG, Jiang *et al.* The effect of non-covalent interaction of chlorogenic acid with whey protein and casein on physicochemical and radical-scavenging activity of *in vitro* protein digests. **Food Chemistry**, v. 268, p. 334–341, 2018.

JOMOVA, Klaudia; VALKO, Marian. Health protective effects of carotenoids and their interactions with other biological antioxidants. **European Journal of Medicinal Chemistry**, v. 70, p. 102–110, 2013.

KACZOR, Agnieszka; BARANSKA, Malgorzata; CZAMARA, Krzysztof. Carotenoids: Overview of Nomenclature, Structures, Occurrence, and Functions. *In*: BARANSKA, Malgorzata; KACZOR, Agnieszka. **Carotenoids**. 1. ed. Chichester: Wiley, 2016. p. 1–13.

KHORSHIDIAN, Nasim *et al.* An Overview of Antimicrobial Activity of Lysozyme and Its Functionality in Cheese. **Frontiers in Nutrition**, v. 9, p. 833618, 2022.

KUMAR, Naresh; GOEL, Nidhi. Phenolic acids: Natural versatile molecules with promising therapeutic applications. **Biotechnology Reports**, v. 24, p. e00370, 2019.

KUMAR, Naresh; PRUTHI, Vikas. Potential applications of ferulic acid from natural sources. **Biotechnology Reports**, v. 4, n. 1, p. 86–93, 2014.

KUPIKOWSKA-STOBBA, Barbara; DOMAGAŁA, Jacek; KASPRZAK, Mirosław M. Critical Review of Techniques for Food Emulsion Characterization. **Applied Sciences**, v. 14, n. 3, p. 1069, 2024.

LAVELLI, Vera; SEREIKAITĖ, Jolanta. Kinetic Study of Encapsulated β-Carotene Degradation in Dried Systems: A Review. **Foods**, v. 11, n. 3, p. 437, 2022.

LI, Dan *et al.* Ferulic acid: A review of its pharmacology, pharmacokinetics and derivatives. **Life Sciences**, v. 284, p. 119921, 2021.

LI, Hui *et al.* Lysozyme–phenolics bioconjugates with antioxidant and antibacterial bifunctionalities: Structural basis underlying the dual-function. **Food Chemistry**, v. 406, p. 135070, 2023.

LINKE, Christina; DRUSCH, Stephan. Pickering emulsions in foods - opportunities and limitations. **Critical Reviews in Food Science and Nutrition**, v. 58, n. 12, p. 1971–1985, 2018.

LIU, Fuguo *et al.* Food-Grade Covalent Complexes and Their Application as Nutraceutical Delivery Systems: A Review. **Comprehensive Reviews in Food Science and Food Safety**, v. 16, n. 1, p. 76–95, 2017.

LIU, Fuguo *et al.* Novel Colloidal Food Ingredients: Protein Complexes and Conjugates. **Annual Review of Food Science and Technology**, v. 14, n. 1, p. 35–61, 2023.

LIU, Jun *et al.* Recent advances in phenolic–protein conjugates: synthesis, characterization, biological activities and potential applications. **RSC Advances**, v. 9, n. 61, p. 35825–35840, 2019.

LIU, Yuqing *et al.* Food emulsions stabilized by proteins and emulsifiers: A review of the mechanistic explorations. **International Journal of Biological Macromolecules**, v. 261, p. 129795, 2024.

LIYANAPATHIRANAGE, Anuradhi *et al.* Recent Developments in Edible Films and Coatings for Fruits and Vegetables. **Coatings**, v. 13, n. 7, p. 1177, 2023.

LOVEDAY, Simon M. Food Proteins: Technological, Nutritional, and Sustainability Attributes of Traditional and Emerging Proteins. **Annual Review of Food Science and Technology**, v. 10, n. 1, p. 311–339, 2019.

MAJEED, Massarat; RATHER, Mushtaq Ahmad. Enhancing Shelf Life and Bioavailability of Vitamin D Through Encapsulation: A Comprehensive Review. **Food Biophysics**, v. 20, n. 1, p. 15, 2025.

MARTĂU, Gheorghe Adrian; MIHAI, Mihaela; VODNAR, Dan Cristian. The Use of Chitosan, Alginate, and Pectin in the Biomedical and Food Sector—Biocompatibility, Bioadhesiveness, and Biodegradability. **Polymers**, v. 11, n. 11, p. 1837, 2019.

MATLOOB, Anam *et al.* A Review on Edible Coatings and Films: Advances, Composition, Production Methods, and Safety Concerns. **ACS Omega**, v. 8, n. 32, p. 28932–28944, 2023.

MAURYA, Vaibhav Kumar; BASHIR, Khalid; AGGARWAL, Manjeet. Vitamin D microencapsulation and fortification: Trends and technologies. **The Journal of Steroid Biochemistry and Molecular Biology**, v. 196, p. 105489, 2020.

MCCLEMENTS, David Julian. **Food Emulsions**. 2. ed. Boca Raton: CRC Press, 2004.

MCCLEMENTS, David Julian. **Nanoparticle and microparticle based delivery systems**. 1. ed. Boca Raton: CRC Press, 2014.

MCCLEMENTS, David Julian; DECKER, Eric. Interfacial Antioxidants: A Review of Natural and Synthetic Emulsifiers and Coemulsifiers That Can Inhibit Lipid Oxidation. **Journal of Agricultural and Food Chemistry**, v. 66, n. 1, p. 20–35, 2018.

MCCLEMENTS, David Julian; PENG, Sheng Feng. Current status in our understanding of physicochemical basis of bioaccessibility. **Current Opinion in Food Science**, v. 31, p. 57–62, 2020.

MEGANAHARSHINI, M. *et al.* Review on recent trends in the application of protein concentrates and isolates – A food industry perspective. **Food and Humanity**, v. 1, p. 308–325, 2023.

MEHTA, Nitin *et al.* Microencapsulation as a Noble Technique for the Application of Bioactive Compounds in the Food Industry: A Comprehensive Review. **Applied Sciences**, v. 12, n. 3, p. 1424, 2022.

MÉNDEZ, Daniel A. *et al.* Sustainable bioactive pectin-based films to improve fruit safety via a circular economy approach. **Food Hydrocolloids**, v. 137, p. 108327, 2023.
NAWAZ, Nida *et al.* Lysozyme and Its Application as Antibacterial Agent in Food Industry. **Molecules**, v. 27, n. 19, p. 6305, 2022.

NEEKHRA, Somya *et al.* Innovative approaches for microencapsulating bioactive compounds and probiotics: An updated review. **Journal of Food Processing and Preservation**, v. 46, n. 11, p. 1–21, 2022.

NISBET, Andrew D. *et al.* The Complete Amino-Acid Sequence of Hen Ovalbumin. **European Journal of Biochemistry**, v. 115, n. 2, p. 335–345, 1981.

NIU, Ben *et al.* Co-encapsulation of chlorogenic acid and cinnamaldehyde essential oil in Pickering emulsion stablized by chitosan nanoparticles. **Food Chemistry: X**, v. 14, p. 100312, 2022.

NOOSHKAM, Majid; VARIDI, Mehdi. Maillard conjugate-based delivery systems for the encapsulation, protection, and controlled release of nutraceuticals and food bioactive ingredients: A review. **Food Hydrocolloids**, v. 100, p. 105389, 2020.

OLDONI, Fernanda C. A. *et al.* Valorization of mangoes with internal breakdown through the production of edible films by continuous solution casting. **LWT**, v. 145, p. 111339, 2021.

OTERO-HERRERA, Ana *et al.* Development of edible films based on sweet potato (*Ipomoea batatas*) starch and their application in candy packaging. **International Journal of Biological Macromolecules**, v. 299, p. 140031, 2025.

OTONI, Caio G. *et al.* Recent Advances on Edible Films Based on Fruits and Vegetables—A Review. **Comprehensive Reviews in Food Science and Food Safety**, v. 16, n. 5, p. 1151–1169, 2017.

OU, Shiyi; KWOK, Kin-Chor. Ferulic acid: pharmaceutical functions, preparation and applications in foods. **Journal of the Science of Food and Agriculture**, v. 84, n. 11, p. 1261–1269, 2004.

PAN, Li *et al.* Effects of fabrication of conjugates between different polyphenols and bovine bone proteins on their structural and functional properties. **Food Bioscience**, v. 52, p. 102375, 2023.

PHILLIPS, G. O.; WILLIAMS, P. A. **Handbook of Food Proteins**. 1. ed. Cambridge: Woodhead Publishing, 2011.

QIN, Xin Sheng; GAO, Qun Yu; LUO, Zhi Gang. Enhancing the storage and gastrointestinal passage viability of probiotic powder (*Lactobacillus plantarum*) through encapsulation with pickering high internal phase emulsions stabilized with WPI-EGCG covalent conjugate nanoparticles. **Food Hydrocolloids**, v. 116, p. 106658, 2021.

QING, Rui *et al.* Protein Design: From the Aspect of Water Solubility and Stability. **Chemical Reviews**, v. 122, n. 18, p. 14085–14179, 2022.

QUAN, Tran Hong *et al.* Protein–polyphenol conjugates: Antioxidant property, functionalities and their applications. **Trends in Food Science and Technology**, v. 91, p. 507–517, 2019.

RANI, Priya *et al.* Material, antibacterial and anticancer properties of natural polyphenols incorporated soy protein isolate: A review. **European Polymer Journal**, v. 152, p. 110494, 2021.

RAYEES, Rahiya *et al.* General approaches to biopolymer-based Pickering emulsions. **International Journal of Biological Macromolecules**, v. 267, p. 131430, 2024.

RAZI, Saeed Mirarab *et al.* An overview of the functional properties of egg white proteins and their application in the food industry. **Food Hydrocolloids**, v. 135, p. 108183, 2023.

REN, Gerui *et al.* The fabrication of novel zein and resveratrol covalent conjugates: Enhanced thermal stability, emulsifying and antioxidant properties. **Food Chemistry**, v. 374, p. 131612, 2022a.

REN, Gerui *et al.* Fabrication of Antioxidant Pickering Emulsion Based on Resveratrol-Grafted Zein Conjugates: Enhancing the Physical and Oxidative Stability. **Foods**, v. 11, n. 23, p. 3851, 2022b.

REQUE, Priscilla Magro; BRANDELLI, Adriano. Encapsulation of probiotics and nutraceuticals: Applications in functional food industry. **Trends in Food Science & Technology**, v. 114, p. 1–10, 2021.

RIBEIRO, Marisa A.; ESTEVINHO, Berta N.; ROCHA, F. Microencapsulation of polyphenols - The specific case of the microencapsulation of *Sambucus nigra* L. extracts - A review. **Trends in Food Science & Technology**, v. 105, p. 454–467, 2020.

ROSS, A. C. **Dietary Reference Intakes for Calcium and Vitamin D**. Washington, D.C.: National Academies Press, 2011.

ROSTAMABADI, Hadis *et al.* Ovalbumin, an outstanding food hydrocolloid: Applications, technofunctional attributes, and nutritional facts, A systematic review. **Food Hydrocolloids**, v. 139, p. 108514, 2023.

SHAHIDI, Fereidoon; DISSANAYAKA, Chandrika Sewwandi. Phenolic-protein interactions: insight from in-silico analyses – a review. **Food Production, Processing and Nutrition**, v. 5, n. 1, p. 2, 2023.

SILVA, Pablo Teixeira da *et al.* Microencapsulation: concepts, mechanisms, methods and some applications in food technology. **Ciência Rural**, v. 44, n. 7, p. 1304–1311, 2014.

SONG, Haizhao *et al.* Pectin: Structural Characteristics, ADME Profiles, and Their Interrelationship. **Chemistry & Biodiversity**, v. 22, n. 6, p. e202402532, 2025.

SULJAGIC, Jasmin; BRATOVCIC, Amra. Micro- and nano-encapsulation in food industry. **Croatian journal of food science and technology**, v. 11, n. 1, p. 113–121, 2019.

SUN, Xiaohong; SARTESHNIZI, Roghayeh Amini; UDENIGWE, Chibuike C. Recent advances in protein–polyphenol interactions focusing on structural properties related to antioxidant activities. **Current Opinion in Food Science**, v. 45, p. 100840, 2022.

SUN, Ying *et al.* Preparation and characterization of lactoferrin-polyphenol conjugate with stabilizing effects on fish oil high internal phase Pickering emulsions. **Food Chemistry: X**, v. 24, p. 101836, 2024.

TAMILVANAN, S. Oil-in-water lipid emulsions: Implications for parenteral and ocular delivering systems. **Progress in Lipid Research**, v. 43, n. 6, p. 489–533, 2004.

THONGZAI, Hataikan *et al.* Interfacial Properties and Antioxidant Activity of Whey Protein-Phenolic Complexes: Effect of Phenolic Type and Concentration. **Applied Sciences**, v. 12, n. 6, p. 2916, 2022.

TSAO, Rong. Chemistry and Biochemistry of Dietary Polyphenols. **Nutrients**, v. 2, n. 12, p. 1231–1246, 2010.

ULRIH, Nataša Poklar. Analytical techniques for the study of polyphenol–protein interactions. **Critical Reviews in Food Science and Nutrition**, v. 57, n. 10, p. 2144–2161, 2017.

WANG, Yan *et al.* Insights into interactions between food polyphenols and proteins: An updated overview. **Journal of Food Processing and Preservation**, v. 46, n. 5, p. e16733, 2022.

WILSON, Louise R. *et al.* Vitamin D deficiency as a public health issue: using vitamin D2 or vitamin D3 in future fortification strategies. **Proceedings of the Nutrition Society**, v. 76, n. 3, p. 392–399, 2017.

WISEMAN, Elina Manusevich; BAR-EL DADON, Shimrit; REIFEN, Ram. The vicious cycle of vitamin a deficiency: A review. **Critical Reviews in Food Science and Nutrition**, v. 57, n. 17, p. 3703–3714, 2017.

WU, Tiantian *et al.* What is new in lysozyme research and its application in food industry? A review. **Food Chemistry**, v. 274, p. 698–709, 2019.

XIAO, Liyuan *et al.* Development of β-carotene microcapsules based on collagen peptides: Improving bioaccessibility and application in functional biscuits. **Journal of Food Engineering**, v. 407, p. 112842, 2026.

XU, Haoxie *et al.* Effect of chlorogenic acid covalent conjugation on the allergenicity, digestibility and functional properties of whey protein. **Food Chemistry**, v. 298, p. 125024, 2019.

XUE, Yu Ting *et al.* Effect of ferulic acid covalent conjugation on the functional properties and antigenicity of β-lactoglobulin. **Food Chemistry**, v. 406, p. 135095, 2023.

YAN, Xiaojia *et al.* Protein-stabilized Pickering emulsions: Formation, stability, properties, and applications in foods. **Trends in Food Science and Technology**, v. 103, p. 293–303, 2020.

YANG, Xi *et al.* An overview of classifications, properties of food polysaccharides and their links to applications in improving food textures. **Trends in Food Science & Technology**, v. 102, p. 1–15, 2020.

YE, Qianyu; GEORGES, Nicolas; SELOMULYA, Cordelia. Microencapsulation of active ingredients in functional foods: From research stage to commercial food products. **Trends in Food Science and Technology**, v. 78, p. 167–179, 2018.

YE, Yang *et al.* Pickering emulsions stabilized with SPI-Cur conjugates: Effects on storage, gastrointestinal viability of *Lactobacillus plantarum*. **LWT**, v. 217, p. 117379, 2025.

YIN, Yongpeng *et al.* Lysozyme-(-)-epigallocatechin gallate covalent conjugates: preparation, structure and functional properties. **Journal of Food Measurement and Characterization**, v. 18, n. 6, p. 4741–4750, 2024.

ZHANG, Bingyan; WANG, Yunping; LU, Rongrong. Pickering emulsion stabilized by casein–caffeic acid covalent nanoparticles to enhance the bioavailability of curcumin *in vitro* and *in vivo*. **Journal of the Science of Food and Agriculture**, v. 103, n. 7, p. 3579–3591, 2023.

ZHANG, Qiaozhi *et al.* Dietary protein-phenolic interactions: characterization, biochemical-physiological consequences, and potential food applications. **Critical Reviews in Food Science and Nutrition**, v. 61, n. 21, p. 3589–3615, 2021.

ZHANG, Yun *et al.* Probiotic encapsulation in water-in-oil high internal phase emulsions: Enhancement of viability under food and gastrointestinal conditions. **LWT**, v. 163, p. 113499, 2022.

ZHAO, Weiping *et al.* pH-modulated pea protein-β-glucan and carboxymethyl chitosan double-layer complex coacervate microcapsules: Efficient vitamin D3 encapsulation and functional fortification of surimi. **International Journal of Biological Macromolecules**, v. 311, p. 143472, 2025.

ZHAO, Xinlei *et al.* Construction of vitamin D delivery system based on pine nut oil Pickering emulsion: effect of phenols. **Journal of the Science of Food and Agriculture**, v. 103, n. 8, p. 4034–4046, 2023.

ZHAO, Xinru; LI, Chen; XUE, Feng. Effects of whey protein-polyphenol conjugates incorporation on physicochemical and intelligent pH-sensing properties of carboxymethyl cellulose based films. **Future Foods**, v. 7, p. 100211, 2023.

CAPÍTULO II. IMPACT OF THE COVALENT INTERACTION BETWEEN FERULIC ACID AND OVALBUMIN ON THE STRUCTURE AND FUNCTIONAL PROPERTIES OF THE PROTEIN

Publicado em 2025 na *Food Biophysics*

DOI: https://doi.org/10.1007/s11483-024-09919-6

Abstract

Protein-polyphenol conjugates, formed through chemical modifications, can alter the structure of proteins, thereby enhancing their functional properties and enabling the development of novel ingredients for diverse applications. Despite this potential, the covalent conjugation of ovalbumin (OVA) with ferulic acid (FA) and the determination of their optimal binding ratios have not been previously studied. To address this gap, we investigated the formation of OVA-FA conjugates using an alkaline method and identified an optimal ratio of 0.9 g of FA per g of OVA. The resulting conjugates displayed substantial alterations in the secondary and tertiary structures of OVA, increased hydrophobicity, and a higher molar mass. These structural modifications significantly improved the solubility, emulsification capacity, and foam-forming ability of OVA, while also enhancing its antioxidant activity compared to the unmodified protein. These findings demonstrate the potential of OVA-FA conjugates as multifunctional emulsifiers with antioxidant properties, broadening their applications in the food and nutraceutical industries.

Keywords: conjugate, polyphenol, protein, antioxidant activity, alkaline method, techno-functional properties.

1 Introduction

Egg is one of the main sources of protein in the human diet, it is composed of shell, yolk and white. Ovalbumin (OVA) is one of the main egg proteins, representing about 55% of the egg white mass, it is a glycoprotein with a molar mass of 45 kDa and has 385 amino acid residues [1]. Ovalbumin is recognized for its high nutritional value, serving as a rich source of essential amino acids. Its abundance in egg whites and ease of accessibility make it a cost-effective option for various applications [2,3]. Additionally, it holds significant importance in the food industry due to its diverse techno-functional properties, such as the ability to form gels, emulsions and its ability to form and stabilize foams. These characteristics are due to its amino acid composition, which is made up of approximately 50% hydrophobic amino acids [2,4].

The compound 4-hydroxy-3-methoxycinnamic acid, known as ferulic acid (FA), is a polyphenol from the category of phenolic hydroxycinnamic acids, having only one benzene ring and three carbons forming a side chain, creating a C6-C3 structure, its molar mass is 194.18 g/mol [5,6]. It is an abundant substance in nature, being found in several natural sources such as wheat, rice and corn, and found mainly in the cell walls of vegetables [7]. It has a notable antioxidant activity that is also accompanied by preventive properties in relation to cardiovascular diseases, cancer, diabetes, and other [8,9]. However, its use in industry is limited due to its low solubility and low bioavailability [5].

The chemical modification of proteins together with polyphenols is called conjugate, it is non-reversible and occurs from a C-N and C-S covalent bond, which occurs in the nucleophilic residues of proteins, mainly in the amino acids methionine, lysine, tryptophan and cysteine [10]. One of the most common techniques for the formation of conjugates between proteins and polyphenols is the alkaline method [11], which is defined by exposing polyphenols to alkaline environments with a pH close to 9.0. In this situation, these compounds begin an oxidation reaction, which rearranges their structure to a highly reactive substance, quinones, which bind to the amino acid groups of the protein [11,12]. The alkaline method is a simple and efficient technique for conjugating proteins with phenolics, it requires fewer reagents and steps than the free radical method and offers a more cost-effective alternative to enzymatic methods, making it a suitable approach for protein modification[11–13]. Chemical interactions are intended to improve the functional capabilities of ovalbumin and add new capabilities to the protein, such as the ability to form and stabilize emulsions, form and stabilize foams, increase solubility, and modify its biological properties, such as increasing antioxidant capacity and antimicrobial, in addition to altering its allergenic properties and bioaccessibility [11,13]. Protein-polyphenol conjugates have the capacity to generate new ingredients for various

technological applications, these with new characteristics or better techno-functional properties. With the conjugation, it was possible to improve the emulsifying and foaming capabilities of ovalbumin [3] and increase its antioxidant capacity [14]. Conjugates formed between ferulic acid and β-lactoglobulin were also reported in the literature, which showed an increase in the emulsion capacity and antioxidant activity of the protein [15].

Several studies have investigated the interaction between ovalbumin and ferulic acid [16–18]. However, these studies focus on elucidating physical interactions (formation of complexes), no studies were found that study the formation of conjugates between these biomolecules. Consequently, the present study aims to investigate the formation of conjugates using the alkaline method with ferulic acid and ovalbumin. This investigation includes assessing the influence of ferulic acid concentration on its binding capacity to ovalbumin, as well as examining alterations in the protein's secondary and tertiary structures, which was accessed by circular dichroism and intrinsic fluorescence analysis, respectively. Additionally, we explore the effects of conjugation on techno-functional properties such as solubility, emulsification capacity, and foam stability. The potential applications of this approach include future developments in food systems, where it could enhance emulsifying stability while delivering antioxidant benefits. These findings open avenues for further research into its use in functional foods and innovative food formulations.

2 Material and Methods

2.1 Material

Ferulic acid, ovalbumin (62-88% purity), Folin-Ciocalteu, 5,5'-dithiobis-(2-nitrobenzoic acid (DTNB), ethylenediamine tetraacetic acid (EDTA), bromophenol blue, acrylamide, 2,2-diphenyl-1-picrylhydrazyl (DPPH), acid 2 ,2′-azino-bis (3-ethylbenzothiazoline-6-sulfonic acid) (ABTS), were obtained from Sigma-Aldrich® (St. Louis, USA). Soybean oil used in this study was obtained from the local market (Rio de Janeiro, Brazil) with a refractive index of 1.47. The compound tetramethyl ethylenediamine (TEMED), the brilliant blue dye Coomassie G-250 and the molecular weight standard for electrophoresis (10-250 KDa, 4-20% gel) were purchased from Bio-Rad (California, USA). Analytical grade ultrapure water with conductivity 0.05 μS/cm (Gehaka, Master-P&D, Brazil) was used in in all solutions.

2.2 Formation of OVA-FA Conjugates

The procedure to form the conjugate between the OVA and FA proteins using the alkaline method followed the method described by He *et al.* [3]. An aqueous solution of OVA was prepared at a concentration of 5 mg/mL, and the pH was adjusted to 9.0 using NaOH. The pH was measured using a pH meter (PG2000, Gehaka, Brazil). After the pH adjustment, the solution was kept under agitation for 2 hours.

Then, different concentrations of FA were added into the OVA solution to reach a concentration ranging from 0.2 to 1.0 g FA/g OVA. The addition was carried out under continuous stirring using a magnetic stirrer (HS7, IKA, Germany) at room temperature and the solution was stirred for 24 hours. Afterwards, unbound FA was removed by dialysis (D9527, Sigma Aldrich, USA) over 48 hours. The resulting solution was frozen using liquid nitrogen (-160 ºC) and then lyophilized (Enterprise I, Terroni, Brazil).

2.3 Determination of FA Binding Equivalent Capacity to OVA

The Folin-Ciocalteu method adapted by Hu *et al.* [19] was used to evaluate the total content of phenols linked to OVA. OVA and OVA-FA samples (0.5 mL, 1 mg/mL) were solubilized in Folin-Ciocalteu reagent (2.5 mL, 0.2 mol/L) in the dark for a period of 5 minutes. Subsequently, a sodium carbonate solution (2 mL, 7.5% w/v) was added, and the mixture was left to rest for 2 hours. Absorbance measurement was performed at 760 nm using a Biomate 3S spectrophotometer (Thermo Fisher Scientific, USA), ultrapure water was used as a blank. The FA content bound in the conjugates was calculated using the FA standard curve and expressed as mg of FA equivalents per g (mg FA/g of OVA-FA) for each of the concentrations evaluated.

The relationship between the concentration of equivalent bound ferulic acid (FA) in the FA-OVA conjugate prepared (mg FA/g) and various ferulic acid concentrations used in the preparation was plotted on an S- type curve [20,21] defined by the following Equation:

$$C = \frac{q_m}{1+\left(\frac{x}{a}\right)^b} \qquad (1)$$

where the coefficients a and b are model parameters, the parameter q_m (mg FA/g) is the maximum capacity of FA bound to OVA, C is the concentration identified after the Folin-Ciocalteu method (mg FA/ g), x is initial concentration of the phenolic compound in g FA/g OVA.

The model standard deviation (SD) and relative sum of squared errors (RSSE) values were used to evaluate the adjustment of Equation 10 to the experimental data [22], they are described in Equations 11 and 12:

$$SD\ (mg\ FA/\ g) = \left(\frac{\sum_{i=1}^{m}(C_{exp,i}-C_{calc,i})^2}{m-p}\right)^{0,5} \quad (2)$$

$$RSSE\ (\%) = \frac{100}{m}\left(\sum_{i=1}^{m}\left(\frac{\left|(C_{exp})^2-(C_{exp,i}-C_{calc,i})^2\right|}{C^2{}_{exp,i}}\right)\right) \quad (3)$$

where C_{exp} and C_{calc} are experimental and calculated values of the concentration identified after the Folin-Ciocalteu method (mg FA/g), m is the number of experimental points of the model and p is the number of adjusted parameters.

2.4 Determination of the Thiol Sulfhydryl Group

Thiol sulfhydryl groups (SH) were observed using the methodology adapted from Pan *et al.* [23], in which a solution of 5 mg/mL of DTNB (Ellman's reagent) was dissolved in a buffer solution of 0.086 mol/ L Tris, 0.09 mol/L glycine and 4 mmol EDTA, at pH 8.0. Samples of OVA and OVA-FA were mixed with the same buffer solution at a concentration of 3 mg/mL Then, 50 mL of the reagent and 5 mL of the protein solutions were mixed and stirred for 30 minutes, the absorbance was recorded on a spectrophotometer at a wavelength of 412 nm. The number of thiol groups was determined by Equation:

$$\text{Sulfhydryl group}\ (\mu\text{mol/g}) = \frac{73,53\times A}{C} \quad (4)$$

where A is the recorded absorbance and C is the sample concentration.

2.5 Structural Analysis of the OVA-FA Conjugate

2.5.1 SDS-PAGE

Sodium dodecyl sulfate-polyacrylamide gel electrophoresis (SDS-PAGE) was conducted following the adapted protocol of He *et al.* [3]. One milliliter of OVA and OVA-FA samples (2.5 mg/mL) was combined with 1 mL of 2 x loading buffer (2% w/v SDS, 25% w/v glycerol, 12.5% w/v Tris(hydroxymethyl) aminomethan 0.5 mol/L pH 6.8, 0.1% w/v bromophenol blue, and 5% w/v mercaptoethanol). Subsequently, the samples were heated at 90 ºC for 5 minutes. The heated solutions were then loaded into the wells of a polyacrylamide gel (12% resolving gel and 5% stacking gel). Electrophoresis was conducted at a constant voltage

of 150 V using an electrophoresis apparatus (K33, Kasvi, Brazil). The gel was stained with Coomassie Blue G-250 for 30 minutes.

2.5.2 Circular dichroism

Circular dichroism (CD) analysis was conducted at 25 ºC following the protocol described by He *et al.* [3]. Solutions of ovalbumin (OVA) and the OVA-FA conjugate were prepared at a concentration of 0.2 mg/mL in phosphate-buffered saline (PBS) pH 7.4. Far-UV CD spectra were recorded from 200 to 250 nm with a spectral resolution of 0.2 nm and a scan speed of 100 nm/min using a Chirascan spectropolarimeter (Applied Photophysics, UK) equipped with a 1 mm path-length quartz cuvette. Data analysis was performed using the DICHROWEB tool [24].

2.5.3 FTIR

A Fourier transform infrared spectrophotometer (Bruker, Vertex 70, Germany) was used to analyze the OVA and OVA-FA samples. The spectrum obtained was analyzed in the range from 4000 to 400 cm-1.

2.5.4 Surface hydrophobicity

The surface hydrophobicity of the OVA and OVA-FA samples was obtained using the methodology adapted from Yu *et al.* [25]. Initially, a solution of 200 µL of bromophenol blue (1 mg/mL) was mixed with the samples (5 mg/mL) using a magnetic stirrer for 10 minutes. After that, the solutions were centrifuged at 5,600 g for 15 minutes at 4 ºC. Ultrapure water was used as control. Absorbance values were recorded with a spectrophotometer at 595 nm. The surface hydrophobicity values were determined by the Equation:

$$\text{Hydrophobicity (µg)} = \frac{200 \times (A_C - A_S)}{A_C} \qquad (5)$$

where A_c is the absorbance recorded by the control and A_s the absorbance of the sample.

2.5.5 UV-VIS

The UV-VIS spectra of the samples were determined according to the adapted methodology of He *et al.* [3]. The reading was taken in the wavelength range from 230 to 450 nm in a spectrophotometer, the samples read had a concentration of 1 mg/mL for OVA and OVA-FA and 0.2 mg/mL for pure FA.

2.5.6 Fluorescence

For the analysis of intrinsic fluorescence emission, the methodology of Cheng *et al.* [26] was adopted. Samples containing OVA-FA and OVA (0.2 mg/mL) were subjected to analysis using an RF-5301 PC Spectrofluorometer (Shimadzu, Japan). Excitation was performed at a wavelength of 280 nm, with analysis being conducted in the range of 300 to 400 nm.

2.5.7 Particle Size and Zeta Potential

The hydrodynamic diameter (in nanometers) of the OVA and OVA-FA solutions (1 mg/mL) and their zeta potential were determined using a Zetasizer Nano ZS90 (Malvern Instruments, UK) with a He-Ne laser at 25°C following the methodology described by Ju *et al.* [27].

2.6 Techno-Functional Properties

2.6.1 Solubility

Solubility was determined using the adapted method of Xu *et al.* [28]. The OVA and OVA-FA samples (1 mg/mL) were solubilized using a magnetic stirrer for 2 hours After that, 2 mL aliquots were centrifuged (Digicen 21R, OrtoAlresa, Spain) at 5.900 g for 10 minutes. Protein concentrations were determined before and after centrifugation using the Bradford method. Solubility was obtained using the Equation:

$$\text{Solubility (\%)} = \frac{C_f}{C_0} \qquad (6)$$

where C_0 is the concentration before centrifugation and C_f is the concentration obtained after the centrifugation.

2.6.2 Emulsion properties

The emulsion capacity index (EAI) and the emulsion stability index (ESI) were identified using the methodology adapted from Ren *et al.* [29]. Emulsions were formed using an UltraTurrax T25 homogenizer (IKA, Germany) by mixing 10 mL of protein solution (1 mg/mL) and 0.5 mL of soybean oil, homogenization was carried out at 10,000 RPM for 2 minutes. Soon after, 50 □L of emulsion was mixed with 4.95 mL of 10% w/v SDS. Another 50 □L aliquot was removed after 10 minutes of emulsion formation. The absorbance values of these solutions were identified at 500 nm obtained using a spectrophotometer. The EAI and ESI values were obtained using Equations:

$$\text{EAI } (m^2/g) = \frac{4{,}606 \times A_0 \times D}{N \times C \times 10000} \quad (7)$$

$$\text{ESI } (minutes) = \frac{A_0 \times T}{A_0 - A_{10}} \quad (8)$$

where A_0 and A_{10} is the absorbance recorded immediately after the emulsion and after 10 minutes of rest, D is the dilution factor (100), N is the oil/water ratio in the emulsion (0.048), C is the sample concentration (0.001 g/ mL) and T is the resting time in minutes.

2.6.3 Foam Properties

The foam properties of the proteins studied were obtained using the methodology adapted from Chang *et al.* [30]. Solutions of 12.5 mL (5 mg/mL) of OVA and OVA-FA were prepared at pH 6.5 and were placed in 25 mL beakers and homogenized by UltraTurrax T25 at 10,000 rpm for 2 minutes. The foam volume was measured immediately after finishing homogenization and after 30 minutes of rest. The values of foaming capacity (FC) and foam stability (FS) were found by Equations:

$$\text{FC } (\%) = 100\% \times \frac{V_1}{V} \quad (9)$$

$$\text{FS } (\%) = 100\% \times \frac{V_2}{V_1} \quad (10)$$

where V is the initial volume of the protein before homogenization, V1 is the volume of the foam immediately after homogenization and V2 is the volume of the foam after 30 minutes of rest.

2.7 Antioxidant Activity

2.7.1 DPPH radical scavenging activity determination

The radical scavenging activity determined by the DPPH method was obtained using the adapted methodology of Pan *et al.* [23], in which 2.5 mL of the OVA and OVA-FA solution (0.5 mg/mL) were mixed with 1 mL of DPPH reagent (1.75 x 104 M). The samples were incubated in the dark for 30 minutes, and finally, the absorbance values were measured by a spectrophotometer at 517 nm. Ultrapure water was used as control. The DPPH radical scavenging activity was calculated by the Equation:

$$\text{DPPH scavenging } (\%) = 100\% \times \left(1 - \frac{A_S}{A_c}\right) \quad (11)$$

where A_s is the absorbance recorded by the sample and A_c is the absorbance of the control.

2.7.2 ABTS radical scavenging activity determination

For the ABTS radical scavenging method, the methodology from Ren *et al.* [29] was adapted. Initially, potassium persulfate (2.45 mmol/L) and ABTS (7 mmol/L) solutions were mixed in a 1:1 ratio and stored in the dark overnight to produce free radicals. After that, 0.5 mL (0.25 mg/mL) solutions of OVA and OVA-FA are mixed with 2 mL of the ABTS solution and stored in the dark to react for one hour. Finally, absorbance values were recorded by a spectrophotometer at 734 nm. Ultrapure water was used as control. ABTS radical scavenging activity was determined by Equation:

$$\mathrm{ABTS}^{+}\text{scavenging}\ (\%) = 100\% \times \left(1 - \frac{A_s}{A_c}\right) \qquad (12)$$

where A_s is the absorbance recorded by the sample and A_c is the absorbance of the control.

2.8 Statistical analysis

Data evaluation was carried out using Tukey analysis and analysis of variance using the SISVAR®5.6 program, with a significance level of ($p < 0.05$). The experiments were performed in triplicate, and the results were presented as mean ± standard deviation.

3 Results and Discussion

3.1 Ferulic Acid Binding Capacity

Figure 14 presents the concentration of equivalent bound ferulic acid (FA) in the FA-OVA conjugate (mg FA/g) as a function of various ferulic acid concentrations (0.2~1 g FA/g OVA). The concentration of ferulic acid was determined using the Folin-Ciocalteu method. In an alkaline environment, provided by sodium carbonate, the phenolic proton dissociates, leading to the formation of a phenolate ion. This phenolate ion reduces the Folin-Ciocalteu reagents, producing a blue-colored complex [31]. The intensity of the blue color is directly proportional to the phenolic concentration and was quantified using a spectrophotometer.

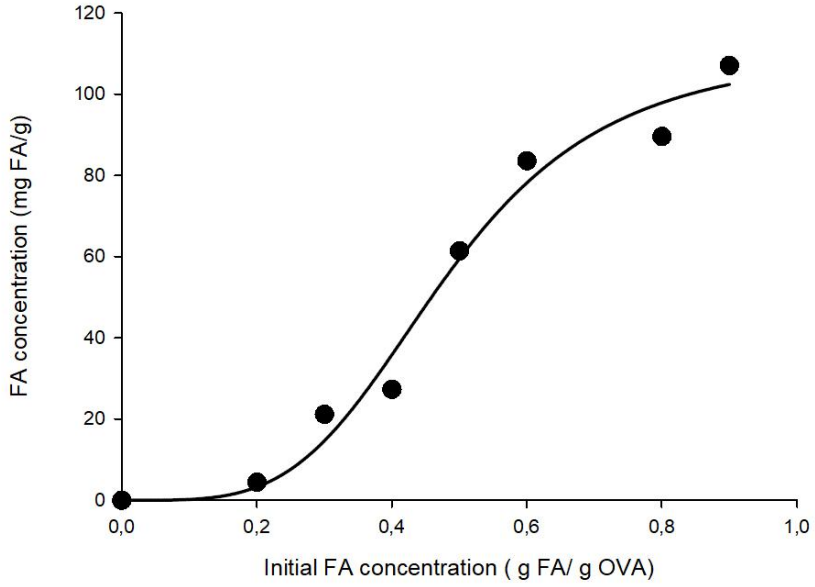

Figure 14. S-type model (Equation 10) of the binding capacity of ferulic acid in the OVA-FA conjugate as a function of the initial concentration of FA added to the system.

This figure shows an increase in FA bound to the conjugate as the FA content per gram of OVA increases, tending to stabilize at 0.8 g FA/g OVA. Similar behavior was observed in the literature, Thongzai *et al.* [32] reported the same behavior in conjugates formed between FA and whey proteins. Additionally, Wang *et al.* [33] observed that up to 25% FA concentration in rice bran protein conjugates resulted in a corresponding increase in FA concentration. However, none of these studies proposed identifying a maximum value for this concentration. This figure shows S-type model (Equation 1), which was employed to fit the experimental data of FA binding per gram of OVA.

The S-type model showed a good fit to the experimental data, presenting an SD of 6.92 mg FA/g and an RSSE of 96.65%. The parameters obtained by the model, qm, a and b, were defined as 111.06, 0.4822, and -3.9699, respectively.

Increasing the initial FA concentration gradually raises the final ferulic acid concentration in the conjugate until a maximum is reached, beyond that point, no significant change is observed. This point is identified by the parameter qm being 111.06 mg FA/g. This maximum point can be explained by the formation of dimers generated by the high concentration of ferulic acid in the system, preventing further binding of ferulic acid to the protein [15]. Thus, the maximum binding point obtained by the S-type model corresponds approximately to an initial concentration ratio of 0.9 g FA/g OVA.

The values of free SH groups are presented in Figure 15 and indicate a decrease in SH content with the increase in the concentration of added FA. This is due to the quinones formed

from the oxidation of FA interacting with the SH groups of ovalbumin, forming C-S bonds, thereby decreasing the amount of free SH groups in the system [26]. The SH groups are one of the main binding sites between polyphenols and proteins. The ovalbumin has four free SH groups, as out of its six cysteine residues in its structure, only two are involved in disulfide bonds [34], thus, identifying the free SH groups is an important factor for determining the formation of OVA-FA conjugates. After the concentration of ferulic acid exceeds 0.7 g FA/g OVA, no significant decreases in SH groups are observed, which may indicate that most of the binding sites have already been utilized for covalent binding.

The reduction of SH groups due to covalent binding between proteins and phenolic compounds is well-documented in literature. Chang *et al.* [30] identified a decrease in SH groups in OVA-caffeic acid complexes, as the concentration of caffeic acid increased, the amount of free SH decreased by about 36% and stabilized. Xue *et al.* [15] also observed a decrease in SH groups in β-lactoglobulin after conjugation with ferulic acid, identifying a maximum interaction point at a ratio of 0.6 g FA/g β-lactoglobulin. The reduction of SH groups may indicate the formation of OVA-FA conjugates.

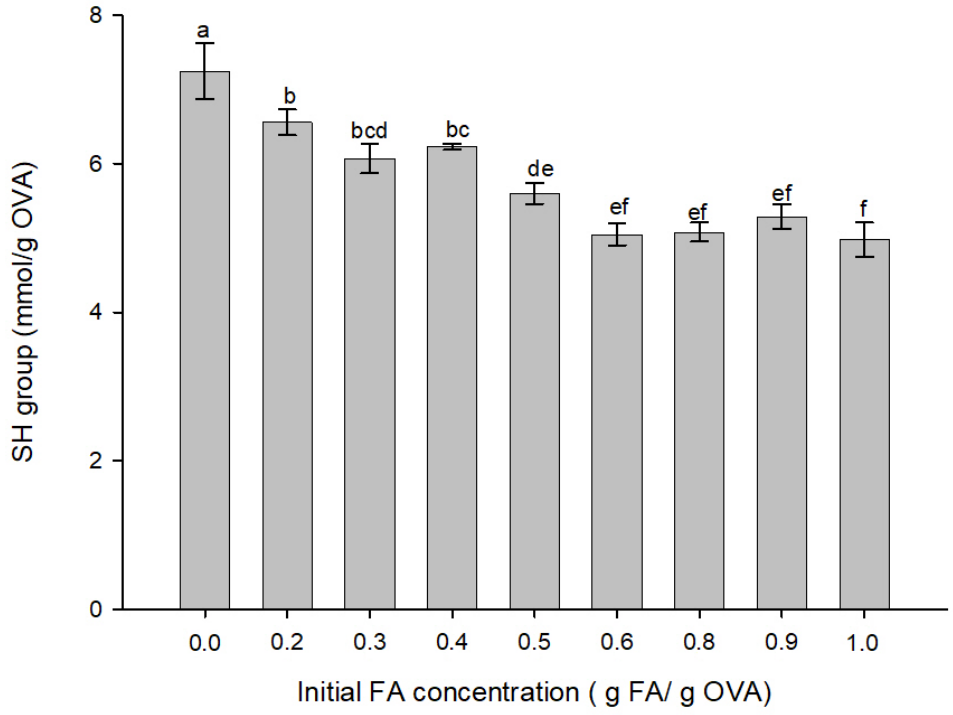

Figure 15. Free SH groups in control ovalbumin and in OVA-FA conjugates formed from different initial concentrations of FA added to the system. Values followed by the same letters do not present statistically significant difference in the Tukey test ($p < 0.05$).

The S-type model (Equation 1) suggests that the maximum binding capacity of FA with OVA is at a ratio close to 0.9 g FA/g OVA. This FA/OVA ratio is also observed by the reduction in free SH groups, as beyond the ratio of 0.8 g FA/g OVA, there are no significant differences in free SH groups, defining 0.9 g FA/g OVA as the ideal point for conjugate formation, with its maximum ferulic acid binding capacity. Therefore, the concentration of 0.9 g FA/g OVA was used in subsequent studies on the structure and functional properties of the conjugate, referred to as the OVA-FA conjugate.

3.2 Structural Analysis of the OVA-FA Conjugate.

Figure 16 presents the electrophoretic diagram of OVA and the OVA-FA conjugate. The SDS-PAGE analysis aims to identify the protein structure, in the diagram, it can be observed that the analyzed OVA presented three distinct bands. The main band, in the range of 45 kDa, corresponds to ovalbumin, the principal component of the analyzed protein. However, there are residues of other proteins, indicated by a higher band in the range of 75 kDa, corresponding to ovotransferrin, and a smaller band around 15 kDa, corresponding to lysozyme. Upon analyzing the OVA-FA conjugate, a shift in the main band to a higher position compared to OVA is observed, due to the increased molar mass of the conjugate compared to OVA. This shift is attributed to polyphenols covalently binding to the protein, altering its structure and increasing its molar mass [12]. Other studies have also reported an increase in molar mass due to the conjugation between proteins and phenolic compounds using the SDS-PAGE technique [3,23,35] Since SDS and mercaptoethanol used in sample preparation are reagents capable of breaking non-covalent bonds in a [15], it is identified that the binding between ferulic acid and ovalbumin in this study is indeed covalent.

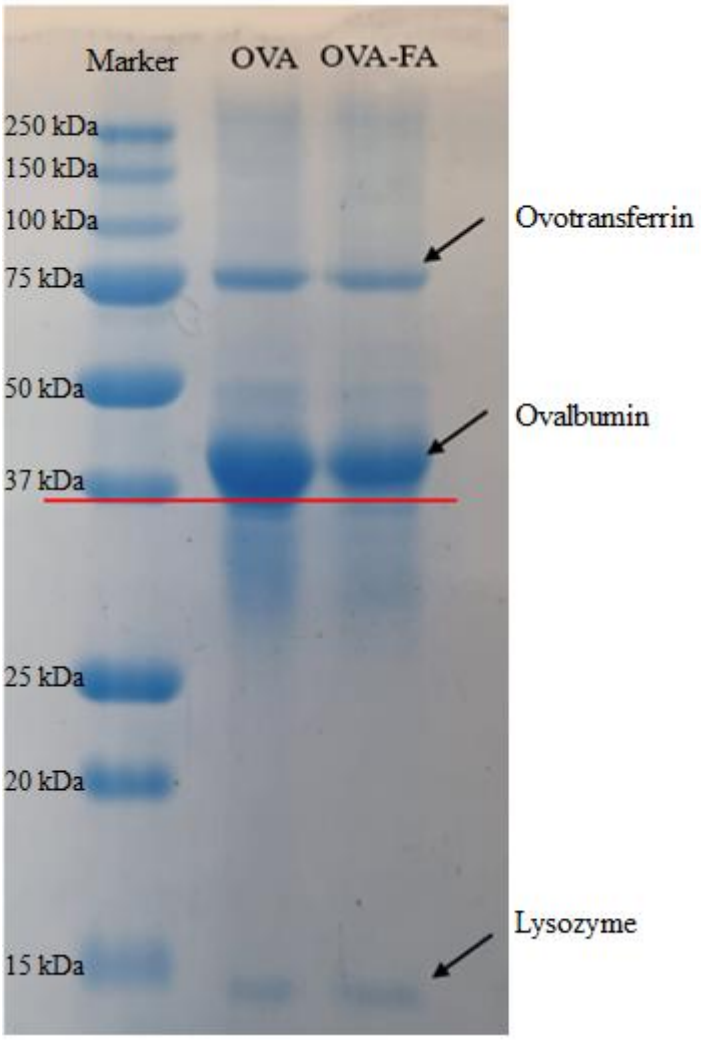

Figure 16. SDS-PAGE (12% resolution gel) of control ovalbumin and OVA-FA conjugate.

The CD spectra of OVA and the OVA-FA conjugate are presented in Figure 17. In this figure, it is observed that the absolute value of ellipticity of the OVA-FA conjugate decreased, indicating a modification in the secondary structure, specifically a decrease in the α-helix content of the protein. DICHROWEB analysis using the CDSSTR algorithm [36] showed that OVA has the following distribution of secondary structure components: 41% α-helix, 31% β-sheets, 7% β-turns, and 21% disordered structures. After conjugation, there was a decrease in α-helix structures to 37%, approximately a 10% reduction from the initial value, with an increase in β-sheets and β-turns to 34% and 9%, respectively. This phenomenon was also identified by Lu et al [37], who observed a decrease of about 12% in the α-helix fraction of ovalbumin when conjugated with chlorogenic acid.

Far UV CD spectra of control ovalbumin (green) and the OVA-FA conjugate (purple).

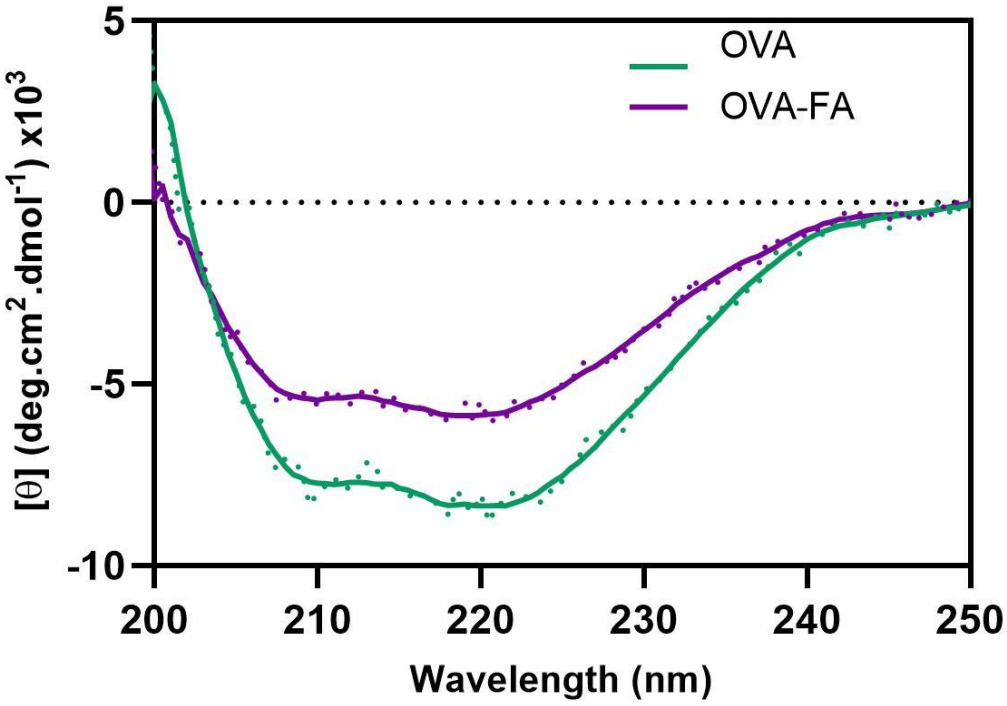

Figure 17. Far UV CD spectra of control ovalbumin (green) and the OVA-FA conjugate (purple).

Figure 18 presents the FTIR spectra for OVA and OVA-FA in the 3,500 to 1,000 cm-1 mid-IR region. The amide I region spans from 1600 to 1700 cm-1 [38,39], OVA exhibits a peak at 1635.43 cm-1, while the OVA-FA conjugate shows a peak at 1633.51 cm-1. A peak shift in the amide II region, around 1530 cm-1 [38,39], was observed, where the OVA peak of 1529.36 shifted to 1523.58 for the OVA-FA conjugate. The amide I and amide II bands are directly related to the secondary structure of a protein [39], the peak shifts in OVA-FA compared to OVA indicate a change in the protein's secondary structure, as also indicated by circular dichroism analysis.

The region around 1400 cm-1, associated with C-N bonds in the protein, showed a peak shift from 1392.43 for OVA to 1386.65 for OVA-FA. The N-H bonds in proteins, peaking around 3300 cm-1, were observed at 3280.52 and 3278.59 for OVA and OVA-FA, respectively. The shifts in peaks at 1400 cm-1 and 3400 cm-1 define a change in the atomic bonds within the structure [38,39], indicating that ferulic acid bound to the ovalbumin structure.

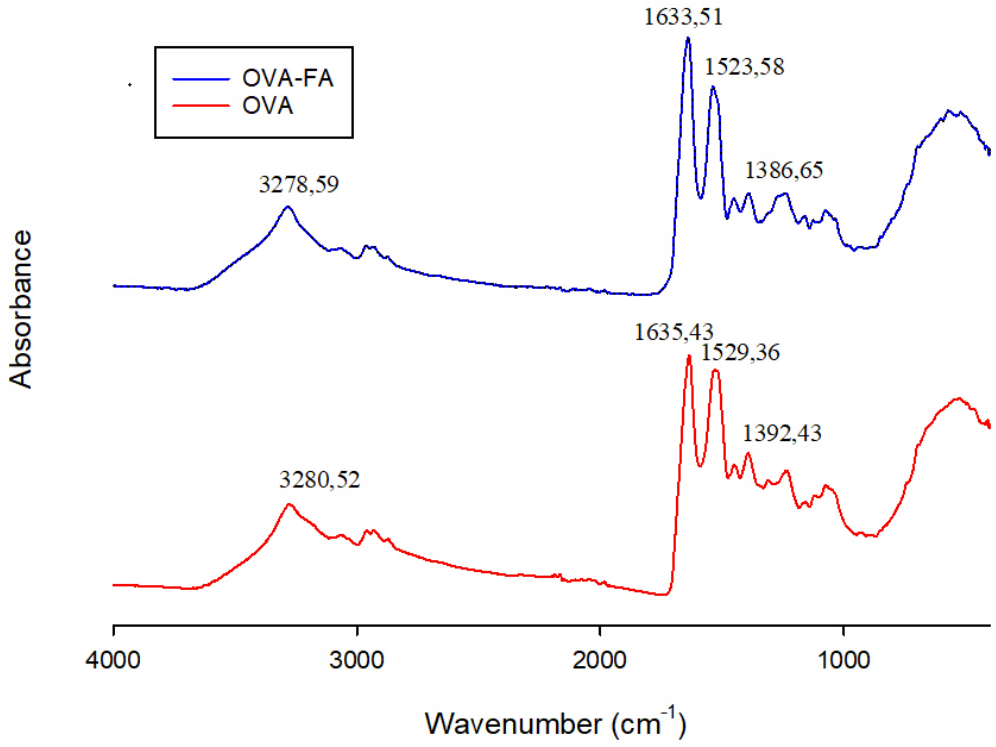

Figure 18. FTIR spectra of ovalbumin (red) and OVA-FA conjugate (blue). Peaks are shown by arrows.

In the surface hydrophobicity analyses, control OVA presented a hydrophobicity of 19.46 ± 1.39 µg, while the OVA-FA conjugate showed a significant increase in hydrophobicity, observed at 68.68 ± 2.07 µg. This increase is due to the addition of ferulic acid to the protein structure, modifying and exposing its hydrophobic sites. This effect is also reported in studies by Xue *et al.* [15], which identified a substantial increase in surface hydrophobicity in β-lactoglobulin and ferulic acid conjugates. Feng *et al.* [40] also identified an almost threefold increase in hydrophobicity in conjugates formed by ovalbumin and epigallocatechin gallate (EGCG).

The fluorescence intensity is presented in Figure 19. The primary residues responsible for fluorescence at 280 nm are tyrosine and tryptophan [41]. Ovalbumin has 10 tyrosine residues and 3 tryptophan residues in its sequence [42]. The interaction of proteins with polyphenols modifies the intrinsic fluorescence of the system. After conjugation, fluorescence intensity decreased, indicating that tyrosine and tryptophan residues were affected by covalent interaction with ferulic acid, thereby reducing their fluorescence [28]. Moreover, the exposure of these residues to a more polar environment, such as the solvent, contributes to the reduction in fluorescence intensity [40]. A red shift is also observed, with the ovalbumin fluorescence

peak shifting from 337 nm to 339 nm (Figure 19, dashed line), indicating a change in the environment of the residue, transitioning from a nonpolar to a more polar environment, suggesting ovalbumin unfolding and a change in its tertiary structure. He *et al.* [3] identified a decrease in fluorescence intensity and a red shift of 1.4 nm in the conjugation between ovalbumin and EGCG.

The fluorescence spectroscopy analysis is further supported by the increase in surface hydrophobicity, as ferulic acid conjugation exposes additional hydrophobic residues of the ovalbumin. This exposure alters the local environment of tyrosine and tryptophan residues, leading to reduced fluorescence due to their interaction with the more polar medium [40]. The increased surface hydrophobicity, resulting from the exposure of these hydrophobic residues, aligns with the structural changes observed in the fluorescence spectroscopy, providing additional evidence of protein modification.

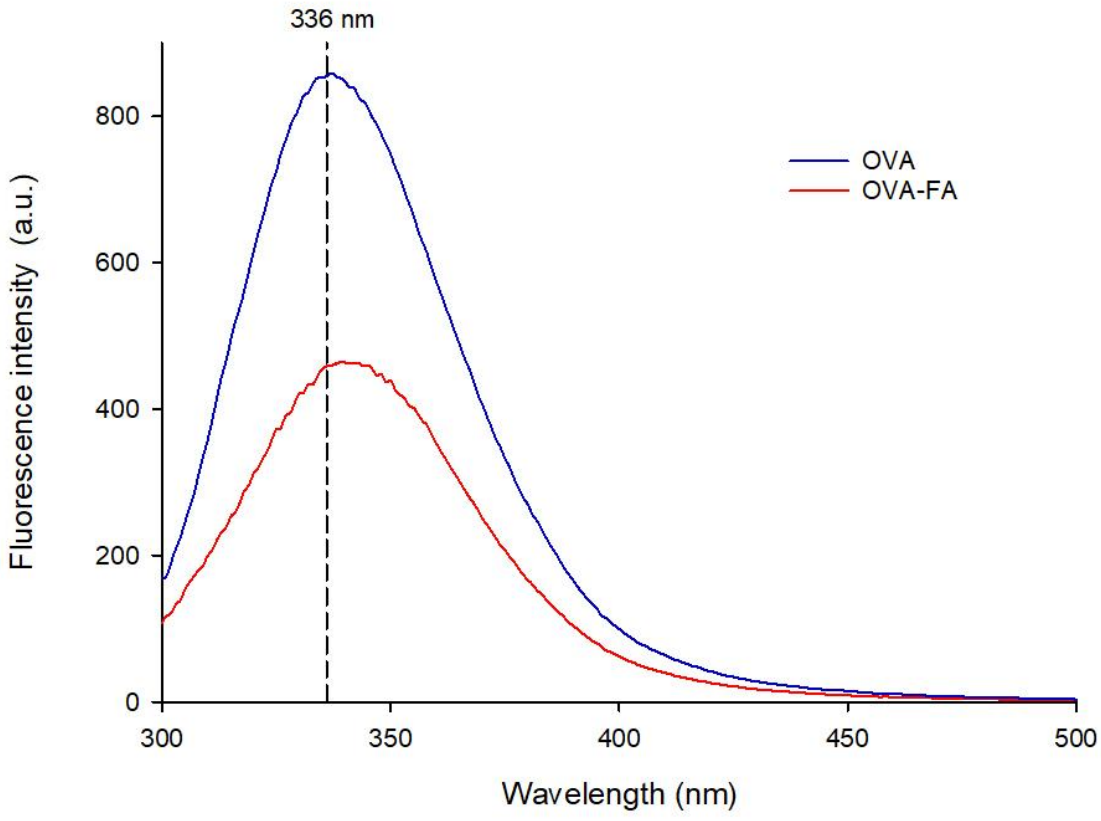

Figure 19. Intrinsic fluorescence spectra of control ovalbumin (blue line) and OVA-FA conjugate (red line). Excitation was set at 280 nm, and dashed line is the peak of control OVA.

The UV-VIS spectrum is presented in Figure 20. A single peak in the range of 280 nm is observed for pure OVA, while the OVA-FA conjugate shows peaks at 280 nm and 310 nm. The absorbance peak at 280 nm in proteins is explained by the double bonds in the aromatic

rings of tyrosine, tryptophan, and phenylalanine residues, which confer UV absorption properties. Phenolic acids have peaks in the range of 280 nm and 305 to 330 nm [12]. The increase in absorbance intensity at the 280 nm peak indicates an increase in covalent bonds in the system, thus indicating the formation of conjugates between ovalbumin and ferulic acid. The peak at 310 nm is explained by the presence of oxidized parts of FA, which have a peak in this range. Yang *et al.* [43] also observed an increase in absorbance at 280 nm after forming conjugates between pumpkin protein and different polyphenols. Xue *et al.* [15] identified peaks at 280 and 310 nm for β-lactoglobulin and ferulic acid conjugates, along with an increase in the 280 nm peak with increased ferulic acid presence.

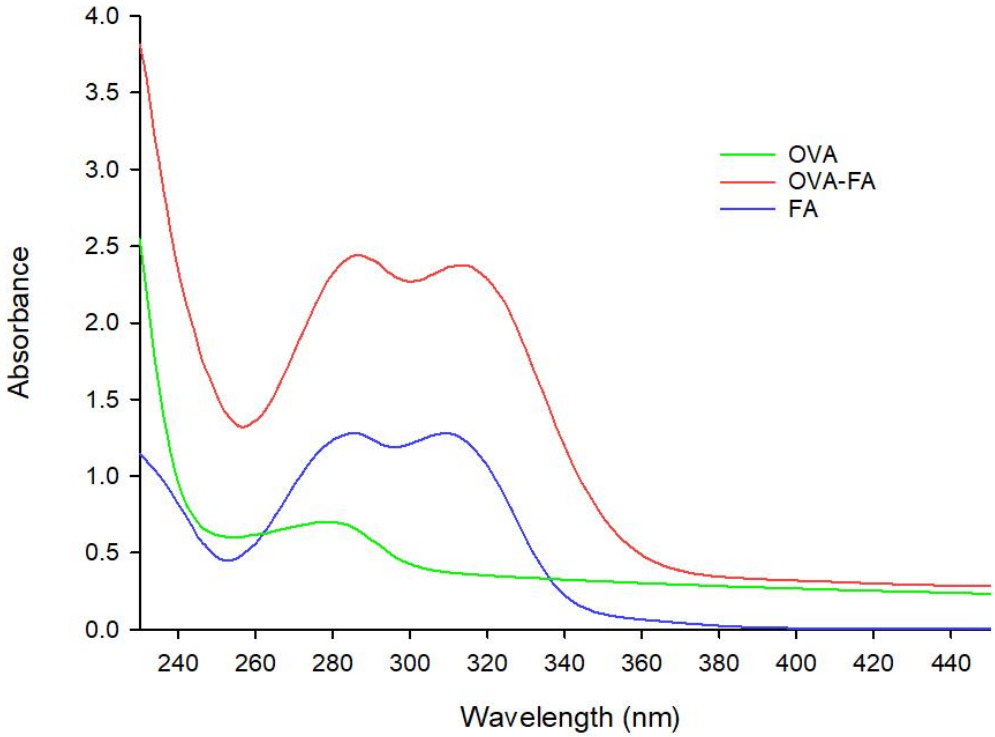

Figure 20. UV-VIS spectrum of ovalbumin and OVA-FA conjugate.

The Z-average particle size of OVA and OVA-FA was evaluated to investigate the impact of ferulic acid on particle characteristics. The results indicated that OVA-FA particles exhibited a smaller size compared to OVA particles, with diameters of 1007.60 ± 67.52 d.nm and 1323.67 ± 43.14 d.nm, respectively. This significant reduction ($p < 0.05$) in particle size is consistent with previous studies, such as those by Ju *et al.* [27], who observed a similar decrease in particle size of soy protein isolate upon conjugation with anthocyanins.

The zeta potential of OVA and OVA-FA was assessed to investigate their surface charge properties. The results showed that OVA-FA exhibited a significantly ($p < 0.05$) more negative zeta potential compared to OVA, with values of -21.00 ± 0.20 mV and -13.29 ± 1.31 mV,

respectively. This shift in zeta potential is likely attributable to the conjugation of ferulic acid, which modifies the surface characteristics of the particles [27]. These findings are in agreement with those of Geng *et al.* [44], who observed an increase in absolute values of zeta potential following the conjugation of EGCG with soy protein isolate.

3.3 Functional Properties of the Conjugate Formed by OVA-FA

The solubility values for OVA and the OVA-FA conjugate are presented in Figure 21 (A). The OVA-FA conjugate exhibited a solubility of 86.47 ± 1.35%, compared to 80.14 ± 0.86% for OVA. Approximately 50% of ovalbumin residues are hydrophobic, which can facilitate interactions leading to aggregation under certain conditions, thereby decreasing its solubility [2]. Similarly, Hu *et al.* [45] reported that the solubility of native, unmodified ovalbumin was approximately 75%. A significant increase ($p < 0.05$) in solubility of 7.92% was observed after the conjugation of OVA, attributed to the unfolding of OVA's structure, which exposed its hydrophilic amino acids, facilitating water interaction and enhancing solubility [28]. Similar increases in solubility through conjugate formation were reported by Cheng *et al.* [26], who observed a significant increase in whey protein concentrate upon quercetin conjugation.

The conjugation also affected significantly ($p < 0.05$) the emulsifying properties of ovalbumin, as shown in Figures 21 (B) and 14 (C). The EAI of the protein increased from 102.81 ± 4.96 m^2/g to 113.76 ± 3.66 m^2/g in the OVA-FA conjugate. The emulsion stability properties showed significant improvement, with OVA's ESI increasing from 21.6 ± 0.75 minutes to 30.4 ± 3.30 minutes in the OVA-FA conjugate, marking a 41% enhancement after covalent interaction. This enhancement in emulsifying properties was also observed in other studies. He *et al.* [3] noted higher emulsion stability in ovalbumin-EGCG conjugates formed via both alkaline and free radical methods. Similarly, Xue *et al.* [15] observed significant changes in EAI and ESI in β-lactoglobulin-ferulic acid conjugates formed by the alkaline method. The enhancements in EAI and ESI are explained by changes in surface hydrophobicity due to covalent interactions, which exposed the hydrophobic groups of the proteins, thereby improving their emulsifying capabilities.

Foaming capacity (FC) and foam stability (FS) data are presented in Figure 21 (D). The FC of ovalbumin increased by approximately 30%, from 56.9 ± 1.19% to 73.6 ± 1.39% post-conjugation, while FS increased by about 30%, from 48.5 ± 1.19% to 63.0 ± 3.23%, indicating significant enhancements ($p < 0.05$) in both foam formation and stability. The structural changes induced by FA conjugation improved the protein's ability to bind within a water-air structure, thereby enhancing foam formation and stability. He *et al.* [3] also observed increased FC and

FS in ovalbumin upon covalent interaction with EGCG, noting higher values in free radical method compared to the alkaline method.

3.4 Antioxidant Activity of the OVA-FA Conjugate

The antioxidant capacity was evaluated using the ABTS radical scavenging and DPPH methods, as shown in Figure 21 (E). The presence of ferulic acid significantly enhanced the antioxidant capacity of ovalbumin. This enhancement is attributed to the covalent bonding of FA, which introduces additional hydroxyl groups to the protein, making the conjugate a more reactive ingredient [28]. Using the ABTS method, the antioxidant capacity of OVA increased from 10.82 ± 1.19% to 53.96 ± 1.39% in the OVA-FA conjugate, representing approximately a fivefold increase in antioxidant capacity. Similarly, the DPPH method showed an increase of about 5.2 times, from 17.28 ± 2.90% in OVA to 89.87 ± 2.77% in the OVA-FA conjugate. This significant improvement in antioxidant activity has been observed in several other studies. For instance, He *et al.* [3] reported an increase of 4 to 6 times in DPPH radical scavenging activity and 2 to 5 times in ABTS activity for various OVA-EGCG conjugates formed via free radical and alkaline methods. Feng *et al.* [40] found that the antioxidant activity of ovalbumin conjugated with different phenolic compounds also increased by about 3 to 5 times compared to the control in both DPPH and ABTS assays.

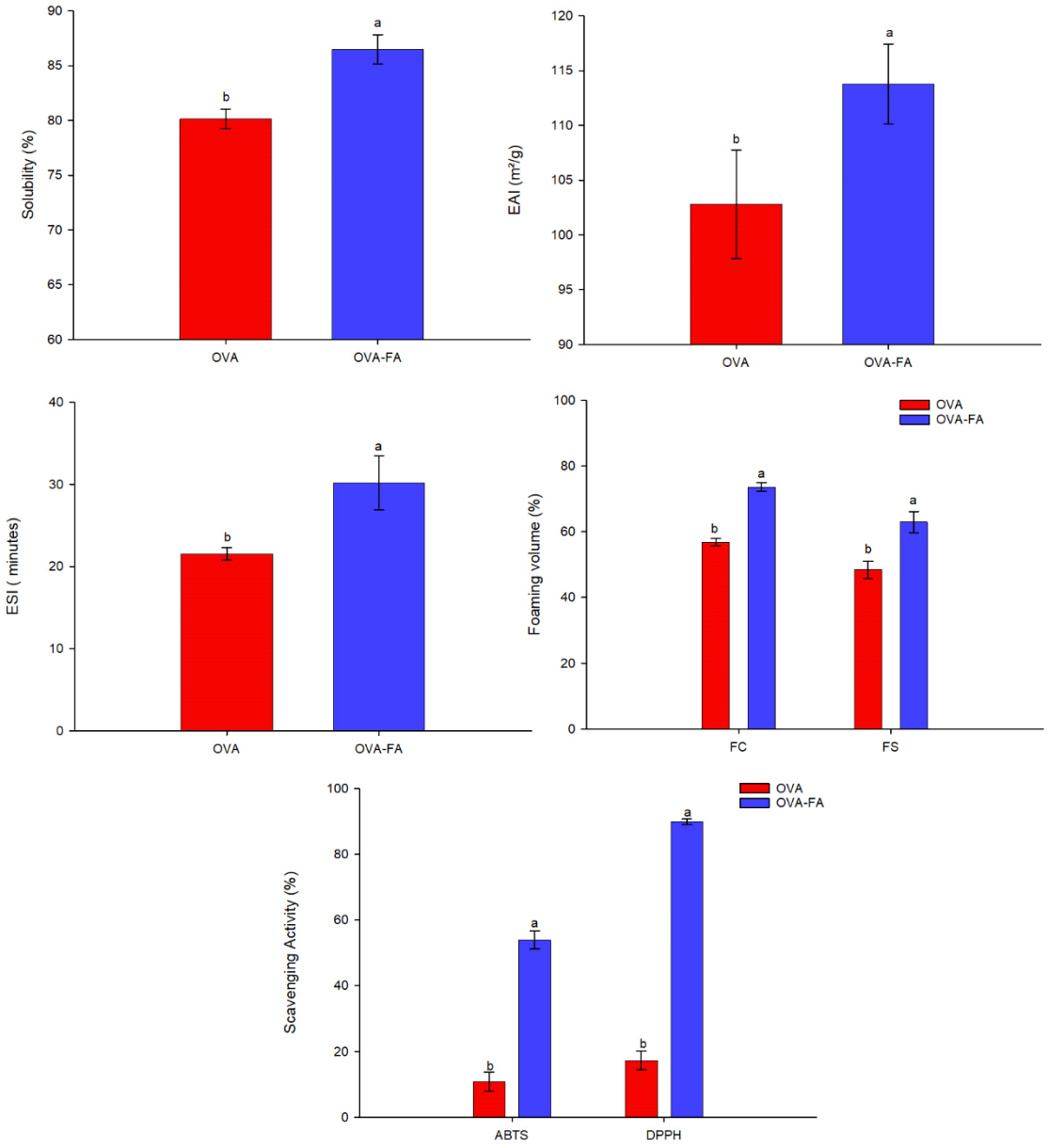

Figure 21. Techo-functional properties of ovalbumin and the OVA-FA conjugate. Solubility (A), emulsion properties (B), foaming properties (C) and antioxidant activity (D) are presented as mean ± standard deviation. Values followed by the same letters do not present statistically significant difference in the Tukey test ($p < 0.05$).

4 Conclusions

Conjugates of ferulic acid and ovalbumin were efficiently formed at a ratio of 0.9 g FA/g OVA using the alkaline method for synthesis. The resulting covalent reaction induced alterations in the secondary and tertiary structures of ovalbumin, imparting new techno-functional properties. The OVA-FA conjugate exhibited a significant increase in solubility, emulsifying capacity, and foaming ability, in addition to demonstrating superior antioxidant activity compared to unmodified ovalbumin. These results clearly indicate that OVA-FA is a promising ingredient with significant potential as an emulsifier with an antioxidant activity.

CRediT authorship contribution statement

Bruno Sérgio Toledo Barbosa: Conceptualization, Methodology, Validation, Investigation, Writing – original draft, Writing – review & editing. **Sanclayver Corrêa Araújo:** Methodology, Investigation, Writing – original draft,. **Yraima Cordeiro**: Methodology, Investigation, Writing – original draft, Writing – review & editing. **Edwin Elard Garcia-Rojas**: Conceptualization, Methodology, Resources, Writing – review & editing, Supervision, Project administration, Funding acquisition.

Conflict of interest

The authors declare that they have no known competing financial interests or personal relationships that could have appeared to influence the work reported in this paper.

Data availability

Data will be made available on request.

Acknowledgments

The authors thank the CNPq, Brazil (313928/2021-5); CAPES, Brazil (Código 001) and FAPERJ, Brazil (E-26/210.052/2023; E-26/201.030/2021) for the financial support.

5 References

1. J.A. Huntington, P.E. Stein, Structure and Properties of Ovalbumin (2001).

2. H. Rostamabadi, V. Chaudhary, N. Chhikara, N. Sharma, M. Nowacka, I. Demirkesen, K. Rathnakumar, S. R. Falsafi, Food Hydrocoll. 139, 108514 (2023)

3. W. He, H. Xu, Y. Lu, T. Zhang, S. Li, X. Lin, B. Xu. X. Wu, J. Funct. Foods 61, 103490 (2019).

4. T. Strixner and U. Kulozik, in Handbook of Food Proteins (Elsevier, 2011), pp. 150–209.

5. N.D. Raj and D. Singh, Health Sci. Rev. 5 100063 (2022).

6. B. Warren, Ferulic Acid: Antioxidant Properties, Uses and Potential Health Benefits, UK ed. (Nova Science Pub Inc, 2014).

7. S. Mathew and T.E. Abraham, Crit. Rev. Biotechnol. 24, 59 (2004).

8. S. Ou and K.C. Kwok, J. Sci. Food. Agric. 84, 1261 (2004).

9. A.V. Phadke, A.A. Tayade. M.P. Khambete, Chem. Biol. Drug. Des. 98, 713 (2021).

10. F. Shahidi and C.S. Dissanayaka, Food Prod. Process. Nutr. 5, (2023).

11. T.H. Quan, S. Benjakul, T. Sae-leaw, A.K. Balange. S. Maqsood, Trends Food Sci. Technol. 91, 507 (2019).

12. J. Liu, H. Yong, X. Yao, H. Hu, D. Yun. L. Xiao, RSC Adv. 9, 35825 (2019).

13. W.N. Baba, D.J. McClements. S. Maqsood, Food Chem. 365, 130455 (2021).

14. J. Sun, H. Jing, Y. Mu, D.J. McClements, S. Dong. B. Xu, Food Hydrocoll. 108, 106019 (2020).

15. Y.T. Xue, Y.N. Han, Y. Wang, Y.H. Zhang, Y.Q. Yin, B.H. Liu, H.L. Zhang. X.H. Zhao, Food Chem. 406, (2023).

16. K. Chang, J. Liu, W. Jiang, R. Zhang, T. Zhang. B. Liu, Food Res. Int. 136, (2020).

17. L. Chen, M. Zhu, X. Hu, J. Pan. G. Zhang, J. Sci. Food Agric. 102, 3835 (2022).

18. Z. Huang, X. Yang, S. Liang, L. Chen, L. Dong, A. Rahaman, S. He, Y. Shen. D. Su, Int. J. Biol. Macromol. 211, 150 (2022).

19. Q. Hu, T. Wang, M. Zhou, J. Xue. Y. Luo, J Agric. Food. Chem. 64, 5893 (2016).

20. C.H. Giles, T.H. MacEwan, S.N. Nakhwa. D. Smith, J. Chem. Soc. (Resumed) 3973 (1960).

21. E.E. Garcia Rojas, J.S. dos Reis Coimbra. L.A. Minim, Eur. Food Res. Technology 223, 705 (2006).

22. X.D. Tong, B. Xue. Y. Sun, Biochem. Eng. J. 16, 265 (2003).

23. L. Pan, J. Chen, H. Fu, N. Wang, J. Zhou, S. Zhang, S. Lu, J. Dong, Q. Wang. H. Yan, Food. Biosci. 52, (2023).

24. A.J. Miles, S.G. Ramalli. B.A. Wallace, Protein Sci. 31, 37 (2022).

25. Z. Yu, L. Ma, B. Liu, W. Wang, Z. Shang, H. Dang. C. Liu, Ultrason. Sonochem. 101, 106672 (2023).

26. J. Cheng, O.E. Dudu, J. Zhang, Y. Wang, L. Meng, W. Wei, X. Li. T. Yan, Food Hydrocoll. 142, 108787 (2023).

27. M. Ju, G. Zhu, G. Huang, X. Shen, Y. Zhang, L. Jiang. X. Sui, Food Hydrocoll. 99, 105329 (2020).

28. H. Xu, T. Zhang, Y. Lu, X. Lin, X. Hu, L. Liu, Z. He. X. Wu, Food Chem. 298, (2019).

29. G. Ren, J. Shi, S. Huang, C. Liu, F. Ni, Y. He, X. Luo, T. Li, Y. Song, M. Huang. H. Xie, Food Chem. 374, 131612 (2022).

30. K. Chang, J. Liu, W. Jiang, Y. Fan, B. Nan, S. Ma, Y. Zhang, B. Liu. T. Zhang, Lwt 146, 111383 (2021).

31. J.C. Sánchez-Rangel, J. Benavides, J.B. Heredia, L. Cisneros-Zevallos. D.A. Jacobo-Velázquez, Anal. Methods 5, 5990 (2013).

32. H. Thongzai, N. Matan, P. Ganesan. T. Aewsiri, Appl.Sci. (Switzerland) 12, (2022).

33. S. Wang, X. Li, J. Zhu, H. Liu, T. Liu, G. Yu. M. Shao, J. Agric. Food Chem. 69, 7777 (2021).

34. S. Guha, K. Majumder. Y. Mine, Egg Proteins (2018).

35. M.G. Tang, M. Yang, L.K. Xu, Y.L. Wang, L. Tao, J.H. Dai, J. Sheng. Y. Tian, LWT 115991 (2024).

36. L.C. Curtisjohnson, Anal. Biochem. 155, 155 (1986).

37. Y. Lu, S. Li, H. Xu, T. Zhang, X. Lin. X. Wu, J Agric Food Chem 66, 9794 (2018).

38. A. Barth, Biochim. Biophys. Acta. Bioenerg. 1767, 1073 (2007).

39. S.A. Tatulian, Methods Mol. Biol. 974, 177 (2013).

40. J. Feng, H. Cai, H. Wang, C. Li. S. Liu, Food Chem. 241, 60 (2018).

41. J.R. Lakowicz, Principles of Fluorescence Spectroscopy (Springer, 2006).

42. A.D. Nisbet, R.H. Saundry, A.J.G. Moir, L.A. Fothergill. J.E. Fothergill, Eur. J. Biochem. 115, 335 (1981).

43. C. Yang, J. Liu, Y. Han, B. Wang, Z. Liu, H. Hu, Z. Guan, Y. Yang. J. Wang, Food Biosci. 55, (2023).

44. M. Geng, L. Li, X. Feng, J. Xu, Y. Huang, F. Teng. Y. Li, J. Mol. Liq. 360, (2022).

45. G. Hu, J. Zhang, Q. Wang, M. Ma, L. Ma, and S. Li, Foods 11, (2022).

CAPÍTULO III. EFFECT OF OVALBUMIN-FERULIC ACID CONJUGATES ON THE STABILITY AND BIOACCESSIBILITY OF VITAMIN D3 IN PICKERING EMULSIONS

Publicado em 2025 na *International Journal of Biological Macromolecules*

DOI: https://doi.org/10.1016/j.ijbiomac.2025.146397

Abstract

Vitamin D is essential for human health, but its instability under environmental stressors poses challenges for effective supplementation. In this study, ovalbumin–ferulic acid (OVA–FA) conjugates were evaluated as emulsifiers in Pickering emulsions for the encapsulation of vitamin D_3. Emulsions formulated with 50%, 60%, and 70% oil phase fractions and 4.0% (w/w) OVA–FA in the aqueous phase exhibited the highest kinetic stability and greatest protein adsorption at the oil–water interface. The emulsions displayed pseudoplastic behavior and showed enhanced antioxidant capacity, with scavenging rates exceeding 80%. They also demonstrated greater oxidative stability, with peroxide values around 43 mmol/kg oil, compared to 186 mmol/kg in ovalbumin-only emulsions. Encapsulation efficiency exceeded 90%. The system protected vitamin D3 from photodegradation, significantly reducing degradation to 26% versus nearly 40% with ovalbumin alone. Bioaccessibility reached up to 49.86% after *in vitro* gastrointestinal digestion. These findings highlight the potential of OVA–FA-stabilized Pickering emulsions as robust delivery systems for bioactive compounds in food fortification, offering improved stability, protection, and functional performance.

Keywords: Covalent interaction, Polyphenol, Cholecalciferol, *in vitro* digestion, Emulsifier.

1 Introduction

Vitamin D is a fat-soluble prohormone present in two forms: vitamin D3 (cholecalciferol), derived from mammals, and vitamin D2 (ergocalciferol), found in fungi and plants. Both forms follow similar metabolic pathways in the human body [1–3]. Its deficiency is associated with several conditions, such as osteoporosis, cardiovascular diseases, and immune disorders, and is a global concern. In Brazil, approximately 4.3% of newborns exhibit vitamin D deficiency, and approximately 15% of the adult population may be affected [4]. The main source of vitamin D3 for the body is cutaneous synthesis induced by exposure to UVB rays from sunlight [5]. However, factors such as limited sun exposure, poor diet, and aging contribute to vitamin D deficiency. Therefore, strategies for effective vitamin D3 supplementation have been widely studied. However, challenges arise due to the high sensitivity of vitamin to light and their susceptibility to oxidation [6,7].

Microencapsulation has emerged as a promising approach to protect vitamin D3 from oxidative degradation and increase its bioaccessibility [8]. Various techniques have been explored for this purpose, including spray-drying [9], complex coacervation [10], and emulsions [6,11]. Emulsions are homogeneous mixtures composed of two immiscible liquids [12]. However, owing to their thermodynamic instability, emulsifiers that bind to the oil–water interface are required to prevent phase separation [13,14]. These emulsifiers can be either surfactants or solid particles, the latter of which are used in Pickering emulsions [15,16].

Pickering emulsions have garnered significant interest because of their greater stability than conventional emulsions stabilized by surfactants [16]. This type of emulsion is stabilized by solid particles that form a physical barrier at the oil/water interface, reducing coalescence and increasing the stability of the system [15,17,18]. However, the choice of the appropriate emulsifier is essential to ensure the functionality and efficiency of the encapsulation system. Conjugates are products of covalent interactions, which may occur between a variety of molecules, including phenolic compounds, polysaccharides, and proteins, resulting in materials with improved emulsifying properties and the capacity to provide antioxidant benefits [19,20]. This modification can be performed by different methods, with the alkaline technique being one of the most commonly used methods because of its simplicity, lower cost, and reduced use of reagents [20,21]. In this method, the reaction occurs under high pH conditions, promoting the oxidation of phenolic compounds and the formation of quinones, highly reactive intermediates that can form covalent bonds with proteins [22]. In this context, ovalbumin (OVA) and ferulic acid (FA) are promising candidates for the formulation of emulsifying conjugates.

Ovalbumin is a protein that is widely used in food systems because of its emulsifying and foaming properties [23,24], whereas ferulic acid, a phenolic compound primarily found in plant cell walls, enhances the techno-functional properties of ovalbumin and provides biological activities to the conjugate [22,25]. The combination of these molecules to form the OVA-FA conjugate may result in more stable emulsions with better functional characteristics.

Although protein–polyphenol conjugates have been investigated for use in Pickering emulsions [26–28], their application in vitamin D3 encapsulation remains limited. In particular, the use of an ovalbumin–ferulic acid conjugate for this purpose has not been previously reported. Moreover, the systematic evaluation of oil phase variation in such systems has not been explored in the context of vitamin D3 encapsulation. Compared with other protein–polyphenol conjugates, OVA–FA offers a unique combination of high emulsifying capacity and potent antioxidant activity, which contributes to improved emulsion stability and oxidative protection.

This study aimed to investigate the efficacy of OVA–FA conjugates on the kinetic and oxidative stability of oil-in-water (O/W) Pickering emulsions, as well as to characterize their structural and rheological properties. Additionally, the efficiency of these emulsions in the encapsulation, stability, bioaccessibility, and release of vitamin D_3 during an *in vitro* simulated gastrointestinal digestion assay was evaluated, along with the influence of varying the oil phase fraction on these parameters. This approach enabled the assessment of the structural and functional behavior of the emulsions under different formulation conditions.

2 Material and Methods

2.1 Material

Ferulic acid (128708), ovalbumin (A5253, purity 62–88%), cholecalciferol (C9756), 2,2-diphenyl-1-picrylhydrazyl (DPPH-D9132), 2,2′-azino-bis(3-ethylbenzothiazoline-6-sulfonic acid) (ABTS-A1888), cumene hydroperoxide (247502,80%), porcine pepsin (P6887), porcine pancreatin (P7545), and porcine bile extract (B8631) were acquired from Sigma–Aldrich® (St. Louis, USA). The soybean oil used in this study was obtained from a local market (Rio de Janeiro, Brazil). The Coomassie Brilliant Blue G-250 dye (1610406) was purchased from Bio-Rad (California, USA). The water used in the experiments was ultrapure, with a conductivity of 0.05 μS/cm (Gehaka, Master-P&D, Brazil). All other reagents used in the study were of analytical grade.

2.2 Preparation of OVA-FA Conjugates

The conjugate between OVA and FA was obtained following the method described by Barbosa *et al.* [1]. Briefly, a 5 mg/mL OVA solution was prepared, and its pH was adjusted to 9.0 with NaOH. The mixture was left to stand for 2 h. Subsequently, 0.9 g of FA was added to the solution under continuous stirring (HS7, IKA, Germany) at room temperature, and the mixture was stirred for 24 h. After this period, the excess FA was removed by dialysis (D9527, Sigma Aldrich, USA) in ultrapure water for 48 h. The final solution was then frozen with liquid nitrogen (-160 °C) and subsequently lyophilized (Enterprise I, Terroni, Brazil).

2.3 Characterization of OVA-FA Conjugates

2.3.1 Interfacial Tension

The interfacial tension between different concentrations of OVA-FA (1.0, 2.0, 3.0, and 4.0% w/w) and the oil phase was measured using an Easytrack tensiometer (Teclis Scientific, France) with the drop shape method, adapted from Barbosa & Garcia–Rojas [2]. Measurements were performed at 25 ± 0.01 °C using a CD-BC4 thermostatic bath (Julabo, Germany). The model (Equation 1) developed by Shi *et al.* [2] was fitted to the interfacial tension data obtained between OVA-FA solution systems and soybean oil.

$$\sigma(t) = \sigma_f + \exp\left(-t/\tau_1\right)\left(\sigma_1 - \sigma_f\right) + \exp\left(-t/\tau_2\right)\left(\sigma_2 - \sigma_f\right) \qquad (1)$$

where σf is the asymptotic interfacial tension (mN/m) as $t \rightarrow \infty$, t is the time in s, σ_1 and σ_2 are kinetic parameters of the interfacial tension, τ_1 is the migration time (s) of the emulsifier at the interface, and τ_2 is the time (s) for reorganization and potential changes in the macromolecules at the interface.

2.3.2 Three-Phase Contact Angle

The oil–water three-phase contact angle of the OVA–FA conjugate was determined using the sessile drop method, as described by Qin *et al.* [2], which employs an Easytrack system coupled with a contact angle module. Lyophilized samples of OVA-FA were compacted onto a glass slide to form a uniform layer. The slide was then positioned in contact with soybean oil, and a droplet of distilled water (2 μL) was deposited onto the surface using a precision syringe. The droplet image was recorded by a camera attached to the system after 2 min of equilibration. The contact angle was automatically calculated, and the average was obtained from three repetitions at two distinct points on the droplet.

2.4 Formation of O/W Pickering Emulsions

Particle formation was carried out according to the methodology of Ju *et al.* [3]. Solutions of 5.0% (w/v) OVA-FA were subjected to a water bath at 95 °C for 15 min, followed by immediate cooling in an ice bath until reaching room temperature. The final solution was rapidly frozen in liquid nitrogen (-160 °C) and then subjected to lyophilization.

The Pickering emulsion was prepared following the methodology of Ji *et al.* [4], where emulsions were formulated with different soybean oil fractions (φ) of 0.25, 0.50, 0.60, and 0.70, as well as varying concentrations of OVA-FA diluted in the aqueous phase (1.0, 2.0, 3.0, and 4.0% w/w). Accordingly, A1 corresponds to the emulsion with an oil fraction of 0.25 and an OVA-FA concentration of 1.0%, A2 corresponds to the emulsion with 0.25 oil and 2.0% OVA-FA, etc., and D4 corresponds to the emulsion with 0.70 oil and 4.0% OVA-FA. Emulsification was performed using an Ultra-Turrax T25 homogenizer (IKA, Germany) at 18,000 rpm for 6 min.

2.4.1 Kinetic Stability

The methodology described by Ren *et al.* [5] was employed to evaluate the kinetic stability of the emulsions. Samples of 10 mL of O/W emulsions were placed in transparent tubes and maintained at 25 °C for 7 days in a Shaker SL222 incubator (Solab, Brazil). During this period, the height of the transparent layer at the bottom of each tube was monitored. The stability of the emulsions was evaluated using the creaming index, which was calculated with the following equation:

$$CI(\%) = \frac{H_c}{H_t} \qquad (2)$$

where CI is the creaming index, H_c is the height of the transparent part, and H_t is the total height of the system.

2.4.2 Protein Adsorption at the Emulsion Interface

The methodology described by Chen *et al.* [6] was used to identify the adsorption of OVA-FA at the interface of Pickering emulsions. Aliquots of 1 mL of freshly prepared Pickering emulsions were subjected to centrifugation for 30 min at 15,000 × g. After centrifugation, the oil layer was removed, while the lower layer was extracted and sequentially filtered through membranes with pore sizes of 0.45 and 0.22 μm. The protein content in the filtrate after centrifugation was quantified using the Bradford method, and the amount of nonadsorbed protein, C_f, was recorded. The initial protein mixture used in the preparation of the emulsion was similarly centrifuged under the same conditions, and the adsorbed protein content was

evaluated using the Bradford method and recorded as C_i. The adsorption of OVA-FA was determined using the following equation:

$$Adsorption(\%) = \frac{C_i - C_f}{C_i} \qquad (3)$$

2.5 Characterization of Pickering Emulsions

The characterization of the Pickering emulsions to determine the particle size, zeta potential, and rheology was carried out on emulsions B4, C4, and D4, which demonstrated the highest kinetic stability over eight days and the greatest protein adsorption at the interface. Additionally, an OVAE emulsion, prepared using only ovalbumin (4% w/w) in the aqueous phase as the emulsifier with φ = 0.5, was included in the analyses of peroxide formation and antioxidant capacity, as well as in subsequent experiments involving vitamin D3 encapsulation and stability.

2.5.1 Particle Size and Zeta Potential

The particle size and zeta potential analyses of freshly prepared emulsions were performed on samples diluted 100 times in water using the Zetasizer Nano ZS90 (Malvern Instruments, United Kingdom) measurements carried out at 25 °C.

2.5.2 Morphological Evaluation

The formed emulsions were placed between slides and analyzed using an optical microscope (K220, Kasvi, Brazil).

2.5.3 Rheology

The rheological characterization of the emulsions was performed using an MCR 92 rheometer (Anton Paar, Austria). The tests were conducted with a parallel plate geometry of 50 mm in diameter (PP50), with the gap adjusted to 1 mm. The measurements were made immediately after the preparation of the emulsions. The apparent viscosity was determined over a shear rate range of 0.1-100 s^{-1}. The power law model (Equation 4), Bingham model (Equation 5), and Herschel-Bulkley model (Equation 6) were used to describe the rheological behavior of the emulsions. Additionally, dynamic shear rate variation analyses were performed to identify the linear viscoelastic region, followed by frequency sweep analysis to determine the storage modulus (G') and loss modulus (G"), within a frequency range of 0.1-10 Hz.

$$\tau = K(\dot{\gamma})^n \quad (4)$$

$$\tau = \tau_0 + \mu_p\dot{\gamma} \quad (5)$$

$$\tau = K(\dot{\gamma})^n + \tau_0 \quad (6)$$

where τ is the shear stress (Pa), τ_0 is the yield stress (Pa), μ_p is the Bingham plastic viscosity (Pa.s), K is the consistency index (Pa.s^n), n is the fluid behavior index and $\dot{\gamma}$ is the shear rate (1/s).

2.5.4 Antioxidant Capacity

The antioxidant capacity was determined using the DPPH method according to the methodology adapted from Ren *et al.* [7]. For this purpose, an aliquot of 1.0 mL each from emulsions B4, C4, D4, and OVAE, as well as a ferulic acid solution (0.1 mg/mL), was mixed with 1.0 mL of DPPH solution (1.75×10^{-4} mol/L), and the mixture was incubated in the dark for 30 min. After this period, the absorbance of the solution was measured at 517 nm using a UV–Vis spectrophotometer. The antioxidant capacity was expressed as the percentage of DPPH radical sequestration, which was calculated according to the following equation:

$$DPPH\ Scavenging\ Rate\ (\%) = \left[1 - \frac{A_1 - A_2}{A_0}\right] x100 \quad (7)$$

where A_0 is the absorbance without sample, A_1 is the absorbance with sample, and A_2 is the absorbance of the blank (without DPPH).

The capacity to scavenge the $ABTS^{+\bullet}$ radical was determined on the basis of the methodology described by Liu *et al.* [8], with modifications. For the preparation of the working solution, stock solutions of ABTS (7.4 mmol/L) and potassium persulfate (2.6 mmol/L) were combined at a 1:1 ratio and kept in the dark for 12 h to allow for radical formation. The solution was then diluted with ethanol until an absorbance between 0.7 and 0.8 at 734 nm was achieved. Subsequently, 500 µL of the ABTS working solution was mixed with 500 µL of the emulsion. The reaction mixture was incubated in the dark for 10 min, and the absorbance was measured at 734 nm using a UV–Vis spectrophotometer. The antioxidant capacity was expressed as the percentage of $ABTS^+$ radical sequestration, which was calculated according to the following equation:

$$ABTS^+\ Scavenging\ Rate\ (\%) = \left[1 - \frac{A_1 - A_2}{A_0}\right] x100 \quad (8)$$

where A_0 is the absorbance without sample, A_1 is the absorbance with sample, and A_2 is the absorbance of the blank (without $ABTS^+$).

2.5.5 Oxidative Stability

The oxidative stability analysis was performed by identifying lipid hydroperoxides, following the methodology described by Zhang *et al.* [9]. Freshly prepared emulsions were transferred to glass vials and stored in a TE-424 incubator (Tecnal, Brazil) at 37 °C for 14 days in the dark. Aliquots of 0.2 mL of the emulsion were collected immediately after preparation and on the first, fourth, seventh, eleventh, and fourteenth days and mixed with 1 mL of an isooctane/2-propanol solution (3:1, v/v) in a vortex for 10 s, which was repeated three times. The emulsion was then centrifuged at 7200 × g for 8 min. A 0.2 mL aliquot of the organic phase located at the top after centrifugation was removed and added to 2.8 mL of a methanol/1-butanol solution (2:1, v/v), followed by the addition of 15 µL of ammonium thiocyanate (3.94 mol/L) and 15 µL of an iron solution (0.132 mol/L barium chloride and 0.144 mol/L ferrous sulfate). The resulting mixture was incubated at room temperature in the dark for 20 min. After the reaction time, the absorbance of the solution was measured at 510 nm using a spectrophotometer. The quantification of hydroperoxides present in the emulsions was performed on the basis of a standard curve constructed with cumene hydroperoxide. An OVAE emulsion, as described in Section 2.5, was also analyzed.

2.6 Microencapsulation of Vitamin D3 in O/W Pickering Emulsions

The emulsions were prepared as described in Section 2.4, with the addition of vitamin D3 to the oil phase at a concentration of 1.0% (w/w).

2.6.1 Encapsulation Efficiency of Vitamin D3

The encapsulation efficiency of vitamin D3 was determined according to the methodology of Zhang *et al.* [10]. First, 1 mL of the freshly prepared emulsion was mixed with 2 mL of ethanol for 10 s, followed by the addition of 2 mL of hexane and further mixing for 10 s. The mixture was then centrifuged at 4000 × g for 2 min, after which the oil phase was collected. This process was repeated three times. After centrifugation, 6 mL of hexane was added to compensate for evaporation loss. The total amount of vitamin D3 was determined by measuring the absorbance at 265 nm using spectrophotometry on the basis of a standard curve of vitamin D3 dissolved in hexane. The amount of free vitamin D3 in the system was determined by mixing 1 mL of emulsion with 2 mL of hexane, followed by centrifugation at 700 × g for 2 min. The hexane layer was collected, and the process was repeated two more times. Free

vitamin D3 was quantified using the previously described spectrophotometric technique. The encapsulation efficiency (EE) was calculated using the following equation:

$$EE(\%) = \frac{Total\ Vitamin\ D3 - Free\ Vitamin\ D3}{Total\ Vitamin\ D3} \quad (9)$$

2.6.2 Photochemical Stability of Vitamin D3

The method for determining the photochemical stability of vitamin D3 was based on the methodology of Zhang *et al.* [10], with adaptations. The freshly prepared emulsions were exposed to ultraviolet (UV) light irradiation for 3 h in a UV darkroom chamber (AG-DC-02, ACS Gold, Brazil). Aliquots of the emulsions were taken at different time intervals (0, 60, 120, and 180 min). The photochemical stability of vitamin D3 was determined as the percentage of vitamin D3 remaining in the emulsions after UV irradiation.

2.7 *In vitro* Gastrointestinal Simulation of Vitamin D3 Microcapsules

The INFOGEST 2.0 method [11] was used for the preparation of simulated digestion fluids, including saliva (SSF), gastric juice (SGF), and intestinal fluid (SIF). In the simulation, emulsions containing OVA-FA as the emulsifier, as well as the OVAE emulsion, as described in Section 2.5, were used at an initial amount of 1 g per sample. A control sample containing 1% (w/w) vitamin D3 in oil was also analyzed.

The digestion process was carried out in three sequential stages: the oral phase, the gastric phase, and the intestinal phase, using sealed tubes to maintain controlled conditions throughout the procedure. All procedures were performed under controlled agitation at a temperature of 37 °C in a TE-424 incubator. During the oral phase (2 min), each emulsion was mixed with 0.8 mL of SSF, 0.1 mL of salivary amylase solution (75 U/mL), 5 μL of $CaCl_2$ (0.3 mol/L), and 0.095 mL of distilled water. In the gastric phase (2 h), the entire volume from the oral phase was combined with 1.6 mL of SGF, 0.2 mL of pepsin solution (2000 U/mL), 1 μL of $CaCl_2$ (0.3 mol/L), and 0.2 mL of distilled water. The pH was adjusted to 3.0 with HCl. During the intestinal phase (2 h), the gastric mixture was further combined with 1.7 mL of SIF, 1 mL of pancreatin solution (100 U/mL), 0.5 mL of bile solution (10 mmol/L), 8 μL of $CaCl_2$ (0.3 mol/L), and 0.792 mL of distilled water. The pH was adjusted to 7.0 with NaOH.

Aliquots of 100 μL were collected at 0, 2, 30, 60, 90, 120, 150, 180, 210, and 240 min throughout the digestion. Following each sampling, an equal volume of the respective simulated digestive fluid was added to maintain constant reaction conditions. The collected aliquots were centrifuged at 10,000 × g for 30 min at 4 °C, and the transparent phase was recovered. The

concentration of vitamin D3 was determined according to the procedure described in Section 2.6.1.

2.7.1 Bioaccessibility of Vitamin D3

The bioaccessibility was determined according to the methodology of Winuprasith *et al.* [12]. After the completion of the gastrointestinal simulation, 10 mL of the digested samples were subjected to centrifugation at 4000 × g for 30 min at 25 °C. After centrifugation, 2 mL of the transparent phase was collected, and the concentration of vitamin D3 was determined. Bioaccessibility was calculated as the ratio between the concentration obtained in the transparent phase (micelle) and the concentration found at 240 min of digestion (digesta).

2.8 Statistical Analysis

The data were evaluated through Tukey's test and analysis of variance using the SISVAR® 5.6 software, with a significance level of $p < 0.05$. The experiments were performed in triplicate, and the results are presented as the means ± standard deviations.

3 Results and discussion

3.1 Characterization of the OVA-FA Conjugate

3.1.1 Interfacial Tension

Figure 22A shows the variation in the dynamic interfacial tension between different concentrations of the OVA-FA conjugate and an oil phase. The parameters obtained from Equation 1 are detailed in Table 5. The proposed model demonstrated excellent fit to the experimental data, with the average absolute deviation (AAD) varying up to a maximum of 0.86% for the sample with a 2.0% OVA-FA concentration, whereas the standard deviation (SD) did not exceed 0.06 mN/m. As the OVA-FA concentration increased, a gradual decrease in interfacial tension was observed, ranging from 5.96 mN/m for a 1.0% OVA-FA concentration to 4.03 mN/m in systems with 4.0% OVA-FA. This behavior can be explained by the fact that protein–oil and protein–water interactions are more favorable than oil–water interactions are [13]. Thus, the increase in protein concentration increases the number of molecules bound to the oil–water interface, resulting in a reduction in interfacial tension.

Table 5. Dynamic interfacial tension parameters between the external aqueous phase with different concentrations of OVA-FA conjugate and soybean oil estimated from equation 1.

Concentration (%)	σ_f (mN/m)	σ_1 (mN/m)	σ_2 (mN/m)	τ_1 (s)	τ_2 (s)	AAD* (%)	SD** (mN/m)
1.0	5.96	9.41	8.84	40.42	428.78	0.27	0.05
2.0	5.45	7.29	7.89	16.58	405.45	0.86	0.06
3.0	5.00	6.90	7.04	89.17	667.33	0.41	0.05
4.0	4.03	5.09	5.59	28.29	426.83	0.12	0.02

$$*AAD(\%) = \left(\frac{100}{m}\right)\left[\sum_{i=1}^{m}\frac{\sigma_{exp,i}-\sigma_{cal,i}}{\sigma_{exp,i}}\right] \quad ;**SD = \sqrt{\frac{\sum_{i=1}^{m}\left(\sigma_{exp,i}-\sigma_{cal,i}\right)^2}{m-p}}$$

3.1.2 Three-Phase Contact Angle

Figure 22B shows an image of a water droplet on the lyophilized OVA–FA conjugate coated with soybean oil, where a contact angle of 84.25 ± 1.15° was observed. The three-phase contact angle of particles plays a crucial role in determining the type and stability of Pickering emulsions [14]. When this angle is close to 90°, there is no clear affinity between the aqueous and oil phases, which promotes the adsorption of particles at the oil–water interface. This arrangement forms an effective steric barrier, preventing the coalescence of oil droplets. Angles lower than 90° indicate greater affinity for the aqueous phase, favoring the stabilization of oil-in-water (O/W) emulsions. On the other hand, angles greater than 90° indicate greater affinity for the oil phase, facilitating the formation of water-in-oil (W/O) emulsions [15–17]. The value obtained for the OVA-FA conjugate, close to 90°, suggests a strong interaction with the oil–water interface. Additionally, since it is slightly lower than 90°, OVA-FA has potential as an emulsifier for O/W emulsions. Similar results were reported by Yi *et al.* [18], who reported that OVA-tannic acid complexes exhibited a contact angle of 85.01 ± 0.50° and acted as effective emulsifiers in stabilizing Pickering emulsions.

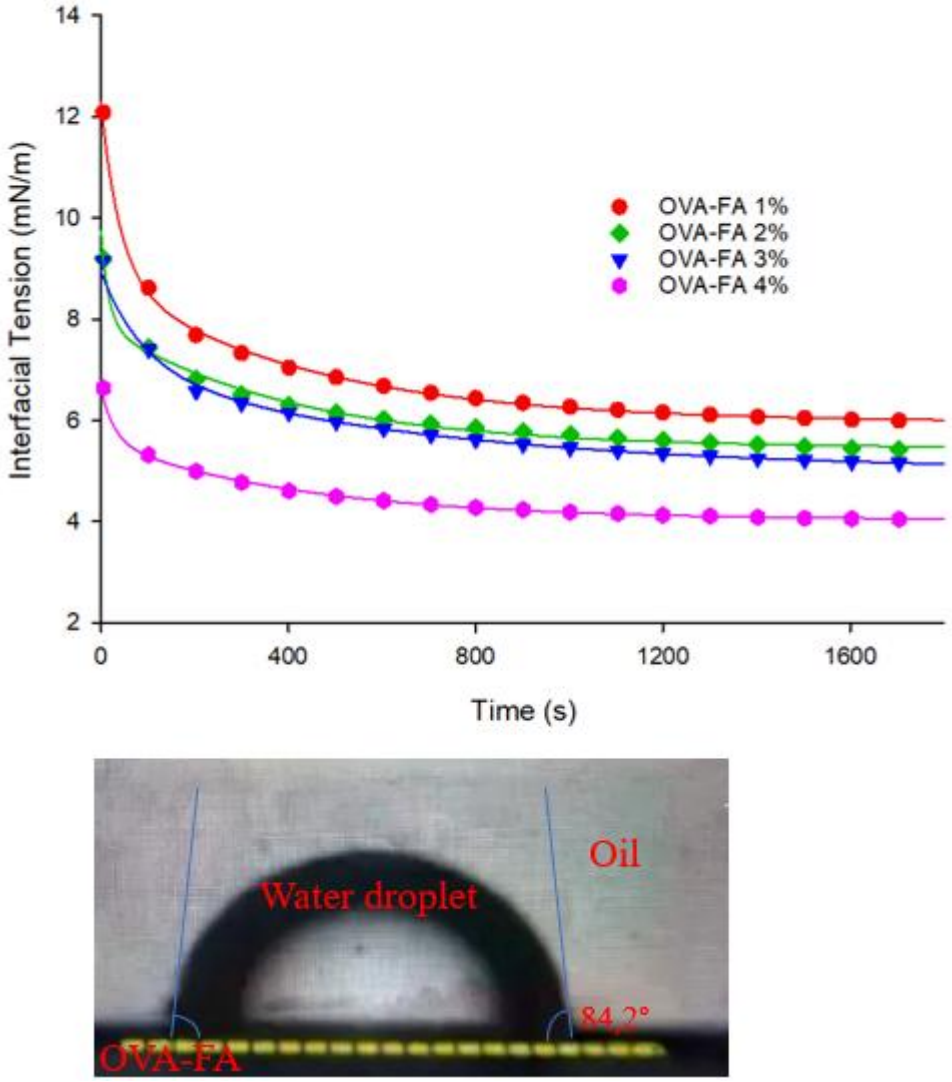

Figure 22. (A) Dynamic interfacial tension of different OVA-FA concentrations at the oil-water interface, with the model proposed by Equation 1 (–). (B) Oil-water three-phase contact angle with the OVA-FA conjugate.

3.2 Formation and Stability of Pickering Emulsions

3.2.1 Kinetic Stability

Figure 23 shows the creaming index of emulsions with different oil fractions over eight days of storage at 25 °C. The emulsion with a lower oil content (Figure 23A, $\varphi = 0.25$) exhibited lower kinetic stability, with phase separation observed after only 2 h. Sample A1, for example, presented a creaming index of 27.42 ± 6.46% in the first h, which increased to 33.65 ± 4.8% on the last day. The emulsions containing $\varphi = 0.5$ (Figure 23B) were more stable than the emulsions in Group A. Sample B1, for example, presented an increase in the creaming index from 5.08 ± 2.26% on the first day to 12.63 ± 1.89% on the seventh day, suggesting a gradual separation

process. Similar trends were observed for B2 and B3, which maintained relatively stable indices after an initial increase. Notably, emulsion B4 remained at 0% throughout the storage period, indicating that no phase separation occurred. The emulsion with φ = 0.60 (Figure 23C) exhibited a similar behavior to that of the B emulsions. Sample C1 presented an increase in the creaming index from 4.38 ± 2.07% on the first day to 14.02 ± 5.20% on the seventh day. Sample C3 remained stable for the first few days but increased in the final stage of storage. However, sample C4 maintained a creaming index of 0% throughout the period.

The emulsion with a high oil content (Figure 23D, φ = 0.7) demonstrated resistance to phase separation during the initial days of storage. Sample D1 showed no visible phase separation until the second day, after which creaming increased from 1.33 ± 2.31% to 19.11 ± 5.39% by the seventh day, indicating progressive destabilization. Sample D3 also remained stable in the early days, but creaming reached 11.66 ± 5.70% on the sixth day. Sample D4 exhibited the highest stability, with no observable phase separation throughout the entire experimental period.

Emulsions B4, C4, and D4 remained stable throughout the entire storage period, highlighting the critical roles of both the oil volume fraction and emulsifier concentration in preventing phase separation. At high oil loadings, droplets are densely packed, forming a percolating network within the continuous phase that significantly increases their effective viscosity and mechanically restricts droplet movement. This crowding effect slows both creaming and coalescence[19,20]. Simultaneously, the higher concentration of OVA-FA at the oil–water interface reduces the interfacial tension and introduces electrostatic repulsion between droplets. This repulsive force prevents them from approaching closely enough to merge, thereby maintaining a uniform and stable dispersion [13,20]. Qin *et al.* [2] reported a greater stability of Pickering O/W emulsions when the oil fraction in the system was increased. In systems with an oil fraction of 0.8, the emulsions remained stable throughout the analysis period without significant changes in their creaming index. Huang *et al.* [21] reported a lower creaming index in Pickering O/W emulsions using a higher concentration of protein conjugate from moringa seed residue and tannic acid, ranging from 8.2% for more concentrated systems to 32.7% for less concentrated systems after the entire experimental period.

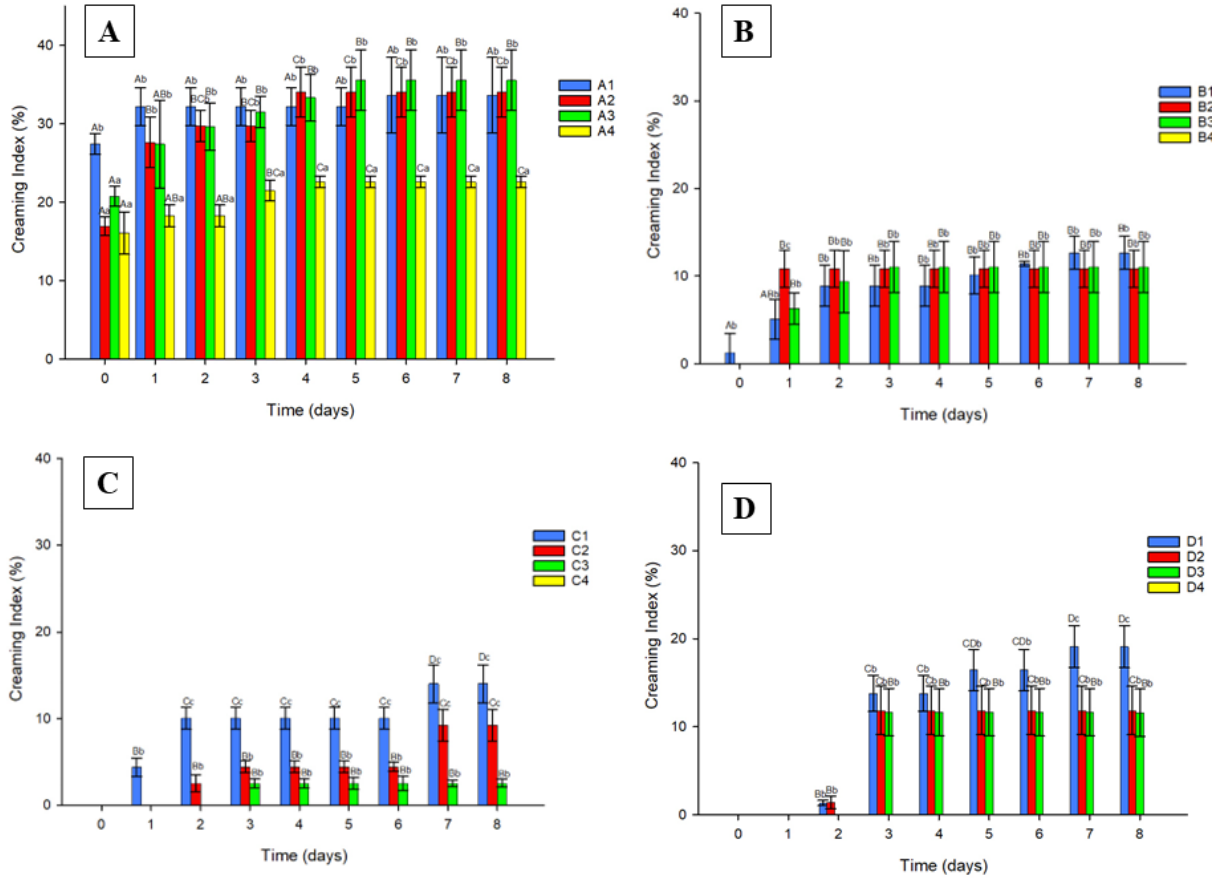

Figure 23. Creaming index of the different Pickering O/W emulsion samples, where (A), (B), (C), and (D) correspond to oil fractions of 0.25, 0.5, 0.6, and 0.7, respectively. Values followed by the same letters do not show statistically significant differences in the Tukey test ($p < 0.05$). Lowercase letters match samples and uppercase letters match time.

3.2.2 Protein Adsorption at the Emulsion Interface

Figure 24 shows the protein adsorption data at the oil–water interface of the emulsions. The A emulsions resulted in the lowest protein adsorption values at the interface. Compared with the other emulsions, emulsion A1 had the lowest concentration, at 13.97 ± 0.82%, whereas that of A4 reached 23.51 ± 1.17%, which was still lower than most. In contrast, emulsion B4 presented significantly higher values, at 48.30 ± 2.74%, indicating greater protein adsorption. Emulsions C4 and D4 had even higher adsorption values, with values of 51.30 ± 1.39% and 52.62 ± 0.97%, respectively, which can be correlated with the greater presence of the OVA-FA emulsifier. The emulsions with higher concentrations of OVA-FA showed greater protein adsorption, which was also supported by the interfacial tension data, where these solutions exhibited the lowest interfacial tension. This behavior suggests that higher concentrations of OVA-FA promote the formation of more stable interfaces, with a greater protein density at the droplet surfaces.

The above findings suggest that increasing the concentration of the OVA-FA emulsifier and the oil concentration increased the emulsifier's adsorption capacity due to the increase in surface area and the number of proteins available to bind to the interface. The increase in adsorption at the water–oil interface inhibits phase separation effects in the emulsion, such as flocculation and coalescence [22]. Thus, systems with greater adsorption tend to be more stable, and in this work, systems with greater protein adsorption at the interface presented lower creaming indices over time. Chen *et al.* [6] reported higher adsorption indices in Pickering O/W emulsions when whey protein isolate (WPI)-tannic acid conjugates were used as emulsifiers. Qin *et al.* [2] reported higher protein concentrations at the interface of a Pickering O/W emulsion when the concentration of the WPI-EGCG (epigallocatechin gallate) conjugate used as an emulsifier was increased and when the oil fraction in the emulsion was increased.

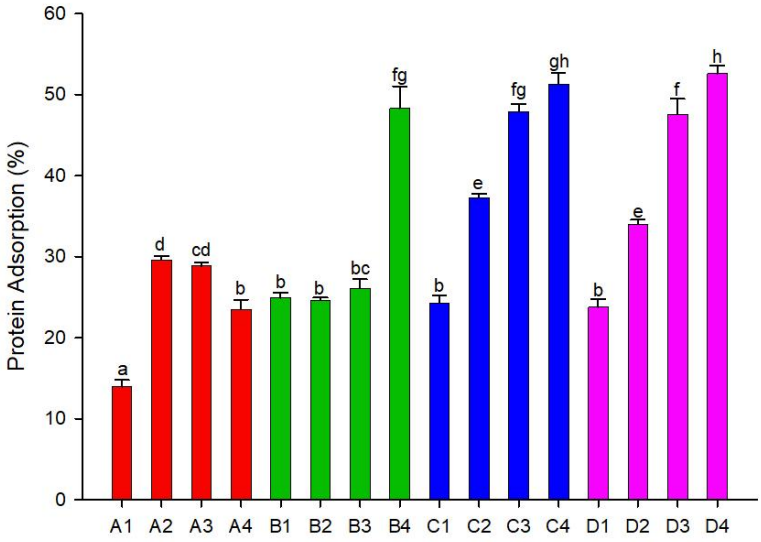

Figure 24. Adsorption of the OVA-FA conjugate at the oil-water interface of Pickering O/W emulsions. Values are presented as mean ± standard deviation. Values followed by the same letters do not show statistically significant differences in the Tukey test ($p < 0.05$).

3.3 Characterization of Pickering Emulsions

Samples B4, C4, and D4 showed no phase separation over the eight days of the experiment and presented relatively high values of protein adsorption at the oil–water interface. Therefore, these samples were selected for subsequent characterization and microencapsulation analyses of vitamin D3.

3.3.1 Particle Size and Zeta Potential

The particle size results indicated that sample B4 had an average size of 922.9 ± 50.5 nm, whereas sample C4 had an average size of 845.3 ± 46.9 nm. Sample D4, on the other hand, presented the smallest average particle size, measuring 733.3 ± 38.4 nm. Cui *et al.* [23] reported a decrease in the particle size distribution when the oil fraction increased in Pickering O/W emulsions from 0.2 to 0.78.

The zeta potential values for the samples were -41.3 ± 0.36 mV for B4, -41.63 ± 1.83 mV for C4, and -41.47 ± 1.15 mV for D4. No significant difference was observed between the zeta potential values of the samples ($p < 0.05$). High charge densities indicate high kinetic stability of the emulsion, resulting from repulsion between the droplets dispersed in the emulsion [13]. This stability was further supported by the results, as the samples remained stable for eight days.

3.3.2 Morphology

Figure 25 shows microscopy images of emulsions B4, C4, and D4. The images show dark circles, which correspond to the oil droplets, surrounded by a lighter region representing the aqueous phase. This distribution confirms that the OVA-FA conjugate was able to form and stabilize emulsions. Emulsion B had a lower density of dispersed droplets, whereas emulsions C4 and D4 had a greater number of droplets distributed in the aqueous phase.

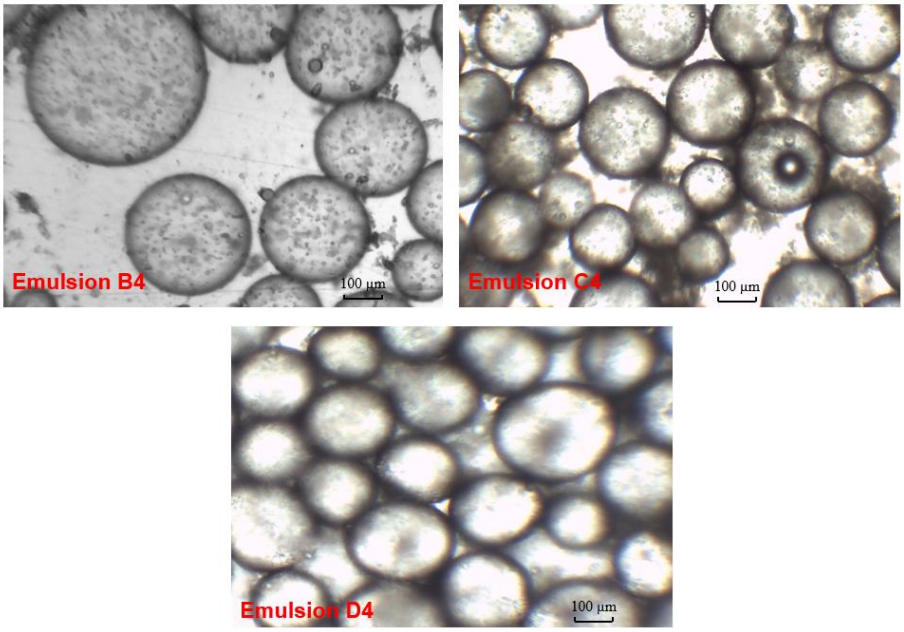

Figure 25. Optical microscopy image of B4, C4, and D4 samples, Pickering O/W emulsions, composed of an aqueous phase containing 4% OVA-FA and different oil fractions (0.5, 0.6, and 0.7, respectively).

3.3.3 Rheology

Figure 26A shows the apparent viscosity versus time graph for emulsions B4, C4, and D4. The emulsions exhibited a reduction in apparent viscosity with increasing shear rate, indicating pseudoplastic behavior [12]. This result is consistent with the literature, where several studies also identified pseudoplastic behavior in Pickering O/W emulsions [24,25]. Additionally, the increase in the oil fraction resulted in a higher apparent viscosity, possibly due to the closer proximity between the oil droplets, which intensifies interactions and hinders flow [24]. This behavior was also reported by Wan *et al.* [26], who reported an increase in the apparent viscosity of Pickering O/W emulsions up to an oil fraction of 0.85.

The fitted rheological models are presented in Table 6. The power law model showed a good fit to the experimental data, with high determination coefficient values. The index n was lower than 1 for all the samples, confirming the pseudoplastic nature of the emulsions. These results are consistent with other studies on Pickering emulsions reported in the literature. Wang *et al.* [27] reported a good correlation with the power law model in Pickering O/W emulsions formed by short-chain fatty acids and modified starch, with a high determination coefficient for all the systems studied. Additionally, they noted that the values of n for all systems were less than 1, ranging from 0.25-0.71. Similarly, Ren *et al.* [28] reported pseudoplastic behavior and excellent correlation with the power law model ($R^2 = 0.989$) in Pickering emulsions stabilized by lotus root starch and xanthan gum particles, with an n value of 0.216. The Bingham model, which assumes the existence of a yield stress, showed a less precise fit for the samples, suggesting that the rheological behavior of the emulsions cannot be fully described by this model. On the other hand, the Herschel–Bulkley model, which combines aspects of the two previous models, demonstrated good predictive ability for emulsion behavior, indicating the presence of yield stress followed by pseudoplastic behavior. Li *et al.* [29] also reported a more suitable response for the Herschel-Bulkley model than for the power law for Pickering O/W emulsions formed by a chitosan-starch complex, identifying pseudoplastic behavior in the presence of yield stress.

Table 6. Rheological models fit with Power Law, Bingham, and Herschel-Bulkley for emulsions with oil fractions of 0.5 (B4), 0.6 (C4), and 0.7 (D4), and 4% w/w OVA-FA as the emulsifier in the aqueous phase.

Model	Parameters	B4	C4	D4
Power Law	K (Pa.s^n)	1.331	1.765	2.422
	n	0.297	0.228	0.189
	Adjusted R^2	0.917	0.900	0.966
Bingham	τ_0 (Pa)	2.500	2.834	3.574
	μ_p (Pa.s)	0.031	0.026	0.026
	Adjusted R^2	0.838	0.852	0.867
Herschel-Bulkley	τ_0 (Pa)	0.894	2.408	1.602
	K (Pa.s^n)	0.705	0.125	1.046
	n	0.397	0.680	0.304
	Adjusted R^2	0.924	0.980	0.979

Dynamic shear rate sweep analysis revealed that all emulsions exhibited linear viscoelastic behavior at a deformation of 0.5%, from which the frequency sweep was performed, as shown in Figure 26B. The results show that the storage modulus was greater than the loss modulus for all emulsions studied, indicating predominantly elastic behavior [30]. Additionally, it is possible to observe that the tan δ values were consistently below 1, remaining close to 0.2 in all experiments. These low values indicate that elastic responses dominate over viscous ones, reinforcing that the emulsions exhibit elastic behavior with limited viscous flow under the tested conditions. This behavior can be attributed to the formation of a network structured by the OVA–FA conjugate in the continuous phase of the emulsion [31]. Furthermore, an increase in the oil fraction resulted in higher G' and G'' values, indicating that emulsion D4 exhibited a stronger and more viscoelastic gel. These findings are in line with those of Cui *et al.* [23], who reported a continuous increase in G' and G'' values in Pickering emulsions as the oil fraction was increased, with the highest fraction analyzed (0.78) showing the highest values for these moduli.

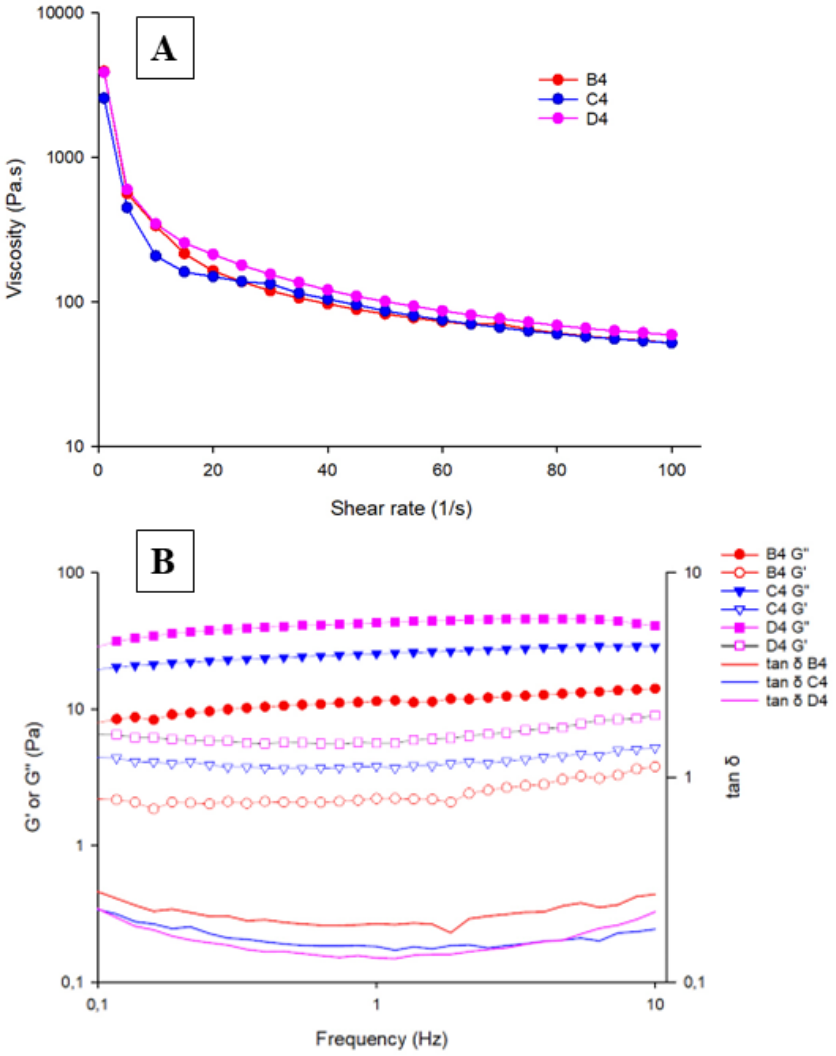

Figure 26. Rheological properties of Pickering emulsions at different oil fractions: (A) Apparent viscosity as a function of time; (B) Storage modulus (G'), loss modulus (G'') and damping factor (tan δ).

3.3.4 Antioxidant Capacity

The antioxidant capacity of the emulsions analyzed is shown in Figure 27. The $ABTS^{+}$ antioxidant capacity (Fig. 20A) of the emulsions formulated with OVA-FA was significantly greater than that of the OVAE emulsion, which used only ovalbumin as the emulsifier. The OVAE emulsion exhibited an antioxidant capacity of 21.89 ± 4.94%, whereas the emulsions containing the OVA–FA conjugate presented significantly higher values ($p < 0.05$): 87.98 ± 0.67% (sample B4), 89.53 ± 1.54% (sample C4), and 87.79 ± 1.01% (sample D4). This difference was also observed using the DPPH assay (Fig. 20B). The OVAE emulsion exhibited an antioxidant capacity of 23.51 ± 2.37%, whereas the B4, C4, and D4 emulsions presented significantly higher values ($p < 0.05$) of 83.37 ± 0.16%, 81.68 ± 0.91%, and 90.36% ± 0.27%,

respectively. The ferulic acid solution resulted in increased antioxidant capacity, with values of 94.17 ± 0.12% in the DPPH assay and 99.33 ± 0.44% in the ABTS assay.

These results suggest that the incorporation of ferulic acid enhanced the antioxidant capacity of the emulsions. Ferulic acid has high antioxidant activity due to its chemical structure; specifically, its phenolic hydroxyl groups can donate hydrogen atoms to neutralize free radicals and reactive oxygen species[32,33]. This mechanism contributes to the high radical scavenging activity of the OVA–FA conjugate and results in a significantly greater antioxidant capacity than that of pure ovalbumin. Zhang *et al.* [34] also reported greater antioxidant capacity in Pickering emulsions that used a casein–ferulic acid conjugate as an emulsifier than in emulsions that employed only casein.

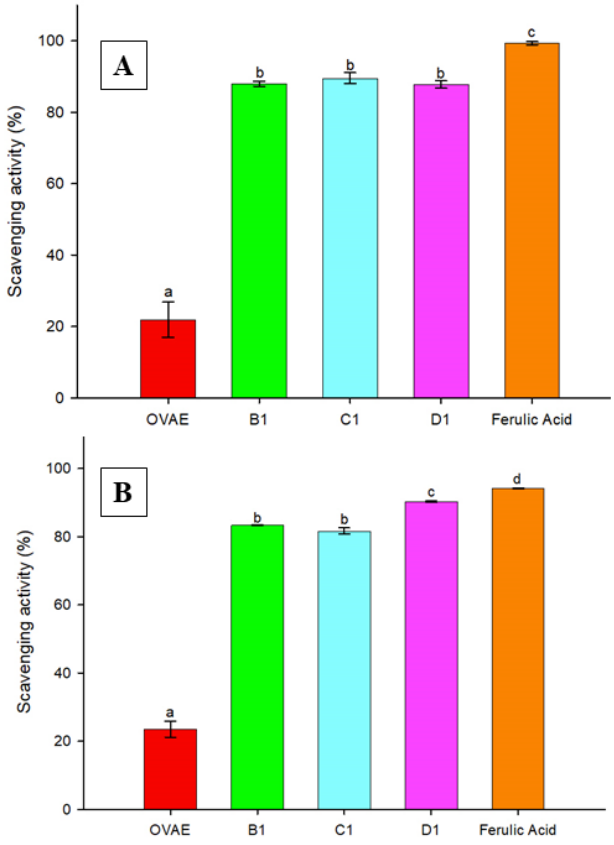

Figure 27. Antioxidant capacity, evaluated using the $ABTS^{+}$ (A) and DPPH (B) assays, of emulsions containing different oil fractions (B4 = 0.5, C4 = 0.6, D4 = 0.7), an emulsion stabilized with ovalbumin only (OVAE), and a ferulic acid solution (0.1 mg/mL). Results are expressed as mean ± standard deviation. Means followed by the same letter are not significantly different according to the Tukey test ($p < 0.05$).

3.3.5 Oxidative Stability

Figure 28A presents data on the concentration of cumene hydroperoxide (mmol/kg of oil) over time. The OVAE sample was formed with an emulsion containing an oil fraction of 0.5, using only OVA as the emulsifier. On Day 0, the hydroperoxide concentration in the OVAE

was 8.863 ± 0.895^{c} mmol/kg. Over time, this concentration increased significantly, reaching 186.37 ± 4.21^{b} mmol/kg on Day 14.

For treatments B4, C4, and D4, the initial hydroperoxide concentrations on Day 0 were 4.70 ± 0.43^{a} mmol/kg, 6.63 ± 0.61^{b} mmol/kg, and 3.56 ± 0.79^{a} mmol/kg, respectively. At the end of the experiment, on Day 14, the values for B4, C4, and D4 were 42.92 ± 0.45^{a} mmol/kg, 43.028 ± 0.870^{a} mmol/kg, and 39.265 ± 1.797^{a} mmol/kg, respectively. Compared with OVAE, emulsions containing OVA-FA presented lower oxidation levels. This effect is attributed to the presence of ferulic acid in the emulsifier mixture, which, owing to its antioxidant capacity, reduced the extent of lipid hydroperoxides in the emulsion. Consequently, the formation of hydroperoxides occurred more slowly in these emulsions than in OVAE, where oxidation was more pronounced over time. Similar effects were reported by Cui *et al.* [23], who reported that a conjugate of black soybean protein isolate and the anthocyanin cyanidin-3-glucoside significantly reduced lipid oxidation in Pickering emulsions compared with systems without the conjugate.

3.4 Microencapsulation of Vitamin D3 in O/W Pickering Emulsions

3.4.1 Encapsulation Efficiency of Vitamin D3

The results of the vitamin D3 encapsulation efficiency analysis are presented in Table 7, which shows that there was no significant difference between emulsions B4, C4, D4, and OVA ($p > 0.05$). The OVAE emulsion exhibited an encapsulation efficiency of 88.33 ± 1.20%, whereas the B4, C4, and D4 formulations achieved efficiencies of 91.59 ± 0.85%, 92.59 ± 0.73%, and 92.13 ± 1.14%, respectively. This could be explained by the ability of the emulsifier to form a sterically hindering interfacial layer that entraps the oil phase, thereby enhancing the barrier performance against the diffusion of vitamin D3 from the oil core [35].

Similar results were also noted by Jan *et al.* [36], who reported an encapsulation efficiency of approximately 90% for vitamin D3 in an optimized O/W nanoemulsion formulation composed of medium-chain triglyceride (MCT) oil, ethylene glycol (EG), and Kolliphor RH-40. Similarly, Shah *et al.* [37] reported an encapsulation efficiency of 91.8% for vitamin D3 in Pickering emulsions stabilized by zein and chitosan complexes.

Table 7. Encapsulation efficiency of vitamin D3 in emulsions with different oil fractions. Values are presented as mean ± standard deviation. Values followed by the same letters do not show statistically significant differences in the Tukey test ($p < 0.05$).

Sample	Encapsulation Efficiency (%)
OVAE	88.33 ± 1.20[a]
B4	91.59 ± 0.85[a]
C4	92.59 ± 0.73[a]
D4	92.13 ± 1.14[a]

3.4.2 Photochemical stability

Figure 28B presents the degradation of vitamin D3 over time for the samples. Compared with the OVAE emulsion, the emulsions containing the OVA-FA conjugate caused less degradation of vitamin D3. After 1 h of exposure, the vitamin D3 loss in the OVAE emulsion reached 25.40 ± 1.78%, whereas the B4, C4, and D4 formulations presented lower losses of 23.38 ± 1.29%, 21.30 ± 2.46%, and 12.78 ± 1.26%, respectively. As the exposure time increased to 3 h, greater protection of the OVA-FA emulsions was maintained, with the D4 emulsion showing the lowest degradation rate of 26.51 ± 2.59%, whereas the OVA emulsion presented a significantly greater ($p < 0.05$) loss of 39.68 ± 0.92%.

Vitamin D3 is highly sensitive to light and significantly degrades over time when exposed to light [38,39]. Emulsions with higher oil fractions (C4 and D4 emulsions) resulted in less degradation of vitamin D3 over time, which can be attributed to greater adsorption of the conjugate at the oil–water interface, forming a barrier that prevents peroxide formation [40]. These results suggest that the addition of FA to the OVA emulsified system can provide significant protection against the photochemical degradation of vitamin D3, with the D4 formulation being the most efficient. Similarly, Zhang *et al.* [10] reported greater retention of vitamin D3 in Pickering O/W emulsions stabilized by soybean peptide nanoparticles (SPNs) than in emulsions stabilized by the surfactant Tween 80. The study indicated that higher concentrations of SPN resulted in increased retention, which was attributed to greater particle coverage at the interface.

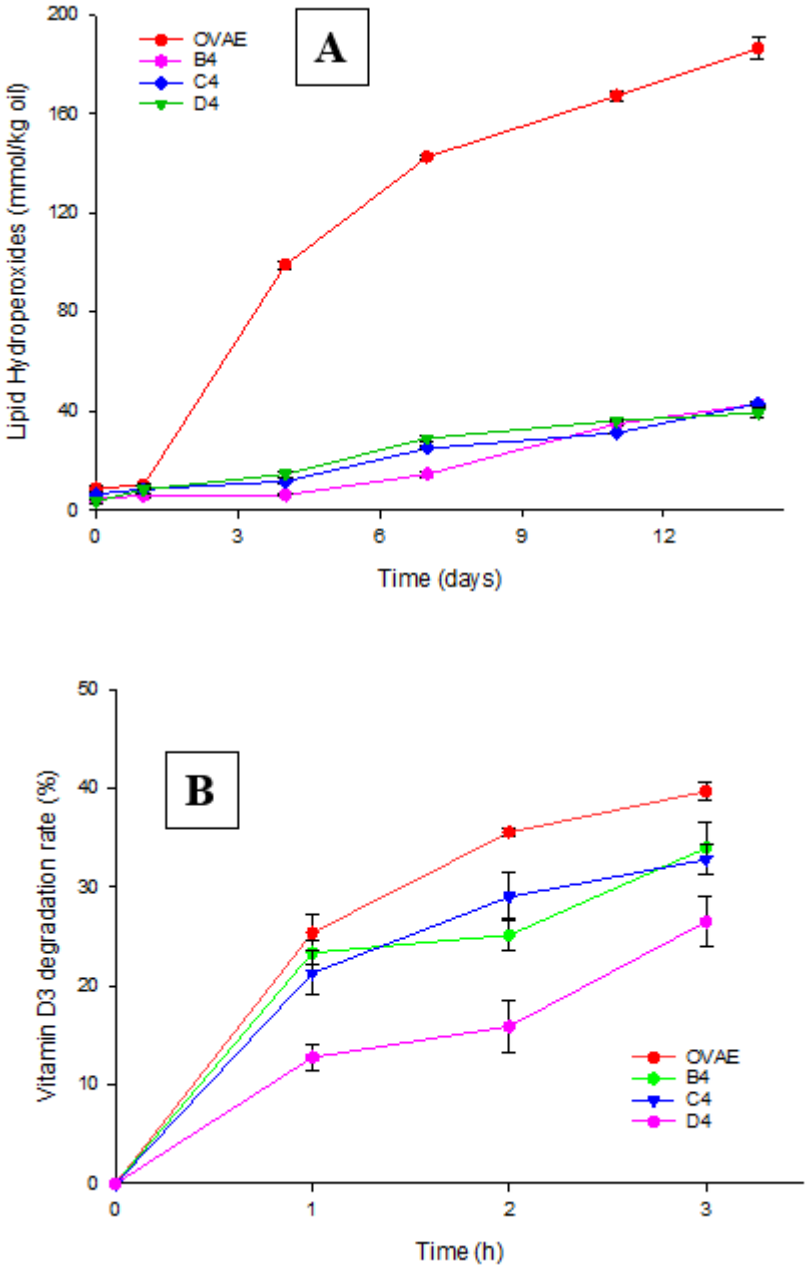

Figure 28. (A) Lipid oxidation of Pickering O/W emulsions at different oil fractions. (B) Photochemical stability of vitamin D3 under UV irradiation in Pickering emulsions stabilized by OVA-FA, with different oil fractions.

3.5 In vitro gastrointestinal simulation of Vitamin D3 microcapsules

3.5.1 Release of Vitamin D3

Figure 29 presents the release profile of vitamin D3 from emulsions B4, C4, D4, OVAE, and the control throughout *in vitro* digestion. A marked decline in vitamin D3 content was observed in the control sample over time, in contrast to the microencapsulated samples. While the control showed a high initial release, its vitamin D3 content decreased drastically after 30 min, reaching less than 5% after 150 min. This degradation is likely due to enhanced oxidation

of vitamin D3 at acidic gastric pH and lipid oxidation resulting from exposure to oxygen in the unprotected oil phase [41].

During the oral phase, the release of microencapsulated vitamin D3 reached 9.15 ± 0.38%, likely due to the dilution of the emulsion by simulated salivary fluid, which may have contributed to its structural destabilization. In the gastric phase, the release of vitamin D3 progressively increased, reaching 37.07 ± 1.53% at the end of this stage in the OVAE emulsion. This significant increase could be attributed to the action of pepsin in an acidic environment, which promotes protein degradation. This process affects ovalbumin molecules at the interface, reducing repulsion between emulsion droplets, favoring phase separation, and consequently enhancing vitamin D3 release [42]. Emulsions B4, C4, and D4 exhibited significantly lower release rates ($p < 0.05$) than did OVAE, with values of 28.69 ± 1.76%, 29.16 ± 1.25%, and 28.62 ± 0.89%, respectively. This reduced release could be attributed to lower degradation of OVA–FA at the oil–water interface compared to native ovalbumin. One possible explanation is that ferulic acid, covalently bound to ovalbumin, may interfere with pepsin activity. Conjugation can induce modifications in the secondary and tertiary structures of proteins [29], resulting in steric hindrance at enzymatic cleavage sites and alterations in surface charge. These structural and electrostatic changes are known to influence enzymatic accessibility and efficiency [67,68]. Additionally, the covalent interaction between ovalbumin and ferulic acid reduces the number of accessible amino acid residues available for pepsin cleavage, further limiting proteolysis[69].These findings align with those of previous studies, where Zhou *et al.* [70] reported that, compared with pure protein, the conjugation of the polyphenol EGCG with soy protein isolate reduced protein hydrolysis, thereby limiting digestion.

In the intestinal phase, the total release of vitamin D3 from OVAE and emulsions B4, C4, and D4 reached 51.99 ± 1.15%, 45.04 ± 1.52%, 46.89 ± 1.38%, and 43.39 ± 1.40%, respectively. This increase was attributed to the action of lipase, which hydrolyzes fat molecules in the oil phase, generating free fatty acids and monoglycerides, thus facilitating the release of vitamin D3 [20].

These results indicate that the OVA-FA conjugate improves the vitamin D3 release profile by reducing its release during the oral and gastric phases. Similar findings were reported by Kouravand *et al.* [40], who reported that emulsions stabilized by conjugates of WPI and basil seed gum presented lower vitamin D3 release rates during the gastric phase (approximately 28%–36%) than emulsions containing only WPI. After two h in the intestinal phase, the release increased to approximately 50%.

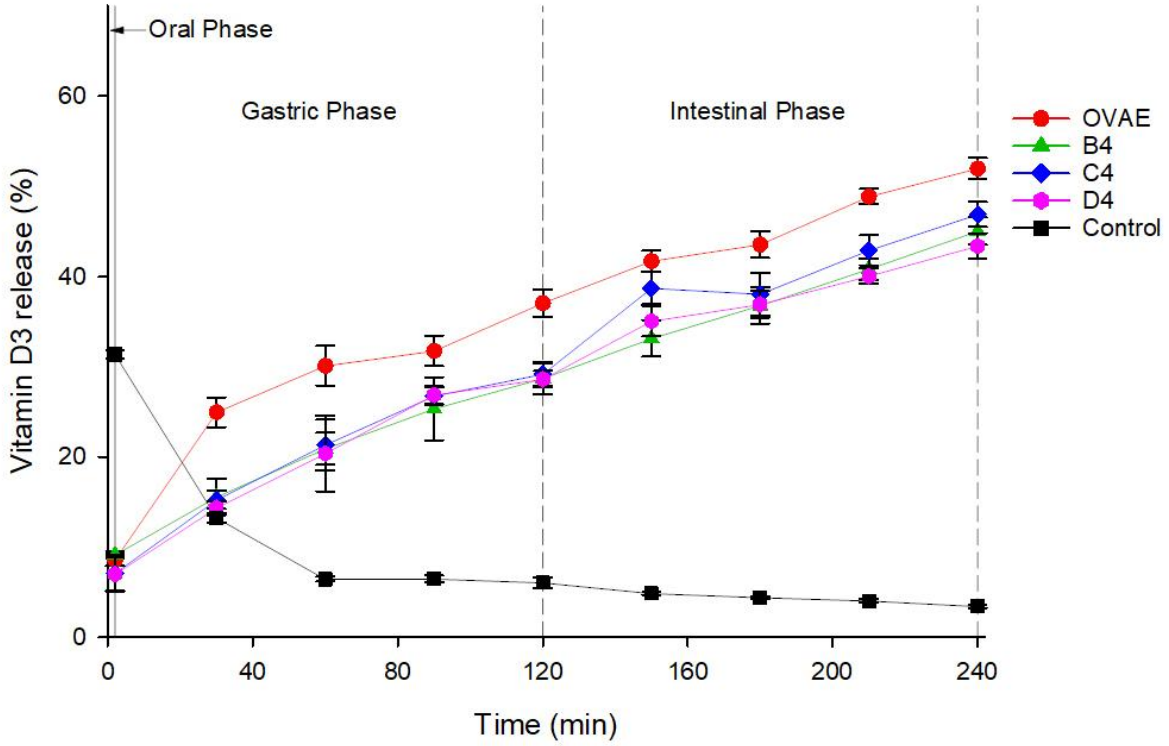

Figure 29. Vitamin D3 release in *in vitro* gastrointestinal simulations of Pickering O/W emulsions with different oil fractions (B4 = 0.5, C4 = 0.6, D4 = 0.7), an emulsion stabilized with ovalbumin only (OVAE), and an unencapsulated vitamin D3 in oil (Control).

3.5.2 Bioaccessibility of Vitamin D3

The bioaccessibility of vitamin D3 after the complete *in vitro* digestion simulation is presented in Figure 30. Compared with the microencapsulated formulations, the no microencapsulated vitamin D3 (control) formulation exhibited significantly lower bioaccessibility ($p < 0.05$), indicating that the microencapsulation process effectively protects vitamin D3 throughout the digestive process. Since vitamin D3 absorption occurs in the small intestine, its availability at this stage of digestion is crucial [45]. Compared with the emulsions stabilized by the OVA-FA conjugate, the OVAE emulsion exhibited significantly lower bioaccessibility ($p < 0.05$). This result may be attributed to the greater stability of emulsions formed by the conjugate, which demonstrated greater resistance to phase separation throughout digestion, as evidenced by the release profile.

Similar findings were reported by Zhao *et al.* [71], where Pickering emulsions stabilized solely by WPI particles presented a bioaccessibility of 22.33%, which was lower than that of emulsions formed using WPI conjugated with tannic acid, gallic acid, tea polyphenols, and vanillic acid (ranging from 25.4% to 60.4%). These results indicate that the incorporation of polyphenolic compounds can significantly increase the bioaccessibility of encapsulated vitamin

D. Additionally, the authors reported that emulsions with higher physical stability tended to exhibit superior bioaccessibility. Similarly, Zhang *et al.* [10] reported that Pickering emulsions stabilized by soy peptide nanoparticles achieved a vitamin D3 bioaccessibility of 55.25%, whereas that of conventional emulsions using Tween 80 as the emulsifier reached 60.17%. These findings highlight the potential of Pickering emulsions to perform comparably to conventional surfactant-based systems commonly used in industry.

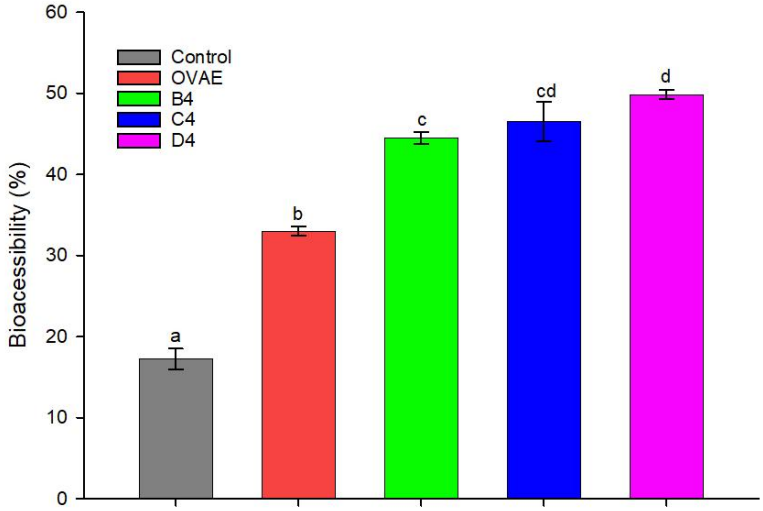

Figure 30. Bioaccessibility of vitamin D3 in a simulated *in vitro* gastrointestinal model from emulsions with different oil fractions (B4 = 0.5, C4 = 0.6, D4 = 0.7), an emulsion stabilized with ovalbumin only (OVAE), and an unencapsulated vitamin D3 in oil (Control). Values followed by the same letters do not show statistically significant differences in the Tukey test ($p < 0.05$).

4 Conclusions

This study demonstrated that Pickering emulsions stabilized by ovalbumin–ferulic acid (OVA–FA) conjugates exhibit high physicochemical stability and antioxidant potential, making them effective for the encapsulation and protection of vitamin D3. Compared with emulsions stabilized with lower conjugate concentrations, emulsions formulated with a higher oil fraction and OVA-FA concentration presented a lower creaming index and greater protein adsorption at the oil–water interface. Additionally, the incorporation of OVA-FA conjugates significantly reduced lipid hydroperoxides and the photochemical degradation of vitamin D3, highlighting their efficiency in preserving this bioactive compound. The *in vitro* digestion simulation revealed that emulsions containing OVA-FA enabled more controlled vitamin D3 release and higher bioaccessibility than the OVAE system did, demonstrating the potential of these conjugates for functional food applications. Thus, the findings emphasize the potential of Pickering emulsions stabilized by ovalbumin–ferulic acid (OVA–FA) conjugates as an effective

strategy for vitamin D3 fortification in foods, offering enhanced stability and antioxidant capacity. Their application could extend to various products, such as dairy alternatives, dressings, and functional beverages. However, further studies are needed to evaluate their performance in real food matrices, as factors like pH, ionic strength, and processing conditions may affect their stability and effectiveness.

Conflict of interest

The authors declare that they have no known competing financial interests or personal relationships that could have appeared to influence the work reported in this paper.

Acknowledgments

The authors thank the CNPq, Brazil (313928/2021-5); CAPES, Brazil (Código 001) and FAPERJ, Brazil (E-26/210.052/2023; E-26/204.182/2024) for the financial support.

CRediT authorship contribution statement

Bruno Sérgio Toledo Barbosa: Conceptualization, Methodology, Validation, Investigation, Writing – original draft, Writing – review & editing. **Edwin Elard Garcia-Rojas**: Conceptualization, Methodology, Resources, Writing – review & editing, Supervision, Project administration, Funding acquisition.

5 References

[1] S. Gallo, A. Phan, C.A. Vanstone, C. Rodd, H.A. Weiler, The change in plasma 25-hydroxyvitamin D did not differ between breast-fed infants that received a daily supplement of ergocalciferol or cholecalciferol for 3 months, J. Nutr. 143 (2013) 148–153. https://doi.org/10.3945/jn.112.167858.

[2] H. Göring, Vitamin D in nature: a product of synthesis and/or degradation of cell membrane components, Biochemistry (Moscow) 83 (2018) 1350–1357. https://doi.org/10.1134/S0006297918110056.

[3] A.C. Ross, Dietary reference intakes for calcium and vitamin D, National Academies Press, Washington, D.C., 2011. https://doi.org/10.17226/13050.

[4] V.Z.C. Borba, M. Lazaretti-Castro, S. da S. Moreira, M.C.C. de Almeida, E.D. Moreira, Epidemiology of vitamin D (EpiVida): a study of vitamin D status among healthy adults in Brazil, J. Endocr. Soc. 7 (2022) bvac171. https://doi.org/10.1210/jendso/bvac171.

[5] L.R. Wilson, L. Tripkovic, K.H. Hart, S.A. Lanham-New, Vitamin D deficiency as a public health issue: using vitamin D2 or vitamin D3 in future fortification strategies, Proc. Nutr. Soc. 76 (2017) 392–399. https://doi.org/10.1017/S0029665117000349.

[6] F. Kouravand, F. Shahidi, M. Fathi, A. Koocheki, S. Roshanak, Physicochemical stability and controlled release of vitamin D3-loaded emulsions stabilised by whey protein isolate–basil seed gum conjugates, J. Microencapsul. 41 (2024) 770–781. https://doi.org/10.1080/02652048.2024.2418615.

[7] K. Liu, X.L. Kong, Q.M. Li, H.L. Zhang, X.Q. Zha, J.P. Luo, Stability and bioavailability of vitamin D3 encapsulated in composite gels of whey protein isolate and lotus root amylopectin, Carbohydr. Polym. 227 (2020) 115337. https://doi.org/10.1016/j.carbpol.2019.115337.

[8] M. Esmaeili, R. Yekta, A.S. Abedi, K. Ghanati, R.Z. Derav, A. Houshyarrad, Z.S. Dehkordi, M. Ajami, M. Mahmoudzadeh, Encapsulating vitamin D: a feasible and promising approach to combat its deficiency, Pharm. Sci. 28 (2022) 194–207. https://doi.org/10.34172/PS.2021.42.

[9] S.R. Bajaj, S.J. Marathe, R.S. Singhal, Co-encapsulation of vitamin B12 and D3 using spray drying: wall material optimization, product characterization, and release kinetics, Food Chem. 335 (2021) 127642. https://doi.org/10.1016/j.foodchem.2020.127642.

[10] M.B. Santos, E.E. Garcia-Rojas, Recent advances in the encapsulation of bioactive ingredients using galactomannans-based delivery systems, Food Hydrocoll. 118 (2021) 106815. https://doi.org/10.1016/j.foodhyd.2021.106815.

[11] Y. Zhang, F. Zhou, X. Zeng, P. Shen, D. Yuan, M. Zhong, Q. Zhao, M. Zhao, pH-driven-assembled soy peptide nanoparticles as particulate emulsifier for oil-in-water Pickering emulsion and their potential for encapsulation of vitamin D3, Food Chem. 383 (2022) 132489. https://doi.org/10.1016/j.foodchem.2022.132489.

[12] D.J. McClements, Nanoparticle and microparticle based delivery systems, 1st ed., CRC Press, Boca Raton, FL, 2014. https://doi.org/10.1201/b17280.

[13] E. Fredrick, P. Walstra, K. Dewettinck, Factors governing partial coalescence in oil-in-water emulsions, Adv. Colloid Interface Sci. 153 (2010) 30–42. https://doi.org/10.1016/j.cis.2009.10.003.

[14] D.J. McClements, E. Decker, Interfacial antioxidants: a review of natural and synthetic emulsifiers and coemulsifiers that can inhibit lipid oxidation, J. Agric. Food Chem. 66 (2018) 20–35. https://doi.org/10.1021/acs.jafc.7b05066.

[15] Y. Chevalier, M.A. Bolzinger, Emulsions stabilized with solid nanoparticles: Pickering emulsions, Colloids Surf. A Physicochem. Eng. Asp. 439 (2013) 23–34. https://doi.org/10.1016/j.colsurfa.2013.02.054.

[16] R. Rayees, A. Gani, N. Noor, A. Ayoub, Z.U. Ashraf, General approaches to biopolymer-based Pickering emulsions, Int. J. Biol. Macromol. 267 (2024) 131430. https://doi.org/10.1016/j.ijbiomac.2024.131430.

[17] C. Albert, M. Beladjine, N. Tsapis, E. Fattal, F. Agnely, N. Huang, Pickering emulsions: preparation processes, key parameters governing their properties and potential for

pharmaceutical applications, J. Control. Release 309 (2019) 302–332. https://doi.org/10.1016/j.jconrel.2019.07.003.

[18] X. Yan, C. Ma, F. Cui, D.J. McClements, X. Liu, F. Liu, Protein-stabilized Pickering emulsions: formation, stability, properties, and applications in foods, Trends Food Sci. Technol. 103 (2020) 293–303. https://doi.org/10.1016/j.tifs.2020.07.005.

[19] F. Liu, D.J. McClements, C. Ma, X. Liu, Novel colloidal food ingredients: protein complexes and conjugates, Annu. Rev. Food Sci. Technol. 14 (2023) 35–61. https://doi.org/10.1146/annurev-food-060721-023522.

[20] W.N. Baba, D.J. McClements, S. Maqsood, Whey protein–polyphenol conjugates and complexes: production, characterization, and applications, Food Chem. 365 (2021) 130455. https://doi.org/10.1016/j.foodchem.2021.130455.

[21] T.H. Quan, S. Benjakul, T. Sae-leaw, A.K. Balange, S. Maqsood, Protein–polyphenol conjugates: antioxidant property, functionalities and their applications, Trends Food Sci. Technol. 91 (2019) 507–517. https://doi.org/10.1016/j.tifs.2019.07.049.

[22] J. Liu, H. Yong, X. Yao, H. Hu, D. Yun, L. Xiao, Recent advances in phenolic–protein conjugates: synthesis, characterization, biological activities and potential applications, RSC Adv. 9 (2019) 35825–35840. https://doi.org/10.1039/C9RA07808H.

[23] J.A. Huntington, P.E. Stein, Structure and properties of ovalbumin, J. Chromatogr. B 756 (2001) 189–198. https://doi.org/10.1016/S0378-4347(01)00108-6.

[24] H. Rostamabadi, V. Chaudhary, N. Chhikara, N. Sharma, M. Nowacka, I. Demirkesen, K. Rathnakumar, S.R. Falsafi, Ovalbumin, an outstanding food hydrocolloid: applications, technofunctional attributes, and nutritional facts—a systematic review, Food Hydrocoll. 139 (2023) 108514. https://doi.org/10.1016/j.foodhyd.2023.108514.

[25] B. Warren, Ferulic acid: antioxidant properties, uses and potential health benefits, Nova Science Pub Inc., Hauppauge, NY, 2014.

[26] S. Ge, R. Jia, Q. Li, W. Liu, M. Liu, D. Cai, M. Zheng, H. Liu, J. Liu, Pickering emulsion stabilized by zein/adzuki bean seed coat polyphenol nanoparticles to enhance the stability and bioaccessibility of astaxanthin, J. Funct. Foods 88 (2022) 104867. https://doi.org/10.1016/j.jff.2021.104867.

[27] Y. Sun, M. Zhao, Z. Liu, H. Shi, X. Zhang, Y. Zhao, Z. Ma, G. Yu, G. Xia, X. Shen, Preparation and characterization of lactoferrin-polyphenol conjugate with stabilizing effects on fish oil high internal phase Pickering emulsions, Food Chem. X 24 (2024) 101836. https://doi.org/10.1016/j.fochx.2024.101836.

[28] Y. Xu, Z. Wei, C. Xue, Pickering emulsions stabilized by zein–gallic acid composite nanoparticles: impact of covalent or non-covalent interactions on storage stability, lipid oxidation and digestibility, Food Chem. 408 (2023) 135254. https://doi.org/10.1016/j.foodchem.2022.135254.

[29] B.S.T. Barbosa, S.C. Araújo, Y. Cordeiro, E.E. Garcia-Rojas, Impact of the covalent interaction between ferulic acid and ovalbumin on the structure and functional properties of the protein, Food Biophys. 20 (2025) 1-12. https://doi.org/10.1007/s11483-024-09919-6.

[30] B.S.T. Barbosa, E.E. Garcia-Rojas, Double emulsions as delivery systems for iron: stability kinetics and improved bioaccessibility in infants and adults, Curr. Res. Food Sci. 5 (2022) 718–725. https://doi.org/10.1016/j.crfs.2022.04.003.

[31] T. Shi, V.E. Ziegler, I.C. Welge, L. An, B.A. Wolf, Evolution of the interfacial tension between polydisperse "immiscible" polymers in the absence and in the presence of a compatibilizer, Macromol. 37 (2004) 1591–1599. https://doi.org/10.1021/ma035616y.

[32] X.S. Qin, Q.Y. Gao, Z.G. Luo, Enhancing the storage and gastrointestinal passage viability of probiotic powder (*Lactobacillus plantarum*) through encapsulation with Pickering high internal phase emulsions stabilized with WPI–EGCG covalent conjugate nanoparticles, Food Hydrocoll. 116 (2021) 106658. https://doi.org/10.1016/j.foodhyd.2021.106658.

[33] M. Ju, G. Zhu, G. Huang, X. Shen, Y. Zhang, L. Jiang, X. Sui, A novel Pickering emulsion produced using soy protein–anthocyanin complex nanoparticles, Food Hydrocoll. 99 (2020) 105329. https://doi.org/10.1016/j.foodhyd.2019.105329.

[34] Y. Ji, C. Han, E. Liu, X. Li, X. Meng, B. Liu, Pickering emulsions stabilized by pea protein isolate–chitosan nanoparticles: fabrication, characterization and delivery EPA for digestion *in vitro* and *in vivo*, Food Chem. 378 (2022) 132090. https://doi.org/10.1016/j.foodchem.2022.132090.

[35] Z. Ren, Z. Chen, Y. Zhang, X. Lin, B. Li, Novel food-grade Pickering emulsions stabilized by tea water-insoluble protein nanoparticles from tea residues, Food Hydrocoll. 96 (2019) 322–330. https://doi.org/10.1016/j.foodhyd.2019.05.015.

[36] C. Chen, K. Shi, X. Qin, H. Zhang, H. Chen, D.G. Hayes, Q. Wu, Z. Hu, G. Liu, Effect of interactions between glycosylated protein and tannic acid on the physicochemical stability of Pickering emulsions, LWT 152 (2021) 112383. https://doi.org/10.1016/j.lwt.2021.112383.

[37] G. Ren, J. Liu, J. Shi, Y. He, Y. Zhu, Y. Zhan, J. Lv, L. Liu, Y. Huang, M. Huang, W. Fang, Q. Lei, H. Xie, Improved antioxidant activity and delivery of peppermint oil Pickering emulsion stabilized by resveratrol-grafted zein covalent conjugate/quaternary ammonium chitosan nanoparticles, Int. J. Biol. Macromol. 253 (2023) 127094. https://doi.org/10.1016/j.ijbiomac.2023.127094.

[38] M. Liu, J. Liang, C. Jing, Y. Yue, Y. Xia, Y. Yuan, T. Yue, Preparation and characterization of *Lycium barbarum* seed oil Pickering emulsions and evaluation of antioxidant activity, Food Chem. 405 (2023) 134906. https://doi.org/10.1016/j.foodchem.2022.134906.

[39] Y. Zhang, F. Zhou, M. Zhao, L. Lin, Z. Ning, B. Sun, Soy peptide nanoparticles by ultrasound-induced self-assembly of large peptide aggregates and their role on emulsion stability, Food Hydrocoll. 74 (2018) 62–71. https://doi.org/10.1016/j.foodhyd.2017.07.021.

[40] A. Brodkorb, L. Egger, M. Alminger, P. Alvito, R. Assunção, S. Ballance, T. Bohn, C. Bourlieu-Lacanal, R. Boutrou, F. Carrière, A. Clemente, M. Corredig, D. Dupont, C. Dufour, C. Edwards, M. Golding, S. Karakaya, B. Kirkhus, S. Le Feunteun, U. Lesmes, A. Macierzanka, A.R. Mackie, C. Martins, S. Marze, D.J. McClements, O. Ménard, M. Minekus, R. Portmann, C.N. Santos, I. Souchon, R.P. Singh, G.E. Vegarud, M.S.J. Wickham, W. Weitschies, I. Recio, INFOGEST static *in vitro* simulation of gastrointestinal food digestion, Nat. Protoc. 14 (2019) 991–1014. https://doi.org/10.1038/s41596-018-0119-1.

[41] T. Winuprasith, M. Suphantharika, Properties and stability of oil-in-water emulsions stabilized by microfibrillated cellulose from mangosteen rind, Food Hydrocoll. 43 (2015) 690–699. https://doi.org/10.1016/j.foodhyd.2014.07.027.

[42] D.J. McClements, Food emulsions, 2nd ed., CRC Press, Boca Raton, FL, 2004. https://doi.org/10.1201/9781420039436.

[43] L.E. Low, S.P. Siva, Y.K. Ho, E.S. Chan, B.T. Tey, Recent advances of characterization techniques for the formation, physical properties and stability of Pickering emulsion, Adv. Colloid Interface Sci. 277 (2020) 102117. https://doi.org/10.1016/j.cis.2020.102117.

[44] Y. Zou, J. Guo, S.W. Yin, J.M. Wang, X.Q. Yang, Pickering emulsion gels prepared by hydrogen-bonded zein/tannic acid complex colloidal particles, J. Agric. Food Chem. 63 (2015) 7405–7414. https://doi.org/10.1021/acs.jafc.5b03113.

[45] X. Yi, Y. Chen, B. Ding, K. Ma, Z. Li, Y. Luo, High internal phase Pickering emulsions prepared by globular protein–tannic acid complexes: a hydrogen bond-based interfacial crosslinking strategy, J. Mol. Liq. 370 (2023) 121025. https://doi.org/10.1016/j.molliq.2022.121025.

[46] G. Zhao, S. Wang, H. Yang, L. Yang, H. Song, G. Zhang, H. Liu, Y. He, Impact of oil volume fraction on stability of Pickering emulsion prepared by silica particles and soy hull polysaccharides, J. Food Eng. 397 (2025) 112601. https://doi.org/10.1016/j.jfoodeng.2025.112601.

[47] Z. Huang, X. Yang, Q. Chen, L. Chen, S. Liang, Q. Zeng, R. Zhang, F. Huang, L. Dong, D. Su, Ferulic acid and EGCG alter the structural characteristics of ovalbumin and its application in mineral loading, Int. J. Food Sci. Technol. 57 (2022) 3060–3068. https://doi.org/10.1111/ijfs.15634.

[48] X. Tao, C. Chen, Y. Li, X. Qin, H. Zhang, Y. Hu, Z. Liu, X. Guo, G. Liu, Improving the physicochemical stability of Pickering emulsion stabilized by glycosylated whey protein isolate/cyanidin-3-glucoside to deliver curcumin, Int. J. Biol. Macromol. 229 (2023) 1–10. https://doi.org/10.1016/j.ijbiomac.2022.12.269.

[49] X. Cui, M. Ma, Y. Xie, Y. Yang, Q. Li, S. Sun, W. Ma, Formation, structure and stability of high internal phase Pickering emulsions stabilized by BSPI–C3G covalent complexes, Food Chem. X 16 (2022) 100455. https://doi.org/10.1016/j.fochx.2022.100455.

[50] M. Geng, L. Li, X. Feng, J. Xu, Y. Huang, F. Teng, Y. Li, Encapsulation of β-carotene in high internal phase Pickering emulsions stabilized by soy protein isolate–epigallocatechin-3-gallate covalent composite microgel particles, J. Mol. Liq. 360 (2022) 119511. https://doi.org/10.1016/j.molliq.2022.119511.

[51] Y. Wan, R. Wang, W. Feng, Z. Chen, T. Wang, High internal phase Pickering emulsions stabilized by co-assembled rice proteins and carboxymethyl cellulose for food-grade 3D printing, Carbohydr. Polym. 273 (2021) 118586. https://doi.org/10.1016/j.carbpol.2021.118586.

[52] R. Wang, M. Li, M. Liu, A. Wang, P. Strappe, C. Blanchard, Z. Zhou, Characterization of Pickering emulsion by SCFAs-modified debranched starch and a potent for delivering

encapsulated bioactive compound, Int. J. Biol. Macromol. 231 (2023) 123164. https://doi.org/10.1016/j.ijbiomac.2023.123164.

[53] X. Ren, C. Zhou, A. Qayum, J. Tang, Q. Liang, Pickering emulsion: a multi-scale stabilization mechanism based on modified lotus root starch/xanthan gum nanoparticles, Int. J. Biol. Macromol. 233 (2023) 123459. https://doi.org/10.1016/j.ijbiomac.2023.123459.

[54] X.M. Li, Q.T. Xie, J. Zhu, Y. Pan, R. Meng, B. Zhang, H.Q. Chen, Z.Y. Jin, Chitosan hydrochloride/carboxymethyl starch complex nanogels as novel Pickering stabilizers: physical stability and rheological properties, Food Hydrocoll. 93 (2019) 215–225. https://doi.org/10.1016/j.foodhyd.2019.02.021.

[55] M.H. Tunick, Small-strain dynamic rheology of food protein networks, J. Agric. Food Chem. 59 (2011) 1481–1486. https://doi.org/10.1021/jf1016237.

[56] W. Xu, S. Zheng, H. Sun, Y. Ning, Y. Jia, D. Luo, Y. Li, B.R. Shah, Rheological behavior and microstructure of Pickering emulsions based on different concentrations of gliadin/sodium caseinate nanoparticles, Eur. Food Res. Technol. 247 (2021) 2621–2633. https://doi.org/10.1007/s00217-021-03827-6.

[57] E. Graf, Antioxidant potential of ferulic acid, Free Radic. Biol. Med. 13 (1992) 435–448. https://doi.org/10.1016/0891-5849(92)90184-I.

[58] Y. Lu, W. Wang, D. Wang, X. Bian, H. Zhang, P. Shi, Reaction mechanism of ferulic acid scavenging OH and NO2 radicals: a theoretical study, Struct. Chem. 33 (2022) 641–647. https://doi.org/10.1007/s11224-021-01855-2.

[59] B. Zhang, Y. Wang, R. Lu, Pickering emulsion stabilized by casein–caffeic acid covalent nanoparticles to enhance the bioavailability of curcumin *in vitro* and in vivo, J. Sci. Food Agric. 103 (2023) 3579–3591. https://doi.org/10.1002/jsfa.12447.

[60] P. Wilde, A. Mackie, F. Husband, P. Gunning, V. Morris, Proteins and emulsifiers at liquid interfaces, Adv. Colloid Interface Sci. 108–109 (2004) 63–71. https://doi.org/10.1016/j.cis.2003.10.011.

[61] Y. Jan, L.A. Al-Keridis, M. Malik, A. Haq, S. Ahmad, J. Kaur, M. Adnan, N. Alshammari, S.A. Ashraf, B.P. Panda, Preparation, modelling, characterization and release profile of vitamin D3 nanoemulsion, LWT 169 (2022) 113980. https://doi.org/10.1016/j.lwt.2022.113980.

[62] B.R. Shah, W. Xu, J. Mráz, Formulation and characterization of zein/chitosan complex particles stabilized Pickering emulsion with the encapsulation and delivery of vitamin D3, J. Sci. Food Agric. 101 (2021) 5419–5428. https://doi.org/10.1002/jsfa.11190.

[63] M. Majeed, M.A. Rather, Enhancing shelf life and bioavailability of vitamin D through encapsulation: a comprehensive review, Food Biophys. 20 (2025) 15. https://doi.org/10.1007/s11483-024-09906-x.

[64] V.K. Maurya, K. Bashir, M. Aggarwal, Vitamin D microencapsulation and fortification: trends and technologies, J. Steroid Biochem. Mol. Biol. 196 (2020) 105489. https://doi.org/10.1016/j.jsbmb.2019.105489.

[65] V. Lavelli, P. D'Incecco, L. Pellegrino, Vitamin D incorporation in foods: formulation strategies, stability, and bioaccessibility as affected by the food matrix, Foods 10 (2021) 1989. https://doi.org/10.3390/foods10091989.

[66] M. Yang, Z. Yang, D.W. Everett, E.P. Gilbert, H. Singh, A. Ye, Digestion of food proteins: the role of pepsin, Crit. Rev. Food Sci. Nutr. (2025) 1–22. https://doi.org/10.1080/10408398.2025.2453096.

[67] B. Wang, B.L. Pham, B. Adhikari, Complexation and conjugation between phenolic compounds and proteins: Mechanism, characterisation and applications as novel encapsulants, Sustainable Food Technol. 2 (2024) 1206–1227. https://doi.org/10.1039/d4fb00013g.

[68] N. Maeda, D. Dulko, A. Macierzanka, C. Jungnickel, Analysis of the factors affecting static *in vitro* pepsinolysis of food proteins, Molecules 27 (2022) 1260. https://doi.org/10.3390/molecules27041260.

[69] W. Shi, H. Xie, K. Ouyang, S. Wang, H. Xiong, M.W. Woo, Q. Zhao, The effect of rice protein–polyphenols covalent and non-covalent interactions on the structure, functionality and *in vitro* digestion properties of rice protein, Food Chem. 450 (2024) 139241. https://doi.org/10.1016/j.foodchem.2024.139241.

[70] S.D. Zhou, Y.F. Lin, X. Xu, L. Meng, M.S. Dong, Effect of non-covalent and covalent complexation of (−)-epigallocatechin gallate with soybean protein isolate on protein structure and *in vitro* digestion characteristics, Food Chem. 309 (2020) 125718. https://doi.org/10.1016/j.foodchem.2019.125718.

[71] X. Zhao, X. Yang, Y. Bao, Y. Guo, J. Luo, S. Jiang, W. Zhang, Construction of vitamin D delivery system based on pine nut oil Pickering emulsion: effect of phenols, J. Sci. Food Agric. 103 (2023) 4034–4046. https://doi.org/10.1002/jsfa.12363.

CAPÍTULO IV. KINETIC AND OXIDATIVE STABILITY OF OIL-IN-WATER PICKERING EMULSIONS STABILIZED BY LYSOZYME-FERULIC ACID CONJUGATES.

Abstract

The demand for ingredients with natural appeal has driven the development of multifunctional natural emulsifiers. This study aimed to synthesize covalent conjugates of lysozyme (LYS) and ferulic acid (FA) via a free radical reaction and investigate their application in stabilizing soybean oil Pickering emulsions. Conjugate formation was confirmed by SDS-PAGE electrophoresis and FTIR and UV-Vis spectroscopy, indicating alterations in the protein's tertiary structure and an increase in surface hydrophobicity. The LYS-FA conjugate exhibited techno-functional properties superior to native lysozyme, including higher emulsifying capacity and antioxidant activity, with inhibition values above 74% for both DPPH and ABTS. Oil-in-water Pickering emulsions were prepared with different conjugate concentrations from 2 to 4% w/w in the aqueous phase. The formulation with 4% LYS-FA resulted in smaller droplets and excellent kinetic stability, showing no creaming for 8 days. Rheology revealed pseudoplastic behavior with a predominantly elastic character, where G' was higher than G", suggesting the formation of a robust network at the interface. In addition to physical stability, the Pickering emulsions significantly retarded the primary and secondary lipid oxidation of the encapsulated soybean oil compared to the control, attributed to the interfacial barrier and antioxidant action formed by the conjugate. Furthermore, *in vitro* digestion studies demonstrated that conjugation protected FA from degradation in the gastric phase. These results suggest that LYS-FA conjugates are promising candidates as emulsifiers with good techno-functional properties and antioxidant capacity for applications in the food industry.

Keywords: Free radical grafting, Phenolic compounds, Interfacial properties, *in vitro* digestion, egg protein

1 Introduction

The growing demand for natural, safe, and sustainable products has driven the search for alternatives to synthetic additives traditionally used in the food industry (Lima *et al.*, 2023). Natural ingredients with multifunctional properties, such as proteins and phenolic compounds, have been extensively investigated as substitutes for synthetic surfactants and artificial colorants (Echegaray *et al.*, 2023; Schreiner *et al.*, 2022). However, many of these compounds exhibit functional limitations, including high sensitivity to temperature and light, as well as insufficient interfacial performance (Albuquerque *et al.*, 2021; Tian *et al.*, 2024). To overcome these constraints and expand their applications, several strategies for structural and functional modification have been explored, including thermal treatments, ultrasound application, and the formation of complexes and conjugates with polyphenols or polysaccharides (He *et al.*, 2019; Nooshkam *et al.*, 2023; Rahman *et al.*, 2020; Zhang *et al.*, 2020).

Among these approaches, the formation of conjugates has emerged as a particularly promising strategy. Conjugates are products of covalent interactions that may occur between different types of molecules, such as phenolic compounds, polysaccharides, and proteins (Liu *et al.*, 2023). In particular, protein–polyphenol conjugates yield materials with enhanced emulsifying properties while also providing biological benefits, such as increased antioxidant capacity (Baba *et al.*, 2021). These conjugates can be produced using various methods, including enzymatic reactions, alkaline conditions, or free radical–mediated processes (Quan *et al.*, 2019). The free radical method, commonly induced by ascorbic acid and hydrogen peroxide, promotes the formation of radicals on protein side chains, enabling covalent bonding with phenolic groups, mainly at lysine, tyrosine, and tryptophan residues (Baba *et al.*, 2021; Liu *et al.*, 2019). This method is relatively simple and involves few processing steps, occurring under mild conditions such as room temperature and neutral pH, which makes it particularly suitable for food applications (Quan *et al.*, 2019).

Protein–polyphenol conjugates have been widely explored as emulsifiers, as structural modifications and increased hydrophobicity enhance their adsorption at the oil–water interface, resulting in improved emulsion stability (Liu *et al.*, 2023). Emulsions are thermodynamically unstable systems and therefore require emulsifiers—ingredients that adsorb at the oil–water interface, forming a physical barrier that prevents phase separation and ensures emulsion stability (Fredrick *et al.*, 2010; McClements, 2004). In this context, the presence of phenolic groups can provide additional protection against lipid oxidation, contributing to improved physicochemical stability of emulsions (Ren *et al.*, 2022). Consequently, the application of

these conjugates in emulsified systems has shown strong potential for the development of stable and functional food formulations.

Among the most recent and sustainable approaches for emulsion stabilization, Pickering emulsions have gained increasing attention. These systems are stabilized by solid particles adsorbed at the oil–water interface rather than by conventional surfactants (Chevalier & Bolzinger, 2013; Rayees *et al.*, 2024). Particles based on protein–polyphenol conjugates can act as effective emulsifiers in Pickering systems, combining strong interfacial activity with high antioxidant capacity (McClements & Decker, 2018; Quan *et al.*, 2019).

Lysozyme (LYS) is a globular protein with low molecular weight (~14.3 kDa), composed of 129 amino acid residues, widely found in egg white and present in animal secretions such as tears and saliva (Guha *et al.*, 2018; Strixner & Kulozik, 2011). It is well recognized for its antimicrobial activity and plays an important role in the innate immune system, exhibiting strong action against a wide range of pathogens, including bacteria, fungi, and viruses (Nawaz *et al.*, 2022). However, its low hydrophobicity and relatively high surface charge at neutral pH limit its functionality at oil–water interfaces (Tian *et al.*, 2024). In contrast, the compound 4-hydroxy-3-methoxycinnamic acid, known as ferulic acid (FA), is a phenolic acid widely distributed in the cell walls of grains, fruits, and vegetables. Its aromatic structure, containing hydroxyl and carboxyl groups, confers strong antioxidant activity and the ability to form covalent bonds with proteins (Ou & Kwok, 2004; Warren, 2014).

Although the literature reports the effectiveness of various protein–polyphenol conjugates as emulsifiers in Pickering emulsions (Pan *et al.*, 2023; Shi *et al.*, 2024; Sun *et al.*, 2024; Yang *et al.*, 2023), no studies have been found investigating the application of lysozyme–ferulic acid (LYS–FA) conjugates as emulsifying agents in Pickering emulsions. Therefore, the aim of this study was to develop and characterize Pickering emulsions stabilized by covalent lysozyme–ferulic acid conjugates obtained via a free radical–mediated pathway, evaluating their structural properties, techno-functional and antioxidant capacities, as well as their ability to stabilize Pickering emulsions, with emphasis on kinetic and oxidative stability.

2 Materials and Methods

2.1 Materials

Lysozyme, ferulic acid, 2,2-diphenyl-1-picrylhydrazyl (DPPH), 2,2′-azino-bis(3-ethylbenzothiazoline-6-sulfonic acid) (ABTS), cumene hydroperoxide (80%), porcine pepsin, porcine pancreatin, porcine bile extract, Folin–Ciocalteu reagent, ascorbic acid, ammonium thiocyanate, and bromophenol blue were purchased from Sigma-Aldrich® (St. Louis, USA). Soybean oil used in this study was obtained from a local market (Rio de Janeiro, Brazil). Coomassie Brilliant Blue G-250 was purchased from Bio-Rad (California, USA). Ultrapure water with a conductivity of 0.05 μS/cm (Gehaka, Master-P&D, Brazil) was used in all experiments. All other reagents employed in this study were of analytical grade.

2.2 Preparation of LYS–FA conjugates

The LYS–FA conjugate was prepared using a free radical–mediated oxidation method as described by Sun *et al.* (2020), with minor modifications. Briefly, a 1% (w/w) LYS solution was prepared by dissolving the protein in 50 mL of ultrapure water. Subsequently, 1 mL of a solution containing hydrogen peroxide (H_2O_2, 5 mol/L) and ascorbic acid (0.25 g) was added as the free radical–generating system. The mixture was maintained under magnetic stirring for 2 h at 25 °C. After this period, FA was added to initiate conjugate formation. Specific molar ratios of FA to LYS were investigated, namely 1, 3, 5, 7.5, 10, and 15 mol FA/mol LYS. Upon completion of the reaction, the mixture was dialyzed against ultrapure water using dialysis membranes (D9527, Sigma-Aldrich, USA) for 48 h at 4 °C, with four water changes, to remove residual reagents and reaction by-products. Finally, the dialyzed solution was rapidly frozen in liquid nitrogen (−160 °C) and lyophilized using a freeze dryer (Enterprise I, Terroni, Brazil).

2.2.1 Fluorescence spectroscopy

Fluorescence spectroscopy was performed according to a method adapted from Cheng *et al.* (2023). Measurements were carried out using a spectrofluorometer (RF-5301 PC, Shimadzu, Japan) at 298 K. The excitation wavelength was set at 280 nm, and emission spectra were recorded over the range of 300–500 nm. To evaluate the interaction between the ligand and the protein, aqueous solutions of LYS and LYS–FA conjugates were prepared with a fixed protein concentration of 0.2 mg/mL. The different conjugate formulations corresponded to a theoretical phenolic compound concentration range from 2.70 to 38.83 μmol/L. Fluorescence quenching was analyzed using the Stern–Volmer equation (Bi *et al.*, 2004):

$$\frac{F_0}{F} = 1 + K_q C_{fa} \tau = 1 + K_{sv} C_{fa} \qquad (1)$$

where F_0 is the fluorescence intensity of native LYS, F is the fluorescence intensity of the LYS–FA conjugates, and C_{fa} is the concentration of FA in the conjugate (mol/L). K_{sv} and K_q are the Stern–Volmer quenching constant (L/mol) and the bimolecular quenching rate constant (L mol^{-1} s^{-1}), respectively. τ represents the average fluorescence lifetime of the fluorophore in the absence of the quencher, which is assumed to be 1.0×10^{-8} s for proteins.

The binding constant (K_a) and the number of binding sites (n) were determined using the double-logarithmic equation, as described by Bi *et al.* (2004).

$$\log\left(\frac{F_0 - F}{F}\right) = \log K_a + n \log C_{fa} \qquad (2)$$

The value of the binding site number was subsequently used to determine the optimal FA concentration in the final LYS–FA conjugate selected for the subsequent analyses.

2.3 Structural characterization of the LYS–FA conjugate

2.3.1 Total phenolic content

Total phenolic content was determined using the Folin–Ciocalteu method, adapted from Hu *et al.* (2016). For this analysis, aqueous solutions of LYS and the selected LYS–FA conjugate, chosen based on the optimal FA concentration previously identified by fluorescence spectroscopy, were prepared at a protein concentration of 1 mg/mL. Subsequently, 0.5 mL of each sample was thoroughly mixed with 2.5 mL of Folin–Ciocalteu reagent (0.2 mol/L), and the mixture was kept in the dark for 5 min. Then, 2.0 mL of sodium carbonate solution (7.5%, w/v) was added, and the reaction was allowed to proceed for 2 h at room temperature. Absorbance was measured at 760 nm using a spectrophotometer (Biomate 3S, Thermo Fisher Scientific, USA), with ultrapure water used as the blank. The amount of FA bound to the conjugate was quantified using a standard calibration curve of FA, and the results were expressed as milligrams of FA equivalents per gram of sample (mg FA/g LYS–FA).

2.3.2 Electrophoresis

Sodium dodecyl sulfate–polyacrylamide gel electrophoresis (SDS–PAGE) was performed according to the method described by He *et al.* (2019), with minor modifications. For sample preparation, LYS and LYS–FA solutions (2.5 mg/mL) were mixed at a 1:1 (v/v) ratio with 2× loading buffer containing 2% SDS, 25% glycerol, 12.5% Tris (0.5 mol/L, pH 6.8), 0.1% bromophenol blue, and 5% β-mercaptoethanol. The mixtures were heated at 90 °C for 5 min to ensure protein denaturation. Subsequently, the samples were loaded onto polyacrylamide gels consisting of a 5% stacking gel and a 15% resolving gel. Electrophoresis was carried out at a constant voltage of 150 V using an electrophoresis system (K33, Kasvi, Brazil). After separation, the gels were stained with Coomassie Brilliant Blue G-250 solution for 30 min.

2.3.3 Fourier transform infrared (FTIR) spectroscopy

Fourier transform infrared (FTIR) spectroscopy was used to analyze LYS and LYS–FA samples using an FTIR spectrometer (Vertex 70, Bruker, Germany). Spectra were recorded in the range of 4000–400 cm^{-1}.

2.3.4 UV-Vis spectroscopy

Ultraviolet–visible (UV–Vis) spectroscopy was performed according to the method described by He *et al.* (2019), with minor modifications. Absorbance spectra were recorded using a spectrophotometer over the wavelength range of 230–450 nm. Sample solutions were prepared at concentrations of 1 mg/mL for LYS and LYS–FA, and 0.2 mg/mL for pure FA.

2.3.5 Surface hydrophobicity

Surface hydrophobicity of LYS and LYS–FA samples was evaluated according to the method described by Yu *et al.* (2023), with minor modifications. Briefly, 200 μL of a bromophenol blue (BPB) solution (1 mg/mL) was mixed with protein samples (5 mg/mL) and stirred using a magnetic stirrer for 10 min at room temperature. The mixtures were then centrifuged at 5600 × g for 15 min at 4 °C. Ultrapure water subjected to the same experimental conditions was used as the control. Absorbance of the supernatants was measured at 595 nm using a spectrophotometer. Surface hydrophobicity was subsequently calculated based on the BPB binding equation described below.

$$\text{BPB bound (μg)} = 200 \times \frac{(A_c - A_s)}{A_c} \quad (3)$$

where A_c is the absorbance measured for the control and A_s is the absorbance of the sample.

2.4 Techno-functional properties of the LYS–FA conjugate

2.4.1 Antioxidant capacity

Free radical scavenging capacity was determined using the DPPH assay, according to a method adapted from Pan *et al.* (2023). For the assay, 2.5 mL of LYS and LYS–FA solutions (0.5 mg/mL) were mixed with 1.0 mL of a DPPH solution (1.75×10^{-4} mol/L). The mixtures were incubated in the dark for 30 min at room temperature. Subsequently, absorbance was measured at 517 nm using a spectrophotometer. Ultrapure water was used as the control. The DPPH radical scavenging capacity was calculated using the following Equation:

$$DPPH\ (\%) = \left[1 - \frac{A_s}{A_c}\right] x100 \quad (4)$$

where A_s is the absorbance of the sample and A_c is the absorbance of the control.

ABTS radical scavenging capacity was determined according to the method described by Ren, Shi, *et al.* (2022), with minor modifications. Briefly, potassium persulfate (2.45 mmol/L) and ABTS solutions (7 mmol/L) were prepared, mixed at a 1:1 ratio, and kept in the dark overnight to allow the formation of $ABTS^+$ radicals. Subsequently, 0.5 mL of LYS and LYS–FA samples (0.25 mg/mL) was added to 2.0 mL of the preformed ABTS solution. The mixtures were incubated in the dark for 1 h at room temperature. After incubation, absorbance was measured at 734 nm using a spectrophotometer. Ultrapure water was used as the control. The ABTS radical scavenging capacity was calculated using the following equation:

$$ABTS\ (\%) = \left[1 - \frac{A_s}{A_c}\right] x100 \quad (5)$$

where A_s is the absorbance of the sample and A_c is the absorbance of the control.

2.4.2 Emulsifying properties

The emulsifying activity index (EAI) and emulsifying stability index (ESI) were determined according to the method described by Ren *et al.* (2022), with minor modifications. Emulsions were prepared using an Ultra-Turrax T25 homogenizer (IKA, Germany) by mixing 10 mL of protein solution (1 mg/mL) with 0.5 mL of soybean oil. Homogenization was performed at 10,000 rpm for 2 min. Immediately after emulsification, a 50 μL aliquot of the emulsion was diluted with 4.95 mL of 10% (w/v) SDS solution. A second 50 μL aliquot was

collected 10 min after emulsion formation and diluted in the same SDS solution. The absorbance of both dilutions was measured at 500 nm using a spectrophotometer. EAI and ESI values were calculated using the corresponding equations, based on absorbance readings at 0 and 10 min, respectively.

$$\text{EAI } (\text{m}^2/\text{g}) = \frac{4{,}606 \times A_0 \times D}{N \times C \times 10000} \quad (6)$$

$$\text{ESI } (minutes) = \frac{A_0 \times T}{A_0 - A_{10}} \quad (7)$$

where A_0 and A_{10} represent the absorbance measured immediately after emulsion formation and after 10 min of standing, respectively. D corresponds to the dilution factor (100), N represents the oil-to-water ratio in the emulsion (0.048), C indicates the sample concentration (0.001 g/mL), and T refers to the standing time, in minutes.

2.4.3 Foaming properties

Foaming properties of the proteins were evaluated according to a method adapted from Chang *et al.* (2021). LYS and LYS–FA solutions (5 mg/mL) were prepared in volumes of 12.5 mL and transferred to 25 mL beakers. The samples were then homogenized using an Ultra-Turrax T25 homogenizer at 10,000 rpm for 2 min. Foam volume was recorded immediately after homogenization and again after 30 min of standing. Foam capacity (FC) and foam stability (FS) were calculated using the following Equations:

$$\text{FC } (\%) = 100\% \times \frac{V_1}{V} \quad (8)$$

$$\text{FS } (\%) = 100\% \times \frac{V_2}{V_1} \quad (9)$$

where V represents the initial volume of the protein solution before homogenization (mL), V_1 is the foam volume measured immediately after homogenization (mL), and V_2 corresponds to the foam volume after 30 min of standing (mL).

2.4.4 Interfacial tension

Interfacial tension between the oil phase and aqueous solutions containing different concentrations of LYS–FA (2.0, 3.0, and 4.0%, w/w) was measured using an Easytrack tensiometer (Teclis Scientific, France) by the rising drop method, following a procedure adapted from Barbosa and Garcia-Rojas (2022). Measurements were performed at a controlled temperature of 25 ± 0.01 °C, maintained using a thermostatic bath (CD-BC4, Julabo, Germany).

The interfacial tension data obtained for the systems composed of LYS–FA solutions and soybean oil were fitted to the mathematical model described in Equation 10, as proposed by Shi *et al.* (2004).

$$\sigma(t) = \sigma_f + \exp(t/\tau_1)(\sigma_1 - \sigma_f) + \exp(t/\tau_2)(\sigma_2 - \sigma_f) \qquad (10)$$

where σ_f represents the asymptotic interfacial tension ($mN \cdot m^{-1}$) as $t \to \infty$; t is the time (s); σ_1 and σ_2 are kinetic parameters associated with the interfacial tension; τ_1 corresponds to the migration time (s) of the emulsifier toward the interface; and τ_2 represents the characteristic time (s) related to molecular rearrangement and possible conformational changes of macromolecules at the interface.

2.4.5 Three-phase contact angle

The oil–water three-phase contact angle of the LYS–FA conjugate was determined using the sessile drop technique, as described by Qin *et al.* (2021), employing an Easytrack goniometer equipped with a specific module for this measurement. Lyophilized LYS–FA samples were first compressed onto glass slides to form a homogeneous layer. Each slide was then placed in direct contact with soybean oil, and a droplet of distilled water (2 μL) was carefully deposited onto the surface using a high-precision syringe. After a stabilization period of 2 min, the droplet image was captured by a camera coupled to the system, and the contact angle was automatically calculated. The final value was expressed as the mean of three measurements taken at two different points on the droplet.

2.5 In vitro gastrointestinal digestion simulation of the LYS–FA conjugate

The stability of LYS–FA conjugates during gastrointestinal digestion was evaluated based on the retention of DPPH radical scavenging activity, according to the methodology described by Yang *et al.* (2023). For this purpose, samples were subjected to an *in vitro* gastrointestinal digestion simulation using the standardized INFOGEST 2.0 protocol (Brodkorb *et al.*, 2019).

Solutions containing LYS–FA and LYS were prepared at a concentration of 1 mg/mL, using an initial amount of 1 g per sample. In addition, a control sample consisting of ferulic acid (FA) solution at 0.2 mg/mL was analyzed. The digestion was carried out in three sequential stages, oral, gastric, and intestinal phases, in sealed tubes under constant agitation at a controlled

temperature of 37 °C, using a TE-424 incubator (Tecnal, Brazil). Aliquots were collected at 2, 30, 60, 90, 120, 150, 180, 210, and 240 min throughout the digestion process.

During the oral phase (2 min), each sample was mixed with 0.8 mL of simulated salivary fluid (SSF), 0.1 mL of salivary amylase solution (75 U/mL), 5 μL of $CaCl_2$ (0.3 mol/L), and 0.095 mL of distilled water. For the gastric phase (2 h), the total volume from the oral phase was combined with 1.6 mL of simulated gastric fluid (SGF), 0.2 mL of pepsin solution (2000 U/mL), 1 μL of $CaCl_2$ (0.3 mol/L), and 0.2 mL of distilled water, with the pH adjusted to 3.0 using HCl solution. In the intestinal phase (2 h), the gastric mixture was supplemented with 1.7 mL of simulated intestinal fluid (SIF), 1.0 mL of pancreatin solution (100 U/mL), 0.5 mL of bile solution (10 mmol/L), 8 μL of $CaCl_2$ (0.3 mol/L), and 0.792 mL of distilled water, with the pH adjusted to 7.0 using NaOH.

The retention of antioxidant capacity was expressed as the percentage of DPPH radical scavenging activity, as described in Section 2.4.1, throughout the digestion process and calculated according to Equation (11).

$$\text{Retention Rate } (\%) = 100\% \times \frac{A_t}{A_0} \qquad (11)$$

where A_t is the DPPH radical scavenging capacity measured during the digestion simulation, and A_0 is the initial DPPH radical scavenging capacity.

2.6 Oil-in-water (O/W) Pickering emulsion formation

Particle preparation was carried out according to the methodology described by Ju *et al.* (2020). Briefly, LYS–FA solutions at 5% (w/v) were heated in a water bath at 95 °C for 15 min, followed by immediate cooling in an ice bath until room temperature was reached. The resulting solution was then rapidly frozen in liquid nitrogen (−160 °C) and subsequently freeze-dried to obtain the particulate material. Pickering emulsions were formulated following the protocol described by Ji *et al.* (2022), using soybean oil as the dispersed phase and LYS–FA conjugate particles as the emulsifier in the continuous phase at concentrations of 2.0%, 3.0%, and 4.0% (w/w). The emulsions were prepared with a fixed oil volume fraction (φ) of 0.70. Samples were designated as LYSFA2%, LYSFA3%, and LYSFA4% according to the emulsifier concentration. Emulsification was performed using an Ultra-Turrax T25 homogenizer operating at 18,000 rpm for 3 min.

2.6.1 Kinetic stability

The kinetic stability of the emulsions was assessed following the methodology described by Ren *et al.* (2019). For this purpose, 10 mL samples of oil-in-water (O/W) emulsions were transferred to transparent tubes and incubated at 25 °C for 7 days in a Shaker incubator (Model SL222, Solab, Brazil). During this period, the formation of a transparent phase at the bottom of the tubes was monitored. Emulsion stability was quantified using the creaming index, calculated according to Equation 12:

$$CI(\%) = \frac{H_c}{H_t} \qquad (12)$$

where CI is the creaming index, H_c is the height of the transparent layer (mm), and H_t is the total height of the system (mm).

2.6.2 Protein adsorption at the emulsion interface

The adsorption of LYS-FA at the interface of Pickering emulsions was analyzed according to the methodology described by Chen *et al.* (2021). For this purpose, 1 mL of freshly prepared emulsion was centrifuged at 15,000 x g for 30 min. After centrifugation, the oil layer was carefully removed, while the lower phase was collected and subjected to sequential filtration using 0.45 and 0.22 μm pore membranes. The protein content in the filtrate was determined by the Bradford method and denoted as c_f (unadsorbed protein content). In parallel, the initial protein solution used in the emulsion formulation was subjected to the same centrifugation procedure to determine the total available protein, denoted as c_i (mg/mL). The adsorption of LYS-FA at the interface was then calculated using Equation 13:

$$\text{Adsorption } (\%) = \frac{c_i - c_f}{c_i} \qquad (13)$$

2.7 Characterization of O/W Pickering emulsions

2.7.1 Particle size and zeta potential

Particle size and zeta potential analyses of the emulsions were performed on samples diluted 100-fold in distilled water, using a Zetasizer Nano ZS90 (Malvern Instruments, UK). Measurements were conducted at 25 °C. For the zeta potential analysis, DTS 1060 cells were used.

2.7.2 Rheology

The rheological characterization of the emulsions was performed using an MCR 92 rheometer (Anton Paar, Austria). Tests were conducted using a 50 mm diameter parallel plate geometry (PP50) with the gap set to 1 mm. Measurements were taken immediately after emulsion preparation. Apparent viscosity was determined over a shear rate range of 1 to 100 s^{-1}. To describe the rheological behavior of the emulsions, the Power Law (Equation 14), Bingham (Equation 15), and Herschel-Bulkley (Equation 16) models were applied. Furthermore, a dynamic strain sweep was performed to identify the linear viscoelastic region (LVR), followed by a frequency sweep to determine the storage (G') and loss (G'') moduli within a frequency range of 0.1 to 10 Hz.

$$\tau = K(\dot{\gamma})^{n-1} \quad (14)$$

$$\tau = K + \frac{\tau_0}{\dot{\gamma}} \quad (15)$$

$$\tau = K(\dot{\gamma})^{n-1} + \frac{\tau_0}{\dot{\gamma}} \quad (16)$$

where τ is the shear stress (Pa), *K* is the consistency index ($Pa \cdot s^n$), *n* is the flow behavior index, and $\dot{\gamma}$ is the shear rate (s^{-1}).

2.7.3 Antioxidant capacity

The antioxidant capacity of the studied emulsions was determined using the DPPH and $ABTS^+$ methods. For this purpose, 1 mL aliquots of the freshly prepared emulsions were used. The determination of the radical scavenging rate was performed according to the procedures described in section 2.4.1.

2.7.4 Oxidative stability

Lipid oxidation was evaluated by determining primary and secondary oxidation products in Pickering emulsions (LYSFA2%, LYSFA3%, and LYSFA4%), as well as in a control sample containing only soybean oil. Freshly prepared emulsions were transferred to glass vials and stored in a TE-424 incubator (Tecnal, Brazil) at 40 °C for 14 days in the absence of light. Aliquots were collected immediately after emulsion preparation and on days 1, 4, 7, 11, and 14 of storage.

Primary lipid oxidation analysis was performed by identifying lipid hydroperoxides, following the methodology of Zhang *et al.* (2018). Aliquots of 0.2 mL of sample were mixed

with 1 mL of isooctane/2-propanol solution (3:1, v/v) by vortexing for 10 s, repeated three times. Subsequently, the samples were centrifuged at 7200 × g for 8 min. A 0.2 mL volume of the organic phase (upper layer) was withdrawn and added to 2.8 mL of methanol/1-butanol solution (2:1, v/v), followed by the addition of 15 μL of ammonium thiocyanate (3.94 mol/L) and 15 μL of ferrous iron solution (0.132 mol/L barium chloride and 0.144 mol/L ferrous sulfate). The resulting mixture was incubated at room temperature in the dark for 20 min. After this period, the solution absorbance was measured at 510 nm using a spectrophotometer. Quantification of hydroperoxides in the emulsions was performed based on a standard curve constructed using cumene hydroperoxide.

Secondary lipid oxidation was monitored by quantifying malondialdehyde (MDA) using the thiobarbituric acid reactive substances (TBARS) assay, as described by Cui *et al.* (2022). A TBA reagent was prepared from a solution containing 15% (w/v) trichloroacetic acid and 0.375% (w/v) thiobarbituric acid dissolved in 0.25 mol/L HCl. For the analysis, 1 mL of sample was mixed with 2 mL of TBA reagent, and the mixture was heated in a boiling water bath for 15 min. After heating, the samples were immediately cooled to room temperature and filtered. The absorbance of the filtrate was determined in a spectrophotometer at 532 nm. Quantification of secondary lipid oxidation products was performed based on a 1,1,3,3-tetraethoxypropane standard curve.

2.8 Statistical analysis

Data were analyzed using analysis of variance (ANOVA) followed by Tukey's test ($p < 0.05$). All experiments were performed in triplicate, and results are presented as mean ± standard deviation.

3 Results and Discussion

3.1 Formation of the LYS–FA conjugate

The interaction between LYS and FA was investigated through intrinsic protein fluorescence quenching. Figure 31A shows the emission spectra of native LYS and systems containing increasing concentrations of FA.

The intrinsic fluorescence of LYS is attributed to its natural fluorophores, specifically six tryptophan residues and three tyrosine residues (Wu *et al.*, 2019). The native protein exhibited a maximum emission intensity at 344 nm. However, as the FA ratio increased, a progressive and significant decrease in fluorescence intensity was observed, indicating effective interaction of FA with the protein fluorophores and alterations in their microenvironment (Xu *et al.*, 2019). Alongside quenching, a redshift of the maximum emission peak was noted, shifting from 344 nm in native LYS to 348 nm at the highest ligand concentration. This redshift suggests that tryptophan residues became exposed to a more polar environment, indicating conformational changes in the tertiary structure of LYS induced by binding with FA, resulting in partial unfolding of the protein (Lakowicz, 2006). Similar results were reported by Yin *et al.* (2024), who observed a 5 nm redshift in LYS emission upon conjugation with epigallocatechin-3-gallate (EGCG), accompanied by a similar decrease in fluorescence intensity with increasing polyphenol concentration.

The Stern–Volmer equation was fitted to the experimental data (Figure 31B), showing satisfactory linearity ($R^2 = 0.9156$). This linearity indicates that a single fluorescence quenching mechanism predominates within the studied concentration range. The nature of the interaction was determined from the quenching rate constant, calculated as 2.61×10^{12} $L \cdot mol^{-1} \cdot s^{-1}$. Since this value exceeds the maximum diffusion-collision quenching limit of 2.0×10^{10} $L \cdot mol^{-1} \cdot s^{-1}$, it is concluded that the quenching mechanism is static, confirming the interaction between LYS and FA (Czubinski & Dwiecki, 2017). In this context, the K_{sv} of 2.61×10^4 mol^{-1} reflects the strength of this association. Chen *et al.* (2024) reported a static fluorescence quenching mechanism for interactions between ovalbumin and FA, with a K_q of 1.0×10^{11} $L \cdot mol^{-1} \cdot s^{-1}$. Similarly, Jia *et al.* (2019) described strong interactions between rice protein and FA, with a K_q of 2.42×10^{12} and a K_{sv} of 2.42×10^4, indicating high affinity between the phenolic compound and the protein matrix. These findings support the occurrence of strong and predominantly static interactions between proteins and FA.

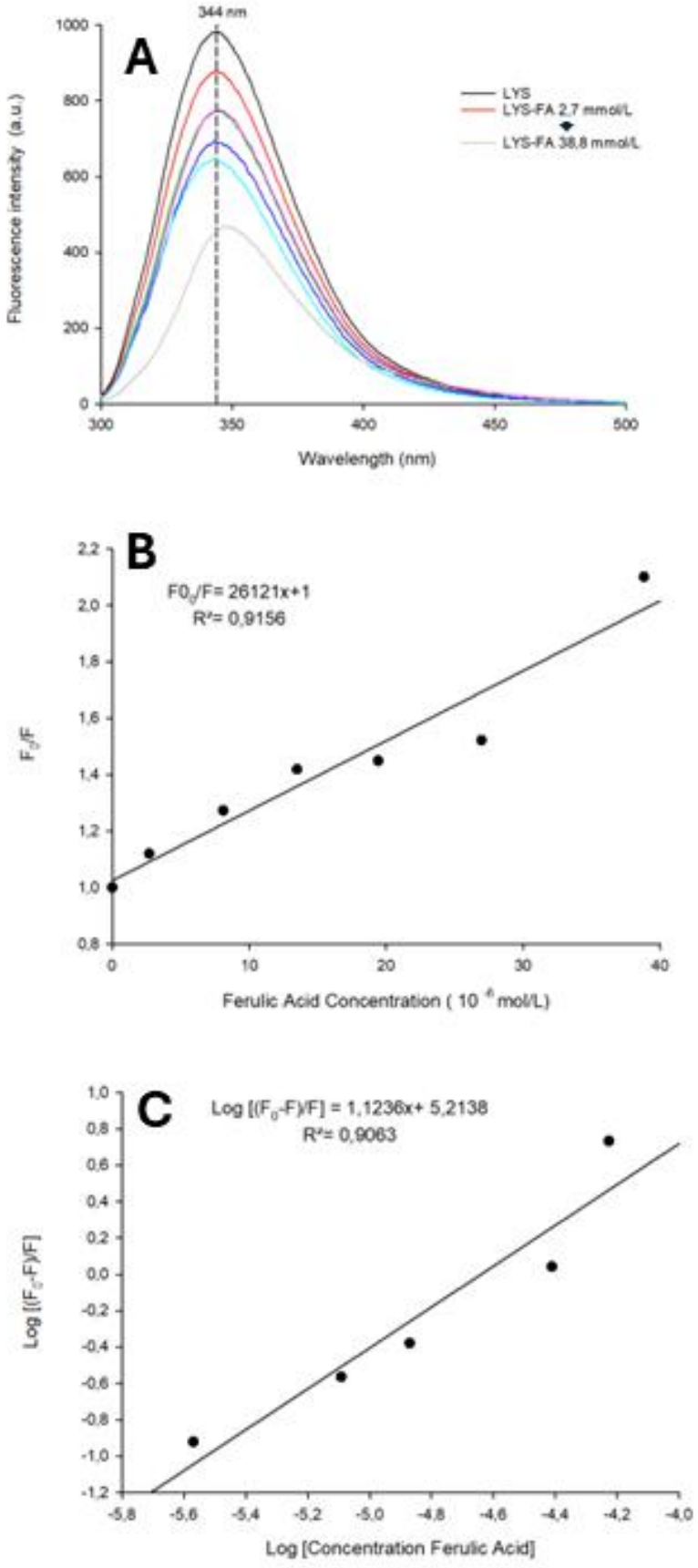

Figure 31. (A) Fluorescence emission spectra of LYS and LYS-FA in the presence of increasing concentrations of FA, ranging from 2.7 to 38.8 µmol/L with excitation at 280 nm. (B) Stern-Volmer plot of LYS fluorescence quenching as a function of FA concentration. (C) Double logarithm plot for LYS-FA conjugates.

The binding constant and the number of binding sites were determined using the double logarithmic plot (Figure 31C), which exhibited satisfactory correlation (R^2 = 0.9063). The parameter n, obtained from the slope, represents the number of binding sites between LYS and FA and was found to be 1.12, indicating approximately one binding site per protein molecule. The binding constant K_a was 1.64 × 10^5 L·mol^{-1}, demonstrating significant affinity between lysozyme and ferulic acid under the evaluated conditions. Similar results were reported by Cheng *et al.* (2023), who observed n = 1.255 and K_a = 9.18 × 10^5 L·mol^{-1} for conjugates formed between whey protein concentrate and quercetin.

Therefore, a molar ratio of 1.12 mol of FA per mol of LYS was adopted for preparing the samples used in subsequent analyses, and the resulting conjugate was designated LYS–FA. Finally, the FA content in the conjugate was quantified using the Folin–Ciocalteu method, revealing a value of 24.94 ± 1.23 mg FA equivalent per gram of protein. This confirms the effectiveness of the conjugation reaction and demonstrates successful incorporation of the phenolic compound into the LYS structure.

3.2 Structural Analysis of the LYS–FA conjugate

3.2.1 Electrophoresis

Figure 32 presents the results of SDS-PAGE analysis of LYS and the LYS–FA conjugate. This technique, which separates proteins according to molecular weight, showed a characteristic band at approximately 15 kDa for native LYS. In the case of the LYS–FA conjugate, a shift of this band toward a higher molecular weight was observed, indicating an increase in protein mass. Considering that SDS and β-mercaptoethanol were used during sample preparation, reagents capable of disrupting only non-covalent interactions, these results suggest that the structural modification of the protein is due to the formation of stable covalent bonds between LYS and FA. These findings are consistent with previous reports, which also describe an increase in protein molecular weight after conjugation with phenolic compounds, confirming the covalent nature of these interactions (Barbosa *et al.*, 2025; Huang *et al.*, 2022; Xiong *et al.*, 2023).

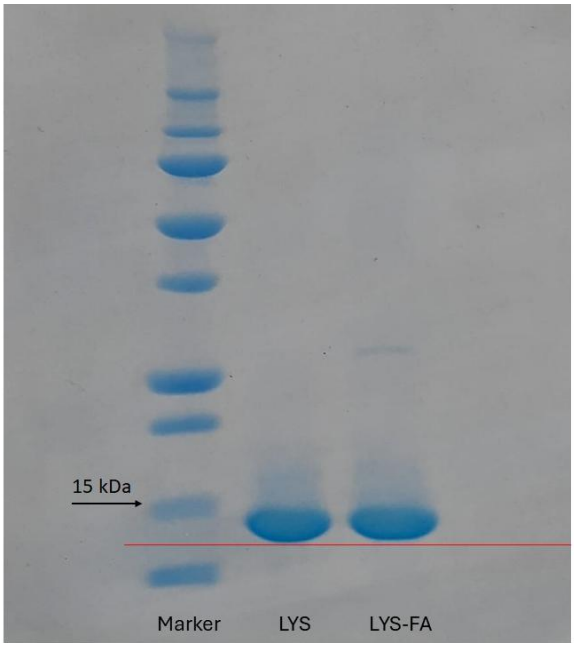

Figure 32. SDS-PAGE analysis of LYS and LYS-FA performed on a 15% polyacrylamide gel showing the molecular weight marker, native LYS and LYS-FA conjugates.

3.2.2 FTIR

Figure 33 shows the FTIR spectra of LYS and the LYS–FA conjugate in the mid-infrared region (4000–400 cm^{-1}). In the amide I region, primarily associated with C=O stretching vibrations, LYS exhibited a peak at 1648 cm^{-1}, while the LYS–FA conjugate showed a shift to 1641 cm^{-1}. A similar trend was observed in the amide II region, associated with N–H bending and C–N stretching, where the LYS peak at 1537 cm^{-1} shifted to 1529 cm^{-1} in the conjugate. Since amide I and II bands are sensitive indicators of the polypeptide backbone conformation, these shifts confirm that the reaction induced alterations in the protein secondary structure (Barth, 2007; Tatulian, 2013). The shift of peaks toward lower wavenumbers has also been reported by Huang *et al.* (2022), who observed a migration of the band from 1656 to 1652 cm^{-1} in walnut protein isolate conjugates with ellagic acid.

Additionally, in the amide A region, associated with N–H stretching vibrations around 3300 cm^{-1}, a shift from 3278 cm^{-1} in LYS to 3284 cm^{-1} in the LYS–FA conjugate was observed. Similar shifts toward higher wavenumbers following conjugation have been reported by Moreno-Vásquez *et al.* (2024) when LYS was conjugated with EGCG, and by İşçimen (2025) for pea protein conjugated with FA, which shifted from 3272 to 3280 cm^{-1}. Changes in the ~3300 cm^{-1} region indicate structural modifications of the protein, suggesting interactions between FA and the LYS structure (Barth, 2007; Tatulian, 2013).

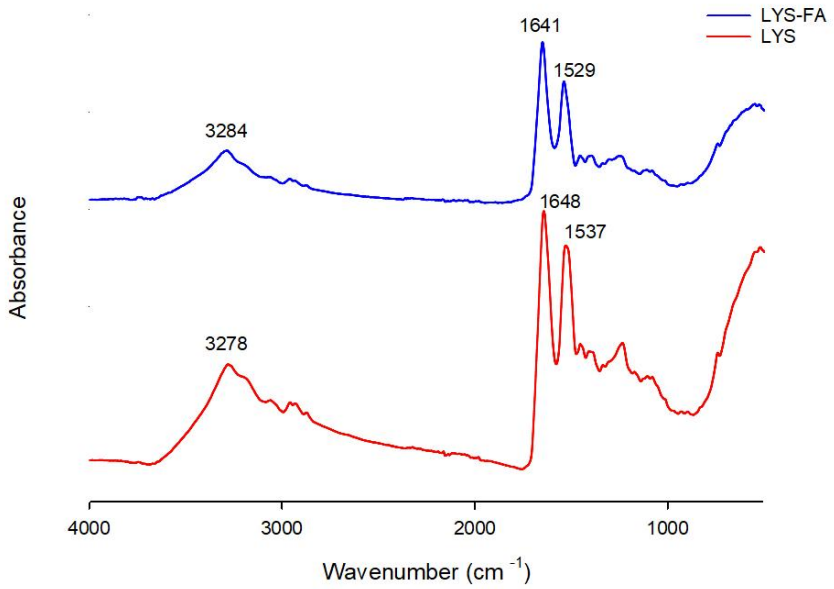

Figure 33. FTIR spectra of LYS and LYS-FA conjugates recorded in the spectral range of 400 to 4000 cm-1.

3.2.3 UV-Vis

The UV–Vis spectra of LYS, FA, and the LYS–FA conjugate are shown in Figure 34. LYS exhibited a single peak at 280 nm, whereas the LYS–FA conjugate showed peaks at both 280 nm and 310 nm. The absorbance at 280 nm in proteins is attributed to the conjugated double bonds in the aromatic rings of tyrosine and tryptophan residues, which confer UV absorption properties (Layne, 1957; Li *et al.*, 2022). Phenolic acids typically absorb at 280 nm and between 305–330 nm (Liu *et al.*, 2019). The increase in absorbance at 280 nm observed for LYS–FA is associated with the presence of the phenolic compound, indicating interactions between the protein and FA. Similar results have been reported in studies evaluating protein conjugation with phenolic compounds, showing enhanced absorbance in this region (Huang *et al.*, 2022; Pi *et al.*, 2023; Yang *et al.*, 2023). The peak at 310 nm can be attributed to oxidized portions of FA, which exhibit characteristic absorption in this region (Xue *et al.*, 2023). Consistently, Li *et al.* (2022) observed a similar behavior when LYS was conjugated with gentisic acid, reporting a peak between 310–330 nm associated with covalent interactions between the compounds.

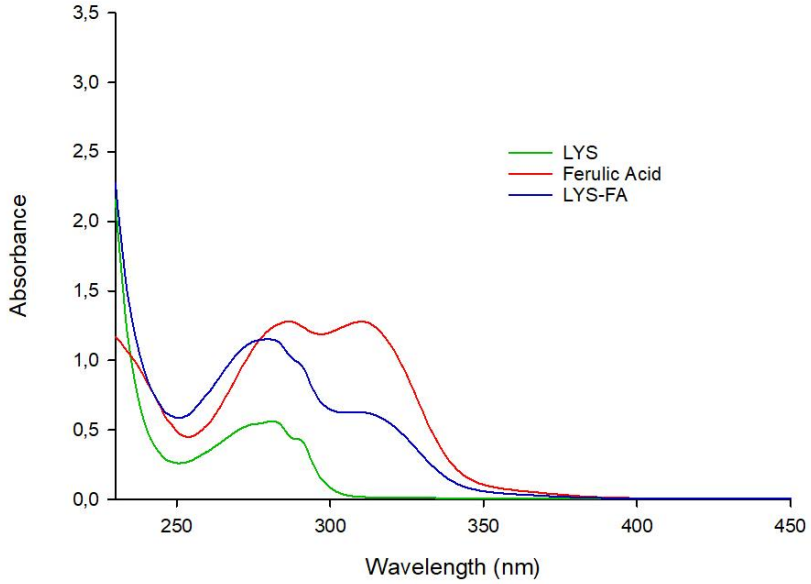

Figure 34. UV-Vis absorption spectra of LYS and LYS-FA conjugates recorded in the wavelength range of 240 to 450 nm.

3.2.4 Surface hydrophobicity

The surface hydrophobicity of LYS was significantly altered ($p < 0.05$) after conjugation with FA. LYS exhibited a hydrophobicity index of 8.79 ± 1.04 µg, whereas the LYS–FA conjugate increased to 15.52 ± 1.85 µg. This increase is attributed to the incorporation of FA into the protein structure, which induced conformational changes and greater exposure of hydrophobic sites. Consistently, Xue *et al.* (2023) also reported increased surface hydrophobicity following FA conjugation to β-lactoglobulin. The increase in surface hydrophobicity aligns with fluorescence intensity changes, as exposure of hydrophobic regions can alter the microenvironment of tryptophan and tyrosine residues, resulting in reduced fluorescence intensity (Feng *et al.*, 2018). Collectively, the changes observed in FTIR and UV–Vis spectra indicate structural modifications in the protein resulting from the conjugation process.

3.3 Characterization of the LYS–FA conjugate

3.3.1 Antioxidant capacity

The antioxidant capacity of LYS and the LYS–FA conjugate is presented in Figure 35A, evaluated using DPPH and ABTS radical scavenging assays. LYS exhibited limited antioxidant activity, with inhibition values of 14.10 ± 1.40% for DPPH and 35.03 ± 1.93% for ABTS radicals. In contrast, conjugation with FA resulted in a pronounced enhancement of antioxidant capacity. LYS–FA showed 74.00 ± 2.31% inhibition in the DPPH assay and 74.76 ± 0.52% in

the ABTS assay. This significant increase is directly related to the incorporation of FA into the protein structure. The antioxidant activity of free FA was measured under the same conditions, showing high values of 94.17 ± 0.12% (DPPH) and 99.33 ± 0.44% (ABTS). The high antioxidant activity of FA is attributed to its phenolic structure, which efficiently donates hydrogen atoms or electrons to stabilize free radicals. Therefore, these results confirm that conjugation effectively transferred the bioactive properties of the phenolic compound to LYS, endowing LYS–FA with enhanced antioxidant potential. This trend aligns with previous reports demonstrating that covalent modification of proteins with phenolic compounds is an effective strategy to enhance system antioxidant capacity (Lu *et al.*, 2018; Parolia *et al.*, 2022; Shi *et al.*, 2024). Specific studies on FA conjugation have reported similar increases in antioxidant activity (Xue *et al.*, 2023).

3.3.2 Emulsifying properties

The ability of LYS and its conjugate to form and stabilize emulsions was assessed through the EAI and ESI, as shown in Figure 35B and Figure 35C. Regarding EAI, a significant increase was observed, from 1162.51 ± 23.92 m^2/g for LYS to 1276.08 ± 35.16 m^2/g for the conjugate. Similarly, ESI improved markedly, with stability time increasing from 16.36 ± 0.45 min for the native protein to 30.29 ± 3.65 min for LYS–FA, indicating a substantial enhancement in emulsion durability. These increases in EAI and ESI can be attributed to the enhanced surface hydrophobicity due to covalent interactions, which expose protein hydrophobic groups, facilitating adsorption at the oil–water interface and thus improving emulsifying properties (Ghribi *et al.*, 2015). Pi *et al.* (2023) reported increased EAI in soy protein isolate conjugates with various polyphenols (gallic acid, caffeic acid, tannic acid), although no significant ESI improvement was observed. In contrast, Xue *et al.* (2023) reported increases in both EAI and ESI after FA conjugation to β-lactoglobulin via an alkaline method.

3.3.3 Foaming properties

FC and FS were evaluated, as shown in Figure 35D. LYS exhibited limited foaming ability, with FC of 3.6 ± 0.43% and FS of 25.3 ± 3.18%. Conjugation significantly enhanced these properties: LYS–FA showed an FC of 9.8 ± 0.49% and FS of 36.5 ± 1.55%. The superior foaming performance of LYS–FA can be attributed to structural modifications induced by FA conjugation. Covalent interactions altered the protein's secondary and tertiary structures, increasing surface hydrophobicity and molecular flexibility. These changes facilitate adsorption

at the air–water interface, promoting bubble formation and stabilization, thereby improving both foam capacity and stability (He *et al.*, 2019). Similar results were reported by Vasava *et al.* (2022), who observed significant increases in foam capacity and stability after conjugating whey protein concentrate with FA, regardless of the conjugation method used, compared to the native protein.

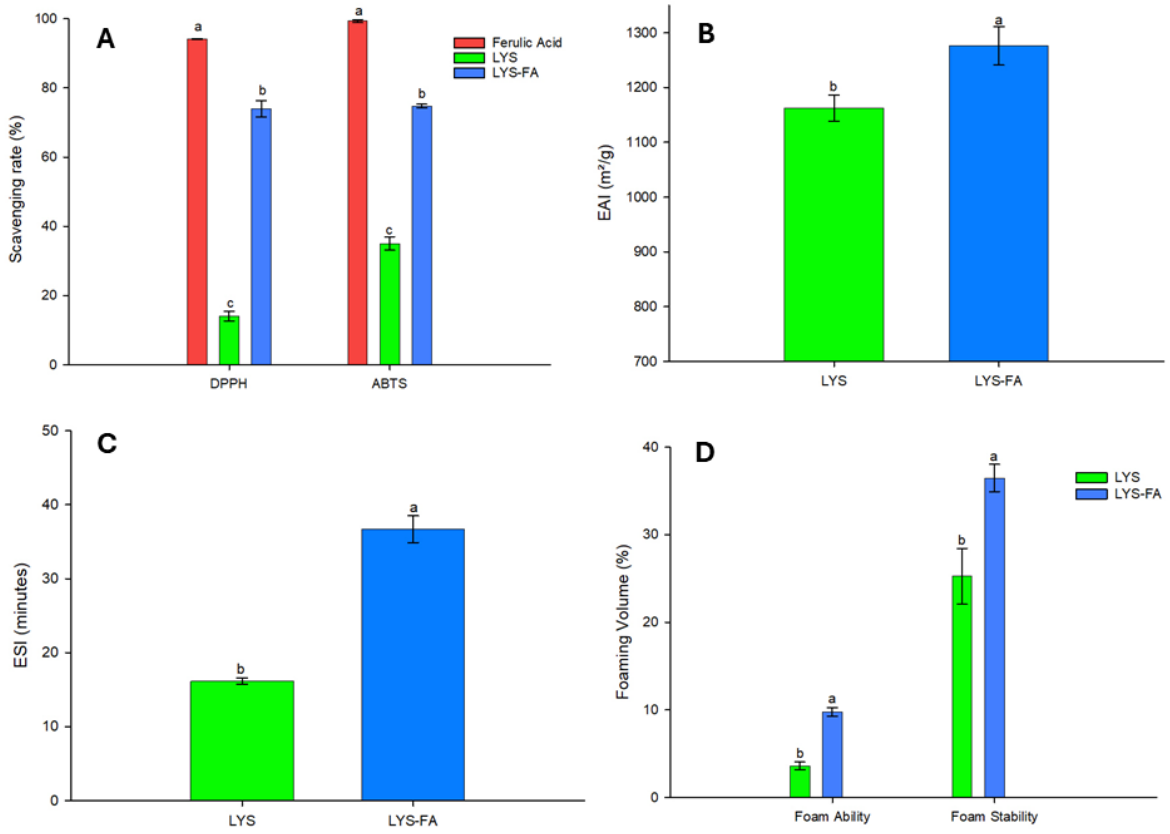

Figure 35. (A) Antioxidant activity of FA, LYS and LYS-FA conjugates evaluated by DPPH and ABTS radical scavenging assays. Emulsifying properties of LYS and LYS-FA conjugates expressed as (B) Emulsifying Activity Index (EAI), and (C) Emulsion Stability Index (ESI). (D) Foaming ability and stability of LYS and LYS-FA samples. Values are presented as mean ± standard deviation. Different letters indicate statistically significant differences according to the Tukey test ($p < 0.05$).

3.3.4 Interfacial tension

Figure 36A illustrates the dynamic interfacial tension behavior of LYS–FA at 2%, 3%, and 4% concentrations. The model described in Equation 10 provided an excellent fit to the experimental data, as evidenced by mean absolute deviations (AAD) below 0.42% and standard deviations (SD) under 0.06 mN/m. Model-derived parameters are presented in Table 8. Increasing the conjugate concentration continuously reduced interfacial tension, from 7.82 mN/m (2%) to 7.07 mN/m (3%) and 5.26 mN/m (4%). This decrease can be attributed to the higher availability of amphiphilic molecules for adsorption at the oil–water interface,

promoting replacement of oil–water interactions with protein–oil and protein–water interactions, which are energetically more favorable (McClements, 2004). This behavior highlights the superior interfacial efficiency of LYS–FA at higher concentrations.

Table 8. Dynamic interfacial tension parameters between the external aqueous phase with different concentrations of LYS-FA conjugate and soybean oil estimated from Equation 10.

Concentration (%)	σ_f (mN/m)	σ_1 (mN/m)	σ_2 (mN/m)	τ_1 (s)	τ_2 (s)	AAD* (%)	SD** (mN/m)
2.0	7.82	11.02	9.21	21.97	694.10	0.35	0.05
3.0	7.07	9.28	9.30	24.13	602.76	0.42	0.06
4.0	5.26	7.03	6.86	31.34	587.23	0.16	0.03

σ_{exp} is the experimental interfacial tension (mN·m^{-1}), σ_{cal} is the interfacial tension calculated by Equation (10) (mN·m^{-1}), m is the number of experimental points, and p is the number of adjusted parameters.

$$*AAD(\%) = \left(\frac{100}{m}\right)\left[\sum_{i=1}^{m}\frac{\sigma_{exp,i}-\sigma_{cal,i}}{\sigma_{exp,i}}\right] \quad ;**SD = \sqrt{\frac{\sum_{i=1}^{m}\left(\sigma_{exp,i}-\sigma_{cal,i}\right)^2}{m-p}}$$

3.3.5 Three-phase contact angle

Figure 36B shows the behavior of a water droplet on the surface of LYS–FA saturated with soybean oil. The measured three-phase contact angle was 85.37 ± 2.99°. In particle-stabilized systems, the three-phase contact angle is a key parameter for determining emulsion type and stability (Albert *et al.*, 2019). Angles above 90° indicate a predominantly hydrophobic character, favoring water-in-oil emulsion formation, whereas angles below 90° indicate higher affinity for the aqueous phase, promoting oil-in-water emulsions. Particles with contact angles near 90° exhibit high desorption energy, which enhances their fixation at the oil–water interface, creating a barrier that prevents coalescence of the dispersed phase (Low *et al.*, 2020). The LYS–FA conjugate, with an angle slightly below 90°, demonstrates ideal characteristics for acting as an emulsifier in oil-in-water emulsions. Similarly, Sun *et al.* (2024) reported a contact angle of 87.5 ± 0.5° for a lactoferrin–EGCG conjugate, demonstrating high efficiency as a Pickering emulsifier in oil-in-water systems.

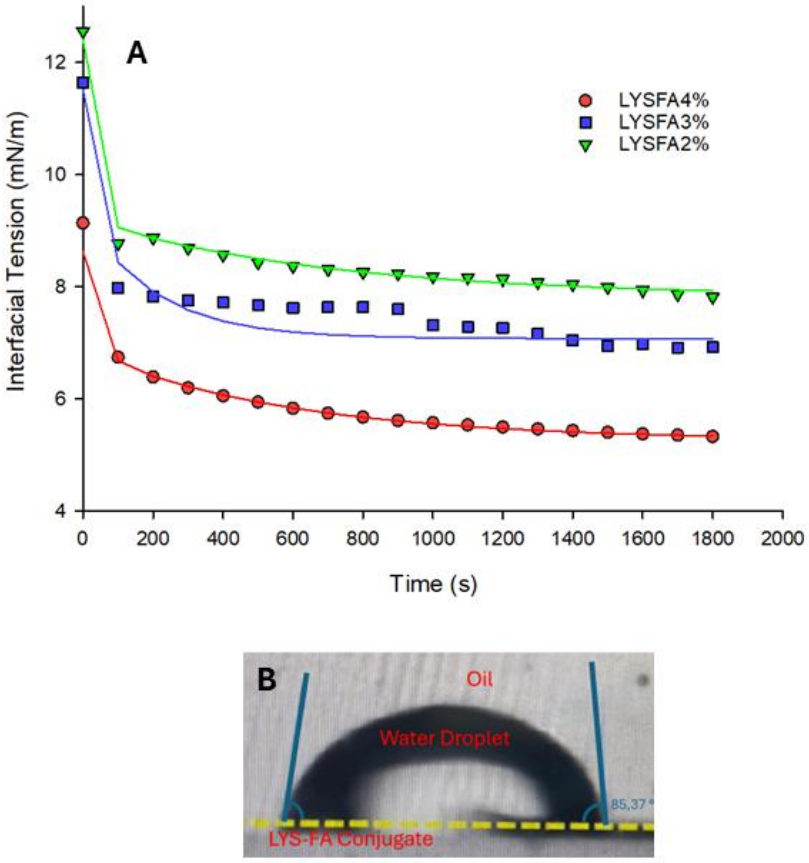

Figure 36. (A) Dynamic interfacial tension of different LYS-FA concentrations at the oil-water interface, with the model proposed by Equation 10 (–). (B) Oil-water three-phase contact angle with the LYS-FA conjugate.

3.4 *In vitro* gastrointestinal digestion simulation of the LYS–FA conjugate

Figure 37 presents the antioxidant profile, evaluated by DPPH radical scavenging, of LYS–FA, native LYS, and free FA during an *in vitro* simulated gastrointestinal digestion. In the oral phase, all systems exhibited the highest antioxidant capacity, with native LYS showing the lowest value (11.05 ± 1.41%), while free FA presented the highest (85.03 ± 0.23%), reflecting its strong reducing potential.

During the gastric phase, a significant reduction in antioxidant capacity was observed for all systems. Native LYS decreased to 4.84 ± 1.51%, likely due to pepsin-induced denaturation and the acidic environment. Similarly, free FA decreased to 50.86 ± 0.78%, indicating partial degradation of the phenolic compound under extreme pH and enzymatic activity. In contrast, the LYS–FA conjugate showed lower loss of activity (53.87 ± 0.67%), suggesting that covalent binding of FA to LYS provides structural protection to the phenol, delaying its degradation in the gastric environment (Shi *et al.*, 2024).

In the intestinal phase, antioxidant capacity of native LYS remained low (3.09 ± 1.53%), while free FA was almost completely degraded, retaining only 5.45 ± 1.49% activity. This sharp decrease is attributed to deprotonation of FA under the more alkaline conditions of simulated intestinal fluid (SIF), which facilitates oxidation (Liu *et al.*, 2016). Conversely, LYS–FA retained 13.05 ± 1.13% antioxidant capacity, more than twice that of free FA. These results indicate that conjugation of FA to LYS significantly ($p < 0.05$) enhances the stability of the phenolic compound under simulated digestive conditions, reinforcing its potential as a functional ingredient. Similar findings were reported by Yang *et al.* (2023), who observed a pronounced reduction in the DPPH-scavenging activity of EGCG upon reaching the intestinal phase, whereas the pumpkin seed protein isolate–EGCG conjugate maintained higher antioxidant activity at the end of digestion.

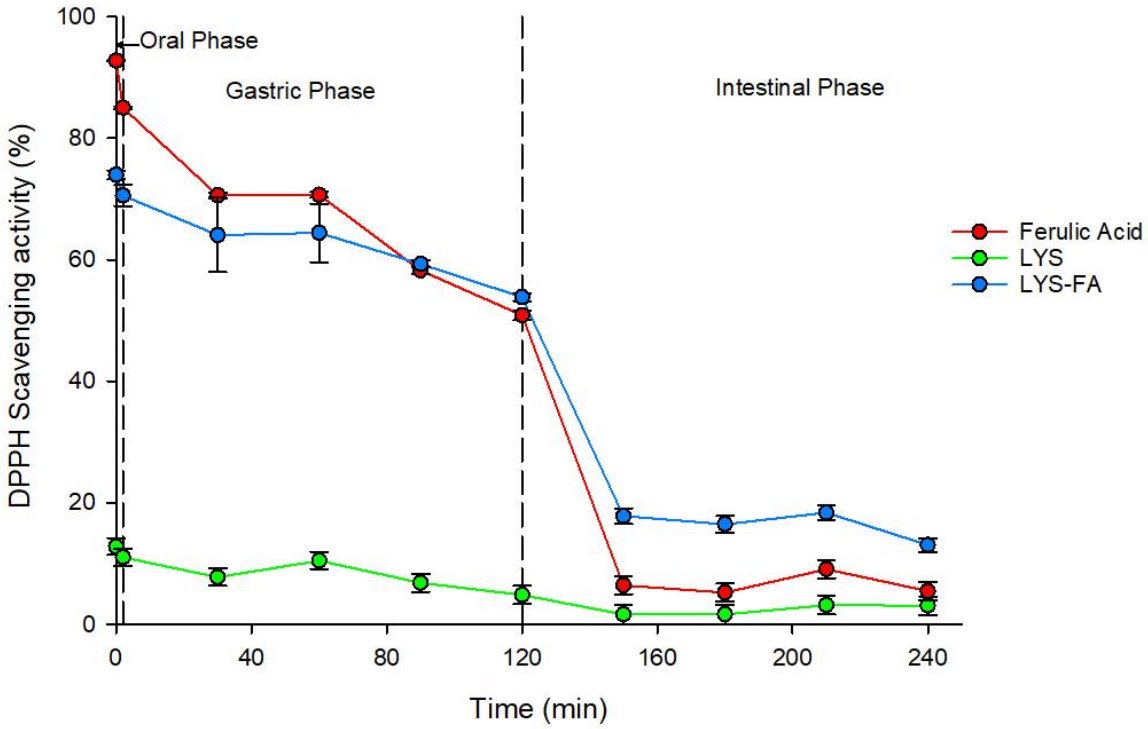

Figure 37. DPPH radical scavenging activity of FA, LYS and LYS-FA conjugates during in vitro simulated gastrointestinal digestion.

3.5 Formation and stability of Pickering emulsions

Figure 38A shows the creaming index of Pickering emulsions stabilized with different concentrations of the LYS–FA conjugate over eight days of storage at 25 °C. The results indicate that the LYSFA2% emulsion exhibited the lowest stability, with phase separation beginning on the first day and a creaming index of 15.84 ± 1.3% at the end of the period. The LYSFA3% emulsion demonstrated intermediate performance, with separation starting on the second day

and reaching 11.78 ± 1.12% on the eighth day. In contrast, the LYSFA4% emulsion remained stable throughout the entire storage period, showing no phase separation and a creaming index of zero.

Figure 38B presents the protein adsorption at the oil–water interface for Pickering emulsions stabilized with different concentrations of LYS–FA. Adsorption values were 26.08 ± 3.14% for LYSFA2%, 33.48 ± 1.92% for LYSFA3%, and 41.63 ± 2.85% for LYSFA4%. It is evident that emulsions with higher LYS–FA concentrations resulted in greater amounts of protein adsorbed at the interface. This behavior directly indicates that increased availability of emulsifying agents enhances their coverage at the surface of the oil droplets.

The results of this study demonstrate that higher concentrations of LYS–FA are directly associated with increased kinetic stability of the emulsions, with the LYSFA4% system being the most stable, supported by its higher protein adsorption at the interface. This enhanced stability arises from greater conjugate adsorption at the oil–water interface, which reduces interfacial tension and strengthens electrostatic repulsion between oil droplets. Such effects create an effective barrier that inhibits droplet aggregation and coalescence, ensuring a stable dispersion during storage (McClements, 2014; Tao *et al.*, 2023).

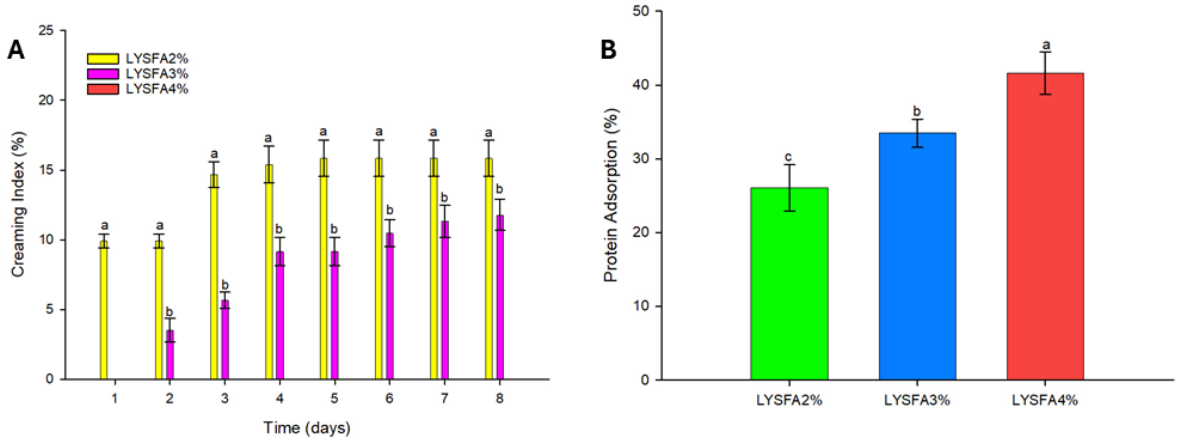

Figure 38. (A) Creaming index of Pickering O/W emulsions stabilized by LYS-FA conjugates at concentrations of 2%, 3%, and 4% as a function of storage time. (B) Protein adsorption of the LYS-FA conjugates at the oil-water interface of the emulsions. Values are presented as mean ± standard deviation. Different letters indicate statistically significant differences according to the Tukey test ($p < 0.05$).

3.6 Characterization of Pickering emulsions

3.6.1 Particle Size and Zeta Potential

The particle size results indicated that increasing the concentration of the LYS–FA conjugate led to a reduction in the average hydrodynamic diameter of the droplets. The sample with the lowest concentration showed a Z-average of 522.43 ± 15.17^{a} d.nm, which differed

significantly ($p < 0.05$) from the highest-concentration sample, which exhibited the smallest diameter, 446.33 ± 23.95^{b} d.nm. The LYSFA3% formulation had an intermediate value of 490.87 ± 12.59^{ab} d.nm. The decrease in particle size with increasing conjugate concentration can be attributed to the greater availability of emulsifier, which facilitates coverage of a larger interfacial area during homogenization, resulting in smaller droplets (Liu *et al.*, 2023). Similar behavior was reported by Sun *et al.* (2024), who observed a reduction in droplet size with increasing concentration of a lactoferrin–EGCG conjugate.

Regarding surface charge, zeta potential values increased significantly ($p < 0.05$) as the LYS–FA concentration was raised, with statistically significant differences among all samples. The observed values were 18.47 ± 0.35^{a} mV for LYSFA2%, 21.13 ± 0.97^{b} mV for LYSFA3%, and 25.20 ± 1.15^{c} mV for LYSFA4%. The increase in zeta potential magnitude indicates greater adsorption of the conjugate at the oil–water interface. Higher surface charges, as observed in LYSFA4%, suggest enhanced kinetic stability of the emulsion due to strengthened electrostatic repulsion between dispersed oil droplets (McClements, 2014).

3.6.2 Rheology

The rheological behavior of LYSFA2%, LYSFA3%, and LYSFA4% emulsions is shown in Figure 39A. All formulations exhibited a non-Newtonian, shear-thinning behavior. To mathematically describe the emulsion behavior, the rheological data were fitted to the Power Law, Bingham, and Herschel–Bulkley models, with parameters presented in Table 9.

The Herschel–Bulkley model provided the best fit to the experimental data. This model highlighted the presence of a yield stress, followed by pseudoplastic behavior. Similar results were reported by Li *et al.* (2019), who observed better fitting of the Herschel–Bulkley model compared to the Power Law for oil-in-water Pickering emulsions stabilized by a chitosan–starch complex.

Oscillatory frequency sweep tests, performed at 0.5% strain within the linear viscoelastic region, are shown in Figure 39B. For all formulations, the storage modulus (G') remained higher than the loss modulus (G") across the evaluated angular frequency range. Furthermore, tan δ values were consistently below 1, ranging from 0.2 to 0.3. These low values indicate a dominant elastic behavior over the viscous contribution (Xu *et al.*, 2021). These results suggest that the emulsions possess a predominantly elastic character, indicative of a stable three-dimensional network structure (Tunick, 2011). Additionally, the magnitudes of G'

and G" increased with rising LYS–FA concentration, demonstrating that higher conjugate content promotes a more rigid internal structure resistant to deformation.

Table 9. Rheological parameters of Power Law, Bingham, and Herschel-Bulkley models for Pickering emulsions stabilized with different LYS-FA conjugate concentrations.

Model	Parameters	LYSFA2%	LYSFA3%	LYSFA4%
Power Law	*K* (Pa.s^n)	1.840	2.866	2.992
	n	0.302	0.234	0.264
	Adjusted R^2	0.937	0.948	0.931
Bingham	τ_0 (Pa)	3.523	4.694	5.255
	μ_p (Pa.s)	0.043	0.043	0.055
	Adjusted R^2	0.856	0.834	0.829
Herschel-Bulkley	τ_0 (Pa)	2.842	3.701	3.586
	K (Pa.s^n)	0.184	0.210	0.367
	n	0.712	0.705	0.652
	Adjusted R^2	0.967	0.959	0.956

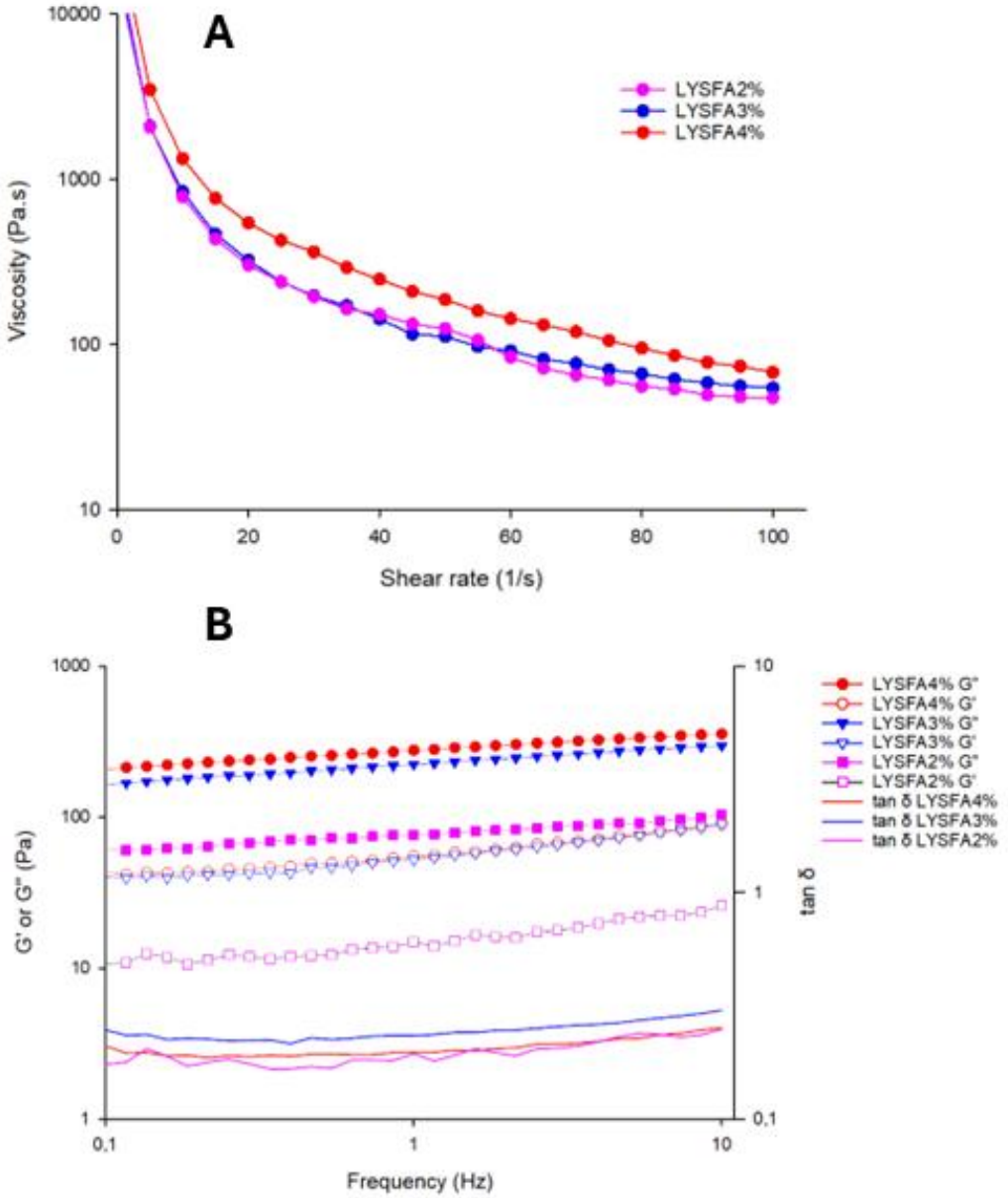

Figure 39. Rheological properties of Pickering emulsions stabilized by LYS-FA conjugates at different concentrations: (A) Apparent viscosity as a function of time; (B) Storage modulus (G') and loss modulus (G").

3.6.3 Antioxidant capacity

Figure 40A shows the antioxidant capacity of Pickering emulsions stabilized with LYS–FA. Antioxidant activity increased significantly with higher conjugate concentrations. In the DPPH assay, LYSFA2% exhibited 69.01 ± 0.67%, LYSFA3% reached 76.80 ± 0.15%, and LYSFA4% achieved 82.64 ± 0.53%. A similar trend was observed in the ABTS assay, with values rising from 67.10 ± 1.14% for LYSFA2% to 78.80 ± 4.93% for LYSFA4%. These results demonstrate that higher conjugate concentrations favor greater radical scavenging capacity.

These findings confirm that emulsions stabilized with LYS–FA maintain the antioxidant capacity conferred by FA. Similar evidence, where protein–polyphenol conjugates preserve

antioxidant activity in emulsions when used as emulsifiers, has been widely reported in the literature (Barbosa & Garcia-Rojas, 2025; Zhang *et al.*, 2023).

3.6.4 Oxidative stability

The oxidative stability of the emulsions was monitored by quantifying lipid hydroperoxides, indicators of primary oxidation, and malondialdehyde (MDA), a marker of secondary oxidation, over 14 days of storage, as shown in Figures 40B and 40C, respectively.

Regarding primary oxidation, the Control sample exhibited the highest deterioration rate, increasing from 13.62 mmol/kg to a peak value of 197.37 mmol/kg. In contrast, the incorporation of the LYS–FA conjugate significantly inhibited ($p < 0.05$) the propagation of oxidative reactions in a concentration-dependent manner. The LYSFA4% formulation showed the best performance, reaching a final value of 68.53 mmol/kg, corresponding to an approximate 65% reduction compared to the Control. The LYSFA3% and LYSFA2% samples followed, with final hydroperoxide contents of 77.14 mmol/kg and 80.96 mmol/kg, respectively.

This effective protection was directly reflected in the MDA results. While the Control exhibited a sharp increase from 4.67 to 39.27 mmol/L, indicating rapid decomposition of hydroperoxides into rancidity-related compounds, the emulsions stabilized with the conjugate maintained significantly lower MDA levels ($p < 0.05$). Once again, the LYSFA4% sample stood out, presenting the lowest MDA value (10.65 mmol/L), corroborating the enhanced stability observed during the primary oxidation stage.

The simultaneous inhibition of both oxidative phases can be attributed to the dual functionality of the LYS–FA conjugate. The formation of a dense interfacial barrier physically hinders the diffusion of oxygen and pro-oxidant species, while the presence of ferulic acid at the interface provides chemical protection by scavenging free radicals before they can initiate or propagate lipid degradation. Similarly, Sun *et al.* (2024) reported reduced lipid oxidation in high internal phase Pickering emulsions stabilized by a lactoferrin–epigallocatechin-3-gallate conjugate, observing lower hydroperoxide formation and a 58.95% reduction in MDA levels. This effect was likewise attributed to the formation of a compact interfacial layer capable of protecting fish oil from pro-oxidative agents.

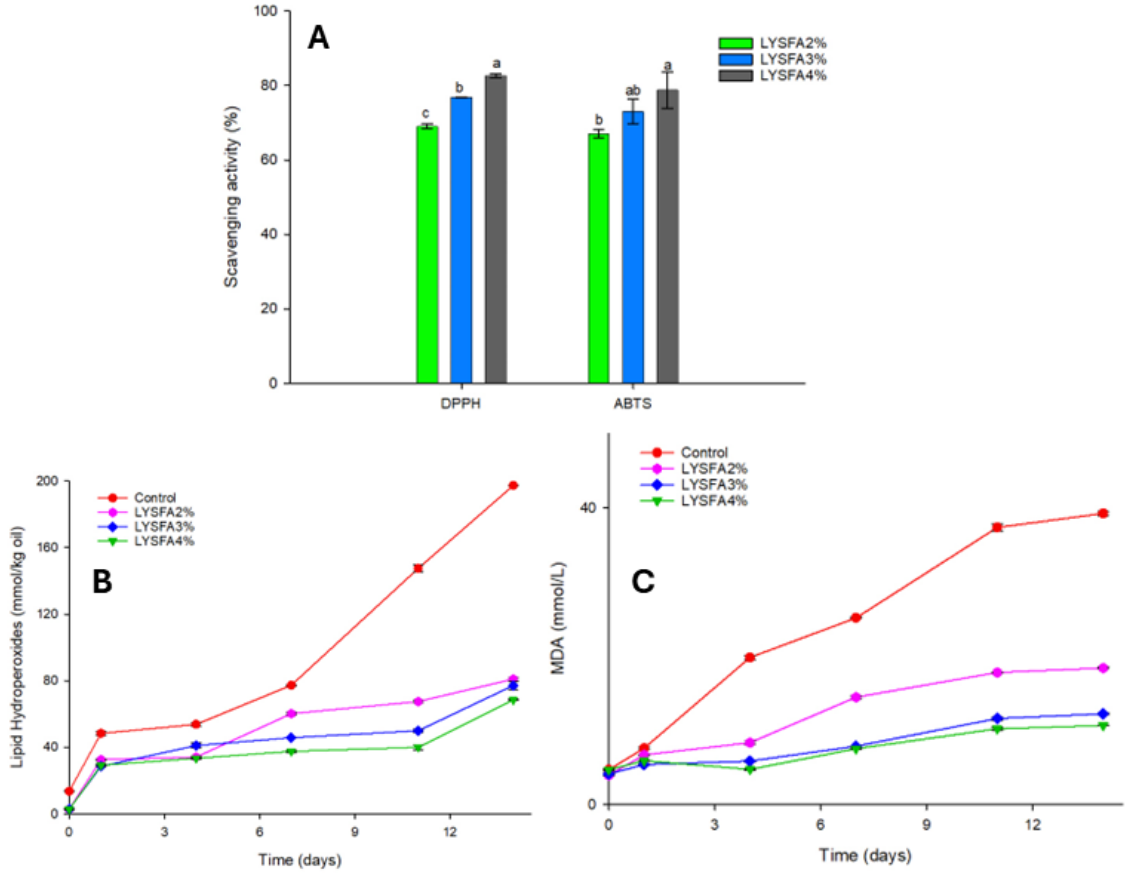

Figure 40. (A) Antioxidant capacity of Pickering O/W emulsions stabilized by LYS-FA conjugates at concentrations of 2%, 3%, and 4%, assessed by DPPH and ABTS radical scavenging assays. (B) and (C) Evaluation of the oxidative stability of the emulsions over time through the quantification of lipid hydroperoxides and malondialdehyde (MDA) content, respectively, compared to soybean oil control. Values are presented as mean ± standard deviation. Different letters indicate statistically significant differences according to the Tukey test ($p < 0.05$).

4 Conclusions

In this study, LYS–FA conjugates were synthesized via a free radical grafting method. Structural analyses confirmed the covalent binding of the polyphenol to the protein, resulting in partial unfolding of the tertiary structure and increased surface hydrophobicity, which are key factors contributing to the improvement of interfacial properties. The LYS–FA conjugate proved to be an efficient bifunctional ingredient, combining the emulsifying capacity of the protein with the antioxidant potential of ferulic acid. In addition, *in vitro* gastrointestinal digestion simulation demonstrated that conjugation provides structural protection to the phenolic compound, ensuring greater preservation of its antioxidant capacity throughout simulated digestion. The application of the conjugate in the formulation of Pickering emulsions was highly effective, particularly at a concentration of 4% (w/w), at which maximum kinetic stability was achieved, as evidenced by complete inhibition of creaming and the formation of a gel-like rheological network. Beyond the physical barrier, the conjugate formed a robust interfacial layer that protected soybean oil against both primary and secondary lipid oxidation. Therefore, LYS–FA conjugates exhibit strong potential as natural antioxidant emulsifiers for the development of functional foods, enabling the encapsulation of bioactive compounds and extending the shelf life of food products.

Conflict of interest

The authors declare that they have no known competing financial interests or personal relationships that could have appeared to influence the work reported in this paper.

Acknowledgments

The authors thank the CNPq, Brazil (309899/2025-7); CAPES, Brazil (Código 001) and FAPERJ, Brazil (E-26/210.052/2023; E-26/ 204.182/2024) for the financial support.

CRediT authorship contribution statement

Bruno Sérgio Toledo Barbosa: Conceptualization, Methodology, Validation, Investigation, Writing – original draft, Writing – review & editing. **Edwin Elard Garcia-Rojas**: Conceptualization, Methodology, Resources, Writing – review & editing, Supervision, Project administration, Funding acquisition.

5 References

Albert, C., Beladjine, M., Tsapis, N., Fattal, E., Agnely, F., & Huang, N. (2019). Pickering emulsions: Preparation processes, key parameters governing their properties and potential for pharmaceutical applications. *Journal of Controlled Release, 309*, 302–332. https://doi.org/10.1016/j.jconrel.2019.07.003

Albuquerque, B. R., Heleno, S. A., Oliveira, M. B. P. P., Barros, L., & Ferreira, I. C. F. R. (2021). Phenolic compounds: Current industrial applications, limitations and future challenges. *Food and Function, 12*, 14–29. https://doi.org/10.1039/d0fo02324h

Baba, W. N., McClements, D. J., & Maqsood, S. (2021). Whey protein–polyphenol conjugates and complexes: Production, characterization, and applications. *Food Chemistry, 365*, Article 130455. https://doi.org/10.1016/j.foodchem.2021.130455

Barbosa, B. S. T., Araújo, S. C., Cordeiro, Y., & Garcia-Rojas, E. E. (2025). Impact of the Covalent Interaction Between Ferulic Acid and Ovalbumin on the Structure and Functional Properties of the Protein. *Food Biophysics, 20,* Article 28. https://doi.org/10.1007/s11483-024-09919-6

Barbosa, B. S. T., & Garcia-Rojas, E. E. (2022). Double emulsions as delivery systems for iron: Stability kinetics and improved bioaccessibility in infants and adults. *Current Research in Food Science, 5*, 718–725. https://doi.org/10.1016/j.crfs.2022.04.003

Barbosa, B. S. T., & Garcia-Rojas, E. E. (2025). Effect of ovalbumin-ferulic acid conjugates on the stability and bioaccessibility of vitamin D3 in pickering emulsions. *International Journal of Biological Macromolecules, 321*, Article 146397. https://doi.org/10.1016/j.ijbiomac.2025.146397

Barth, A. (2007). Infrared spectroscopy of proteins. *Biochimica et Biophysica Acta - Bioenergetics, 1767*, 1073–1101. https://doi.org/10.1016/j.bbabio.2007.06.004

Bi, S., Ding, L., Tian, Y., Song, D., Zhou, X., Liu, X., & Zhang, H. (2004). Investigation of the interaction between flavonoids and human serum albumin. *Journal of Molecular Structure, 703*, 37–45. https://doi.org/10.1016/j.molstruc.2004.05.026

Chang, K., Liu, J., Jiang, W., Fan, Y., Nan, B., Ma, S., Zhang, Y., Liu, B., & Zhang, T. (2021). Structural characteristics and foaming properties of ovalbumin - Caffeic acid complex. *Lwt, 146*, Article 111383. https://doi.org/10.1016/j.lwt.2021.111383

Chen, Q., Liu, Y., Li, Y., Dong, L., Liu, Y., Liu, L., Farag, M. A., & Liu, L. (2024). Interaction and binding mechanism of ovalbumin with cereal phenolic acids: improved structure, antioxidant activity, emulsifying and digestion properties for potential targeted delivery systems. *Food Research International, 175*, Article 113726. https://doi.org/10.1016/j.foodres.2023.113726

Cheng, J., Dudu, O. E., Zhang, J., Wang, Y., Meng, L., Wei, W., Li, X., & Yan, T. (2023). Impact of binding interaction modes between whey protein concentrate and quercetin on protein structural and functional characteristics. *Food Hydrocolloids, 142*, Article 108787. https://doi.org/10.1016/j.foodhyd.2023.108787

Chevalier, Y., & Bolzinger, M.-A. (2013). Emulsions stabilized with solid nanoparticles: Pickering emulsions. *Colloids and Surfaces A: Physicochemical and Engineering Aspects, 439*, 23–34. https://doi.org/10.1016/j.colsurfa.2013.02.054

Cui, X., Ma, M., Xie, Y., Yang, Y., Li, Q., Sun, S., & Ma, W. (2022). Formation, structure and stability of high internal phase Pickering emulsions stabilized by BSPI-C3G covalent complexes. *Food Chemistry: X, 16*, Article 100455. https://doi.org/10.1016/j.fochx.2022.100455

Czubinski, J., & Dwiecki, K. (2017). A review of methods used for investigation of protein–phenolic compound interactions. *International Journal of Food Science and Technology, 52*, 573–585. https://doi.org/10.1111/ijfs.13339

Echegaray, N., Guzel, N., Kumar, M., Guzel, M., Hassoun, A., & Lorenzo, J. M. (2023). Recent advancements in natural colorants and their application as coloring in food and in intelligent food packaging. *Food Chemistry, 404*, Article 134453. https://doi.org/10.1016/j.foodchem.2022.134453

Feng, J., Cai, H., Wang, H., Li, C., & Liu, S. (2018). Improved oxidative stability of fish oil emulsion by grafted ovalbumin-catechin conjugates. *Food Chemistry, 241*, 60–69. https://doi.org/10.1016/j.foodchem.2017.08.055

Fredrick, E., Walstra, P., & Dewettinck, K. (2010). Factors governing partial coalescence in oil-in-water emulsions. *Advances in Colloid and Interface Science, 153*, 30–42. https://doi.org/10.1016/j.cis.2009.10.003

Guha, S., Majumder, K., & Mine, Y. (2018). Egg Proteins. In L. Melton, F. Shahidi, & P. Varelis (Eds.), *Encyclopedia of Food Chemistry*. Elsevier.

He, W., Xu, H., Lu, Y., Zhang, T., Li, S., Lin, X., Xu, B., & Wu, X. (2019). Function, digestibility and allergenicity assessment of ovalbumin–EGCG conjugates. *Journal of Functional Foods, 61*, Article 103490. https://doi.org/10.1016/j.jff.2019.103490

Hu, Q., Wang, T., Zhou, M., Xue, J., & Luo, Y. (2016). *In Vitro* Antioxidant-Activity Evaluation of Gallic-Acid-Grafted Chitosan Conjugate Synthesized by Free-Radical-Induced Grafting Method. *Journal of Agricultural and Food Chemistry, 64*, 5893–5900. https://doi.org/10.1021/acs.jafc.6b02255

Huang, X., Yan, C., Lin, M., He, C., Xu, Y., Huang, Y., & Zhou, Z. (2022). The effects of conjugation of walnut protein isolate with polyphenols on protein solubility, antioxidant activity, and emulsifying properties. *Food Research International, 161*, Article 111910. https://doi.org/10.1016/j.foodres.2022.111910

İşçimen, E. M. (2025). Production of a food-grade pickering emulsion stabilized by pea protein-different phenolic acids. *Journal of the Science of Food and Agriculture, 105*, 6862–6873. https://doi.org/10.1002/jsfa.14397

Ji, Y., Han, C., Liu, E., Li, X., Meng, X., & Liu, B. (2022). Pickering emulsions stabilized by pea protein isolate-chitosan nanoparticles: fabrication, characterization and delivery EPA for digestion *in vitro* and *in vivo*. *Food Chemistry, 378*, Article 132090. https://doi.org/10.1016/j.foodchem.2022.132090

Jia, X., Zhao, M., Xia, N., Teng, J., Jia, C., Wei, B., Huang, L., & Chen, D. (2019). Interaction between plant phenolics and rice protein improved oxidative stabilities of emulsion. *Journal of Cereal Science, 89*, Article 102818. https://doi.org/10.1016/j.jcs.2019.102818

Ju, M., Zhu, G., Huang, G., Shen, X., Zhang, Y., Jiang, L., & Sui, X. (2020). A novel pickering emulsion produced using soy protein-anthocyanin complex nanoparticles. *Food Hydrocolloids, 99*, Article 105329. https://doi.org/10.1016/j.foodhyd.2019.105329

Lakowicz, J. R. (2006). *Principles of fluorescence spectroscopy*. Springer.

Layne, E. (1957). Spectrophotometric and Turbidimetric Methods for Measuring Proteins. *Methods in Enzymology, 3*, 447–454. https://doi.org/10.1016/S0076-6879(57)03413-8

Li, H., Pan, Y., Li, C., Yang, Z., Rao, J., & Chen, B. (2022). Design, synthesis and characterization of lysozyme–gentisic acid dual-functional conjugates with antibacterial/antioxidant activities. *Food Chemistry, 370*, Article 131032. https://doi.org/10.1016/j.foodchem.2021.131032

Li, X.-M., Xie, Q.-T., Zhu, J., Pan, Y., Meng, R., Zhang, B., Chen, H.-Q., & Jin, Z.-Y. (2019). Chitosan hydrochloride/carboxymethyl starch complex nanogels as novel Pickering stabilizers: Physical stability and rheological properties. *Food Hydrocolloids, 93*, 215–225. https://doi.org/10.1016/j.foodhyd.2019.02.021

Lima, R. R., Stephani, R., Perrone, Í. T., & de Carvalho, A. F. (2023). Plant-based proteins: A review of factors modifying the protein structure and affecting emulsifying properties. *Food Chemistry Advances, 3*, Article 100397. https://doi.org/10.1016/j.focha.2023.100397

Liu, F., Ma, C., McClements, D. J., & Gao, Y. (2016). Development of polyphenol-protein-polysaccharide ternary complexes as emulsifiers for nutraceutical emulsions: Impact on formation, stability, and bioaccessibility of β-carotene emulsions. *Food Hydrocolloids, 61*, 578–588. https://doi.org/10.1016/j.foodhyd.2016.05.031

Liu, F., McClements, D. J., Ma, C., & Liu, X. (2023). Novel Colloidal Food Ingredients: Protein Complexes and Conjugates. *Annual Review of Food Science and Technology, 14*, 35–61. https://doi.org/10.1146/annurev-food-060721-023522

Liu, J., Yong, H., Yao, X., Hu, H., Yun, D., & Xiao, L. (2019). Recent advances in phenolic–protein conjugates: synthesis, characterization, biological activities and potential applications. *RSC Advances, 9*, 35825–35840. https://doi.org/10.1039/C9RA07808H

Liu, X., Xie, F., Zhou, J., He, J., Din, Z., Chen, S., & Cai, J. (2023). High internal phase Pickering emulsion stabilized by zein-tannic acid-sodium alginate complexes: β-Carotene loading and 3D printing. *Food Hydrocolloids, 142*, Article 108762. https://doi.org/10.1016/j.foodhyd.2023.108762

Low, L. E., Siva, S. P., Ho, Y. K., Chan, E. S., & Tey, B. T. (2020). Recent advances of characterization techniques for the formation, physical properties and stability of Pickering emulsion. *Advances in Colloid and Interface Science, 277*, Article 102117. https://doi.org/10.1016/j.cis.2020.102117

Lu, Y., Li, S., Xu, H., Zhang, T., Lin, X., & Wu, X. (2018). Effect of covalent interaction with chlorogenic acid on the allergenic capacity of ovalbumin. *Journal of Agricultural and Food Chemistry, 66*, 9794–9800. https://doi.org/10.1021/acs.jafc.8b03410

McClements, D. J. (2004). *Food Emulsions* (2nd ed.). CRC Press.

McClements, D. J. (2014). *Nanoparticle and microparticle based delivery systems* (1st ed.). CRC Press.

McClements, D. J., & Decker, E. (2018). Interfacial Antioxidants: A Review of Natural and Synthetic Emulsifiers and Coemulsifiers That Can Inhibit Lipid Oxidation. *Journal of Agricultural and Food Chemistry, 66*, 20–35. https://doi.org/10.1021/acs.jafc.7b05066

Mokni Ghribi, A., Maklouf Gafsi, I., Sila, A., Blecker, C., Danthine, S., Attia, H., Bougatef, A., & Besbes, S. (2015). Effects of enzymatic hydrolysis on conformational and functional properties of chickpea protein isolate. *Food Chemistry, 187*, 322–330. https://doi.org/10.1016/j.foodchem.2015.04.109

Moreno-Vásquez, M. J., Carretas-Valdez, M. I., Luque-Alcaraz, A. G., Quintero-Reyes, I. E., Tapia-Hernández, J. A., Arvizu-Flores, A. A., Moreno-Córdova, E. N., & Graciano-Verdugo, A. Z. (2024). Conjugation of Lysozyme and Epigallocatechin Gallate for Improving Antibacterial and Antioxidant Properties. *Current Microbiology, 81*, Article 295. https://doi.org/10.1007/s00284-024-03776-9

Nawaz, N., Wen, S., Wang, F., Nawaz, S., Raza, J., Iftikhar, M., & Usman, M. (2022). Lysozyme and Its Application as Antibacterial Agent in Food Industry. *Molecules, 27*, Article 196305. https://doi.org/10.3390/molecules27196305

Nooshkam, M., Varidi, M., Zareie, Z., & Alkobeisi, F. (2023). Behavior of protein-polysaccharide conjugate-stabilized food emulsions under various destabilization conditions. *Food Chemistry: X, 18*, Article 100725. https://doi.org/10.1016/j.fochx.2023.100725

Ou, S., & Kwok, K. C. (2004). Ferulic acid: Pharmaceutical functions, preparation and applications in foods. *Journal of the Science of Food and Agriculture, 84*, 1261–1269. https://doi.org/10.1002/jsfa.1873

Pan, L., Chen, J., Fu, H., Wang, N., Zhou, J., Zhang, S., Lu, S., Dong, J., Wang, Q., & Yan, H. (2023). Effects of fabrication of conjugates between different polyphenols and bovine bone proteins on their structural and functional properties. *Food Bioscience, 52*, Article 102375. https://doi.org/10.1016/j.fbio.2023.102375

Parolia, S., Maley, J., Sammynaiken, R., Green, R., Nickerson, M., & Ghosh, S. (2022). Structure – Functionality of lentil protein-polyphenol conjugates. *Food Chemistry, 367*, Article 130603. https://doi.org/10.1016/j.foodchem.2021.130603

Pi, X., Liu, J., Sun, Y., Ban, Q., Cheng, J., & Guo, M. (2023). Protein modification, IgE binding capacity, and functional properties of soybean protein upon conjugation with polyphenols. *Food Chemistry, 405*, Article 134820. https://doi.org/10.1016/j.foodchem.2022.134820

Qin, X. S., Gao, Q. Y., & Luo, Z. G. (2021). Enhancing the storage and gastrointestinal passage viability of probiotic powder (Lactobacillus Plantarum) through encapsulation with pickering high internal phase emulsions stabilized with WPI-EGCG covalent conjugate nanoparticles. *Food Hydrocolloids, 116*, Article 106658. https://doi.org/10.1016/j.foodhyd.2021.106658

Quan, T. H., Benjakul, S., Sae-leaw, T., Balange, A. K., & Maqsood, S. (2019). Protein–polyphenol conjugates: Antioxidant property, functionalities and their applications. *Trends in Food Science and Technology, 91*, 507–517. https://doi.org/10.1016/j.tifs.2019.07.049

Rahman, M. M., Byanju, B., Grewell, D., & Lamsal, B. P. (2020). High-power sonication of soy proteins: Hydroxyl radicals and their effects on protein structure. *Ultrasonics Sonochemistry, 64*, Article 105019. https://doi.org/10.1016/j.ultsonch.2020.105019

Rayees, R., Gani, A., Noor, N., Ayoub, A., & Ashraf, Z. U. (2024). General approaches to biopolymer-based Pickering emulsions. *International Journal of Biological Macromolecules, 267*, Article 131430. https://doi.org/10.1016/j.ijbiomac.2024.131430

Ren, G., Shi, J., Huang, S., Liu, C., Ni, F., He, Y., Luo, X., Li, T., Song, Y., Huang, M., & Xie, H. (2022). The fabrication of novel zein and resveratrol covalent conjugates: Enhanced thermal stability, emulsifying and antioxidant properties. *Food Chemistry, 374*, Article 131612. https://doi.org/10.1016/j.foodchem.2021.131612

Ren, G., Zhu, Y., Shi, J., Liu, J., He, Y., Sun, Y., Zhan, Y., Lv, J., Huang, M., & Xie, H. (2022). Fabrication of Antioxidant Pickering Emulsion Based on Resveratrol-Grafted Zein Conjugates: Enhancing the Physical and Oxidative Stability. *Foods, 11*, Article 3851. https://doi.org/10.3390/foods11233851

Schreiner, T. B., Dias, M. M., Barreiro, M. F., & Pinho, S. P. (2022). Saponins as Natural Emulsifiers for Nanoemulsions. *Journal of Agricultural and Food Chemistry, 70*, 6573–6590. https://doi.org/10.1021/acs.jafc.1c07893

Shi, T., Ziegler, V. E., Welge, I. C., An, L., & Wolf, B. A. (2004). Evolution of the Interfacial Tension between Polydisperse "Immiscible" Polymers in the Absence and in the Presence of a Compatibilizer. *Macromolecules, 37*, 1591–1599. https://doi.org/10.1021/ma035616y

Shi, W., Xie, H., Ouyang, K., Wang, S., Xiong, H., Woo, M. W., & Zhao, Q. (2024). The effect of rice protein-polyphenols covalent and non-covalent interactions on the structure, functionality and *in vitro* digestion properties of rice protein. *Food Chemistry, 450*, Article 139241. https://doi.org/10.1016/j.foodchem.2024.139241

Strixner, T., & Kulozik, U. (2011). Egg proteins. In G. O. Phillips & P. A. Williams (Eds.), *Handbook of Food Proteins* (pp. 150–209). Woodhead Publishing. https://doi.org/10.1533/9780857093639.150

Sun, J., Jing, H., Mu, Y., McClements, D. J., Dong, S., & Xu, B. (2020). Fabrication of antioxidant emulsifiers from natural ingredients: Conjugation of egg white proteins with catechin and chlorogenic acid. *Food Hydrocolloids, 108*, Article 106019. https://doi.org/10.1016/j.foodhyd.2020.106019

Sun, Y., Zhao, M., Liu, Z., Shi, H., Zhang, X., Zhao, Y., Ma, Z., Yu, G., Xia, G., & Shen, X. (2024). Preparation and characterization of lactoferrin-polyphenol conjugate with stabilizing effects on fish oil high internal phase Pickering emulsions. *Food Chemistry: X, 24*, Article 101836. https://doi.org/10.1016/j.fochx.2024.101836

Tao, X., Chen, C., Li, Y., Qin, X., Zhang, H., Hu, Y., Liu, Z., Guo, X., & Liu, G. (2023). Improving the physicochemical stability of Pickering emulsion stabilized by glycosylated whey protein isolate/cyanidin-3-glucoside to deliver curcumin. *International Journal of Biological Macromolecules, 229*, 1–10. https://doi.org/10.1016/j.ijbiomac.2022.12.269

Tatulian, S. A. (2013). Structural characterization of membrane proteins and peptides by FTIR and ATR-FTIR spectroscopy. *Methods in Molecular Biology, 974*, 177–218. https://doi.org/10.1007/978-1-62703-275-9_9

Tian, Y., Lv, X., Oh, D. H., Kassem, J. M., Salama, M., & Fu, X. (2024). Emulsifying properties of egg proteins: Influencing factors, modification techniques, and applications. *Comprehensive Reviews in Food Science and Food Safety, 23*, Article 70004. https://doi.org/10.1111/1541-4337.70004

Tunick, M. H. (2011). Small-strain dynamic rheology of food protein networks. *Journal of Agricultural and Food Chemistry, 59*, 1481–1486. https://doi.org/10.1021/jf1016237

Vasava, H., Singh, R., & Yadav, T. (2022). Characterisation of whey protein–polyphenol conjugates prepared by the noncovalent and covalent methods for their effect on the functional properties of whey proteins. *International Journal of Dairy Technology, 75*, 563–574. https://doi.org/10.1111/1471-0307.12874

Warren, B. (2014). *Ferulic Acid: Antioxidant Properties, Uses and Potential Health Benefits*. Nova Science Pub Inc.

Wu, T., Jiang, Q., Wu, D., Hu, Y., Chen, S., Ding, T., Ye, X., Liu, D., & Chen, J. (2019). What is new in lysozyme research and its application in food industry? A review. *Food Chemistry, 274*, 698–709. https://doi.org/10.1016/j.foodchem.2018.09.017

Xiong, Y., Li, Z., & Yang, X. (2023). Whey protein-tannic acid conjugate stabilized high internal phase Pickering emulsions: Interfacial stability based on covalent crosslinking. *Colloids and Surfaces A: Physicochemical and Engineering Aspects, 672*, Article 131690. https://doi.org/10.1016/j.colsurfa.2023.131690

Xu, H., Zhang, T., Lu, Y., Lin, X., Hu, X., Liu, L., He, Z., & Wu, X. (2019). Effect of chlorogenic acid covalent conjugation on the allergenicity, digestibility and functional properties of whey protein. *Food Chemistry, 298*, Article 125024. https://doi.org/10.1016/j.foodchem.2019.125024

Xu, W., Zheng, S., Sun, H., Ning, Y., Jia, Y., Luo, D., Li, Y., & Shah, B. R. (2021). Rheological behavior and microstructure of Pickering emulsions based on different concentrations of gliadin/sodium caseinate nanoparticles. *European Food Research and Technology, 247*, 2621–2633. https://doi.org/10.1007/s00217-021-03827-6

Xue, Y. T., Han, Y. N., Wang, Y., Zhang, Y. H., Yin, Y. Q., Liu, B. H., Zhang, H. L., & Zhao, X. H. (2023). Effect of ferulic acid covalent conjugation on the functional properties and antigenicity of β-lactoglobulin. *Food Chemistry, 406*, Article 135095. https://doi.org/10.1016/j.foodchem.2022.135095

Yang, C., Liu, J., Han, Y., Wang, B., Liu, Z., Hu, H., Guan, Z., Yang, Y., & Wang, J. (2023). Fabrication of polyphenol-pumpkin seed protein isolate (PSPI) covalent conjugate microparticles to protect free radical scavenging activity of polyphenol. *Food Bioscience, 55*, Article 102982. https://doi.org/10.1016/j.fbio.2023.102982

Yin, Y., Luo, D., Jin, W., Sun, Y., Yue, M., Li, P., & Xu, W. (2024). Lysozyme-(-)-epigallocatechin gallate covalent conjugates: preparation, structure and functional properties. *Journal of Food Measurement and Characterization, 18*, 4741–4750. https://doi.org/10.1007/s11694-024-02530-w

Yu, Z., Ma, L., Liu, B., Wang, W., Shang, Z., Dang, H., & Liu, C. (2023). Improvement of foaming properties of ovalbumin: Insights into the synergistic effect of preheating and high-intensity ultrasound on physicochemical properties and structure analysis. *Ultrasonics Sonochemistry, 101*, Article 106672. https://doi.org/10.1016/j.ultsonch.2023.106672

Zhang, B., Wang, Y., & Lu, R. (2023). Pickering emulsion stabilized by casein–caffeic acid covalent nanoparticles to enhance the bioavailability of curcumin *in vitro* and *in vivo*. *Journal of the Science of Food and Agriculture, 103*, 3579–3591. https://doi.org/10.1002/jsfa.12447

Zhang, Y., Zhou, F., Shen, P., Zhao, Q., & Zhao, M. (2020). Influence of thermal treatment on oil-water interfacial properties and emulsion stabilization prepared by sono-assembled soy peptide nanoparticles. *Food Hydrocolloids, 103*, Article 105646. https://doi.org/10.1016/j.foodhyd.2020.10

CAPÍTULO V. BIOACTIVE PECTIN FILMS INCORPORATED WITH BETA-CAROTENE PICKERING EMULSIONS USING LYSOZYME-FERULIC ACID CONJUGATES AS EMULSIFIERS

Abstract

The development of active and sustainable food packaging is an alternative to replace conventional plastics. This study developed bioactive pectin films incorporating β-carotene, a lipophilic and photosensitive bioactive compound, using Pickering emulsions stabilized by novel lysozyme-ferulic acid (LYS-FA) conjugates. The conjugates were synthesized via a free-radical grafting method. These particles were used to prepare oil-in-water Pickering emulsions loaded with β-carotene. The emulsion with the highest conjugate concentration (4% w/w) showed superior encapsulation efficiency and significantly enhanced the photostability of β-carotene under UV light. This optimal emulsion was incorporated into pectin film-forming solutions at various concentrations (1.0, 3.0, and 5.0% w/w). The incorporation of the LYS-FA Pickering emulsions notably modified the properties of the pectin films. It increased surface hydrophobicity and antioxidant capacity, while reducing water solubility, moisture content, and water vapor permeability. Films containing β-carotene exhibited a distinct yellow coloration. Release kinetics studies revealed that the β-carotene release from the films was governed by a Fickian diffusion mechanism, as described by the Ritger-Peppas and Peppas-Sahlin models. The results demonstrate that LYS-FA conjugates are effective natural particulate emulsifiers for developing multifunctional pectin-based active packaging.

Keywords: Active food packaging, Release kinetics, Covalent interaction, protein-polyphenol, Sustainable packaging

1 Introduction

The growing concern about the environmental impacts of conventional plastics, together with the demand for safer and more sustainable products, has driven the development of alternative packaging systems in the food industry (Espitia *et al.*, 2014). In this context, active packaging stands out for its ability to interact with the food or its surrounding environment by incorporating functional compounds that enhance product shelf life and quality, preferably derived from natural and biodegradable materials. Within this scenario, biopolymer-based films have received considerable attention as sustainable alternatives to conventional packaging (Nair *et al.*, 2023). Among them, pectin stands out due to its wide availability, non-toxicity, biodegradability, and excellent film-forming ability. It is an anionic polysaccharide predominantly composed of partially methyl-esterified α-(1→4)-D-galacturonic acid units, typically extracted from agro-industrial residues such as citrus peels and apple pomace, exhibiting high water affinity and the ability to form continuous polymeric networks (Espitia *et al.*, 2014; Freitas *et al.*, 2021).

Despite these advantages, pectin films present important limitations associated with their highly hydrophilic nature, resulting in high water vapor permeability and solubility. These characteristics restrict their application as functional packaging materials (Huang *et al.*, 2022). Therefore, strategies aimed at modifying the polymer matrix structure have been widely investigated to improve the physical, mechanical, and functional performance of these films. In parallel, increasing interest has been observed in the incorporation of bioactive compounds such as essential oils (Yang *et al.*, 2024), vitamins (Zickuhr *et al.*, 2025), polyphenols (Zhao *et al.*, 2023), and carotenoids (Chhoden *et al.*, 2025) into polymeric matrices.

β-Carotene is a lipophilic carotenoid widely found in fruits and vegetables, recognized for its antioxidant activity, provitamin A function, and ability to impart natural coloration to foods (Bogacz-Radomska & Harasym, 2018). However, its practical application is limited by its low water solubility and high sensitivity to light, oxygen, and heat, which promote rapid degradation and consequent loss of bioactivity (Gul *et al.*, 2015). Therefore, encapsulation of β-carotene in systems capable of protecting it and controlling its release is essential to enable its application in polymeric matrices and active packaging.

Emulsions have been widely employed as delivery systems for lipophilic bioactive compounds. In this context, Pickering emulsions, stabilized by solid particles adsorbed at the oil–water interface, have emerged as promising alternatives to conventional emulsions, exhibiting high stability against coalescence and flocculation, as well as enhanced protection of encapsulated compounds (Albert *et al.*, 2019; Chevalier & Bolzinger, 2013). Among the

different natural emulsifiers investigated, proteins stand out due to their amphiphilic nature and ability to form colloidal particles with high interfacial activity (Yan *et al.*, 2020). Lysozyme (LYS), a globular protein widely known for its antimicrobial activity, high purity, and structural stability, shows potential for application as an emulsifier in Pickering emulsions, although it remains underexplored in this context (Nawaz *et al.*, 2022).

The incorporation of Pickering emulsions formed by protein–polyphenol conjugates into films has proven to be a promising strategy for the development of active packaging, as these systems can impart new mechanical and barrier properties to polymeric matrices while enhancing their antioxidant capacity (Xue *et al.*, 2024; Yang *et al.*, 2024; Zhao *et al.*, 2023). Additionally, these emulsions enable the incorporation of bioactive ingredients in microencapsulated form, expanding film functionality. However, to date, no studies have explored the use of Pickering emulsions stabilized by lysozyme–ferulic acid conjugates (LYS–FA) for the microencapsulation of β-carotene and their incorporation into pectin films with controlled release, particularly regarding the potential synergistic effects between the protein–phenolic conjugate and the bioactive compound.

Therefore, the aim of this study was to develop Pickering emulsions using lysozyme–ferulic acid conjugate (LYS–FA) particles as emulsifying agents for β-carotene encapsulation and to evaluate their incorporation into bioactive pectin films. The effects of emulsion concentration on encapsulation efficiency, β-carotene photostability, and the physical, mechanical, optical, antioxidant, and barrier properties of the films were investigated, as well as the controlled release behavior of the bioactive compound.

2 Material and Methods

2.1 Material

Lysozyme, ferulic acid, pectin, β-carotene, ascorbic acid, glycerol, 2,2-diphenyl-1-picrylhydrazyl (DPPH), and 2,2′-azino-bis(3-ethylbenzothiazoline-6-sulfonic acid) (ABTS) were purchased from Sigma-Aldrich (St. Louis, MO, USA). Soybean oil used in this study was obtained from the local market in Rio de Janeiro, Brazil. Potassium sulfate, anhydrous calcium chloride, and magnesium nitrate were purchased from Dinâmica Química Contemporânea Ltda. (São Paulo, Brazil). The water used in all experiments was ultrapure (conductivity 0.05 μS/cm), obtained using a Master-P&D system (Gehaka, Brazil).

2.2 Preparation of Particles from the LYS–FA Conjugate

The LYS-FA conjugate was obtained via a free radical-mediated reaction, according to the method described in a previous study (Barbosa & Garcia-Rojas, 2026). At the end of the process, the conjugates were dialyzed using a D9527 membrane (Sigma-Aldrich, USA) against ultrapure water for 48 h to remove excess reagents and subsequently frozen and freeze-dried in a lyophilizer (Enterprise I, Terroni, Brazil) to obtain the dried material.

Particle formation was conducted according to the methodology described by Ju *et al.* (2020). Briefly, aqueous solutions containing 5% (w/v) LYS–FA were heated in a water bath at 95 °C for 15 min, followed by immediate cooling in an ice bath until reaching room temperature. The resulting solution was then rapidly frozen in liquid nitrogen (−160 °C) and subsequently freeze-dried to obtain the particulate material.

2.3 Formation of β-Carotene-Loaded Pickering Emulsions

Oil-in-water (O/W) Pickering emulsions were formulated according to the protocol described by Ji *et al.* (2022), using soybean oil loaded with β-carotene (2 mg/mL) as the dispersed phase and LYS–FA conjugate particles as stabilizers in the continuous phase at concentrations of 2.0%, 3.0%, and 4.0% (w/w). The emulsions were prepared with an oil volume fraction (φ) of 0.70. The samples were named LYSFA2%, LYSFA3%, and LYSFA4% according to the emulsifier concentration in the aqueous phase. Emulsification was performed using an Ultra-Turrax T25 homogenizer (IKA, Germany) operating at 18,000 rpm for 6 min, ensuring emulsion formation under controlled conditions.

2.4 Stability of β-Carotene in Pickering Emulsions

2.4.1 β-carotene Quantification

The quantification of β-carotene in the emulsions was performed based on the method described by Yin *et al.* (2024). Briefly, 1 mL aliquots of the emulsions were diluted tenfold and then mixed with 1 mL of ethanol and 2 mL of n-hexane to extract β-carotene retained in the Pickering emulsions. The mixture was vortexed for 10 s to ensure complete dissolution of the dispersed phase. After standing for 10 min, absorbance readings were obtained using a BioMate 3S spectrophotometer (Thermo Fisher Scientific, USA) at 450 nm. The β-carotene concentration was determined from a standard calibration curve constructed under the same experimental conditions.

2.4.2 Encapsulation Efficiency

Encapsulation efficiency (EE) of freshly prepared emulsions was determined according to Equation (1):

$$EE\ (\%) = \frac{\text{Encapsulated } \beta\text{−carotene}}{\text{Total } \beta\text{−carotene}} \qquad (1)$$

where encapsulated β-carotene (g) represents the amount of the compound retained in the Pickering emulsions, while total β-carotene (g) corresponds to the total amount of the nutrient incorporated into the formulation.

2.4.3 Photochemical Stability of β-carotene

The method used to determine the photochemical stability of β-carotene was based on the methodology described by Wei *et al.* (2022), with modifications. Freshly prepared emulsions were exposed to ultraviolet (UV) radiation for 3 h in a dark chamber equipped with a UV lamp (AG-DC-02, ACS Gold, Brazil). Emulsion aliquots were collected at different time intervals (0, 60, 120, and 180 min). The photostability of β-carotene was evaluated based on the percentage of the compound remaining in the emulsions after UV exposure, according to Equation (2):

$$\beta - \text{caroten retention}\ (\%) = \frac{C_t}{C_0} \qquad (2)$$

where C_t represents the β-carotene concentration (mg/mL) at the analyzed time, while C_0 corresponds to the initial β-carotene concentration (mg/mL), determined immediately after emulsion preparation.

2.5 Preparation of Pectin-Based Films

Pectin-based films were prepared according to Almasi *et al.* (2020) using the casting method. Initially, an aqueous pectin solution (3.5% w/w) was magnetically stirred overnight at room temperature to ensure complete hydration. After solubilization, the previously selected Pickering emulsion was incorporated. The final pectin concentration was 3.0% (w/w) and the glycerol concentration was 0.6% (w/w). The emulsion was added at concentrations of 1.0, 3.0, and 5.0% (w/w), yielding the formulations LYSFA1%, LYSFA3%, and LYSFA5% (emulsion without β-carotene) and BC-LYSFA1%, BC-LYSFA3%, and BC-LYSFA5% (emulsion containing encapsulated β-carotene). The film-forming solutions, with a surface density of 0.3183 g/cm², were cast onto Petri dishes and dried at 25 °C for 48 h. After drying, the films

were stored in desiccators containing saturated magnesium nitrate solution, maintaining 55% relative humidity.

2.6 Characterization of Pectin-Based Films

2.6.1 Light Transmission and Opacity

Light transmission and opacity analyses of the films were performed according to the methodology described by Zhao *et al.* (2022). Film transparency was evaluated using a UV–Vis spectrophotometer over a wavelength range of 190–800 nm, with film specimens measuring 4 cm × 0.5 cm. In addition, film opacity was determined based on the absorbance measured at 600 nm and calculated according to Equation (3):

$$Opacity = \frac{A_{600}}{E} \qquad (3)$$

where A_{600} is the film absorbance at 600 nm and E is the film thickness (mm).

2.6.2 Color Properties

Film color analysis was performed using a colorimeter (SHE TEC200, Tecnal, Brazil). The samples were evaluated according to the Commission Internationale de l'Éclairage (CIE Lab*) color system. Chroma (C*) and hue angle (h°) were calculated according to Equations (4) and (5), respectively. The yellowness index (YI) was determined according to the methodology described by Shen *et al.* (2021), using Equation (6).

$$C^* = \sqrt{(a^{*2} + b^{*2})} \qquad (4)$$

$$h° = \arctan\left(\frac{b^*}{a^*}\right) \qquad (5)$$

$$Yi = \frac{142{,}86 \times b^*}{L^*} \qquad (6)$$

2.6.3 Fourier Transform Infrared (FTIR) Spectroscopy

A Fourier transform infrared (FTIR) spectrophotometer (Vertex 70, Bruker, Germany) was used to analyze LYS and LYS–FA samples. The spectra were recorded in the range of 4000–400 cm^{-1}.

2.6.4 Film Thickness

Film thickness was measured using a digital micrometer (Mitutoyo, Japan). Measurements were taken at ten random points on each film, and the final value was calculated as the average of these measurements.

2.6.5 Mechanical Properties

The mechanical properties of the films were determined using a TA.XTplus texture analyzer (Stable Micro Systems, UK). Film samples were cut into strips (1 × 10 cm) and subjected to tensile strength (TS) and elongation at break (EAB) tests using A/TG tensile grips (Stable Micro Systems, UK).

2.6.6 Moisture Content

The moisture content (%) of the films was determined according to the methodology described by Khedri *et al.* (2021), based on the initial mass loss of the samples. For this purpose, the samples were weighed before and after drying in an oven at 105 ± 1 °C until constant weight was achieved. The moisture content was calculated according to Equation (7):

$$Moisture\ Content\ (\%) = \frac{W_1 - W_2}{W_1} \qquad (7)$$

where W_1 is the initial mass of the sample (g) and W_2 corresponds to the dry mass (g).

2.6.7 Solubility

Film solubility was determined by the gravimetric method according to the methodology described by Taghizadeh *et al.* (2018). Film samples (3 cm × 2 cm) were initially weighed and immersed in 50 mL of distilled water. The system was maintained under constant stirring at 25 °C for 24 h. After this period, the suspension was filtered using filter paper previously dried in an oven at 105 °C for 30 min to retain the undissolved residues. The filter paper containing the residue was then dried again at 105 °C until constant mass, and the final mass was recorded. The mass of the dried residue was obtained from the difference between the final mass of the filter paper with residue and the initial mass of the filter paper. Film solubility was calculated according to Equation (8):

$$Solubility\ (\%) = \frac{W_1 - W_2}{W_1} \qquad (8)$$

where W_1 is the initial mass of the film (g) and W_2 is the mass of the dried residue after filter paper drying (g).

2.6.8 Antioxidant Capacity

The antioxidant capacity of the films was evaluated using DPPH and ABTS radical scavenging assays. For both tests, 100 mg of each film sample were dispersed in 2 mL of water under constant stirring for 2 min.

The free radical scavenging capacity determined by the DPPH method was evaluated based on the methodology described by Pan *et al.* (2023). Briefly, 1 mL of the extract obtained from the film dispersion was mixed with 0.4 mL of a DPPH solution (1.75×10^{-4} mol/L). The mixtures were kept in the dark at room temperature for 30 min. After incubation, the absorbance of the samples was measured at 517 nm using a spectrophotometer. Ultrapure water was used as the reaction blank. The percentage of DPPH radical scavenging was calculated according to Equation (9):

$$DPPH\ (\%) = \left[1 - \frac{A_1 - A_2}{A_0}\right] x100 \qquad (9)$$

where A_0 is the absorbance of the control sample (without extract), A_1 is the absorbance in the presence of the film extract, and A_2 corresponds to the absorbance of the blank (without DPPH).

The ABTS radical scavenging assay was performed based on the adapted methodology described by Ren *et al.* (2022). Initially, potassium persulfate (2.45 mmol/L) and ABTS (7 mmol/L) solutions were mixed at a 1:1 ratio and kept in the dark overnight to generate ABTS radicals. Subsequently, 0.5 mL of the film extract was mixed with 2 mL of the ABTS solution, and the mixture was incubated in the dark for 1 h to allow the reaction to occur. Finally, the absorbance of the samples was measured at 734 nm using a spectrophotometer. Ultrapure water was used as the control. The ABTS radical scavenging capacity was calculated according to Equation (10):

$$ABTS\ (\%) = \left[1 - \frac{A_1 - A_2}{A_0}\right] x100 \qquad (10)$$

where A_0 is the absorbance of the control sample (without extract), A_1 is the absorbance in the presence of the film extract, and A_2 corresponds to the absorbance of the blank (without ABTS).

2.6.9 Water Vapor Permeability

Water vapor permeability (WVP) of the films was determined by the gravimetric method according to ASTM E96-05 (ASTM, 2005), based on the methodology described by Fathi *et al.* (2018). Film samples were sealed over permeation cells containing anhydrous calcium chloride. The assemblies were placed in desiccators containing saturated potassium sulfate

solution, and mass changes were monitored daily. The water vapor transmission rate (WVTR) was calculated according to Equation (11):

$$WVTR = \left(\frac{\Delta m}{\Delta t}\right)\frac{1}{A} \qquad (11)$$

Where Δ_m/Δ_t is the slope obtained by linear regression of mass change as a function of time (g/h), and A is the effective permeation area of the film. (3.14×10^{-4} m^2).

The WVP was calculated according to Equation (12):

$$WVP = \frac{WVTR \times E}{\Delta P} \qquad (12)$$

where E is the average film thickness (m) and ΔP is the partial water vapor pressure difference across the film, equal to 3073.93 Pa. The ΔP value was calculated considering the saturated water vapor pressure at 25 °C (3169 Pa) and a relative humidity difference of 0.97.

2.6.10 Water Contact Angle

The water contact angle on the film surface was used to evaluate the hydrophobicity of the material, according to the methodology described by Liu *et al.* (2025). For this purpose, the samples were fixed onto glass slides, and a 5 μL drop of distilled water was carefully deposited on the film surface using a precision syringe. The contact angle formed between the droplet and the film surface was measured using a tensiometer EasyTrack (Teclis Scientific, France), coupled with a contact angle analysis module.

2.7 β-Carotene Release Kinetics from Pectin-Based Films

The controlled release kinetics study was conducted according to the methodology described by Zickuhr *et al.* (2025), aiming to investigate the release of β-carotene from films containing LYS–FA Pickering emulsions. For this purpose, 1 g film samples containing β-carotene were immersed in 25 mL of absolute ethanol, shaken in amber flasks, and kept protected from light at room temperature. The quantification of released β-carotene was performed as described in Section 2.4.1. Aliquots were collected at 10, 20, 30, 40, 50, 60, 90, 120, 150, 180, and 210 min. To evaluate the release mechanism, first-order (Equation 13), Higuchi (Equation 14), Ritger–Peppas (Equation 15), and Peppas–Sahlin (Equation 16) kinetic models were applied:

$$\frac{M}{M_\infty} = 1 - e^{-kt} \quad (13)$$

$$\frac{M}{M_\infty} = Kt^{0,5} \quad (14)$$

$$\frac{M}{M_\infty} = Kt^{n} \quad (15)$$

$$\frac{M}{M_\infty} = K_1 t^{m} + K_2 t^{2m} \quad (16)$$

where M_t/M_∞ is the fraction of β-carotene released at time t; t is elapsed time (s); K, K_1, and K_2 (s^{-1}) are the release constants of each model; and n and m are the diffusion exponents.

2.8 Statistical Analysis

Data analysis was performed using analysis of variance (ANOVA) followed by Tukey's *post hoc* test for mean comparisons. Differences were considered statistically significant at $p < 0.05$. All experiments were conducted in triplicate, and results are expressed as mean ± standard deviation.

3 Results and Discussion

3.1 Microencapsulation of β-Carotene in Pickering Emulsions

3.1.1 Encapsulation Efficiency of β-Carotene

The encapsulation efficiency results of β-carotene in Pickering emulsions prepared with different concentrations of the LYS–FA emulsifier are shown in Figure 41A. A direct influence of conjugate concentration on the retention of the bioactive compound was observed. The formulations prepared with higher emulsifier concentrations, LYSFA3% and LYSFA4%, exhibited the highest encapsulation efficiencies, reaching 89.48% ± 4.03%[a] and 88.99% ± 2.02%[a], respectively. In contrast, the formulation with the lowest concentration, LYSFA2%, showed a significantly lower encapsulation efficiency of 80.24% ± 3.13%[b].

This behavior indicates that increasing the LYS–FA conjugate concentration was a determining factor in improving the encapsulation system. The greater availability of conjugate molecules in solution favors adsorption kinetics at the oil–water interface, enabling faster and more efficient coverage of the entire surface area of the droplets formed during emulsification (Wilde *et al.*, 2004).

3.1.2 Photochemical Stability of β-Carotene

The photochemical stability of encapsulated β-carotene was monitored over the storage period, as shown in Figure 41B. The results highlight the high sensitivity of the compound to

degradation when exposed to light. The control sample underwent abrupt degradation within the first hour, showing a retention of only 19.57%, which further decreased to 16.90% at the end of the experiment. In contrast, the systems encapsulated with the LYS–FA conjugate exhibited a significantly higher protective capacity, maintaining higher retention levels than the control at all evaluated times. The LYSFA4% system preserved 51.58% of the active compound at the end of the period, whereas the LYSFA2% and LYSFA3% samples maintained retention values close to 35%.

This enhanced preservation is attributed to the formation of Pickering emulsions, which act as a physical barrier at the oil–water interface, reducing direct light incidence on the oil phase in which β-carotene is solubilized (Kouravand *et al.*, 2024). The superior performance observed with increasing conjugate concentration is associated with the antioxidant capacity of ferulic acid, whose greater presence at the interface contributes to scavenging free radicals generated in the initial stage of photo-oxidation, thereby delaying photolytic degradation (McClements & Decker, 2018). Similarly, Yin *et al.* (2024) demonstrated that oil-in-water Pickering emulsions stabilized by chitosan were able to reduce β-carotene degradation under light exposure. Emulsions containing higher emulsifier concentrations showed a greater protective effect, which was attributed to the formation of more stable systems with smaller droplet sizes. Notably, the highest chitosan concentration achieved approximately 70% β-carotene retention, whereas lower concentrations reached around 50% at the end of the experiment.

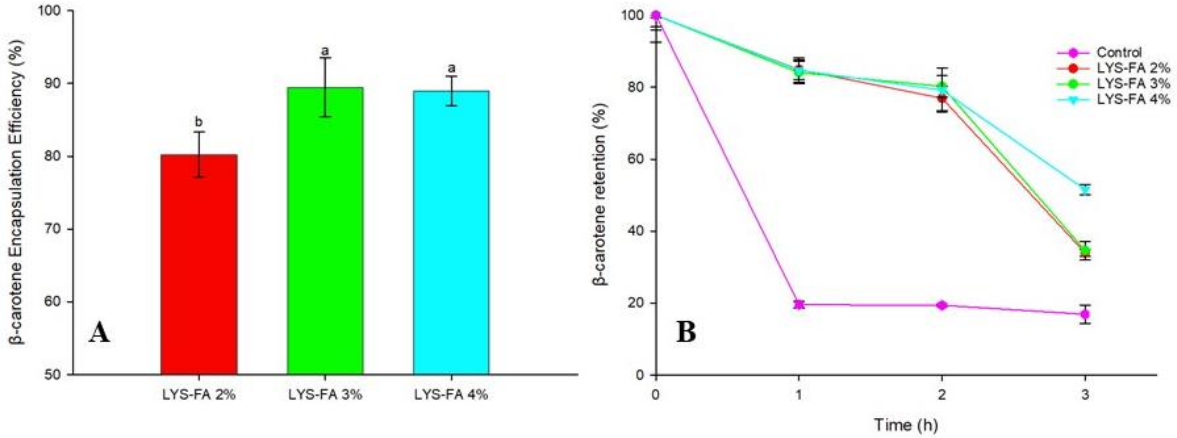

Figure 41. (A) β-carotene encapsulation efficiency of Pickering emulsions prepared using LYS–FA conjugates as emulsifiers at different concentrations. (B) Photochemical stability of β-carotene in soybean oil (control) and in Pickering emulsions prepared using LYS–FA conjugates as emulsifiers during UV exposure. Data are expressed as mean ± standard deviation. Different lowercase letters indicate significant differences among samples ($p < 0.05$).

Based on the encapsulation efficiency and photochemical stability results of β-carotene, the LYS–FA 4% Pickering emulsion was selected for film formation, as it exhibited superior performance, characterized by higher encapsulation efficiency and greater protective capacity against light-induced degradation of β-carotene.

3.2 Characterization of Pectin-Based Films

The pectin-based films are shown in Figure 42, where it can be observed that the control film and the films without β-carotene exhibit a more transparent appearance, whereas those incorporated with β-carotene display yellowish hues due to the coloring properties of the active compound.

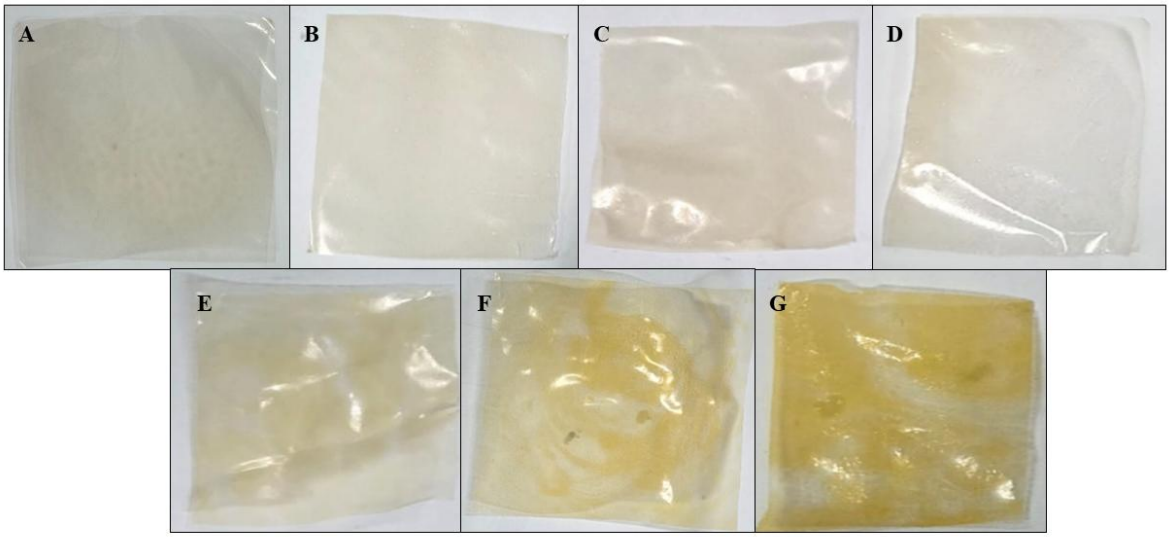

Figure 42. Visual appearance of the pectin-based films: (A) control film; (B) LYSFA 1%; (C) LYSFA 3%; (D) LYSFA 5%; (E) BC–LYSFA 1%; (F) BC–LYSFA 3%; and (G) BC–LYSFA 5%.

3.2.1 Light Transmission and Opacity

The film transmittance results at different wavelengths, presented in Figure 43A, highlight the impact of incorporating Pickering emulsions and β-carotene on the optical and light barrier properties of pectin-based films. The control film exhibited higher transmittance in the ultraviolet region (200–400 nm), indicating a lower capacity to protect against UV radiation. In contrast, the incorporation of Pickering emulsions led to a reduction in transmittance within this spectral range, evidencing an enhanced UV-blocking capacity of the films. This behavior can be attributed to the presence of the oil phase in the emulsions, which exhibits high absorption of radiation near 284 nm, thereby contributing to the light barrier effect (Yang *et al.*, 2024).

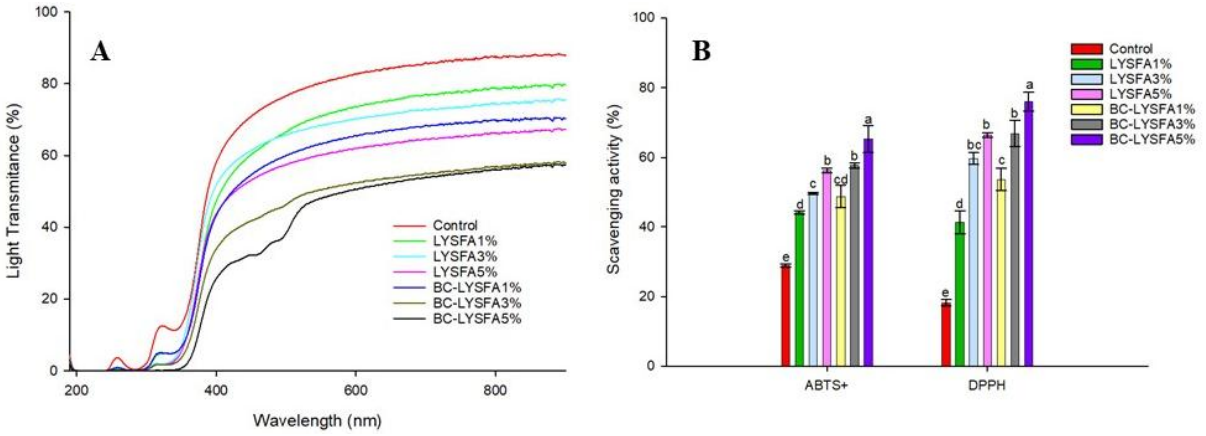

Figure 43. (A) UV–visible light transmittance spectra of pectin-based films containing LYS–FA conjugates at different concentrations, with or without β-carotene. (B) Radical scavenging activity of the films evaluated by $ABTS^{+}$ and DPPH assays. Results are expressed as mean ± standard deviation. Different lowercase letters indicate significant differences among samples within each assay ($p < 0.05$).

As the wavelength increased toward the visible region (400–700 nm), a progressive increase in transmittance was observed for all formulations. However, a clear distinction was observed between the control film and those containing emulsions. The LYSFA films exhibited lower transmittance than control throughout the entire analyzed spectrum, an effect associated with the heterogeneous structure formed by emulsion incorporation, which favors light absorption and scattering (Zhao *et al.*, 2022).

The BC-LYSFA films exhibited the lowest transmittance values among all evaluated systems. This reduction was dependent on emulsion concentration and, consequently, on the amount of β-carotene incorporated. The lower transmittance in these films is attributed to the presence of β-carotene, a carotenoid pigment that absorbs light in the blue and green regions of the visible spectrum, imparting a yellowish color to the films (Britton *et al.*, 2004). Therefore, the incorporation of β-carotene encapsulated in Pickering emulsions reduces system transmittance, providing the films with an enhanced light barrier.

This light barrier effect is reflected in the opacity values presented in Table 10. The control film exhibited an opacity of 0.828 ± 0.054 mm^{-1}, whereas incorporation of LYS–FA conjugates promoted a progressive increase, reaching 1.335 ± 0.047 mm^{-1} for LYSFA1% and 2.079 ± 0.000 mm^{-1} for LYSFA3%. The highest opacity values were observed for films containing β-carotene, with 2.815 ± 0.150 mm^{-1} for BC-LYSFA3% and 2.963 ± 0.044 mm^{-1} for BC-LYSFA5%, confirming the enhanced light barrier promoted by the combined incorporation of Pickering emulsions and encapsulated β-carotene. A similar increase in opacity upon emulsion incorporation was reported by Zhao *et al.* (2022), who observed that films containing Pickering nanoemulsions exhibited opacity values approximately four times higher than those of the anthocyanidin–chitosan control film.

3.2.2 Color Properties

The colorimetric parameters presented in Table 10 highlight the visual impact of incorporating Pickering emulsions and β-carotene into the polymer matrix. The analysis of lightness (L*) and chromatic coordinates (a* and b*) indicates that films containing only Pickering emulsions did not differ statistically from the control ($p < 0.05$). In these samples, L* values remained above 80, while b* values were below 9, indicating that emulsion incorporation, in the absence of the bioactive compound, did not perceptibly alter the original visual appearance of the films.

In contrast, the incorporation of encapsulated β-carotene promoted significant changes in the optical properties of the films. A progressive decrease in lightness was observed with increasing carotenoid concentration, with L* values decreasing to 74.60 ± 0.09 in the BC-LYSFA5% formulation, resulting in visually darker films. Concomitantly, a marked increase in chromatic coordinates was observed, particularly in b*, which increased from 13.80 ± 0.55 at the lowest concentration to 40.27 ± 1.03 in the formulation with the highest concentration of Pickering emulsions containing β-carotene. This increase confirms the predominance of the characteristic yellow coloration of the pigment, indicating its effective incorporation and retention within the film structure (Pathare *et al.*, 2013).

The analysis of C* and h° reinforces these trends. C* values increased sharply with β-carotene addition, rising from 8.40 ± 0.26 in the control to 40.48 ± 1.02 in the BC-LYSFA5% sample, indicating greater color intensity and saturation (Pathare *et al.*, 2013). In parallel, h° values shifted toward higher angles, varying from 76.39 ± 0.36° in the control to 84.06 ± 0.28° in the BC-LYSFA5% formulation, indicating the predominance of purer yellow hues in the active films.

Finally, the behavior of the YI reflects the effect of incorporating encapsulated β-carotene. While the control and films containing only Pickering emulsions exhibited YI values close to 15, the addition of the carotenoid led to a pronounced increase in this index, reaching 61.59 ± 5.34 in BC-LYSFA3% and 77.11 ± 2.01 in BC-LYSFA5%. These results corroborate the visual changes observed in the films. Similar findings were reported by Chhoden *et al.* (2025), who observed an increase in yellowish tone associated with the addition of a carotenoid-rich emulsion to corn starch-based films. At higher extract concentrations, the authors reported an increase in a* and a decrease in L*, indicating color intensification and reduced film lightness. Specifically, L* decreased from 98.44 in the control to 82.21 at the highest concentration, while b* increased from 6.688 to 26.93.

Table 10. Opacity, color parameters (L*, a*, b*), chroma (C*), hue angle (h°), and yellowness index (Yi) of control films and films containing unloaded and β-carotene–loaded Pickering emulsions at different concentrations.

	Opacity (mm^{-1})	L*	a*	b*	C*	h^o (º)	Yi
Control	0,828 ± 0,054^{f}	82.99 ± 0.28^{a}	1.98 ± 0.11^{a}	8.17 ± 0.24^{a}	8.40 ± 0.26^{a}	76.39 ± 0.36^{a}	14.06 ± 0.46^{a}
LYSFA1%	1,335 ± 0,047^{e}	82.05 ± 0.11^{a}	2.21 ± 0.01^{a}	8.48 ± 0.09^{a}	8.77 ± 0.09^{a}	75.42 ± 0.18^{a}	14.77 ± 0.17^{a}
LYSFA3%	1,537 ± 0,000^{d}	80.03 ± 0.78^{a}	2.14 ± 0.06^{a}	8.28 ± 0.18^{a}	8.55 ± 0.18^{a}	75.49 ± 0.32^{a}	14.78 ± 0.18^{a}
LYSFA5%	2,079 ± 0,000^{b}	81.44 ± 0.96^{a}	2.20 ± 0.13^{a}	8.93 ± 0.09^{a}	9.19 ± 0.11^{a}	76.18 ± 0.72^{a}	15.66 ± 0.29^{a}
BC-LYSFA1%	1,841 ± 0,021^{c}	76.09 ± 0.72^{b}	1.94 ± 0.14^{a}	13.80 ± 0.55^{b}	13.94 ± 0.55^{b}	81.99 ± 0.58^{b}	25.91 ± 1.01^{b}
BC-LYSFA3%	2,815 ± 0,150^{a}	74.23 ± 2.40^{b}	3.07 ± 0.25^{b}	32.00 ± 1.80^{c}	32.15 ± 1.77^{c}	84.51 ± 0.73^{c}	61.59 ± 5.34^{c}
BC-LYSFA5%	2,963 ± 0,044^{a}	74.60 ± 0.09^{b}	4.19 ± 0.13^{c}	40.27 ± 1.03^{d}	40.48 ± 1.02^{d}	84.06 ± 0.28^{c}	77.11 ± 2.01^{d}

Values are expressed as mean ± standard deviation. Different superscript letters within the same column indicate significant differences among samples ($p < 0.05$).

3.2.3 FTIR spectroscopy

The FTIR spectra of films are shown in Figure 44. The control film exhibited characteristic bands of pectin, indicating preservation of the polysaccharide structure. A broad band in the range of 3200–3400 cm^{-1} was observed and attributed to O–H stretching vibrations associated with the formation of intermolecular hydrogen bonds between pectin chains (Almasi *et al.*, 2020). The band at 2929 cm^{-1} is related to the stretching vibrations of C–H groups present in the main polymer backbone.

The presence of a peak at 1740 cm^{-1} is associated with the stretching vibration of ester carbonyl groups (C=O), characteristic of the methoxylated groups of pectin. The band observed at 1604 cm^{-1} can be attributed to the asymmetric stretching vibration of free carboxylate groups ($–COO^-$) (Jiang *et al.*, 2019). In the spectral region between 1000 and 1150 cm^{-1}, intense bands corresponding to C–O–C and C–O stretching vibrations, typical of the polysaccharide backbone, were observed, confirming the structural integrity of the pectin matrix in the films (Nisar *et al.*, 2018).

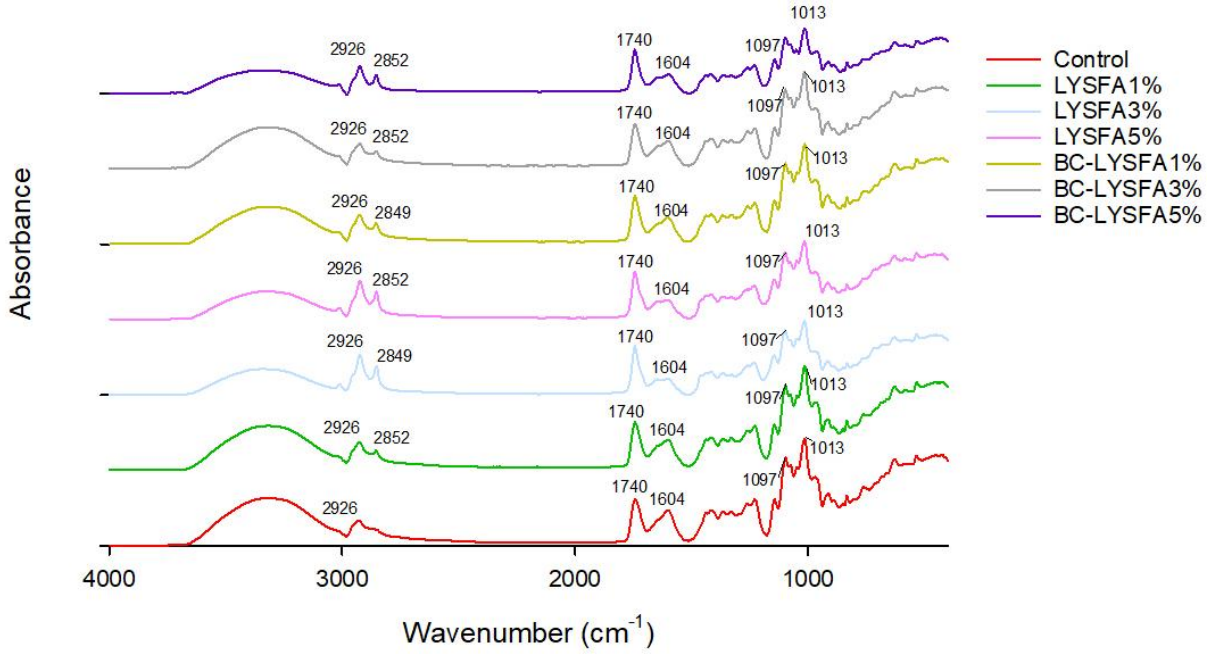

Figure 44. FTIR spectra of pectin-based films: control film, films containing LYS–FA emulsions at different concentrations (1, 3 and 5%), and films incorporating β-carotene–loaded LYS–FA emulsions (BC-LYSFA1%, BC-LYSFA3% and BC-LYSFA5%).

For the films containing Pickering emulsions, an additional peak around 2850 cm^{-1} was identified, which is related to the incorporation of the oil phase. This peak is attributed to symmetric and asymmetric stretching vibrations of methylene groups (–CH2–) in aliphatic C–H chains, characteristic of lipid compounds (Yu *et al.*, 2024).

Overall, the FTIR spectra of the films containing emulsions exhibited profiles similar to that of the control pectin film, with no evidence of new bands or significant peak shifts. These results indicate that the incorporation of Pickering emulsions into the pectin films did not result in the formation of new chemical bonds, suggesting that interactions between the polymer matrix and emulsion components occurred predominantly through physical interactions.

3.2.4 Mechanical Properties

The mechanical properties and thickness of the films are presented in Table 11. Statistical analysis indicated no significant difference ($p < 0.05$) in thickness among the films, suggesting that the incorporation of Pickering emulsions and β-carotene did not alter the final dimensions of the films. In contrast, the mechanical properties showed that the addition of the emulsions directly affected the strength and flexibility of the films.

The tensile strength exhibited a decreasing trend with increasing emulsion concentration, with the control film showing the highest mechanical strength of 29.22 ± 1.68 MPa. Incorporation of the dispersed phase caused a significant reduction in this parameter, reaching the lowest value in the samples containing 5% emulsion. The elongation at break values corroborated the loss of material ductility, as the control film exhibited the highest deformability, 61.82 ± 0.49%, attributed to the effective plasticization provided by glycerol. Addition of 1% emulsion reduced elongation to 54.42 ± 0.26%, while higher concentrations led to nearly similar values, around 51%.

These changes in mechanical properties are attributed to the presence of Pickering emulsions, whose disperse phase functions as structural discontinuities, disrupting the homogeneity of the polymer matrix (Liu *et al.*, 2019; Tongnuanchan *et al.*, 2015). Similar results were reported by Liu *et al.* (2021), who observed a decrease in tensile strength upon incorporation of Pickering emulsions in konjac glucomannan-based films compared to the control film. Liu *et al.* (2022) likewise reported a significant reduction in both tensile strength and EAB in chitosan films containing cinnamon essential oil Pickering emulsions stabilized by cellulose nanocrystals, indicating a decrease in the mechanical integrity of the polymer matrix. The addition of the emulsion reduced tensile strength from 22.42 to 15.66 MPa and elongation at break from 25.12% to 6.65%.

3.2.5 Moisture Content

The moisture content results, presented in Table 11, indicate that the control film retained the highest amount of water, with a moisture content of 17.62 ± 0.49%. A significant reduction ($p < 0.05$) in this parameter was observed as the concentration of Pickering emulsions increased, regardless of the presence of β-carotene. Accordingly, the BC-LYSFA5% sample exhibited the lowest moisture content, 10.49 ± 0.26%. This decrease is associated with the chemical nature of the polymer matrix, since pectin and glycerol are intrinsically hydrophilic and rich in hydroxyl groups, favoring water retention. Incorporation of Pickering emulsions partially replaces this matrix with a hydrophobic oil phase and the LYS-FA conjugate, resulting in films with progressively more hydrophobic character as the emulsion concentration increases (Espitia *et al.*, 2014; Tan *et al.*, 2025). Similarly, Shen *et al.* (2021) observed a reduction in moisture content with the addition of different concentrations of Pickering emulsions. They reported that pure pullulan-gelatin films had a moisture content of 24.40 ± 1.48%, which decreased to 15.07 ± 0.70% at the highest emulsion concentration evaluated.

3.2.6 Solubility

Table 11 shows that the control film exhibited the highest water solubility, with an average value of 92.84 ± 1.55%. Incorporation of Pickering emulsions significantly reduced this parameter, with an effect dependent on the added concentration. Samples containing 1% emulsion maintained high solubility, with values of 86.10 ± 2.62% for LYSFA1% and 85.27 ± 2.72% for BC-LYSFA1%. Increasing the concentration to 3% led to a more pronounced reduction, resulting in values of 67.97 ± 2.03% and 68.86 ± 4.54% for LYSFA3% and BC-LYSFA3%, respectively. The lowest solubility values were observed in films containing 5% emulsion, reaching 57.06 ± 1.45% for LYSFA5% and 56.04 ± 2.05% for BC-LYSFA5%. The presence of encapsulated β-carotene did not significantly alter film solubility, indicating that the bioactive compound did not affect the interaction between the polymer matrix and water. The progressive reduction in solubility can be attributed to the hydrophobic nature of the oil phase and LYS-FA particles, which decrease the overall affinity of the polymer matrix for water (Tan *et al.*, 2025). A similar solubility trend was reported by Liu *et al.* (2021), who observed that incorporation of Pickering emulsions in konjac glucomannan-based films resulted in solubility values ranging from 39.39 to 59.62%, depending on the emulsion oil concentration.

3.2.7 Antioxidant Capacity

The antioxidant capacity of the films, assessed using DPPH and ABTS radical scavenging assays, is presented in Figure 43B. Analysis revealed a significant increase in radical scavenging capacity with increasing emulsion concentration. The control film exhibited the lowest inhibition percentages, 18.22 ± 0.94% for DPPH and 28.86 ± 3.87% for ABTS, consistent with the pure pectin-glycerol matrix, which has limited antioxidant potential. Incorporation of Pickering emulsions resulted in an immediate increase in antioxidant capacity, suggesting that the LYS-FA conjugate actively contributes to this property due to the presence of ferulic acid, a phenolic compound with recognized reducing power. Furthermore, the effect was enhanced in samples containing encapsulated β-carotene, confirming the preservation of its bioactivity after processing. The BC-LYSFA5% sample stood out with the highest absolute inhibition values, reaching 76.04 ± 2.70% in the DPPH assay and 65.28 ± 0.42% in the ABTS assay. These results demonstrate a synergistic effect between the protein–polyphenol emulsifier and β-carotene, yielding a material with high antioxidant capacity. Zhao *et al.* (2023) also observed an increase in antioxidant capacity, measured by ABTS and DPPH methods, upon incorporation of whey protein isolate (WPI) and proanthocyanidin conjugates into carboxymethyl cellulose-based films. Specifically, ABTS scavenging activity increased from approximately 15% in the control to about 85%, while DPPH increased from around 10% to approximately 20% after incorporation.

3.2.8 Water Vapor Permeability

The WVP of the films is presented in Table 11. The control film exhibited the highest WVP value, 4.17×10^{-7} g·m^{-1}·h^{-1}·Pa^{-1}, indicating a limited moisture barrier, characteristic of pectin-based films. Incorporation of Pickering emulsions resulted in a significant reduction ($p < 0.05$) in WVP at all evaluated concentrations, demonstrating an improvement in the barrier properties of the films, with values of $1.618 \pm 0.038 \times 10^{-7}$ g·m^{-1}·h^{-1}·Pa^{-1} for LYSFA5% and $1.539 \pm 0.020 \times 10^{-7}$ g·m^{-1}·h^{-1}·Pa^{-1} for BC-LYSFA5%. This decrease in WVP is attributed to the incorporation of Pickering emulsions, which promoted the formation of a more hydrophobic surface within the polymer matrix, reducing water vapor absorption by the film (Yang *et al.*, 2024). Additionally, the presence of oil due to emulsion incorporation favored the formation of more tortuous diffusion pathways within the polymer matrix, increasing the distance traveled by water molecules and consequently reducing the amount of water permeating the polymer structure (Sánchez-González *et al.*, 2010).

Ding *et al.* (2023) observed that increasing the concentration of Pickering emulsions in pullulan-gelatin film formulations resulted in a decrease in water vapor permeability. A similar effect was observed in pectin-based films; Yu *et al.* (2024) reported that the addition of Pickering emulsions at a concentration of 5% (w/w) led to a reduction of approximately 66% in WVP, values comparable to those obtained in the present study.

3.2.9 Water Contact Angle

The contact angle measurement with water, presented in Figure 45, was used to evaluate the surface hydrophobicity of the films. The control film showed the lowest contact angle, indicating a hydrophilic surface, which corroborates the high affinity of the pectin-glycerol matrix for water observed in the solubility and moisture tests. Incorporation of Pickering emulsions significantly increased ($p < 0.05$) this parameter for all formulations, with values exceeding 90°, indicating a transition to a hydrophobic surface character (Xie *et al.*, 2020). The LYSFA5% and BC-LYSFA5% samples exhibited the highest contact angles, 98.76 ± 1.18° and 97.98 ± 2.38°, respectively. The increase in contact angle is attributed to the fact that Pickering emulsions confer hydrophobic character to the film surface and increase surface roughness, reducing water affinity (Yang *et al.*, 2024). Zhao *et al.* (2023) reported an increase in the contact angle of carboxymethyl cellulose films after incorporation of WPI–polyphenol conjugates. Control films had a contact angle of 85.20 ± 0.20°, while films containing the WPI–curcumin conjugate reached values of up to 101.45 ± 0.25°.

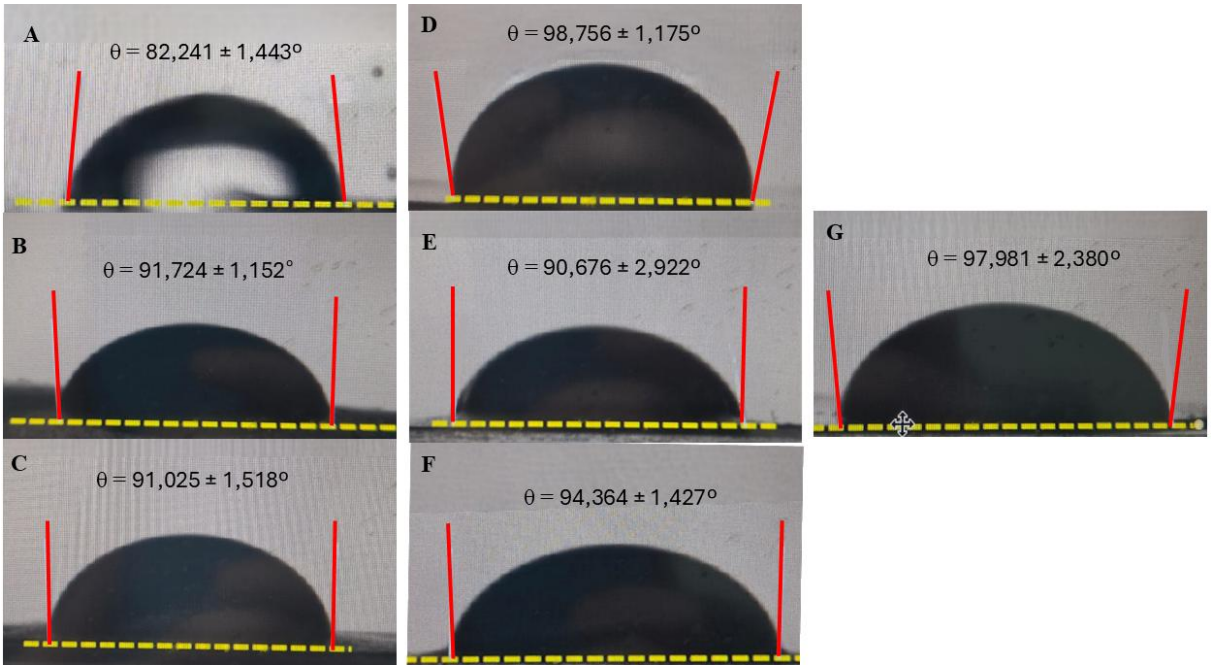

Figure 45. Contact angle images of the pectin-based films: (A) control film; (B) LYSFA 1%; (C) LYSFA 3%; (D) LYSFA 5%; (E) BC–LYSFA 1%; (F) BC–LYSFA 3%; and (G) BC–LYSFA 5%.

Table 11. Thickness, mechanical properties, opacity, moisture content, solubility, water vapor permeability of control films and films incorporated with unloaded and β-carotene–loaded Pickering emulsions at different concentrations.

	Thickness (mm)	Tensile strength (MPa)	Elongation at break (%)	Moisture content (%)	Solubility (%)	WVP (x 10^{-7} g m^{-1} h^{-1} Pa^{-1})
Control	0.099 ± 0.003^{ab}	29.22 ± 1.68^{a}	61.82 ± 0.49a	17.62 ± 0.49^{a}	92.84 ± 1.55^{a}	4.172 ± 0.358^{a}
LYSFA1%	0.101 ± 0.003^{ab}	24.44 ± 1.23^{b}	54.42 ± 0.26^{b}	16.64 ± 0.46^{ab}	86.10 ± 2.62^{ab}	2.831 ± 0.258^{b}
LYSFA3%	0.103 ± 0.003^{a}	18.68 ± 0.40^{c}	51.80 ± 0.24^{c}	13.73 ± 0.73^{c}	67.97 ± 2.03^{c}	2.093 ± 0.125^{c}
LYSFA5%	0.096 ± 0.003^{b}	12.45 ± 0.17^{de}	51.19 ± 0.38^{c}	12.92 ± 0.47^{c}	57.06 ± 1.45^{d}	1.618 ± 0.038^{d}
BC-LYSFA1%	0.098 ± 0.002^{ab}	20.47 ± 1.41^{c}	51.75 ± 0.63^{c}	15.78 ± 0.66^{b}	85.27 ± 2.72^{b}	2.461 ± 0.041^{bc}
BC-LYSFA3%	0.099 ± 0.004^{ab}	15.20 ± 1.75^{d}	50.79 ± 0.09^{c}	12.44 ± 0.59^{c}	68.86 ± 4.54^{c}	2.004 ± 0.087^{c}
BC-LYSFA5%	0.102 ± 0.002^{a}	11.11 ± 0.36^{e}	50.87 ± 0.30^{c}	10.49 ± 0.26^{d}	56.04 ± 2.05^{d}	1.539 ± 0.020^{d}

Values are expressed as mean ± standard deviation. Different superscript letters within the same column indicate significant differences among samples ($p < 0.05$).

3.3 β-Carotene Release Kinetics from Pectin-Based Films

The mathematical models used to describe β-carotene release from the films, along with the corresponding kinetic parameters, are presented in Table 12, while experimental profiles and model fittings are illustrated in Figure 46. The first-order model showed low adjusted R^2 values, especially for the BC-LYSFA5% sample, indicating a limited fit to the experimental data. This behavior suggests that β-carotene release does not occur in direct proportion to the residual concentration of the compound in the film (Askarizadeh *et al.*, 2023). In turn, the Higuchi model exhibited good fitting coefficients for the BC-LYSFA1% and BC-LYSFA3% samples but performed poorly for the BC-LYSFA5% formulation, as evidenced by the reduced adjusted R^2. This result indicates that, although Fickian diffusion contributes to the release process, the fundamental assumptions of the Higuchi model, such as neglecting dissolution and swelling phenomena of the polymer matrix and assuming perfect sink conditions in the release medium (Malekjani & Jafari, 2021), may not be fully met, especially in systems with higher Pickering emulsion content.

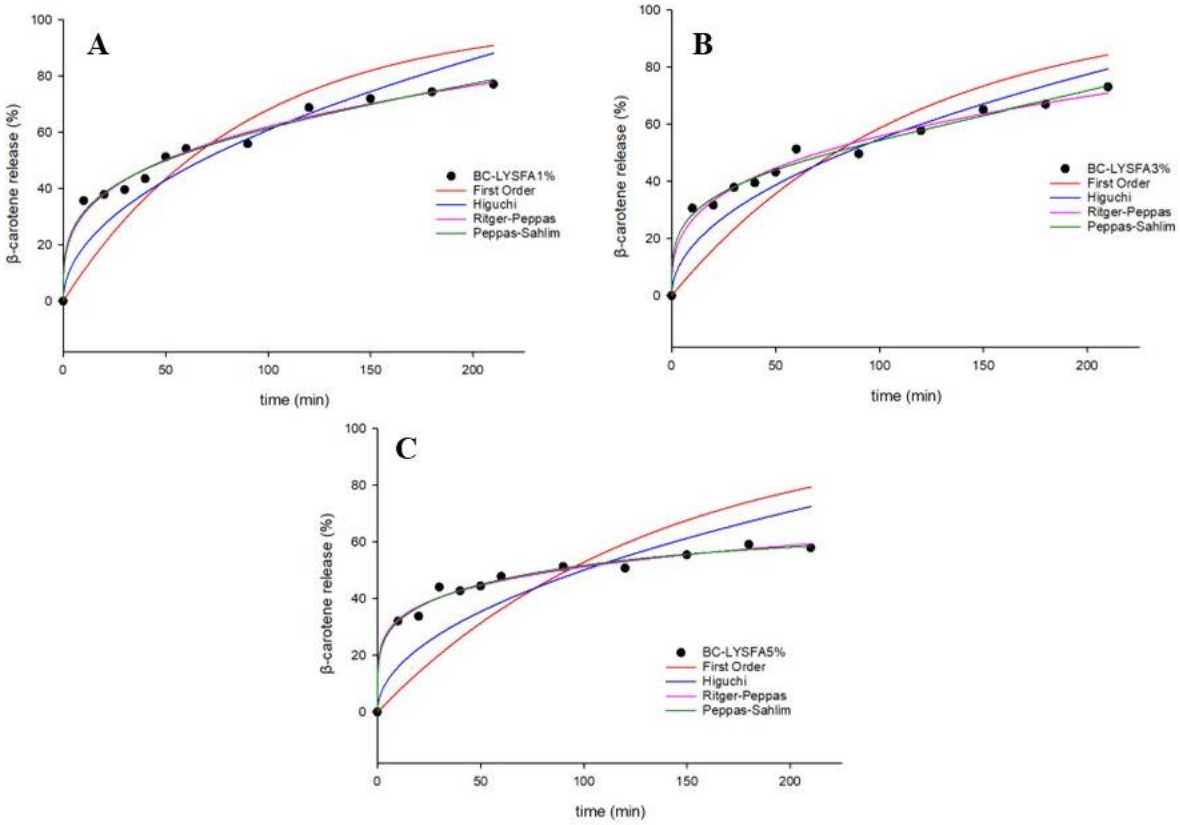

Figure 46. Kinetic modeling of β-carotene release from pectin-based films containing β-carotene-loaded Pickering emulsions prepared using LYS–FA conjugates as emulsifiers at different concentrations: (A) 1%, (B) 3%, and (C) 5% (w/w). Experimental data were fitted to first-order, Higuchi, Ritger–Peppas, and Peppas–Sahlin models. Symbols represent experimental data and solid lines correspond to the predicted values from each kinetic model.

In contrast, the Ritger–Peppas and Peppas–Sahlin models provided the best fits to the experimental data, with R^2 values above 0.98 for all evaluated formulations. In the Ritger–Peppas model, n-values below 0.5 for all samples indicate that β-carotene release is predominantly controlled by Fickian diffusion (Malekjani & Jafari, 2021).

These results are supported by the Peppas–Sahlin model, which considers simultaneous contributions from diffusion and polymer matrix relaxation mechanisms. In this model, the K2 parameter, associated with non-Fickian anomalous transport, was practically negligible in all formulations, indicating that matrix relaxation contribution is minimal. Consequently, K1/K2 > 1, demonstrating that β-carotene release from the films is mainly governed by Fickian diffusion, regardless of the incorporated emulsion concentration (Askarizadeh *et al.*, 2023). Other studies have reported similar findings, indicating that release mechanisms in polymeric films are predominantly Fickian. Sabaghi *et al.* (2022) observed Fickian diffusion behavior in lysozyme release from gelatin films using the Ritger–Peppas model. Similarly, Torres Vargas *et al.* (2026) reported Fickian diffusion in rosemary essential oil release from chitosan films, with n-values near 0.23 in the Korsmeyer–Peppas model.

Table 12. Kinetic parameters of release obtained from different mathematical models for films containing varying concentrations of β-carotene–loaded Pickering emulsions.

Model	Parameters	BC-LYSFA1%	BC-LYSFA3%	BC-LYSFA5%
First Order	K	0.011	0.009	0.008
	Adjusted R^2	0.669	0.626	0.481
Higuchi	K	6.086	5.482	5.007
	Adjusted R^2	0.854	0.883	0.543
Ritger-Peppas	K	15.306	12.666	20.648
	n	0.304	0.322	0.197
	Adjusted R^2	0.983	0.983	0.985
Peppas-Sahlin	K_1	16.518	15.468	19.400
	K_2	0.00034	0.0083	0.00033
	m	0.282	0.264	0.216
	Adjusted R^2	0.982	0.985	0.984

4 Conclusions

In this study, the potential of LYS-FA conjugates as an alternative to synthetic surfactants for the formation of β-carotene-loaded oil-in-water Pickering emulsions and their incorporation into bioactive pectin films was demonstrated. Higher concentrations of the conjugate led to increased encapsulation efficiency and significant protection of β-carotene against photochemical degradation, indicating that the particle-stabilized interface is effective in preserving sensitive lipophilic compounds.

Incorporation of the emulsions into the pectin matrix reduced water solubility, moisture content, and water vapor permeability, while increasing surface hydrophobicity, enhancing the potential application of the films in systems requiring moisture barriers. The films exhibited the characteristic yellow coloration and enhanced antioxidant capacity, attributed to the encapsulated β-carotene. Compound release was predominantly governed by Fickian diffusion.

Overall, the results demonstrate that the combination of LYS-FA-stabilized Pickering emulsions with pectin films represents a promising strategy for the development of active and sustainable packaging capable of incorporating and protecting lipophilic bioactive compounds, while providing antioxidant functionality and improved barrier properties. These findings broaden the potential applications of protein–polyphenol conjugates in smart and functional packaging systems, contributing to the advancement of high-value biodegradable materials.

Conflict of interest

The authors declare that they have no known competing financial interests or personal relationships that could have appeared to influence the work reported in this paper.

Acknowledgments

The authors thank the CNPq, Brazil (309899/2025-7); CAPES, Brazil (Código 001) and FAPERJ, Brazil (E-26/210.052/2023; E-26/204.182/2024) for the financial support.

CRediT authorship contribution statement

Bruno Sérgio Toledo Barbosa: Conceptualization, Methodology, Validation, Investigation, Writing – original draft, Writing – review & editing. Edwin Elard Garcia-Rojas: Conceptualization, Methodology, Resources, Writing – review & editing, Supervision, Project administration, Funding acquisition.

5 References

Albert, C., Beladjine, M., Tsapis, N., Fattal, E., Agnely, F., & Huang, N. (2019). Pickering emulsions: Preparation processes, key parameters governing their properties and potential for pharmaceutical applications. *Journal of Controlled Release*, *309*, 302–332. https://doi.org/10.1016/j.jconrel.2019.07.003

Almasi, H., Azizi, S., & Amjadi, S. (2020). Development and characterization of pectin films activated by nanoemulsion and Pickering emulsion stabilized marjoram (Origanum majorana L.) essential oil. *Food Hydrocolloids*, *99*, Article 105338. https://doi.org/10.1016/j.foodhyd.2019.105338

Askarizadeh, M., Esfandiari, N., Honarvar, B., Sajadian, S. A., & Azdarpour, A. (2023). Kinetic Modeling to Explain the Release of Medicine from Drug Delivery Systems. *ChemBioEng Reviews*, *10*(6), 1006–1049. https://doi.org/10.1002/cben.202300027

ASTM. (2005). *Standard test methods for water vapor transmission of materials* (ASTM E96-05). In *Annual book of ASTM standards*.

Barbosa, B. S. T., & Garcia-Rojas, E. E. (2026). Kinetic and Oxidative Stability of Oil-In-Water Pickering Emulsions Stabilized by Lysozyme-Ferulic Acid Conjugates.

Bogacz-Radomska, L., & Harasym, J. (2018). β-Carotene—properties and production methods. *Food Quality and Safety*, *2*(2), 69–74. https://doi.org/10.1093/fqsafe/fyy004

Britton, G., Liaaen-Jensen, S., & Pfander, H. (2004). *Carotenoids* (1st ed.). Birkhäuser Basel. https://doi.org/10.1007/978-3-0348-7836-4

Chevalier, Y., & Bolzinger, M.-A. (2013). Emulsions stabilized with solid nanoparticles: Pickering emulsions. *Colloids and Surfaces A: Physicochemical and Engineering Aspects*, *439*, 23–34. https://doi.org/10.1016/j.colsurfa.2013.02.054

Chhoden, T., Aggarwal, P., Singh, A., Kaur, S., & Grover, S. (2025). Application of red carrot pomace carotenoids for the development of biofunctional edible film: a sustainable approach. *Biomass Conversion and Biorefinery*, *15*(21), 27575–27592. https://doi.org/10.1007/s13399-024-05339-1

Ding, Z. G., Shen, Y., Hu, F., Zhang, X. X., Thakur, K., Khan, M. R., & Wei, Z. J. (2023). Preparation and Characterization of Eugenol Incorporated Pullulan-Gelatin Based Edible Film of Pickering Emulsion and Its Application in Chilled Beef Preservation. *Molecules*, *28*(19), Article 6833. https://doi.org/10.3390/molecules28196833

Espitia, P. J. P., Du, W.-X., Avena-Bustillos, R. de J., Soares, N. de F. F., & McHugh, T. H. (2014). Edible films from pectin: Physical-mechanical and antimicrobial properties - A review. *Food Hydrocolloids*, *35*, 287–296. https://doi.org/10.1016/j.foodhyd.2013.06.005

Freitas, C. M. P., Coimbra, J. S. R., Souza, V. G. L., & Sousa, R. C. S. (2021). Structure and Applications of Pectin in Food, Biomedical, and Pharmaceutical Industry: A Review. *Coatings*, *11*(8), Article 922. https://doi.org/10.3390/coatings11080922

Gul, K., Tak, A., Singh, A. K., Singh, P., Yousuf, B., & Wani, A. A. (2015). Chemistry, encapsulation, and health benefits of β-carotene - A review. *Cogent Food and Agriculture*, *1*(1), Article 1018696. https://doi.org/10.1080/23311932.2015.1018696

Huang, X., Yan, C., Lin, M., He, C., Xu, Y., Huang, Y., & Zhou, Z. (2022). The effects of conjugation of walnut protein isolate with polyphenols on protein solubility, antioxidant activity, and emulsifying properties. *Food Research International*, *161*, Article 111910. https://doi.org/10.1016/j.foodres.2022.111910

Ji, Y., Han, C., Liu, E., Li, X., Meng, X., & Liu, B. (2022). Pickering emulsions stabilized by pea protein isolate-chitosan nanoparticles: fabrication, characterization and delivery EPA for digestion in vitro and in vivo. *Food Chemistry*, *378*, Article 132090. https://doi.org/10.1016/j.foodchem.2022.132090

Jiang, Y., Zhang, C., Yuan, J., Wu, Y., Li, F., Li, D., & Huang, Q. (2019). Effects of pectin polydispersity on zein/pectin composite nanoparticles (ZAPs)as high internal-phase Pickering emulsion stabilizers. *Carbohydrate Polymers*, *219*, 77–86. https://doi.org/10.1016/j.carbpol.2019.05.025

Ju, M., Zhu, G., Huang, G., Shen, X., Zhang, Y., Jiang, L., & Sui, X. (2020). A novel pickering emulsion produced using soy protein-anthocyanin complex nanoparticles. *Food Hydrocolloids*, *99*, Article 105329. https://doi.org/10.1016/j.foodhyd.2019.105329

Khedri, S., Sadeghi, E., Rouhi, M., Delshadian, Z., Mortazavian, A. M., de Toledo Guimarães, J., Fallah, M., & Mohammadi, R. (2021). Bioactive edible films: Development and characterization of gelatin edible films incorporated with casein phosphopeptides. *LWT*, *138*, Article 110649. https://doi.org/10.1016/j.lwt.2020.110649

Kouravand, F., Shahidi, F., Fathi, M., Koocheki, A., & Roshanak, S. (2024). Physicochemical stability and controlled release of vitamin D3 -loaded emulsions stabilised by whey protein isolate-basil seed gum conjugates. *Journal of Microencapsulation*, *41*(8), 770–781. https://doi.org/10.1080/02652048.2024.2418615

Liu, J., Song, F., Chen, R., Deng, G., Chao, Y., Yang, Z., Wu, H., Bai, M., Zhang, P., & Hu, Y. (2022). Effect of cellulose nanocrystal-stabilized cinnamon essential oil Pickering emulsions on structure and properties of chitosan composite films. *Carbohydrate Polymers*, *275*, Article 118704. https://doi.org/10.1016/j.carbpol.2021.118704

Liu, L., Liu, T., Li, G., Tan, Q., Tang, A., Wen, T. T., Li, Z., Chi, H., Chen, H., Tang, J., & Zhang, X. (2025). Composite antimicrobial films activated by essential oil Pickering emulsions: Preparation, characterization and application in pork preservation. *Food Bioscience*, *68*, Article 106591. https://doi.org/10.1016/j.fbio.2025.106591

Liu, Q. R., Wang, W., Qi, J., Huang, Q., & Xiao, J. (2019). Oregano essential oil loaded soybean polysaccharide films: Effect of Pickering type immobilization on physical and antimicrobial properties. *Food Hydrocolloids*, *87*, 165–172. https://doi.org/10.1016/j.foodhyd.2018.08.011

Liu, Z., Shen, R., Yang, X., & Lin, D. (2021). Characterization of a novel konjac glucomannan film incorporated with Pickering emulsions: Effect of the emulsion particle sizes. *International Journal of Biological Macromolecules*, *179*, 377–387. https://doi.org/10.1016/j.ijbiomac.2021.02.188

Malekjani, N., & Jafari, S. M. (2021). Modeling the release of food bioactive ingredients from carriers/nanocarriers by the empirical, semiempirical, and mechanistic models. *Comprehensive Reviews in Food Science and Food Safety*, *20*(1), 3–47. https://doi.org/10.1111/1541-4337.12660

McClements, D. J., & Decker, E. (2018). Interfacial Antioxidants: A Review of Natural and Synthetic Emulsifiers and Coemulsifiers That Can Inhibit Lipid Oxidation. *Journal of Agricultural and Food Chemistry*, *66*(1), 20–35. https://doi.org/10.1021/acs.jafc.7b05066

Nair, S. S., Trafiałek, J., & Kolanowski, W. (2023). Edible Packaging: A Technological Update for the Sustainable Future of the Food Industry. *Applied Sciences*, *13*(14), Article 8234. https://doi.org/10.3390/app13148234

Nawaz, N., Wen, S., Wang, F., Nawaz, S., Raza, J., Iftikhar, M., & Usman, M. (2022). Lysozyme and Its Application as Antibacterial Agent in Food Industry. *Molecules*, *27*(19), Article 6305. https://doi.org/10.3390/molecules27196305

Nisar, T., Wang, Z. C., Yang, X., Tian, Y., Iqbal, M., & Guo, Y. (2018). Characterization of citrus pectin films integrated with clove bud essential oil: Physical, thermal, barrier, antioxidant and antibacterial properties. *International Journal of Biological Macromolecules*, *106*, 670–680. https://doi.org/10.1016/j.ijbiomac.2017.08.068

Pan, L., Chen, J., Fu, H., Wang, N., Zhou, J., Zhang, S., Lu, S., Dong, J., Wang, Q., & Yan, H. (2023). Effects of fabrication of conjugates between different polyphenols and bovine bone proteins on their structural and functional properties. *Food Bioscience*, *52*, Article 102375. https://doi.org/10.1016/j.fbio.2023.102375

Pathare, P. B., Opara, U. L., & Al-Said, F. A. J. (2013). Colour Measurement and Analysis in Fresh and Processed Foods: A Review. *Food and Bioprocess Technology*, *6*(1), 36–60. https://doi.org/10.1007/s11947-012-0867-9

Ren, G., Zhu, Y., Shi, J., Liu, J., He, Y., Sun, Y., Zhan, Y., Lv, J., Huang, M., & Xie, H. (2022). Fabrication of Antioxidant Pickering Emulsion Based on Resveratrol-Grafted Zein Conjugates: Enhancing the Physical and Oxidative Stability. *Foods*, *11*(23), Article 3851. https://doi.org/10.3390/foods11233851

Sabaghi, M., Joly, C., Adt, I., Ozturk, K., Cottaz, A., & Degraeve, P. (2022). Effect of crosslinking by microbial transglutaminase of gelatin films on lysozyme kinetics of release in food simulants. *Food Bioscience*, *48*, Article 101816. https://doi.org/10.1016/j.fbio.2022.101816

Sánchez-González, L., Cháfer, M., Chiralt, A., & González-Martínez, C. (2010). Physical properties of edible chitosan films containing bergamot essential oil and their inhibitory action on Penicillium italicum. *Carbohydrate Polymers*, *82*(2), 277–283. https://doi.org/10.1016/j.carbpol.2010.04.047

Shen, Y., Ni, Z. J., Thakur, K., Zhang, J. G., Hu, F., & Wei, Z. J. (2021). Preparation and characterization of clove essential oil loaded nanoemulsion and pickering emulsion activated pullulan-gelatin based edible film. *International Journal of Biological Macromolecules*, *181*, 528–539. https://doi.org/10.1016/j.ijbiomac.2021.03.133

Taghizadeh, M., Mohammadifar, M. A., Sadeghi, E., Rouhi, M., Mohammadi, R., Askari, F., Mortazavian, A. M., & Kariminejad, M. (2018). Photosensitizer-induced cross-linking: A novel approach for improvement of physicochemical and structural properties of gelatin edible films. *Food Research International*, *112*, 90–97. https://doi.org/10.1016/j.foodres.2018.06.010

Tan, J. M., Cui, R., Hu, T. G., Li, X. X., & Wu, H. (2025). Preparation of chitosan/shellac nanoparticles-essential oil Pickering emulsion active film and its application in bread preservation. *Food Packaging and Shelf Life*, *49*, Article 101496. https://doi.org/10.1016/j.fpsl.2025.101496

Tongnuanchan, P., Benjakul, S., Prodpran, T., & Nilsuwan, K. (2015). Emulsion film based on fish skin gelatin and palm oil: Physical, structural and thermal properties. *Food Hydrocolloids*, *48*, 248–259. https://doi.org/10.1016/j.foodhyd.2015.02.025

Torres Vargas, O. L., González, M. L., & Loaiza, Y. V. G. (2026). Sustained-release composite films incorporated with rosemary (Rosmarinus officinalis L.) essential oil: Characterization, release kinetics and application for cheese preservation. *Applied Food Research*, *6*(1), Article 101578. https://doi.org/10.1016/j.afres.2025.101578

Wei, Y., Wang, C., Liu, X., Mackie, A., Zhang, M., Dai, L., Liu, J., Mao, L., Yuan, F., & Gao, Y. (2022). Co-encapsulation of curcumin and β-carotene in Pickering emulsions stabilized by complex nanoparticles: Effects of microfluidization and thermal treatment. *Food Hydrocolloids*, *122*, Article 107064. https://doi.org/10.1016/j.foodhyd.2021.107064

Wilde, P., Mackie, A., Husband, F., Gunning, P., & Morris, V. (2004). Proteins and emulsifiers at liquid interfaces. *Advances in Colloid and Interface Science*, *108–109*, 63–71. https://doi.org/10.1016/j.cis.2003.10.011

Xie, B., Zhang, X., Luo, X., Wang, Y., Li, Y., Li, B., & Liu, S. (2020). Edible coating based on beeswax-in-water Pickering emulsion stabilized by cellulose nanofibrils and carboxymethyl chitosan. *Food Chemistry*, *331*, Article 127108. https://doi.org/10.1016/j.foodchem.2020.127108

Xue, F., Li, C., & Adhikari, B. (2024). Physicochemical properties of active films of rose essential oil produced using soy protein isolate-polyphenol conjugates for cherry tomato preservation. *Food Chemistry*, *452*, Article 139614. https://doi.org/10.1016/j.foodchem.2024.139614

Yan, X., Ma, C., Cui, F., McClements, D. J., Liu, X., & Liu, F. (2020). Protein-stabilized Pickering emulsions: Formation, stability, properties, and applications in foods. *Trends in Food Science and Technology*, *103*, 293–303. https://doi.org/10.1016/j.tifs.2020.07.005

Yang, L., Zhou, C., Liu, Y., He, Z., Zhang, M., Wang, C., Yang, Z., & Li, P. (2024). Enhanced mechanical properties and antibacterial activities of chitosan films through incorporating zein-gallic acid conjugate stabilized cinnamon essential oil Pickering emulsion. *International Journal of Biological Macromolecules*, *258*, Article 128933. https://doi.org/10.1016/j.ijbiomac.2023.128933

Yang, W., Zhang, S., Hu, Y., Fu, Q., Cheng, X., Li, Y., Wu, P., Li, H., & Ai, S. (2024). Pectin-based film activated with carboxylated cellulose nanocrystals-stabilized oregano essential oil Pickering emulsion. *Food Hydrocolloids*, *151*, Article 109781. https://doi.org/10.1016/j.foodhyd.2024.109781

Yin, X., Lu, J., Du, W., Wu, Q., Han, L., & Su, S. (2024). Encapsulation of β-carotene in Pickering emulsions stabilized by self-aggregated chitosan nanoparticles: Factors affecting β-carotene stability. *International Journal of Biological Macromolecules*, *277*, Article 133696. https://doi.org/10.1016/j.ijbiomac.2024.133696

Yu, Y., Gong, M., Wang, S., Wang, X., Liu, Y., Huang, D., Guan, H., Liu, H., Chen, Y., Jiang, Y., & Li, D. (2024). Pectin-based cinnamon essential oil Pickering emulsion film with two-sided differential wettability: A major role in the spatial distribution of microdroplets. *International Journal of Biological Macromolecules*, *277*, Article 133727. https://doi.org/10.1016/j.ijbiomac.2024.133727

Zhao, R., Guan, W., Zhou, X., Lao, M., & Cai, L. (2022). The physiochemical and preservation properties of anthocyanidin/chitosan nanocomposite-based edible films containing cinnamon-perilla essential oil pickering nanoemulsions. *LWT*, *153*, Article 112506. https://doi.org/10.1016/j.lwt.2021.112506

Zhao, X., Li, C., & Xue, F. (2023). Effects of whey protein-polyphenol conjugates incorporation on physicochemical and intelligent pH-sensing properties of carboxymethyl cellulose based films. *Future Foods*, *7*, Article 100211. https://doi.org/10.1016/j.fufo.2022.100211

Zickuhr, G. M., Nandi, L. G., Dreyer, J. P., Quadrado, R. F. N., Fajardo, A. R., Carli, L. N., & Bellettini, I. C. (2025). Evaluation of stability, physicochemical properties, in vitro release behavior, and antioxidant activity of α-tocopherol encapsulated in ethyl(hydroxyethyl)cellulose (EHEC) films. *Journal of Molecular Liquids*, *431*, Article 127645. https://doi.org/10.1016/j.molliq.2025.127645

CONCLUSÃO

Esta tese investigou a conjugação covalente entre proteínas da clara de ovo, ovalbumina e a lisozima, e o ácido ferúlico como estratégia para a modificação estrutural e funcional de proteínas alimentares, visando o desenvolvimento de ingredientes multifuncionais com propriedades tecnofuncionais e biológicas aprimoradas, bem como sua aplicação em emulsões Pickering e em matrizes poliméricas para embalagens bioativas.

O estudo das ligações covalentes formadas entre a ovalbumina e o ácido ferúlico, obtidas eficientemente pelo método alcalino, revelou modificações significativas nas estruturas secundária e terciária da proteína. Essas alterações resultaram em aumento expressivo da solubilidade, da capacidade emulsificante e da formação de espuma, além da incorporação de elevada capacidade antioxidante. Os resultados confirmam o potencial do conjugado ovalbumina–ácido ferúlico como ingrediente bifuncional promissor, capaz de atuar simultaneamente como emulsificante e agente antioxidante em sistemas alimentares. A aplicação desses conjugados em emulsões Pickering demonstrou elevada estabilidade físico-química e capacidade antioxidante, sendo eficazes na encapsulação e proteção da vitamina D3. Observou-se redução da formação de hidroperóxidos lipídicos, maior proteção contra degradação fotoquímica e aumento da bioacessibilidade do bioativo após digestão in vitro, em comparação com sistemas estabilizados apenas por ovalbumina.

Já os conjugados formados entre lisozima e ácido ferúlico, obtidos pela técnica de radical livre, apresentaram alterações estruturais que favoreceram a atividade interfacial da proteína e conferiram elevada capacidade antioxidante ao sistema. Esses conjugados mostraram alta eficiência como emulsificantes de emulsões Pickering, promovendo maior estabilidade cinética e proteção efetiva do óleo de soja contra oxidação primária e secundária. Além disso, a simulação de digestão gastrointestinal in vitro evidenciou maior preservação da capacidade antioxidante do ácido ferúlico conjugado, indicando o potencial desses sistemas para aplicações em liberação controlada e alimentos funcionais.

No contexto da aplicação tecnológica, os conjugados lisozima–ácido ferúlico demonstraram atuar de forma eficaz como agentes emulsificantes na formação de emulsões de Pickering contendo β-caroteno. A incorporação dessas emulsões em filmes à base de pectina promoveu melhorias relevantes nas propriedades de barreira à luz e à umidade, redução da solubilidade em água e aumento da hidrofobicidade superficial. Adicionalmente, os filmes apresentaram maior capacidade antioxidante e proteção do β-caroteno frente à degradação fotoquímica, ampliando o potencial de aplicação em embalagens bioativas e sustentáveis.

Por fim, os resultados consolidam os conjugados entre proteínas da clara de ovo e ácido ferúlico como uma estratégia tecnológica robusta para ampliar o desempenho funcional de proteínas alimentares. Essa abordagem viabiliza sua aplicação como emulsificantes em emulsões Pickering com propriedades antioxidantes, permitindo a formação de sistemas com elevada estabilidade, maior proteção de compostos sensíveis e manutenção da bioatividade. Tais achados evidenciam o potencial desses conjugados como ingredientes funcionais na formulação de alimentos fortificados, possibilitando a substituição de surfactantes sintéticos por soluções mais naturais e sustentáveis. Como perspectivas futuras, destacam-se estudos voltados à incorporação desses sistemas em matrizes alimentares reais, como bebidas e molhos funcionais, bem como à aplicação e avaliação de filmes bioativos à base dessas emulsões para uso como revestimentos em alimentos.